Pre-normative research for safety of hydrogen driven vehicles and transport through tunnels and similar confined spaces

Fuel Cells and Hydrogen Joint Undertaking (FCH JU)
Grant Agreement Number 826193

Deliverable 1.2
Report on hydrogen hazards and risks in tunnels and similar confined spaces

Lead authors: UU (D. Cirrone, V. Shentsov, S. Kashkarov, M. Dadashzadeh, D. Makarov, V. Molkov)
Contributing authors: DTU (F. Markert, L. Giuliani)
NCSRD (A. Venetsanos, S. Giannissi, I. Tolias)
KIT (M. Kuznetsov, T. Jordan, Z. Xu)
URS (P. Russo)
USN (K. Vågsæther)
SPFI (T. Van Esbroeck, N. De Backer)
IFA (C. Brauner)
NEN (J. van den Berg, F. de Jong)
PS (J. Grune)
FHA (A. Bernad)

Version: 190830
Delivery date for internal review: 17 August 2019
Due date: 31 August 2019
Dissemination level: Public

FUEL CELLS AND HYDROGEN JOINT UNDERTAKING

Deliverable administration					
Work Package	WP1. The state-of-the-art in safety provisions for underground transportation systems and accident scenarios prioritisation				
N. and title	D1.2. Report on hydrogen hazards and risks in tunnels and similar confined spaces				
Type	Report				
Status	Draft/Working/**Released**	Due	M6	Date	31-08-2019
Comments					

Development and revision			
Version N.	Date	Authors	Description
190403	03-04-2019	D. Cirrone, UU	1st draft ToC
190405	05-04-2019	V. Molkov, UU	Amendments to ToC
190407	07-04-2019	D. Makarov, UU	Amendments to ToC
190527	27-05-2019	D. Cirrone, UU	Amendments to ToC, including KIT suggestions
190630	30-06-2019	D. Cirrone, V. Shenstov, S. Kashkarov, M. Dadashzadeh, UU	Compilation of first draft
190710	10-07-2019	K. Vågsæther, USN	Sections 3.1.4, 3.2.4
190710	10-07-2019	P. Russo, URS	Sections 3.2.3, 5.1
190722	22-07-2019	A. Venetsanos, I. Tolias, S. Giannissi, NCSRD	Sections 3.1.5, 3.1.5.3, 3.1.5.4, 3.1.5.7
190805	05-08-2019	F. Markert, DTU	Sections 3.4.3, 3.5, 5.2
190815	07-08-2019	D. Cirrone, UU	Review and editing of draft
190820	20-08-2019	M. Kuznetsov, KIT	Sections 3.3.2, 3.3.3
190822	22-08-2019	C. Brauner, IFA	Section 3.5.6
190824	24-08-2019	V. Molkov, UU	Review and editing of draft
190827	27-08-2019	P. Russo, URS	Review of the deliverable
190828	28-08-2019	J. van den Berg, NEN F. de Jong, NEN	Review of the deliverable
190830	30-08-2019	J. Grune, PS A. Bernad, FHA Z. Xu, KIT	Addition of section “Ignition of unsteady hydrogen jets” in 3.2.4.2 Review of section 3.4.1 Review of deliverable text
190830	30-08-2019	D. Cirrone, UU	Updated version returned to reviewers

Disclaimer

Acknowledgments

This project has received funding from the Fuel Cells and Hydrogen 2 Joint Undertaking (JU) under grant agreement No 826193. The JU receives support from the European Union's Horizon 2020 research and innovation programme and United Kingdom, Germany, Greece, Denmark, Spain, Italy, Netherlands, Belgium, France, Norway, Switzerland.

Summary

The aim of the present deliverable is to perform a critical analysis of the hazards and associated risks for hydrogen driven vehicles and transport through tunnels or similar confined spaces. The state-of-the-art of the research and guidelines will be discussed thoroughly with the scope of identifying the knowledge gaps and technological bottlenecks for provision of hydrogen safety in underground transportation systems. The review includes aspects of the beyond the state-of-the-art research, e.g. not yet published results of experimental studies, reduced-order engineering tools and contemporary numerical models. First, relevant to use of hydrogen in confined spaces properties are described. Afterwards, hazards associated to possible accident scenarios involving hydrogen-powered vehicle in tunnels and other confined spaces are described and discussed, highlighting where the research focus should be. The available to date tools to assess consequences of different accident scenarios are presented. The results of these tools application should be translated into useful information to ensure protection of life and infrastructure, this includes but is not limited to hazard distances. To provide holistic approach to calculation of hazards distances, a review of the harm to people and damage to buildings criteria is carried out. The existent methodologies for Quantitative Risk Assessment (QRA) are presented and their suitability for hydrogen applications in confined spaces is discussed. In conclusion, the reported information is summarised in a concise list of knowledge gaps that yet need to be closed. The detailed HyTunnel-CS project research programme will be shaped with taking into account the identified gaps.

Keywords

Hydrogen safety, hazards, consequences, accident scenario, assessment tool, unignited release, dispersion, ventilation, jet fire, thermal effects, deflagration, detonation, pressure effects, hydrogen tank rupture in a fire, quantitative risk assessment, prevention and mitigation.

Table of contents

Nomenclature and abbreviations

ADR	The European Agreement Concerning the International Carriage of Dangerous Goods by Road
ASET	Available Safe Egress Time
BA	Breathing Apparatus
BBN	Bayesian Belief Networks
BLEVE	Boiling Liquid Expanding Vapour Explosion
BPS	Best Possible Scenario
BR	Blockage Ratio
CABA	Compressed Air Breathing Apparatus
CFD	Computational Fluid Dynamics
CFRP	Carbon Fibre Reinforced Polymer
CGH_2	Compressed Gaseous Hydrogen
CNG	Compressed Natural Gas
DDT	Deflagration-to-Detonation Transition
DG	Dangerous Goods
DO	Discrete Ordinates
DTRM	Discrete Transfer Radiation Model
EBA	Eisenbahn Bundesamt
EP	Escalating Probability
EV	Expected Value
FCH	Fuel Cell Hydrogen
FCV	Fuel Cell Vehicle
FED	Fractional Effective Dose
FEM	Finite Element Method
FMEA	Failure Mode and Effect Analysis
FRR	Fire Resistance Rating
FSE	Fire Safety Engineering
GTR	Global Technical Regulations
HAZOP	Hazard and operability
HC	Hydrocarbon Curve
HCM	Hydrocarbon Curve Modified
HGV	Heavy Goods Vehicle
HPV	Hydrogen-Powered Vehicles
HRR	Heat Release Rate
IBP	Initial Burst Pressure
IR	Intrinsic Risk
IRSN	Institut de Radioprotection et de Surete Nucleaire
LDV	Light Duty Vehicle
LFL	Lower Flammability Limit
LH_2	Liquid Hydrogen
LNB	Leak-No-Burst
LPG	Liquefied Petroleum Gas
MIE	Minimum Ignition Energy
MPV	Multi Purpose Vehicle
MVKm	Million Vehicle Kilometre
NBP	Normal Boiling Point
NHTSA	National Highway Traffic Safety Administration
NTP	Normal Temperature and Pressure

NWP	Nominal Working Pressure
OECD	Organisation for Economic Co-operation and Development
OEM	Original Equipment Manufacturer
PA	Public Address
PAH	Poly-Aromatic Hydrocarbons
PCDD	Polychlorinated dibenzodioxins
PIARC	Permanent International Association of Road Congresses
PNR	Pre-Normative Research
PPP	Pressure Peaking Phenomena
PRD	Pressure Relief Device
PVC	Polyvinyl Chloride
QRA	Quantitative Risk Assessment
QRAM	Quantitative Risk Assessment Model
RCS	Regulations, Codes and Standards
RSET	Required Safe Egress Time
RTA	Road Tunnel Association
RUD	Run-Up Distance
RWS	Rijks Water Staat
SCBA	Self-Contained Breathing Apparatus
SFPE	Society of Fire Protection Engineers
SHT	Statens Havarikommisjon for Transport
STP	Standard Temperature and Pressure
SUV	Sport Utility Vehicle
TPL	Thermal Protection Layer
TPRD	Thermally activated Pressure Relief Device
UFL	Upper Flammability Limit
VCE	Vapour Cloud Explosion

Definitions

Acceptance criteria are the terms of reference against which safe design of a fuel cell and/or hydrogen (FCH) facility/infrastructure is assessed (definition based on British Standards Institution, 2001).

Accident is an unforeseen and unplanned event or circumstance causing loss or injury.

Flammability range is the range of concentrations between the lower and the upper flammability limits. *The lower flammability limit* (LFL) is the lowest concentration of a combustible substance in a gaseous oxidizer that will propagate a flame. *The upper flammability limit* (UFL) is the highest concentration of a combustible substance in a gaseous oxidizer that will propagate a flame.

Deflagration is the phenomenon of combustion zone propagation at the velocity lower than the speed of sound (sub-sonic) into a fresh, unburned mixture.

Detonation is the process of combustion zone propagating at the velocity higher than the speed of sound (supersonic) in the unreacted mixture.

Fire resistance rating is a measure of time for which a passive fire protection system can withstand a standard fire resistance test.

Harm is physical injury or damage to health.

Hazard is any potential source or condition that has the potential for causing damage to people, property and the environment.

Hazard distance is a distance from the (source of) hazard to a determined (by physical or numerical modelling, or by a regulation) physical effect value (normally, thermal or pressure) that may lead to a harm condition (ranging from “no harm” to “max harm”) to people, equipment or environment.

Hydrogen safety engineering is application of scientific and engineering principles to the protection of life, property and environment from adverse effects of incidents/accidents involving hydrogen.

Incident is something that occurs casually in connection with something else.

Limiting oxygen index is the minimum concentration of oxygen that will support flame propagation in a mixture of fuel, air, and nitrogen.

Mach disk is a strong shock normal to the under-expanded jet flow direction.

Minimum ignition energy of flammable gases and vapours is the minimum value of the electric energy, stored in the discharge circuit with as small a loss in the leads as possible, which (upon discharge across a spark gap) just ignites the quiescent mixture in the most ignitable composition. For a given mixture composition the following parameters of the discharge circuit must be varied to get the optimum conditions: capacitance, inductivity, charging voltage, as well as shape and dimensions of the electrodes and the distance between electrodes.

Normal boiling point (NBP) is the temperature at which a liquid boils at a pressure of 101.325 kPa.

Normal temperature and pressure (NTP) conditions are: temperature 293.15 K and pressure 101.325 kPa.

Permeation is the movement of atoms, molecules, or ions into or through a porous or permeable substance.

Separation distance is the minimum separation between a hazard source and an object (human, equipment or environment) which will mitigate the effect of a likely foreseeable incident and prevent a minor incident escalating into a larger incident.

Standard temperature and pressure (STP) conditions are: temperature 273.15 K and pressure 101.325 kPa.

Risk is the combination of the probability of an event and its consequence.

List of figures

List of tables

1. Introduction and scope (UU, DTU)

The use of FCH vehicle or transport of compressed gaseous hydrogen (CGH_2) and cryogenic liquid hydrogen (LH_2) in tunnels and similar confined spaces, such as underground parks, maintenance shops, garages, etc., creates new challenges to provision of life safety, property and environment protection at the acceptable level of risk. Several studies have showed that confinement or congestion can promote more severe consequences compared to accidents in the open atmosphere. There is a need to develop and validate hazard assessment tools for the prediction of hydrogen behaviour in tunnels, to quantitively assess risk as concluded, e.g., by the HyTunnel internal project of the European Network of Excellence HySafe (NoE HySafe) (HyTunnel-D111, 2009).

The aim of the present deliverable is to perform a critical analysis of hazards and associated risks relevant to the use of FCH vehicles in the underground transportation systems. To achieve this aim, the following objectives are addressed in this deliverable:

- Review and analyse hydrogen hazards in confined spaces and its safety assets using experimental studies.
- Review available reduced-order engineering tools and contemporary CFD models for the assessment of hydrogen hazards and associated risks in tunnels and similar confined spaces.
- Quantify harm for people and damage for underground structures criteria, including unprotected and protected, e.g. firemen.
- Identify the knowledge gaps and technological bottlenecks to be addressed.
- Formulate requirements to engineering tools and CFD models to be developed and validated in the HyTunnel-CS project, keeping in mind their applicability to accident scenarios in road and railway tunnels, underground and multi-storey car parking, etc.

The report structure follows the objectives and is organised as follow. Firstly, hydrogen properties relevant to use in confined spaces are selected and described (Chapter 2). The following chapter delineates the possible accident scenarios and the associated hazards. The specific hydrogen hazards in confined spaces, e.g. the pressure peaking phenomenon, and the main hydrogen safety asset, i.e. its highest among other fuels buoyancy, are analysed from the point of view of the need to whether introduce or not changes to current requirements to safety provisions in tunnels and similar confined spaces, etc. Particular attention is paid to the engineering tools available for hydrogen safety engineering to assess pressure and thermal effects, calculate hazard distances and other parameters relevant to assure an inherently safer deployment and use of hydrogen systems in underground transportation infrastructure. Validated CFD models are presented and discussed. Contemporary CFD models is an essential tool to simulate accident consequences in complex geometries for scenarios where the reduced-order engineering correlations and tools can hardly be applied. Chapter 4 presents the review of harm criteria for both unprotected and protected people, and damage criteria for structures and equipment. Chapter 5 discusses the methodologies of Quantitative Risk Assessment (QRA) and their potential to be applied for hydrogen applications in confines spaces. Chapter 6 summarises identified knowledge gaps to be addressed in the project through complementarities and synergies of experimental, theoretical and numerical studies.

2. Hydrogen properties relevant to safety in confined spaces (UU)

This chapter describes hydrogen properties that are relevant to hazards and safety provisions in tunnels and similar confined spaces.

2.1 Physical properties (UU)

Hydrogen is the lightest known element with an atomic mass of 1.008 g/mol. The atomic configuration for the most diffused isotope in nature (protium) includes a proton in its nucleus and an electron. In hydrogen gas at normal conditions, atoms combine in diatomic molecules through covalent bonds. Each of the two atoms is characterised by a relative spin of the nucleus. If the spins have the same direction, the molecule is defined as ortho-hydrogen. In case of anti-parallel configuration with spins in opposite directions, the molecule is denominated para-hydrogen (NASA, 1997) and it has slightly different physical properties from the ortho-hydrogen molecule. In normal and equilibrium condition, hydrogen is composed by 75% ortho-hydrogen and 25% para-hydrogen. With the decrease of temperature, equilibrium hydrogen gas increases in para-hydrogen component, reaching 99.8% for liquid hydrogen at 20 K. The transition from para- to ortho-hydrogen in cryo-compressed storage is able to receive energy without practically changing the pressure – this helps to practically eliminate the boil-off phenomenon, which is characteristic for LH_2 storage, with little driving per week (the consumption of hydrogen during driving cools it and promote change of ortho-hydrogen to para-hydrogen).

Density of hydrogen at normal conditions (NTP) is as low as 0.0838 kg/m^3 (far below than air density of 1.205 kg/m^3 at the same conditions). To achieve higher capacities, hydrogen is stored at gaseous form at high pressure or as cryo-compressed or liquid hydrogen. Hydrogen critical temperature[1] and pressure[2]are respectively 33.15 K and 12.96 bar, which correspond to a density equal to 31.26 kg/m^3. The triple point[3] is given for a temperature of 13.8 K and pressure of 0.072 bar. The temperature at the normal boiling point (NBP) is 20.37 K (P=1 bar) and density is 70.90 kg/m^3 (NIST website, 2019). A phase change from liquid to gas would cause an expansion of the gas with an increase of volume by approximately 850 times. The expansion ratio is high as well for hydrogen stored at high pressure, e.g. hydrogen at 25 MPa yields an expansion ratio equal to 240 (College of the Desert, 2001). In case of hydrogen release in an enclosure, either as a liquid or as high-pressure gas, the overpressure may rise to a level sufficient to destroy the structure.

Hydrogen gas is colourless, odourless and tasteless. These characteristics make a hydrogen leak difficult to detect. High-pressure hydrogen leak can be recognised in some cases by specific hissing sound. The high purity level needed for use of hydrogen in fuel cells prevents the addition of chemical compounds to scent the gas, as done with mercaptans for scenting natural gas. Despite these properties, hydrogen is non-toxic and dangerous effects on health related to high concentration of hydrogen are mainly associated to deficiency of oxygen. Being

[1] The critical temperature of a substance is the highest temperature at which is possible to liquefy the vapor of a substance.
[2] The critical pressure of a substance is the pressure required to liquefy a gas at its critical temperature.
[3] The triple point of a substance is the temperature and pressure at which there is coexistence of the substance three phases (gas, liquid, and solid) in thermodynamic equilibrium.

non-toxic at high concentration hydrogen nevertheless can cause asphyxiation in confined space.

The small size of the hydrogen molecules leads to a high diffusivity of the gas, with values of hydrogen diffusivity in air ranging from $6.1 \cdot 10^{-5}$ m^2/s, as reported by Alcock et al. (2001), to $6.8 \cdot 10^{-5}$ m^2/s (Baratov et al., 1990). This value is higher than for any other substances. For instance, hydrogen diffusivity in air results to be approximately 3 times the coefficient for methane (HyResponse, 2015a). The diffusivity of hydrogen through gypsum board is as well "unexpectedly" high $1.4 \cdot 10^{-5}$ m^2/s at room temperature (Yang et al., 2013). This can be used in hydrogen safety engineering of garages and other confined spaces (the board could keep heat but mitigate hydrogen accumulation if prover ventilation design is applied).

The heat capacity of hydrogen is similar to that of other diatomic gases despite its low molecular mass (ISO/TR 15916:2004). The specific heat of GH_2 at constant pressure c_p is (in kJ/kg/K): 14.85 (NTP), 14.304 (STP), 12.15 (NBP). The specific heat of LH_2 at boiling point is 9.66 kJ/kg/K (BRHS, 2009). The specific heat at constant pressure of liquid para-hydrogen is c_p=9.688 kJ/kg/K. The gas constant of hydrogen is 4.1243 kJ/kg/K (i.e. the universal gas constant divided by the molecular weight). The specific heats ratio (γ) of hydrogen at NTP is 1.39 and at STP conditions γ is 1.405 (Molkov, 2012).

Thermal conductivity of hydrogen is significantly higher than that of other gases: for GH_2 it is 0.187 W/m/K at NTP, whereas at NBP it is 0.01694 W/m/K for GH_2 and 0.09892 W/m/K for LH_2 (Molkov, 2012).

Speed of sound in gaseous hydrogen is 1304 m/s at NTP and 356 m/s at NBP for gaseous hydrogen, and 1119 m/s for liquid hydrogen (NIST website, 2019). Speed of sound in stoichiometric hydrogen-air mixture is 404 m/s (HyResponse, 2015a).

2.1.1 Buoyancy as the main hydrogen safety asset (UU)

The main hydrogen safety asset, i.e. its highest on The Earth buoyancy, confers the ability to rapidly flow out of an incident scene, and mix with the ambient air to a safe level below the lower flammability limit (LFL) of 4% by volume of hydrogen in air. Indeed, hydrogen has a density of 0.0838 kg/m^3 (NTP) which is far below than air density of 1.205 kg/m^3 at the same conditions. The unwanted consequences of hydrogen releases into the open atmosphere, and in partially confined geometries, where no conditions to allow hydrogen to accumulate exist, are drastically reduced by buoyancy. In case of release in a tunnel, the increase of the ceiling height may create safer conditions to the tunnel users for buoyant releases of H_2 (HyTunnel-D111, 2009). The strategy for inherently safer release in confined space, which would exclude the accumulation of hydrogen above LFL, is to reduce a diameter of release to the value that would guarantee that hydrogen concentration in a jet will be reduced below 4% by volume when hydrogen reaches the ceiling of the confined structure like a tunnel. The similarity law can be used for hydrogen safety engineering in such cases (Molkov, 2012).

Contrary to hydrogen, heavier hydrocarbons can form a huge combustible cloud, usually in a form of pancake being heavier than air. The most known cases of disastrous explosions of hydrocarbons are Flixborough in 1974 (Health and Safety Executive, 1975) and Buncefield in 2005 (Buncefield Investigation, 2010). In many practical situations, hydrocarbons may pose stronger fire and explosion hazards than hydrogen. This statement is valid if hydrogen is

handled properly by professionals in hydrogen safety. Hydrogen high buoyancy affects its dispersion in air considerably more than its high diffusivity.

Pure hydrogen is positively buoyant above a temperature of 22 K, i.e. over almost the whole temperature range of its gaseous state (BRHS, 2009). Buoyancy provides comparatively fast dilution of released hydrogen by surrounding air below LFL. In the open atmosphere only small fraction of released hydrogen would be able to deflagrate in the vicinity of the release where hydrogen concentration is within the flammability limits. Indeed, a hydrogen-air cloud evolving from the inadvertent release upon the failure of a storage tank or pipeline liberates only a small fraction of its thermal energy in case of a deflagration, which is in the range 0.1-10% and in most cases below 1% of the total energy of released hydrogen (Lind, 1975; BRHS, 2009). This makes safety considerations of hydrogen accident with large inventory at the open quite different from that of other flammable gases and vapours with often less or no harmful consequences at all.

Caution should be taken in applying gaseous hydrogen buoyancy observations to releases of hydrogen vapours at cryogenic temperatures. Hydrogen vapours at very low temperature can be denser than air at NTP. Usually the condensation of atmospheric humidity will also add water to the mixture cloud, firstly making it visible, and secondly increasing the molecular mass of the mixture even more (Molkov, 2012).

2.2 Ignition and combustion properties (UU)

Combustion of hydrogen in a clean atmosphere produces an invisible flame. This could make difficult the detection of the flame by eyes in an accident scenario unless dust and other substances from the surrounding are entrained in the jet and burn with visible radiation. Indeed, it is expected that in many cases the flame itself, high turbulence level and hot combustion products will cause variations to the surroundings that can be used to detect the presence of the flame visually and by detectors. The temperature of premixed hydrogen flame can reach 2403 K for stoichiometric mixture, which is somewhat higher than other fuels (BRHS, 2009). A stoichiometric mixture is composed by 29.59 vol % of hydrogen and 70.41 vol % of air, which is assumed to be composed by 21 vol % of oxygen and 79 vol % of nitrogen. Mixtures with hydrogen concentration below the stoichiometric value are defined as “lean”, otherwise for higher values they are defined as “rich”. The minimum amount of oxygen to have flame propagation at NTP conditions is 5 vol % (NASA, 1997).

The lower heat of combustion of hydrogen is 119.93 MJ/kg. The higher heat of combustion is 141.86 MJ/kg and it includes the water vapour heat of condensation. Hydrogen heat of combustion is much higher than other fuels commonly used in the automotive field, as showed in Table 1. Therefore, hydrogen fires in an accident scenario involving FCH vehicle may have temporary heat release rate due to hydrogen greater compared to a conventional car, e.g. at the moment of initiation of thermally activated pressure relief device (TPRD) of large diameter. However, the mass of hydrogen contained in an onboard storage system would be lower than other conventional fuels, which could lower the overall energy released. The duration of automobile fire could be up to 1-2 hours, while release of hydrogen will take usually a shorter time of order of minutes or tens of minutes, if TPRD activated in a right time and being not blocked during an accident. The effect of hydrogen release has not been quantified yet for different fire conditions. Therefore, the research in this project plans to address this issue.

The flammability range of hydrogen is 4-75% (LFL-UFL). It means that a mixture with hydrogen concentration in air included within this range can be ignited and will sustain flame propagation. The flammability range of hydrogen is significantly wider than other fuels (see Table 1). It must be underlined that the flammability limits depend on the direction of flame propagation. Table 1 gives flammability limits for upward flame propagation only. The range narrows down for a horizontal flame propagation to 6.0-7.15% for LFL and 65.7-71.4% for UFL. LFL and UFL change to 8.5-9.45% and 68-74.5% respectively for a downward flame propagation (Coward and Jones, 1952). The flammability range expands linearly with the increase of temperature. As an example, a rise of temperature from 20 °C to 400 °C leads to expansion of the flammability range to 1.5-87.5%.

Table 1. Combustion properties of hydrogen and other common automotive fuels at normal conditions (College of the Desert, 2001[a]; Baratov et al., 1990[b]; Molkov, 2012[c]; Alcock et al., 2001[d]).

Fuel	Hydrogen	Methane	Propane	Gasoline
Higher heating value[a], MJ/kg	141.86	55.53	50.36	47.5
Lower heating value[a], MJ/kg	119.93	50.02	45.6	44.5
Flammability range - concentration in air[a], vol %	4-75	5.3-15	2.2-9.6	1-7.6
Autoignition temperature[b], °C	510	537	470	230-480
Minimum ignition energy[c], mJ	0.017	0.28	0.25	0.23-0.46
Detonability range - concentration in air[d], vol %	11-59.0	6.3-13.5	3.1-7	1.1-3.3

The minimum temperature required to initiate a combustion reaction for a fuel-oxidiser mixture in absence of an external source of ignition is defined by the standard auto-ignition temperature, which is in fact the ignition by the hot surface of flask. At atmospheric pressure, the auto-ignition temperature of hydrogen in air is 510 °C (Baratov et al., 1990). Therefore, contact of hydrogen-air mixture with an object at such temperature may lead to the ignition of the mixture. However, the temperature would increase if, for example, a hot pipe is used for ignition instead of internal surface of flask. The smaller the pipe diameter the higher will be temperature of the pipe able to ignite hydrogen-air mixture.

The minimum ignition energy (MIE) of a hydrogen-air mixture depends on its composition. The absolute MIE is given for a stoichiometric mixture and is equal to 17 μJ. This value is 16 times lower than for methane and 56 times lower than for petrol. MIE increases for compositions different from stoichiometric up to 3 orders of magnitude for hydrogen concentration close to the LFL and UFL (Ono et al., 2007).

The wide flammability range and low ignition energy render hydrogen very easy to ignite. Ignition sources may include sparks from mechanical or electrical equipment, heating equipment, static electricity, etc.

Figure 1 shows the laminar burning velocity, S_u, as function of hydrogen concentration in air as reported by Zimont and Lipantikov (1995) for the experimental studies by Karpov and Severin (1980), and by Tse et al. (2000) and Lamourex et al. (2003). The maximum burning velocity is reached not for stoichiometric mixture but for a mixture with 40.1% hydrogen in air. This is due to the high molecular diffusivity of hydrogen in air (Molkov, 2012).

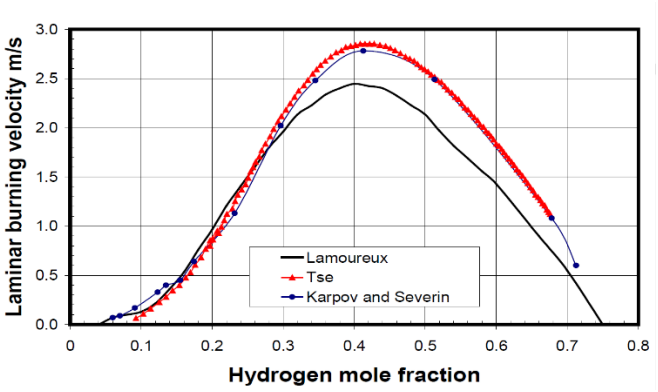

Figure 1. Laminar burning velocity of hydrogen-air mixture (Molkov, 2012).

The flame propagation velocity for a hydrogen-air mixture includes, along burning velocity, the effect of combustion products expansion. It can be calculated for one-dimensional flame propagation, e.g. in a tube from its closed end in the assumption of constant pressure, as $S = S_u E_i$, where E_i is the expansion coefficient, which is the ratio of the fresh mixture density over the one of the burnt mixture. The ratio can be as high as 7.2 for a stoichiometric mixture.

The flame propagation speed can reach a maximum given by the speed of sound of combustion products, which is 975 m/s for a stoichiometric mixture (BRHS, 2009). If the hydrogen concentration is within the range 18.3-59.0 vol %, the mixture may detonate (ISO/TR 15916:2004), leading to a worst case accident scenarios with combustion zone moving into the unburnt zone with a velocity higher than the speed of sound. Alcock et al. (2001) reported an even wider range, 11-59%. The limits depend strongly on the experimental set up dimensions and characteristics. Hydrogen detonability range is wider than for other fuels, see Table 1.

When heat losses from a flame are comparable with the heat generated by combustion (reactions in the flame), the flame can quench. Hydrogen flames are difficult to quench, and they are characterised by short quenching distances, e.g. 0.5 mm for a stoichiometric hydrogen-air mixture (Kim et al., 2001). Furthermore, conventional flame suppression systems, such as water sprays, may induce turbulence and be ineffective, because of the hydrogen-air mixture ability to burn around the water droplets. Details on the current knowledge on the effects of fire suppression systems on hydrogen fires is given in HyTunnel-CS D1.1 “Report on assessment of effectiveness of conventional safety measures in underground transportation systems and similar confined spaces”.

3. Hydrogen hazards (UU, DTU)

This chapter describes the hazards characteristic for the use of hydrogen driven vehicles in tunnels and other confined spaces. Each section describing a hazard and underlying physical phenomena specifies possible associated accident scenarios. The effect of confinement on the accident consequences will be underlined.

3.1 Hydrogen unignited releases (UU)

An unintended hydrogen release of hydrogen may be caused by either a failure of FCV equipment during an accident or unscheduled opening of the TPRD. If initially the release is unignited there is still a possibility that it will be ignited, after a certain delay, if an ignition source is present in the path of the release. If a hydrogen release occurs in confined space the consequences can be more severe compared with those from releases in the open air, as a significant flammable cloud can be build up. The consequences can endanger people, structures and environment, and they depend on the characteristics of the accident scenario and the confined space typology. The hazards associated to unignited releases are presented in the following sections, focusing on the specific hazards associated to a release in a tunnel or other confined spaces. To avoid the build-up of dangerous flammable mixture the hydrogen safety strategies and engineering tools should be applied. They include but not limited for unignited releases to reduction of release diameter (internal diameter of pipes) and pressure in supply lines, proper ventilation system accounting for potential release rate of hydrogen.

3.1.1 Oxygen depletion and asphyxiation (UU)

Hydrogen is not a poisonous gas. However, its release and accumulation in a confined space can create an oxygen-deficient atmosphere. This could lead to asphyxiation of people. Effects on human beings are noticeable for concentration of oxygen below 19%. Human response to different oxygen depletion levels is given in Table 2, along with the corresponding hydrogen concentration in normal conditions (HyResponse, 2015b). Oxygen concentration should be checked before entering the accident scene and first responders should wear a self-contained breathing apparatus. However, it must be noted that if the oxygen depletion is caused by the dilution of hydrogen in air, there is the risk of ignition of the flammable mixture.

Table 2. Human response to oxygen depletion and corresponding hydrogen concentration (conc.) in normal conditions (HyResponse, 2015b; BRHS, 2009).

H_2 conc.by vol %	O_2 conc. by vol %	Physiological effect
0-9	19-21	No specific symptoms
9-28	15-19	Decreased ability to perform tasks, possible early symptoms in persons with heart, lung or blood circulation problems
28-42	12-15	Deeper respiration, faster pulse, poor coordination
42-52	10-12	Dizziness, poor judgement, slightly-blue lips. Risk of death below 11%, tolerance time 30 min
52-62	8-10	Nausea, vomiting, unconsciousness, ashen face, fainting, mental failure, with a tolerance of 5 min
62-71	6-8	Unconsciousness in 3 min, death in 8 min. 50% death and 50% recovery with treatment in 6 min, 100% recovery with treatment in 4-5 min
71-86	3-6	Coma in 40 s, convulsions, respiration ceases, death or permanent brain damage
86-100	0-3	Death within 45 s

3.1.2 Cuts of skin and protective clothing (UU)

High-pressure hydrogen jet can cut bare skin or other tissue. The releases of pressurised hydrogen even from a small leak may penetrate a person's skin. Protective clothing may not prevent skin damage. Scott (1983) reported that gas pressurised at 20 MPa easily penetrated working gloves and clothing. At few centimetres from the leak, a pressure of 0.7 MPa is sufficient to penetrate the skin. The impact and trapping of the gas may cause stop of the blood circulation, which would lead to tissue necrosis (Cadwallader and Zhao, 2016). Pressure of 4.4 MPa is sufficient to cause incision of the skin (Brauer, 2006). This knowledge is important for first responders and applicable to both the open atmosphere and confined space accidents.

3.1.3 Cold burns (cryogenic and liquid hydrogen) (UU)

Severe cold burns can be caused to the skin or tissue when it enters in contact either with cryogenic or liquid hydrogen or with cold surfaces. In case of a prolonged exposure, the damage to the skin or tissue may result in a frostbite.

3.1.4 Hydrogen under-expanded jet releases (UU)

Onboard hydrogen storage systems operate at nominal working pressure (NWP) up to 700 bar. In real life it can be up to 1.25 of NWP and even higher in fire conditions. A release at such a high pressure originates an under-expanded jet. At the nozzle exit, velocity is sonic, and pressure is higher than the atmospheric one. Immediately downstream the nozzle exit the jet expands to the atmospheric pressure through a complex shock structure. The critical pressure ratio between sub-sonic and sonic flow regimes at the nozzle is 1.9 for STP and conditions of no losses in the release tube. It is calculated as $P_R/P_N = ((\gamma+1)/2)^{\gamma/(\gamma-1)}$, where P_R and P_N are the pressures in the storage vessel and at the nozzle, respectively, and γ is the specific heats ratio. Thus, the simple rule to rudely evaluate pressure at the nozzle exit is to divide storage pressure by 1.9, i.e. it is about half of the storage pressure.

Since pressure at the nozzle exit is higher than ambient, the gas must expand outside the nozzle, forming a series of shock waves while reaching the atmospheric pressure. Several theories have been developed to simplify the expansion process for engineering calculations of the release rate and characteristics. Previous approaches are described in the following papers. Birch et al. (1984) described the gas behaviour and concentration decay through an expanded jet originated by a corresponding source, called pseudo-diameter or notional nozzle, with section equal to the area occupied by the mass flow rate released from the real nozzle with uniform sonic velocity at ambient temperature and pressure. The scheme of the under-expanded jet and the related nomenclature are given in Figure 2. The notional nozzle model was based on the conservation of momentum in the expansion region (Birch et al., 1987). Whilst previous studies described the gas behaviour as ideal, Schefer et al. (2007) used a similar to Birch et al. (1987) approach but introduced the Abel-Noble equation of state for real gas to take account of the non-ideal behaviour of hydrogen given the high storage pressure.

The under-expanded jet theory by Molkov et al. (2009) also employed the Abel-Noble equation of state. The flow at the actual nozzle is chocked as in previous theories. Then, the flow undergoes an isentropic expansion from the nozzle exit to the notional nozzle exit, where ambient pressure and uniform velocity equal to the local speed of sound are reached. The system of equations to evaluate the flow characteristics is closed by the conservation of mass and conservation of energy equations. A complete description of the model is available from

the referred publication. The difference with previous theories is in the use of energy conservation instead of momentum conservation equation with chocked flow at the notional nozzle exit. The last assumption is reasonable having in mind huge non-uniformity of flow velocity behind the Mach disk. The previous theories based on the momentum conservation equation end up with velocity at the notional nozzle higher than the local speed of sound. This creates additional difficulties at using parameters at the notional nozzle for CFD simulations of high-pressure jet dispersion.

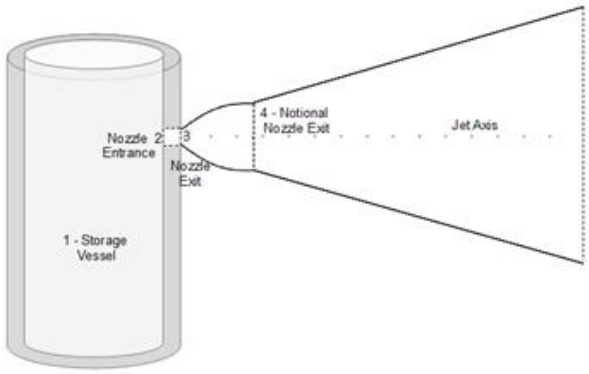

Figure 2. The under-expanded jet scheme.

3.1.4.1 Blowdown of hydrogen storage tank (UU)

The European Regulations on type-approval of hydrogen vehicles require TPRD to be installed on hydrogen onboard tanks to release its content in a fire event and therefore prevent the catastrophic consequences of tank rupture. When a blowdown of hydrogen through TPRD is initiated, temperature inside the tank decreases due to gas expansion and increases due to heat transfer through the tank wall (two competing processes). The heat transfer through the tank wall and the wall degradation are affected by these two competing processes. The wall degradation front propagation slows down in conditions of blowdown compared to the case of closed vessel (Dadashzadeh et al., 2017). The use of larger TPRD diameter could cause serious issues, especially in confined space. These issues include the pressure peaking phenomenon, that could demolish the structure with insufficient vent area by overpressure, and long jet fires, which could affect behaviour in a fire and load bearing capability of elements of underground construction elements. They are presented in detail in sections 3.1.5 and 3.2.2, respectively.

Inherently safer design of a tank-TPRD system is a challenging task with various parameters and processes involved, including tank volume, storage pressure, TPRD release diameter, TPRD initiating time, conductive heat transfer through the wall, convective heat transfer from the ambience/fire to the wall and from the wall to the gas inside the tank, wall material degradation due to the fire, etc. Experimental parametric study of these phenomena is an expensive task, if possible at all. Computational Fluid Dynamics (CFD) is an alternative contemporary method to essentially decrease or even avoid the expensive experiments. However, CFD simulations are not time efficient (Bourgeois et al., 2015).

To predict the pressure and temperature change inside a pressurised tank during a blowdown, the under-expanded jet theory was developed by Molkov et al. (2009) and will be expanded in this project. The theory is based on Abel-Nobel equation of real gas state, mass and total energy conservation equations. The theory performance was compared against blowdown

experiments. However, this theory didn't include heat transfer through the wall. Thus, the comparison with experiments was limited to only two idealised cases: adiabatic discharge (no heat transfer through the wall) and discharge under the constant gas temperature conditions. The effect of various heat transfer boundary conditions on the blowdown dynamic was investigated by (Schefer et al., 2007). It was concluded that the heat transfer due to ambience/fire plays a significant role during the blowdown.

The application of under-expanded jet theory by Molkov et al. (2009) to blowdown phenomenon was further developed by Dadashzadeh et al. (2017) to account for the conductive heat transfer through the tank wall caused by the convective heat transfer at the external side of the wall (either ambient conditions or fire) and the convective heat transfer at the internal side of the tank wall between the gas and the wall plus conductive heat transfer through the wall with a phase change (degradation). The TPRD release orifice size and its activation time are taken into consideration as free not predetermined parameters. Figure 3 shows schematically a tank and the problem formulation for heat transfer.

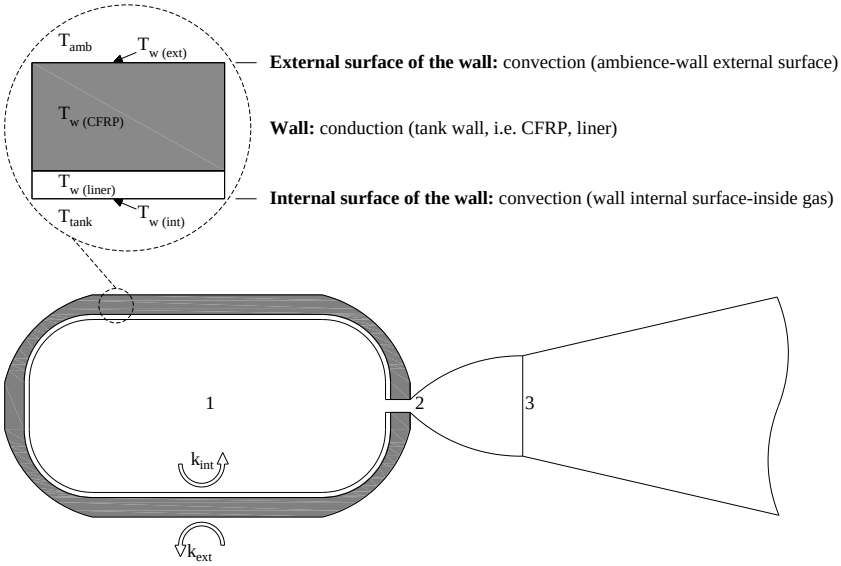

Figure 3. Schematic diagram of a pressurised tank: (1) internal tank space with gas, (2) actual nozzle exit of TPRD, (3) notional nozzle exit.

The modified by heat transfer non-adiabatic under-expanded jet theory (Molkov et al., 2009) is used now to calculate hydrogen parameters at the TPRD exit and at the notional nozzle exit. Conductive heat transfer through the tank wall is calculated by exploiting one dimensional unsteady heat transfer equation using the finite-difference method (Patankar, 1980). To calculate the heat transfer coefficient for the natural and forced convection, Nusselt number correlations are applied (Woodfield et al., 2008). The non-adiabatic blowdown model of Dadashzadeh et al. (2017) can calculate pressure and temperature dynamics inside a tank for arbitrary conditions. Figure 4 demonstrates the measured and calculated pressure (Figure 4a) and temperature (Figure 4b) for both the adiabatic blowdown model and the non-adiabatic blowdown model. The simulated gas pressure with non-adiabatic blowdown model (Dadashzadeh et al., 2017) is in an excellent agreement with the experiment (Figure 4a). It is more accurate compared to the adiabatic model (Molkov et al., 2009) even if its prediction of pressure dynamics during blowdown is not bad. However, the performance of these two versions of the model in the prediction of temperature differs drastically. The non-adiabatic

model prediction of gas temperature inside the tank is accurate (Figure 4b) within 6% deviation from measured values. The former adiabatic model is not able to predict the temperature performance with characteristic minimum. Instead, as expected the temperature decreases monotonically when the adiabatic blowdown model is applied.

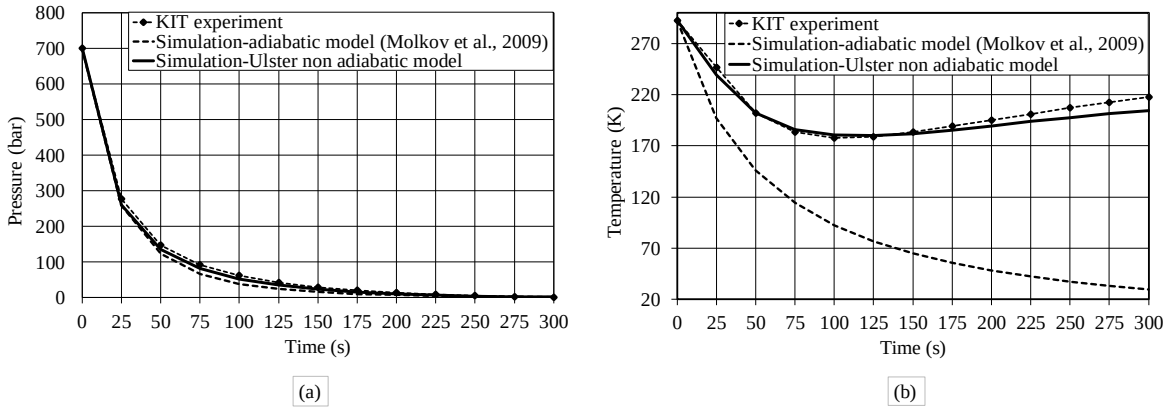

Figure 4. Simulations versus experimental data for the adiabatic blowdown model (Molkov et al., 2009) and the non-adiabatic blowdown model (Dadashzadeh et al., 2017): (a) pressure inside the tank; (b) gas temperature inside the tank.

The non-adiabatic blowdown model allows to calculate accurately hydrogen parameters during the whole process of release. Thus, it should be integrated into analytical models and numerical models to accurately predict, e.g. the effectiveness of ventilation systems in underground facilities when hydrogen release conditions are changing. Furthermore, the non-adiabatic blowdown model should be further developed and validated to include different conditions surrounding a storage tank, e.g. fire. Indeed, it is not yet clear, depending on the time of TPRD initiation after the fire starts to affect the high-pressure tank, what is TPRD exit diameter which will guarantee the release of hydrogen from the tank without its rupture in a fire (rupture is not excluded if time of initiation is comparatively large and release diameter is comparatively small). The project will look for prevention or mitigation technology to exclude tank rupture in a fire with devastating consequences aggravated by confinement of the tunnel and similar confined spaces.

3.1.5 Pressure Peaking Phenomenon (UU, USN)

The information on the pressure peaking phenomenon can be found in the book by Molkov (2012) and recent publications of Ulster University. In vehicles hydrogen is most commonly stored today as a compressed gas in tanks which are required by the Commission Regulation (EU) No 406/2010, to be equipped with pressure relief devices (PRDs), which is usually TPRD. The TPRD is fitted to the fuel tank and starts to release hydrogen when a temperature of about 110^{o}C is reached, e.g. in fire conditions. The TPRD can provide rapid release of hydrogen if a large orifice diameter is used, thus minimising the possibility of tank explosion during too long exposure to fire. High mass flow rates from a TPRD are probably “acceptable” outdoors. However, the hazards resulting from a rapid release in room-like enclosures, e.g. garages and maintenance shops, are different and cannot be accepted to provide life safety and property protection.

Let us consider a hypothetical scenario involving a release from a typical onboard hydrogen storage tank at 35 MPa, through a 5.08 mm diameter orifice, representing a “typical” PRD

(Brennan et al., 2010). The release is assumed to occur vertically upward in the centre, 0.5 m above the floor, of a small garage of size LxWxH=4.5x2.6x2.6 m (SAE J2579, 2009) and volume of 30.4 m^3 with a single vent equivalent in area to a typical brick LxH=25x5 cm located close to the ceiling. A conservative approach is taken, i.e. a constant mass flow rate of 390 g/s is applied (ignoring a pressure drop in the storage tank) after the TPRD opening.

The study (Brennan and Molkov, 2013) describes the pressure peaking phenomenon model accounting either a constant mass flow rate or blowdown. The systems of equations provided by the authors was used to calculate the transient pressure load in the vented enclosure and scenario described above and it is given in Figure 5. It can be observed how the overpressure within the enclosure resulting from the injection of hydrogen reaches a level above 10 kPa, capable of rupturing the garage (Baker et al., 1983), within only 1 s. Evacuation of people in this time is impossible and this life safety issue has to be yet addressed by car manufacturers. There is only one engineering solution that is the reduction of mass flow rate from TPRD, i.e. reduction of release diameter (pressure cannot be reduced to keep driving range competitive to todays fossil fuel vehicles). This in turn will require higher fire resistance level of onboard storage tanks compared to current 3.5-6.5 minutes for type 4 vessels (Stephenson, 2005).

If the garage would not be destroyed by overpressure first, the overpressure within the garage, for the scenario under consideration, would reach a peak in excess of 50 kPa. This maximum pressure then drops off and tends towards a steady state value, considerably lower, and equal to that predicted by the simple steady state orifice equations. It should be noted that this represents a worst-case scenario with constant mass flow rate. Therefore, continuation of a constant mass flow rate release for 60 s included in Figure 5 is to illustrate the time frame before steady state conditions are reached when the garage is occupied by 100% of hydrogen.

In this case, the maximum pressure is reached in less than 10 s. Within this time the entire garage would be destroyed with missiles flying around and creating more damage and life threat. These are consequences of pressure build up without even considering the ignition of released hydrogen. The pressure peaking effect of unignited and ignited hydrogen releases in vented enclosure is a new (specific only for hydrogen) aspect of safety provisions for hydrogen use in confined areas. Hydrogen safety engineers and manufacturers of hydrogen and fuel cell systems must address this issue as required by the international standard ISO 19882 “Gaseous hydrogen – Thermally activated pressure relief devices for compressed hydrogen vehicle fuel containers”. It states: “The adequacy of flow capacity of pressure relief devices for a given application is to be demonstrated by bonfire testing in accordance with ISO 19881, ANSI HGV 2, CSA B51 Part 2, EC79/EU406, SAE J2579, or the UN GTR No. 13 for fuel cell vehicles and by the minimization of the hazardous effects of **the pressure peaking phenomenon** which could take place during high flow rate releases from small diameter vents in enclosed spaces”.

Figure 5 illustrates as well the predicted overpressure versus time for a range of fuels with different molecular mass and the same mass flow rate of 390 g/s at the same garage (with discharge coefficient C=0.6): hydrogen, methane, propane with the molecular masses of 2, 16 and 44 g/mol, respectively. It is clearly showed how the maximum overpressure drops with increasing molecular mass. There is a small pressure peak for methane release as its molecular mass is below that of air. The pressure peaking phenomenon is absent for propane as its molecular mass is higher than air. Instead, the pressure generated by release of hydrogen into the vented enclosure is growing monotonically to reach the maximum and then decreases to a

steady state value, when only hydrogen flows out of the enclosure through the vent(s). The phenomenon must be taken into account when designing TPRDs for the use with different gases for indoor applications. Indeed, the same TPRD used for CNG or LPG should not be assumed to behave in the same way for hydrogen.

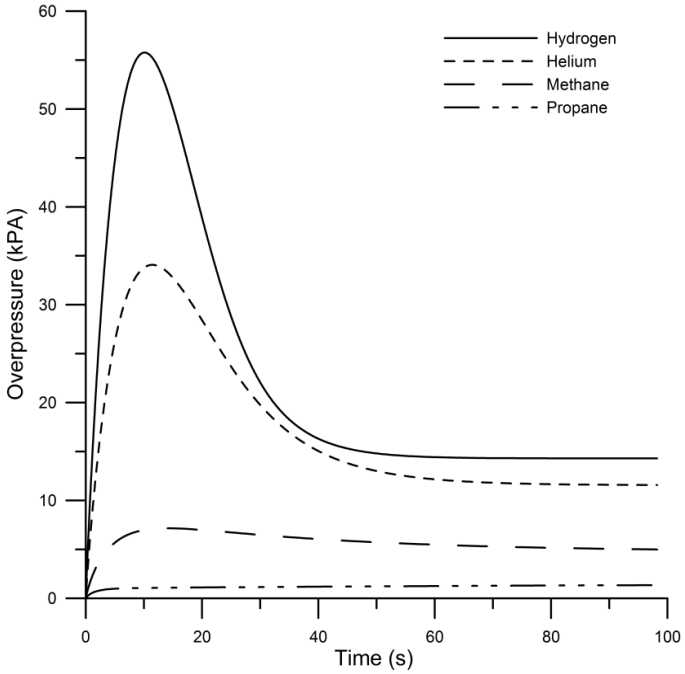

Figure 5. Pressure peaking phenomenon for release of hydrogen with mass flow rate 390 g/s into the enclosure of 30.4 m^3 with a vent of typical brick size 25x5 cm compared with pressure dynamics for releases of helium, methane and propane at the same conditions (Brennan and Molkov, 2018).

A concise description of the phenomenon proposed in (Brennan and Molkov, 2013, 2018) is attempted below. For a given volume and temperature, the pressure in the compartment is dependent on the number of molecules in the volume. Assuming the flow out of the compartment is incompressible, a model for the pressure in the compartment can be derived from a molar balance. Figure 6 shows the schematic of the scenario associated to the model. Two flow rates are competing: 1) hydrogen release from the vehicle, $\dot{m}_{nozz}$, and 2) the flow rate of gas out of the vent, m_{vent}.

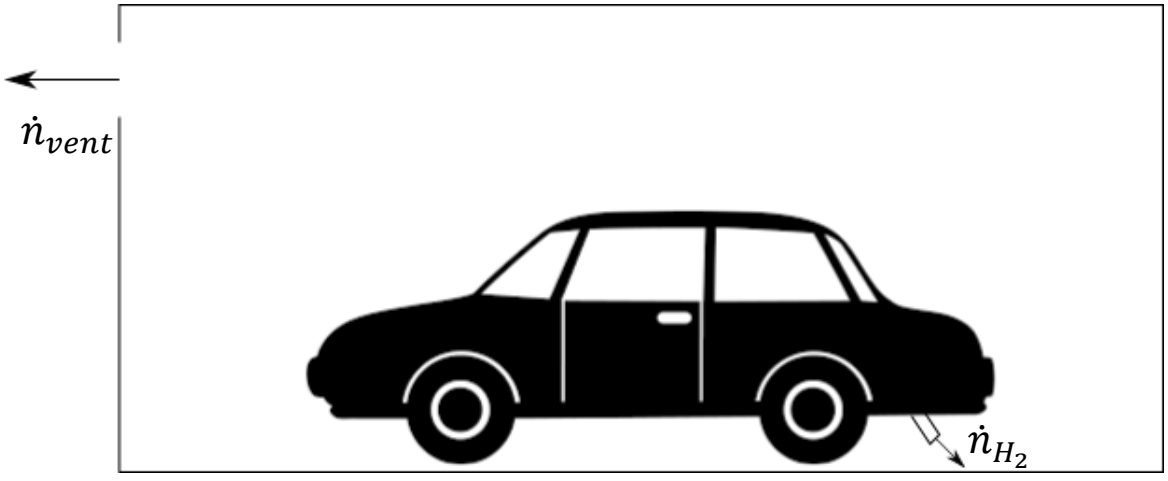

Figure 6. Schematic of the pressure peaking phenomena with a vented garage and hydrogen release from a car.

The system of equations to predict the overpressure dynamics in the assumption of perfect mixing (n – number of moles) is shown below:

$$m_{encl}^{t+\Delta t} = m_{encl}^{t} + (\dot{m}_{nozz}^{t} - \dot{m}_{vent}^{t})\Delta t \tag{3.1}$$

$$n_{encl}^{t+\Delta t} = n_{encl}^{t} + \left(\frac{\dot{m}_{nozz}^{t}}{M_{H_2}} - \frac{\dot{m}_{vent}^{t} n_{encl}^{t}}{m_{encl}^{t}}\right)\Delta t \tag{3.2}$$

$$P_{encl}^{t+\Delta t} = \frac{n_{encl}^{t+\Delta t} RT}{V} \tag{3.3}$$

$$\dot{m}_{vent}^{t+\Delta t} = CA \cdot \left(\frac{m_{encl}^{t+\Delta t}}{V}\right) \cdot \left(\frac{2(P_{encl}^{t+\Delta t} - P_S)V}{m_{encl}^{t+\Delta t}}\right)^{1/2} \tag{3.4}$$

Assuming the flow as incompressible, the volume flow rate out of the vent can be written as:

$$V_{vent} = CA\left\{\left(\frac{2\gamma}{\gamma-1}\right)\frac{P_S}{\rho_{encl}}\left[\left(\frac{P_S}{P_{encl}}\right)^{\frac{2}{\gamma}} - \left(\frac{P_S}{P_{encl}}\right)^{\frac{\gamma+1}{\gamma}}\right]\right\}^{\frac{1}{2}} \tag{3.5}$$

where A is the actual vent area, C is the discharge coefficient, M_{H2} is the molecular weight of vented gas, P_{encl} is the pressure in compartment, P_S is the pressure outside compartment, $\dot{m}_{nozz}$ is the mass flow rate of hydrogen into compartment, $\dot{m}_{vent}$ is the molar flow of gas out of compartment, n_{encl} is the number moles of gas in compartment. If one assumes perfect mixing in the compartment, the density and molecular weight of the vented gas is the same as the mean density and molecular weight inside the compartment. At the beginning of the hydrogen release, density in the enclosure is high due to the large fraction of air present. This leads to a low volumetric flow rate out of the vent, as shown in eq. (3.5). The hydrogen inflow into the enclosure is larger than the outflow through the vent causing the pressure build-up. As the release proceeds further, the hydrogen fraction in the enclosure increases, causing a decrease in density. As a consequence, the volumetric flow rate through the vent increases, leading to the drop in pressure.

Release rates as low as 10 g/s may produce significant overpressure effect according to the enclosure and vent dimensions. Figure 7 shows the pressure peaking dynamics for a 40 m^3 garage with a small vent of 1x10 cm and a constant release of hydrogen of 10 g/s.

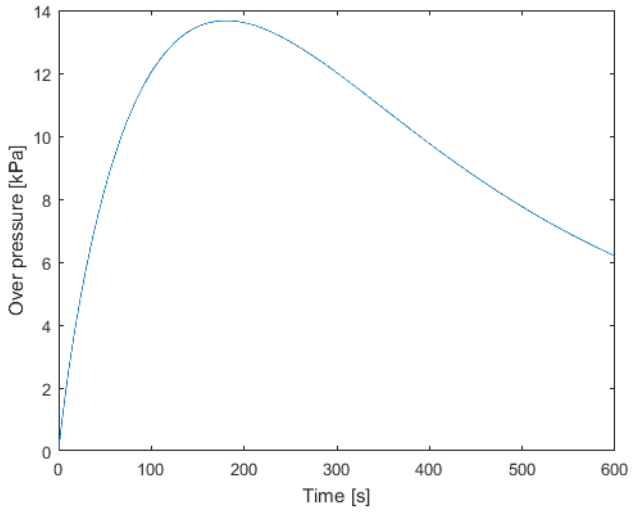

Figure 7.Overpressure in a 40 m^3 compartment with 1x10 cm vent and 10 g/s release of hydrogen.

Validation of the model has been done by (Makarov et al., 2018b) for experiments conducted in a 1 m^3 enclosure and release rates up to 1 g/s at Karlsruhe Institute for Technology. It was achieved a good agreement between model predictions and experimental results. Discrepancies when present were due to the "breathing" effect of the small-scale enclosures. It was observed that for pressures above 1 kPa additional opening areas could form on the structure of experimental chamber, leaking the mixture and decreasing the overall pressure. Additional experimental work, where the "breathing" effect is negligible, is needed to further consolidate the validation of the model. Real-scale garage-like enclosures shall be used to increase the validation domain for PPP tools (the engineering tools are available at https://elab-prod.iket.kit.edu, login: **HyTunnel**, password: **Safety2019**).

Figure 8 shows the simulated pressure dynamics in the garage for two constant hydrogen release rates and four vent sizes equivalent to 1, 2, 3 or 4 bricks using the PPP theory for unignited releases (Brennan et al., 2010; Brennan and Molkov, 2013) and a typical discharge coefficient value: C_D=0.6 for sharp-edged orifice. The pressure transients have a notable pressure peak for each vent size. The peak terminates with a transition to steady-state pressure. For release rate 388 g/s (Figure 8, left), in all but one scenario the pressure peak is above the critical pressure which could be withstood by civil structures like garages, i.e. 10-20 kPa. Only in a scenario with vent area equal to 4 bricks, the pressure peak was below the threshold of 10 kPa, which civil structures can withstand. The larger the vent area the earlier the maximum pressure is achieved. The pressure peak decreases with the increase of vent area. It is worth noting that in many cases the presence of door(s), which fails at overpressures 5.3-9 kPa, and window(s), which glass in 90% of cases breaks at overpressures as low as 3.7 kPa (Mannan, 2005), if available, could mitigate the pressure peaking phenomenon.

Figure 8 (right) shows the pressure dynamics in the four scenarios following the release from a tank with twice higher storage pressure (70 MPa) but 2.5 times smaller TPRD diameter (2 mm). The overpressure with the vent of one brick size is just over the threshold of 10 kPa. For other three scenarios with unignited release and larger vent area, the peak overpressure is significantly below the 10 kPa threshold. Pressure peaks are even below 3.7 kPa threshold, i.e. there is a high probability that even glassing will not be broken.

Figure 8 demonstrates that the unignited (!) hydrogen release from TPRD of 2 mm diameter at storage pressure of 70 MPa will not destroy the garage even if a vent area is equal to only one brick. Thus, we can state that the TPRD diameter is the main parameter affecting the PPP in real life conditions. The reduction of TPRD diameter from 5.08 mm to 2 mm was sufficient in our example to prevent PPP for unignited (!) release, even if the storage pressure increased twice from 35 MPa to 70 MPa. **Unfortunately**, this is not the case for ignited release (jet fire) from the same source as will be demonstrated in section 3.2.4.1.

The pressure peaking phenomenon, i.e. existence of maximum pressure peak that is above the steady state value, during a release of lighter than air gas into vented enclosure should be accounted for when performing safety engineering for use of hydrogen vehicles in confined spaces like garages, maintenance shops and similar enclosures. Overall the conclusion is drawn that TPRDs currently available for hydrogen-powered vehicles should be redesigned, along with the increase of fire resistance rating of onboard hydrogen storage tanks (or use of explosion-free in a fire tanks), and RCS updated if the vehicle is intended for parking in garage, etc.

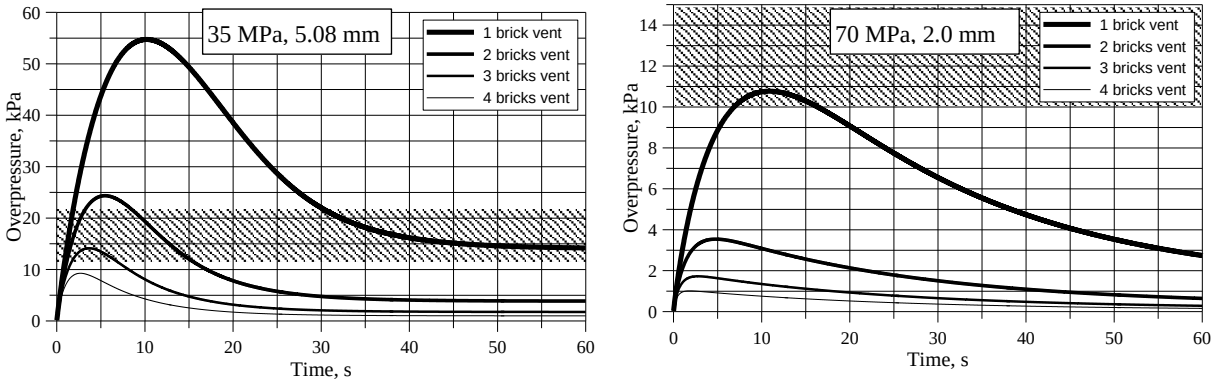

Figure 8. Overpressure dynamics of unignited hydrogen release in the garage for two cases: left - TPRD diameter 5.08 mm, storage pressure 35 MPa (hydrogen release rate of 388 g/s); right - TPRD diameter 2.0 mm, storage pressure 70 MPa (release rate of 107 g/s) (Makarov et al., 2018b).

3.1.6 Formation of a flammable cloud (NCSRD)

An unintended unignited hydrogen release would cause the formation of a flammable cloud. The size and the duration of the flammable cloud depend on several factors, such as the release diameter, pressure and duration, the presence or not of obstacles, the wind intensity, etc. The risks and the hazards can be increased in case of a release inside confined spaces, such as tunnels, if dispersion below LFL is not provided in a system vehicle-tunnel.

Hydrogen release in enclosed spaces can be categorized as follows: release in fully closed space and release in semi-confined space with openings (vents) for natural or forced ventilation. In both categories different hydrogen distribution regimes can be formed dependent on the release rate. In the second category the vent size is an essential factor that influences the gas distribution regimes and their characteristics, such as the maximum concentration in the enclosure.

The next subsections present in detail the release, hydrogen concentration decay in expanded and under-expanded jets, and accumulation of hydrogen inside confined ventilated space and effects of several factors on formation and size of a flammable cloud.

3.1.6.1 Hydrogen concentration decay along jet axis (UU)

Unscheduled hydrogen release from a high-pressure equipment and/or infrastructure will create a highly under-expanded jet. This could lead to formation of a large flammable hydrogen-air envelope which size if proportional to the release nozzle diameter. The size of the flammable envelope is the hazard distance from the release source. Indeed, if the flammable envelope (hydrogen concentration in air equal to the lower flammability limit of 4% by volume) reaches a location of air intake into high-rise buildings, then consequences for occupants and building structure can be catastrophic. It is worth mentioning here that while quiescent 4% hydrogen mixture in air will propagate flame only upward, the turbulent mixture could burn completely with generation of pressure in closed space enough to destroy any civil structure.

Presence of ignition source within the envelope could initiate severe jet fires, deflagration, and potentially deflagration-to-detonation transition. It must be noted that thermal effects of jet fires, pressure effects of deflagration or detonation, fireball size and blast wave after high-pressure hydrogen tank rupture in a fire could override the separation distance determined by the size of flammable envelope. Thus, knowledge of laws describing hydrogen dispersion and

flammable cloud formation, including axial concentration decay, for arbitrary jets with various parameters is essential for reliable hydrogen safety engineering.

The similarity law for concentration decay along the axis of the momentum-controlled jets is shown in Figure 9 along with experimental data for hydrogen under-expanded releases. It is based on the hypothesis of using the original form of the similarity law by (Chen and Rodi, 1980) along with the use of the under-expanded jet theory for calculation of hydrogen density at the nozzle exit (Molkov, 2009). Experimental data on pure hydrogen momentum-controlled subsonic, sonic and supersonic jets were used for validation, involving releases from vessels of different volume pressurized up to 40 MPa, and through nozzles with diameter from 0.25 mm to 100 mm. Hydrogen concentration in air was measured in the range from 1% to 86.6% by volume. Only 60 of total 302 experimental points in the momentum-controlled regime are presented in Figure 9 to avoid overlapping of data on the graph (Molkov et al., 2010). These 60 points are the maximum and minimum values of each experiment and in some cases an additional intermediate value. It is worth noting that cold jets with initial storage gas temperature down to 50 K (Cirrone et al., 2019d) obey the similarity law also.

Figure 9 shows that all the experimental points are on or below the similarity law line. This is thought due to friction and minor losses in experimental equipment, which were not accounted for when the under-expanded jet theory without losses (Molkov et al., 2009) was applied. Indeed, from the similarity law equation it follows that losses decrease pressure at the nozzle exit, reducing hydrogen density and concentration in the jet for a fixed distance from the nozzle. This is equivalent to shifting experimental points down on the graph. If the spouting pressure (actual nozzle exit pressure) is applied instead of the pressure in a storage tank the difference between the similarity law curve and experimental data would reduce to zero in the limit. The universal character of the similarity law for both expanded and under-expanded jets makes it an efficient tool for hydrogen safety engineering.

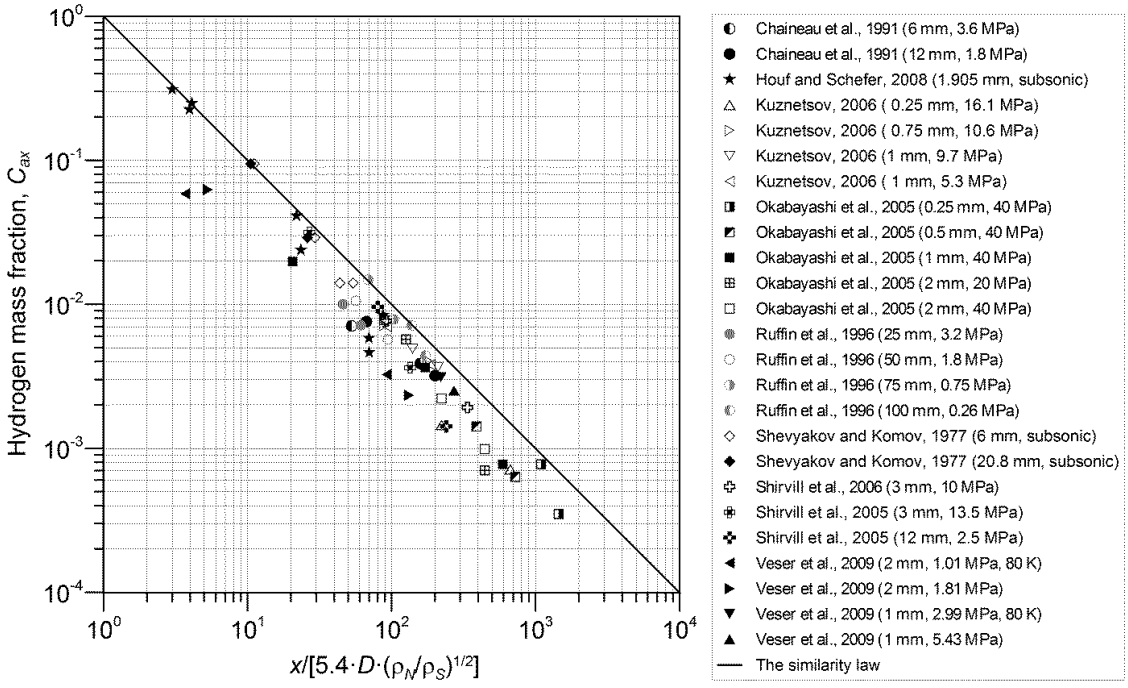

Figure 9. The similarity law (solid line) and experimental data on axial concentration decay in momentum-controlled expanded and under-expanded hydrogen jets (Molkov et al., 2010).

3.1.6.2 Effect of buoyancy on unignited jet hazard distances (NCSRD, UU)

Section 2.1.1 discussed hydrogen buoyancy as a unique safety asset. The identification of the buoyancy effects in unintended hydrogen releases is important to determine the proper hazard distance and to design first responders' intervention strategy and tactics. All jets can be divided into three types based on the effect of buoyancy: momentum-dominant jets, buoyancy-dominant jets and transitional jets. These jet types are showed schematically in Figure 10 for a *horizonta*l jet. Fully momentum-controlled jets are not affected by buoyancy. Fully buoyancy-controlled jets are quickly diverted from the horizontal to vertical flow direction. Transitional jets have a momentum-dominated part closer to the nozzle and buoyancy-controlled flow further downstream when jet velocity drops and jet diameter increases. For hydrogen safety engineering it is important to know when this transition takes place to define more accurately horizontal hazard distance from the release. This has direct implication on the separation distance, thus safety and costs of hydrogen system and/or infrastructure. It is obvious that buoyant-dominant jets decrease the horizontal hazard distances. The buoyance excludes accumulation of flammable cloud near the ground where there are higher risks for ignition sources and human presence.

In *vertical* jets, the effect of buoyancy is to increase the centreline decay rate (Schefer et al., 2008). The faster decay rate in buoyant jets is attributed to the enhanced mixing between hydrogen and ambient air. Thus, there are lower centreline concentrations at the same location downwind the nozzle in buoyant jets compared to momentum-dominant jets, i.e. the hazard distances are smaller in jets where buoyancy dominates.

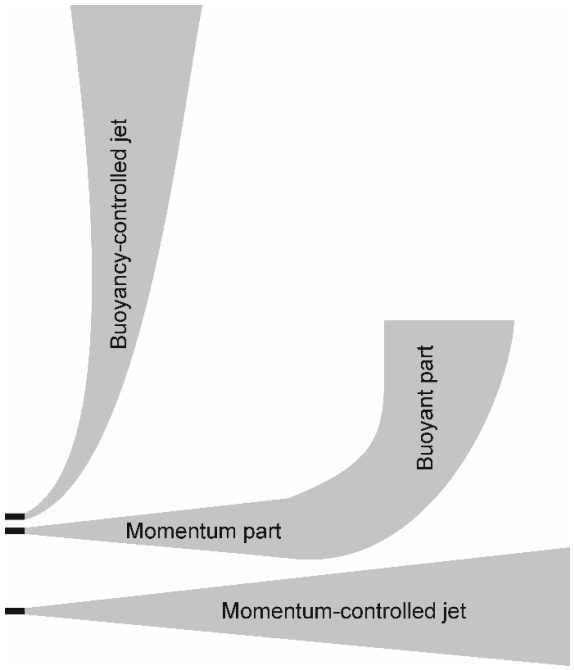

Figure 10. Fully momentum-controlled jet (bottom), transitional jet (middle), and fully buoyancy-controlled jet (top) (Molkov, 2012).

The engineering technique presented here to qualify a hydrogen jet (both expanded and under-expanded) or its part as momentum-controlled, and the rest of the jet downstream as buoyancy-controlled, is based on the work (Shevyakov et al., 1980; Shevyakov and Savelyeva, 2004) that was carried out with expanded jets only. Figure 11 shows in logarithmic coordinates the

dependence of the distance to nozzle diameter ratio *x/D* (ordinate) for a particular concentration of hydrogen in air on the Froude number (abscissa) in its classical form:

$$Fr = \frac{U^2}{gD}, \tag{3.6}$$

where *U* is the velocity at the nozzle exit (notional nozzle exit for under-expanded jets) in m/s, *g* is the gravitational acceleration (standard acceleration of gravity on Earth is 9.80665 m/s^2), and *D* is the nozzle diameter (notional nozzle exit diameter for under-expanded jet) in meters. High Froude number (Fr>1000) indicates momentum-dominant jets, low Froude number (Fr<10) indicates buoyant-dominant jets and intermediate values (10<Fr<1000) stand for transitional jets. Buoyancy effects are present on both horizontal and vertical jets, with the first to underlie greater influence on hazard distances.

For under-expanded jets in Figure 11 the notional nozzle exit diameter and velocity at the notional nozzle exit were calculated by the under-expanded jet theory (Molkov et al., 2009). Both expanded and under-expanded jets obey the same functional dependence with accuracy 20% acceptable for engineering applications.

Practically all under-expanded jets in hydrogen incidents/accidents will be in the momentum-controlled regime as follows from available tests applied to validate the correlation in Figure 11. Four of five theoretical curves in the graph are related to hydrogen concentrations of 4%, 17%, 30%, and 60% by volume respectively. Each of these four curves has an ascending buoyant part and a momentum "plateau" part.

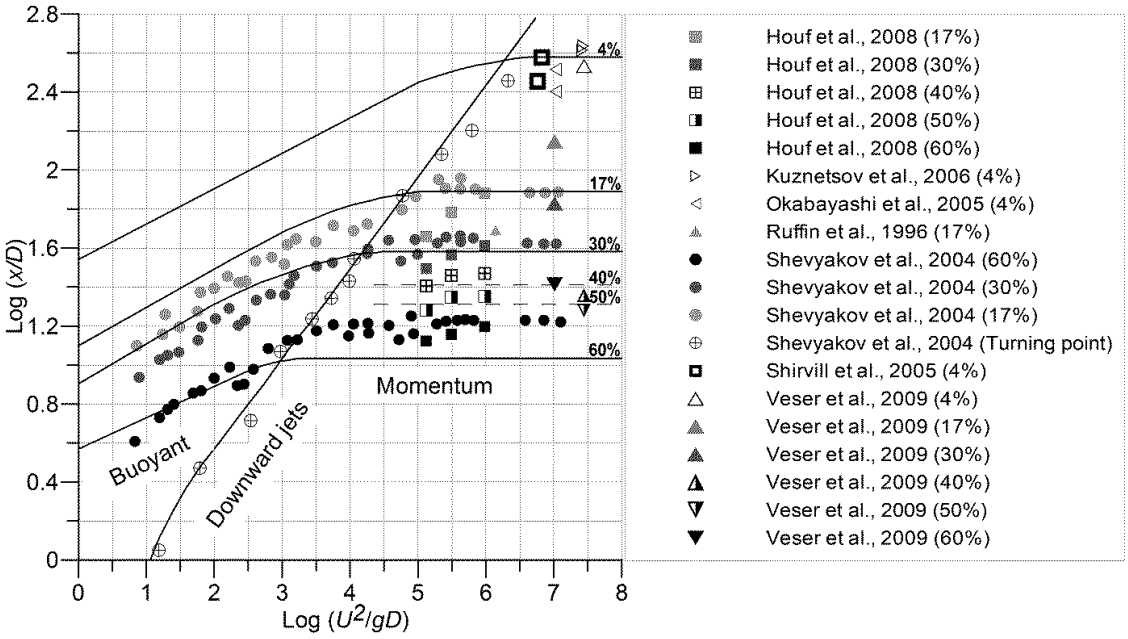

Figure 11. The dependence of the distance to nozzle diameter ratio for particular concentration of hydrogen in air on the Froude number (Molkov et al., 2010).

Firstly, the nozzle exit Froude number is calculated and its logarithm. The under-expanded theory is applied to calculate the notional nozzle exit diameter and the velocity in the notional nozzle exit when applicable. Then, a vertical line is drawn upward from a point on the abscissa axis equal to the calculated Froude number logarithm. The intersection of this vertical line with

the line marked "Downward jets" on the graph indicates the concentration above which the jet is momentum-dominated and below which the jet is buoyancy-controlled.

For example, if a jet is characterised by a *Log* (*Fr*)=4.25 then the jet is in momentum-dominated regime for concentration in the jet above 30% by volume, signalled by the intersection of the vertical line with line "Downward jets". The jet becomes buoyant further downstream of the axial concentration of 30% by vol.

This technique is quite simple to apply and at the same time can be very useful to develop cost-effective hydrogen safety solutions. For instance, the hazard distance for a horizontal jet release can be essentially reduced as only a length of the momentum-dominated part of the jet can be taken as an indication of the hazard distance rather than aggregated (both momentum- and buoyancy-controlled parts of the jet) distance to 4% by volume (LFL).

To sum up, buoyancy effects on unignited jet hazard distances are generally positive by reducing their horizontal length, which is desirable from the safety point of view. However, the vertical hazard distances are increased, and attention should be given to the upper part of the closed and semi-closed spaces and to the design of the ventilation and security systems.

3.1.6.3 Accumulation of hydrogen in a fully closed space (NCSRD)

In case of accidental hydrogen release its buoyant nature would force the flammable cloud to move upwards. In closed spaces hydrogen reaches the ceiling and then spreads to the sidewalls and then descends. Depending on the volumetric Richardson number, three different distribution regimes can be identified in fully closed space (Cleaver et al., 1994), (Cariteau & Tkatschenko, 2012). Decreasing the Richardson's value one can observe stratified, stratified with a homogenous layer and homogeneous mixture inside the enclosure. The volumetric Richardson number is given by:

$$R_{iv} = g\frac{\rho_a - \rho_0}{\rho_0}\frac{V^{1/3}}{u_0^2} \tag{3.7}$$

where g is the gravitational acceleration, ρ_a is the air density, ρ_0 is the hydrogen density, V is the volume of the enclosure and u_0 is the average injection velocity.

For low volumetric Richardson number ($R_{iv} < 3.2 \cdot 10^{-3}$) the initial injected momentum is very high. As a result, the upper layer descends almost until the bottom of the enclosure and a homogeneous layer of height equal to the height of the enclosure is formed. This regime is a limit case of the next regime. The given critical Richardson value is an average and it increases for decreasing hydrogen volume fraction at the injection (Cariteau & Tkatschenko, 2012).

For $3.2 \cdot 10^{-3} < R_{iv} < 3$, a homogeneous layer is formed in the upper layer of the enclosure, while a more or less stratified layer is formed in the lower part of the enclosure. In such Richardson values the decrease in release rate leads to smaller gas velocity and consequently to less local mixing. However, the initial injected momentum is sufficiently large near the ceiling to generate overturning and to form a homogeneous layer in the upper part of the enclosure.

For $R_{iv} > 3$, stratification without homogenous layer is observed. This stratification regime could be linear or parabolic. In this case, the release rates are so slow that the buoyancy dominates over the jet momentum. The momentum is not sufficient for overturning at the edges of the ceiling. Figure 12 illustrates the distribution regimes in closed spaces based on the value of volumetric Richardson number.

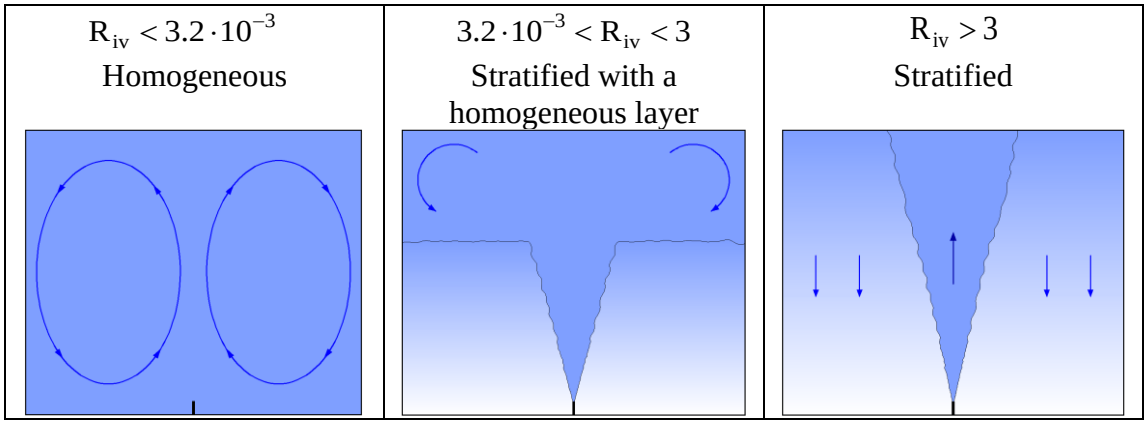

Figure 12. The different distribution regimes inside a fully closed space depending on the volumetric Richardson number (Molkov et al., 2014a).

3.1.6.4 Hydrogen concentration in semi-closed space with passive ventilation (UU)

In case of a hydrogen leak in an enclosure, it is mostly recommended to have a ventilation system aimed to prevent hydrogen concentration above 1% vol of hydrogen mole fraction based on (IEC 60079-10-1, 2015), (NFPA 2, 2011), and (ISO/DIS 19880-1, 2018), which are standards for equipment with gaseous hydrogen. Without an adequate ventilation for a confined space a flammable mixture may be formed, and an accident might occur putting lives in danger.

Enclosures may be provided with a passive ventilation system (to distinguish with natural ventilation, which is usually used to provide air quality rather than control comparatively large release rate). A theory has been developed (Molkov et al., 2014b) to calculate the hydrogen gas concentration, *X*, following a release in passively ventilated enclosure:

$$X = f(X) \cdot \left[\frac{Q_0}{C_D A (g' H)^{1/2}} \right]^{2/3}, \tag{3.8}$$

where function *f*(*X*), which defines the difference between the approximate solution for volumetric fraction of hydrogen by the natural ventilation theory and the exact solution of the problem using the passive ventilation theory, is:

$$f(X) = \left(\frac{9}{8}\right)^{1/3} \cdot \left\{ \left[1 - X \left(1 - \frac{\rho_{H_2}}{\rho_{air}} \right) \right]^{1/3} + (1 - X)^{2/3} \right\}. \tag{3.9}$$

Function *f(X)* gives the deviation of the exact solution of the problem from the approximate solution for unscheduled release of gas using natural ventilation assumptions, which are sufficient to control air quality in buildings but insufficient for calculation of ventilation parameters in a case of comparatively large release rate. Figure 13 shows the change of *f(X)* with hydrogen volumetric fraction in air (solid line) compared to *f(X)*=1 for natural ventilation

(dash line). Figure 13 demonstrates that *f(X)* can be twice more than 1 (natural ventilation value) for small volumetric fractions of hydrogen and twice less than 1 for very high volumetric fractions. This means that hydrogen concentrations predicted by equation for natural ventilation can underestimate real values twice for low and overestimate twice for very high concentrations. This misuse of ventilation theories could have serious safety implications.

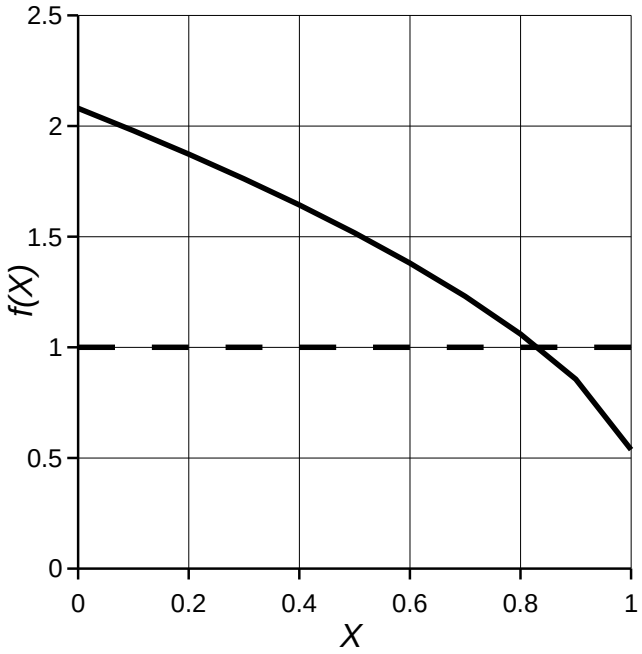

Figure 13. Function f(X) for passive ventilation (solid line) and for natural ventilation (dashed line) (Molkov et al., 2014b).

A hydrogen release from a 700 bar onboard storage in a typical car park was investigated numerically by Hussein et al. (2019). The car park had dimensions LxWxH=30x28x2.6 m. CFD simulations included a natural ventilation system as specified in the British Standards (BS 7346-7:2013). The study compared the flammable clouds (>4% H_2 by vol) formed by two releases through TPRD diameters equal to 3.34 mm and 0.5 mm. Results showed that the flammable cloud formed by release from a TPRD with diameter 3.34 mm covered large part of the car park. On the other hand, the maximum extension of the flammable cloud from a hydrogen release through a 0.5 mm TPRD reduced to ~2 m. The cloud with hydrogen concentration 1% by vol produced by the 3.34 mm TPRD enveloped the car park along all its length (30 m), whereas it reduced to a length of approximately 15 m when the 0.5 mm TPRD was employed. A further reduction of this area was observed when the release was directed downwards.

If the natural (passive in terms of this work) ventilation in areas containing hydrogen systems is not sufficient to provide air quality with hydrogen concentration below the standards requirements, a forced ventilation system is required (Cerchiara et al., 2011).

3.1.6.5 Hydrogen concentration in semi-confined space with forced ventilation (UU, NCSRD)

Based on (IEC 60079-10-1, 2015), (NFPA 2, 2011), and (ISO/DIS 19880-1, 2018) standards for equipment with gaseous hydrogen, the ventilation system must work to maintain hydrogen concentration under 1% volume of hydrogen mole fraction in the air, above this limit there should be a mechanical ventilation sensor activation.

The perfect mixing equation is the simplest that can be used to calculate air flow by forced ventilation depending on hydrogen release rate to keep hydrogen concentration below required level at steady-state conditions (constant flow rates of hydrogen from a leak and air by forced ventilation):

$$C\% = \frac{100 \cdot Qg}{Qa + Qg}, \quad (3.10)$$

where C% is the steady state gas concentration (% by volume), Qa is the air flow rate (m^3/min), and Qg is the gas leakage rate (m^3/min). The unsteady release conservative approach or CFD tools can be applied.

Besides simple equation (3.10) there are more sophisticated models and tools available to calculate parameters of forced ventilation. . In most of realistic releases hydrogen concentration in enclosure will be rather non-uniform. Thus, averaged concentration calculated by Equation (3.10) could be below the maximum concentration under the enclosure ceiling. Here it is worth mentioning that only small fraction of concentration with highest concentration defines non-uniform vented deflagration overpressure in the enclosure (Makarov et al., 2018a). A "forced ventilation" model has been built on the principles of the passive ventilation model (Molkov et al., 2014b) that calculates ventilation flow rate to provide maximum hydrogen concentration in an enclosure below the required level. An application of forced ventilation model in numerical experiments proved the validity of the approach. The engineering tool (based on this model) to calculate parameters of forced ventilation is realised within the European project "Novel Education and Training Tools based on digital Applications related to Hydrogen and Fuel Cell Technology" (NET-Tools). The project is developing a digital platform and providing online contemporary tools and information services for education and training within FCH sector, including online free access e-Laboratory with about 20 tools related to hydrogen safety. The forced ventilation tool is available at https://elab-prod.iket.kit.edu (login: **HyTunnel**, password: **Safety2019**) and it calculates parameters of the forced (mechanical) ventilation system to keep hydrogen concentration below a required level. The parameters include the volume flow rate of air which is needed for the given mass flow rate of hydrogen to keep hydrogen concentration lower than specified threshold in the assumption of perfect mixing.

The comparison of hydrogen concentration calculated by the perfect mixing equation and the "forced ventilation" model is shown in Table 3 for hydrogen release 1 g/s. The perfect mixing equation, which gives an average concentration of hydrogen in the volume underpredicts the maximum concentration calculated by e-Laboratory by 38%. It can be seen that for 1 g/s of hydrogen release and ventilation rate 28.61 m^3/min the predicted concentration is 4% for e-Laboratory and 2.45% for perfect mixing equation. Thus, more experimental validation of existent models for assessment of forced ventilation parameters is required.

Table 3. Comparison between e-Laboratory and perfect mixing equation results.

H_2 mass flow rate (g/s)	1.00
H_2 volumetric flow rate for Eq (3.10), Qg (m^3/min)	0.72
Air volumetric flow rate (m^3/s)	0.48
Air volumetric flow rate for Eq (3.10), Qa (m^3/min)	28.62
Hydrogen concentration: e-Laboratory (based on passive ventilation), %	**4.00**
Hydrogen concentration: perfect mixing equation (3.10), %	**2.45**

The effect of ventilation on hydrogen dispersion in closed spaces has been examined through several numerical studies. Choi et al. (2013) performed CFD simulations in an underground parking garage. Ventilation rates equal to 20, 30 and 60 m^3/min were examined. They observed that the volume of the flammable cloud decreases significantly in the cases of ventilation. However, no differences between the different ventilation rates were observed which was justified by the fact that the air volume of the fan was much larger than the leakage rate of hydrogen (up to 1310 L/min). Matsuura et al. (2010) examined numerically the effect of ventilation velocity in an enclosure with one vent. Various configurations of the vent and the release point were tested. They concluded that strong ventilation may become harmful in some configurations because hydrogen can accumulate near the ground. A control method for the forced ventilation flow rate was proposed to encounter the problem. It is based on the estimated leak flow rates and hydrogen sensor information near the roof, control is conducted considering the plot of acceptable exhaust flow rates to various inflow rates and leak positions.

Overall, further experimental studies should be conducted, as well as analytical and numerical models be developed and validated to assess the effect of ventilation parameters on hydrogen dispersion in enclosed spaces, such as garages and underground parking. The final aim is to analyse the efficiency of ventilation systems and identify general guidelines and requirements to prevent harmful conditions. Furthermore, a scenario that should be investigated is given by the possibility of flammable hydrogen-air mixture formation in the ventilation system.

3.1.6.6 Effect of ventilation velocity on dispersion in tunnels (NCSRD, UU)

Passive ventilation is usually present in a tunnel due to the movement of the vehicles (piston effect) or due to the meteorological conditions, e.g. pressure difference across the portals. Active ventilation is also very likely to exist, especially in long tunnels, in order to remove the pollutants of vehicle emissions or in order to remove the smoke in a case of fire. A detailed presentation of ventilation types in tunnels is presented in the deliverable D1.1 of this project (HyTunnel-CS, 2019).

Ventilation influences strongly hazardous gases dispersion. The exact location of vehicles and the geometry of the tunnel can be important because they affect the generated flow field. Ventilation can have both positive and negative effects on hydrogen dispersion. The positive aspects of ventilation are: it can dilute hydrogen concentrations minimizing the size of the flammable cloud; it can safely transport unlimited amount of hydrogen out of the tunnel through its portals and shafts if hydrogen concentration is below LFL. The negative aspects are: a flammable cloud may be extended further away from the release; the turbulence may be induced by ventilation which can enhance the combustion rate and thus overpressures in the case of ignition (this is why the ventilation rate in tunnels is usually reduced in case of fire detection).

In longitudinal ventilation, a minimum air speed is required in order to remove the hazardous gas or smoke. Hydrogen behaves, in general, similarly to smoke from a fire because of its high buoyancy (smoke is buoyant as well due to higher than surrounding air temperature). For fires in tunnels, a lot of research has been carried out on the effect of ventilation on smoke movement, e.g. (Hu et al., 2008a); (Hu et al., 2008b); (Barbato et al., 2014); (Zhang et al., 2019); (Haddad et al., 2019), and empirical correlations have been developed which estimate the critical velocity as a function of heat release rate. The ventilation velocity value of 3.5 m/s seems to be sufficient for most tunnel fires to prevent the “back-layering” effect, including

large fires of more than 100 MW. More details are presented in deliverable D1.1 of this project (HyTunnel-CS, 2019).

About the effect of ventilation on hydrogen dispersion specifically, few studies have been conducted. Mukai et al. (2005) performed a CFD study examining the effect of ventilation on hydrogen dispersion. 60 m^3 of hydrogen were released from a fuel cell vehicle in a tunnel. Three scenarios were investigated, one with no ventilation, one with 1 m/s ventilation velocity and one with 2 m/s. It was found that hydrogen is moved towards the downstream ventilation direction efficiently. As a result, the area where hydrogen concentration is above LFL decreases significantly, especially for the 2 m/s case.

Houf et al. (2012) performed a similar study investigating the effect of ventilation on the flammable cloud produced by three separate releases from the bottom of a hydrogen fuel-cell vehicle in a tunnel. They concluded that increasing the ventilation rate reduces the peak flammable cloud volume and reduces significantly the time required for dilution below LFL.

Middha and Hansen (2009) investigated the risk from hydrogen releases from cars and buses inside road tunnels. Ventilation flow velocities equal to 2, 3 and 5 m/s were investigated and compared against the case with no ventilation. In the worst case investigated, involving 4mm releases from 4 out of the 8 cylinders at 350 bar on the hydrogen bus, the maximum flammable cloud size was found to be equal to 1800 m^3 in the case with no ventilation, 1500 m^3 in the case of 2 m/s ventilation and 1000 m^3 in the case of 5 m/s. However, no significant differences were found for the effect of ventilation on the equivalent stoichiometric gas cloud (which was used to evaluate explosion hazards). It was concluded that "ventilation is only important if more significant volumes of reactive clouds are seen" and that for the examined high momentum releases the dilution process is dominated by the momentum jet. They suggested that more investigation should be made for lower momentum jets.

Bie & Hao (2017) investigated numerically the distribution of hydrogen in a subsea tunnel of dimensions WxHxL=13.5x5x500 m following a release from the 6 mm TPRD of a vehicle. The onboard storage was assumed to contain 4.96 kg of H_2 in a volume of 150 L at 70 MPa. Four ventilation rates were applied to the tunnel: 0, 1, 3 and 6 m/s. The distributions at 3 s of release for the different ventilation conditions are shown in Figure 14 and Figure 15 for the plane parallel and perpendicular to the tunnel axis, respectively. For absent ventilation, the flammable cloud on the longitudinal plane extends for approximately 15 m under the ceiling (Figure 14). With the increase of ventilation rate, the flammable layer under the ceiling extended to approximately 20 m, being more pronounced in direction of the ventilation flow. Figure 15 shows the transversal hydrogen distribution. For absent ventilation, the high-pressure jet reaches the ceiling and spreads horizontally. Once the flammable cloud reaches the walls it descends along them toward the ground. With the increase of ventilation rate to 6 m/s the flammable cloud reduced in size forming a thin layer under the ceiling extending for approximately 10 m. Overall the increase of ventilation velocity helps reducing greatly the flammable cloud upstream the counter direction to the ventilation flow. The vehicles upstream the car accident are likely to be blocked and/or require longer escape times, whereas downstream vehicles should drive away more easily from the accident scene. If the ventilation flow has same direction as the traffic, the upstream vehicles will be less subject to the flammable cloud, creating less dangerous conditions. However, it is though that the size of flammable cloud can be decreased by reducing TPRD diameter from 6 mm in this study to 2-

3 mm as in today's cars (according to the similarity law the length of flammable envelope is proportional to TPRD diameter).

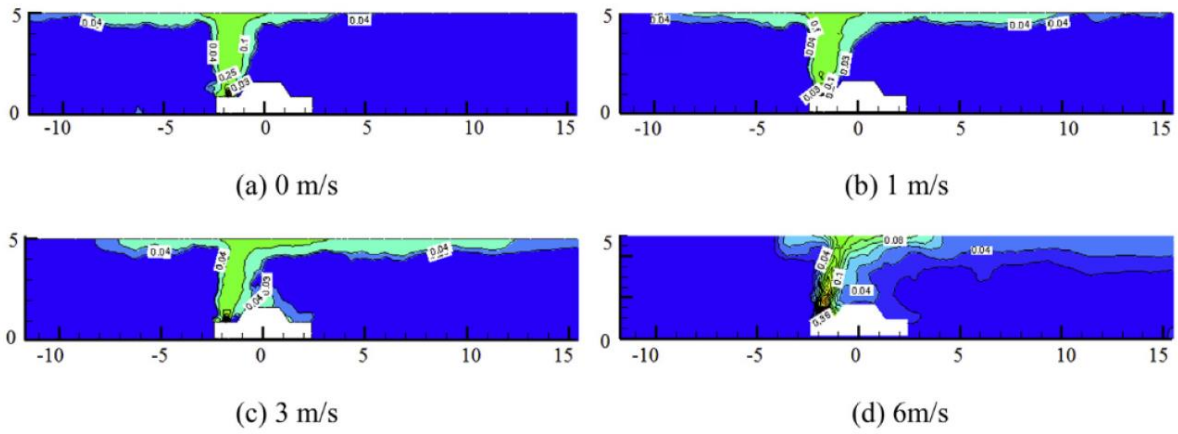

Figure 14. Hydrogen concentration at t=3 s contours through the plane parallel to the tunnel axis (Bie & Hao, 2017).

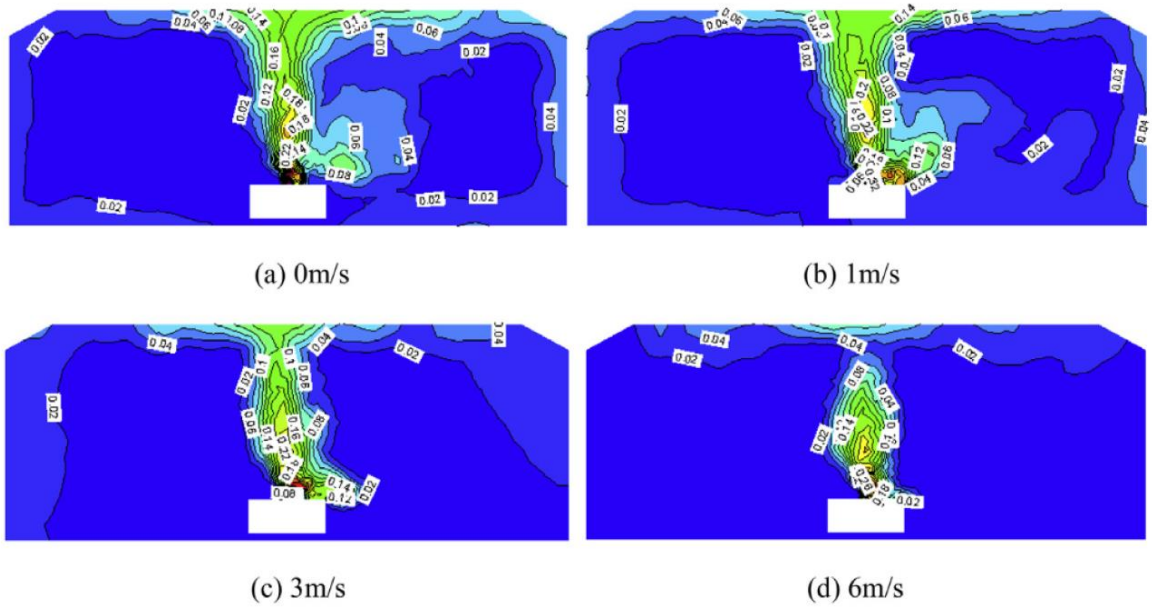

Figure 15. Hydrogen concentration at t=3 s contours through the plane perpendicular to the tunnel axis (Bie & Hao, 2017).

In conclusion, ventilation in a tunnel has generally a beneficial effect diluting the hydrogen cloud and safely removing hydrogen, which is in areas where hydrogen concentration dropped below 4% vol (LFL). However, Bie & Hao (2017)'s study showed how in certain conditions ventilation may transport the cloud of flammable gas and contribute to further extend it. The cloud may thus move towards other vehicles or along ventilation ducts and shafts. Furthermore, the numerical studies presented above have found different effects for the analysed range of ventilation velocities. Therefore, further experimental studies should be conducted to investigate this scenario and create the basis for more general and universal recommendations on the effectiveness of ventilation in tunnels. The produced experimental dataset shall be then used to validate the CFD models to simulate specific scenarios and perform hydrogen safety engineering. In addition, previous works have not included the effect of a tunnel slope in their

analysis on flow and dispersion of hydrogen. The maximum slope allowed by the European Directive 2004/54/EC is 5% for new built longitudinal tunnels. Furthermore, the Directive states that for gradients above 3% additional measures are required to increase level of safety. Further numerical studies should be conducted to assess the effect on hydrogen dispersion in tunnels.

3.1.6.7 Effect of jet impingement and attachment on flammable cloud size (UU)

Presence of surfaces may affect the dispersion of high-pressure hydrogen jets, impacting the size of flammable cloud. Friedrich et al. (2007b) investigated the hydrogen concentration distribution in vertical releases impinging on a horizontal plate (1x1 m) located 1.5 m above the nozzle with diameter 4, 21 and 100 mm. For releases with velocity in the range 100-400 m/s, it was observed that the reciprocal of the hydrogen concentration along the jet axis depends almost linearly from the ratio of the release diameter over the distance from the release point. This is in full agreement with the similarity law (Molkov, 2012). Hydrogen concentration along the radius of the jet showed a distribution like a Gaussian profile. A second scenario considered was the jet impingement on a horizontal plate provided with sidewalls forming a hood structure. In this case, the jet was observed to move vertically, then horizontally when impinging on the plate. However, when reaching the sidewalls, the flow moved in downward direction, resulting in a different radial profile from a free jet. Following a Gaussian profile, hydrogen concentration was maximum on the jet axis, decaying along the radius to reach a minimum at about 0.3 m from the jet axis. However, hydrogen increased in concentration while moving further along the radius towards the sidewalls. For increasing release velocities this behaviour becomes more distinct. Both release configurations were simulated numerically by Middha et al. (2010). The authors used a standard k-ε turbulence model modified to include wall functions. The authors obtained a good agreement with the experimental results especially for the high momentum jets (21 mm release orifice).

Tolias and Venetsanos (2015) investigated the performance of several discretization schemes to reproduce the expected pattern of an impinging hydrogen jet. It was found that the discretisation scheme can greatly affect results, therefore, great care should be given to the numerical scheme employed to solve similar problems.

Li et al. (2015) investigated a realistic accident scenario involving hydrogen release from a 4.2 mm diameter TPRD of fuel cell vehicle. The jet was directed downward (three different angles were studied) and impinged on the ground. Distance to LFL decreased by 60% when compared to a free jet configuration. Hazard distance to LFL was 9.4 m for a storage pressure 35 MPa and 11.8 m for 70 MPa. Validated tools are currently needed to accurately estimate the concentration distribution in impinging jets. The developed models can be used to calculate parameters fundamental for the assessment of accident consequences. An example is given for hydrogen concentration at the stagnation point of a jet impinging a ceiling, as it is an important factor to determine the concentration in the pre-mixed flammable cloud formed within a ventilated compartment.

Releases in proximity of surfaces undergo a reduced entrainment. The reduced air entrainment causes lesser dilution of hydrogen by air, leading to an extension of the distance occupied by the flammable cloud. Hall et al. (2017) observed that the presence of the ground in the proximity of the release may affect significantly the dilution of the gas. For a jet released at 5 cm above the ground with pressure 150 barg and 1.06 mm orifice diameter, the LFL was

reached at approximately 2.5 m. At the same distance, only ¼ of the LFL concentration was measured for a free jet. Releases in proximity of a ceiling were shown to behave similarly to releases in proximity of the ground. Concentration to LFL was reached at a shorter distance, 2.1 m, possibly due to a major spread of the jet caused by the buoyant forces. CFD simulations were performed by the authors and they resulted in overprediction of the jet extent. The deviation may be due to the highly unstable wind conditions during experiments, which could not be reproduced in the numerical modelling.

Hourri et al. (2011) investigated numerically releases up to 700 barg, finding that the distance to LFL could increase by 48% when passing from a free jet configuration to a release height of 7.7 cm above the ground. A previous study by Hourri et al. (2009) analysed the effect provoked by a vertical wall located on the side of the horizontal release. The LFL area extended by 90%, indicating that buoyancy effect has a limited reducing effect.

3.2 Hydrogen jet fires (UU)

A fire around hydrogen tank, e.g. gasoline spill fire during an accident, will lead to venting of hydrogen through the TPRD. The hydrogen flame from TPRD can cover distances of tens of meters (Royle et al., 2011a), and cause life-threatening conditions by the flame itself and thermal radiation. It is worth mentioning here that flame length from TPRD is proportional to TPRD orifice diameter. This knowledge already assisted to reduction of TPRD diameter from 6 mm at early days to 2-3 mm currently. Further decrease of TPRD is needed to make parking of hydrogen cars in garages inherently safer.

If a delay occurs between the opening of the TPRD and ignition of highly turbulent flammable jet, pressure loads must be considered along with above mentioned thermal hazards. The overpressure of turbulent deflagrative combustion of jet can be as high as 0.2 bar at 4 m from the ignition point for a 40 MPa release through a 10 mm orifice (Takeno et al., 2007). This generated overpressure is enough to cause serious injury with eardrum rupture (LaChance et al., 2011). In hydrogen safety analysis, structure response due to the pressure and thermal loads from the combustion is of great concern. It is of high significance to understand not only the combustion process itself, but reaction of structures on pressure and thermal loads.

A jet fire from TPRD in a confined space may have a twofold effect on vehicle fire consequences. The hydrogen jet fire from TPRD may increase the heat release rate (see section 3.5.1). Water vapour produced by combustion may in some situations act as an extinguisher of the primary fire, e.g. wood fire in a garage. The contributions of these two competing phenomena are not known and further research is needed to clarify it. Furthermore, current standard requirements for ventilation in an underground parking may not be adequate and sufficient when the TPRD is activated during a FCH vehicle fire and it may actually worsen the blaze consequences or the evacuation conditions. There is a lack of knowledge on this aspect, which can only be fulfilled by further experimental tests and modelling studies. The HyTunnel-CS project considers a system vehicle-confined structure. There is a full understanding of partners that it is much more efficient to develop inherently safer hydrogen-driven vehicle that could safely enter underground transportation infrastructure rather than invest heavily into changes of existent infrastructure and novel prevention-mitigation technologies related to infrastructure itself.

3.2.1 Oxygen depletion and asphyxiation (UU)

The effects of oxygen depletion and asphyxiation are presented in section 3.1.1. They are valid as well for hydrogen ignited releases. In fire conditions, the oxygen depletion is caused not only by substitution of air by other gases but its direct consumption in the combustion process.

3.2.2 Flame length and hazard distances for hydrogen jet fires (UU)

Figure 16 presents a dimensionless hydrogen flame length correlation. In this correlation the experimental data on flame length are normalized by the actual (not notional) nozzle diameter and are correlated with the product of the dimensionless density ratio ρ_N/ρ_S and the Mach number (the ratio of flow velocity to speed of sound at actual nozzle exit) to the power of three $M^3 = (U_N/C_N)^3$.

One of the advantages of this universal correlation, which includes all regimes of jet and plume fires, is the absence of parameters at the notional nozzle exit. The parameters needed to predict the flame length are those at the actual nozzle exit only: diameter, hydrogen density and flow velocity, the speed of sound at pressure and temperature at the nozzle exit. The use of the correlation requires application of the under-expanded jet theory that can be found elsewhere (Molkov, 2012). There is lesser uncertainty in calculation of flow parameters in the actual nozzle exit compared to uncertainties at the notional nozzle. Indeed, it is well known that there is a strong non-uniformity of velocity immediately downstream of the Mach disk that deviates from the common for all under-expanded jet theories assumption of uniform velocity at the notional nozzle exit. By this fact, the methodology excludes from consideration the questionable issue of use of flow parameters at the notional nozzle exit.

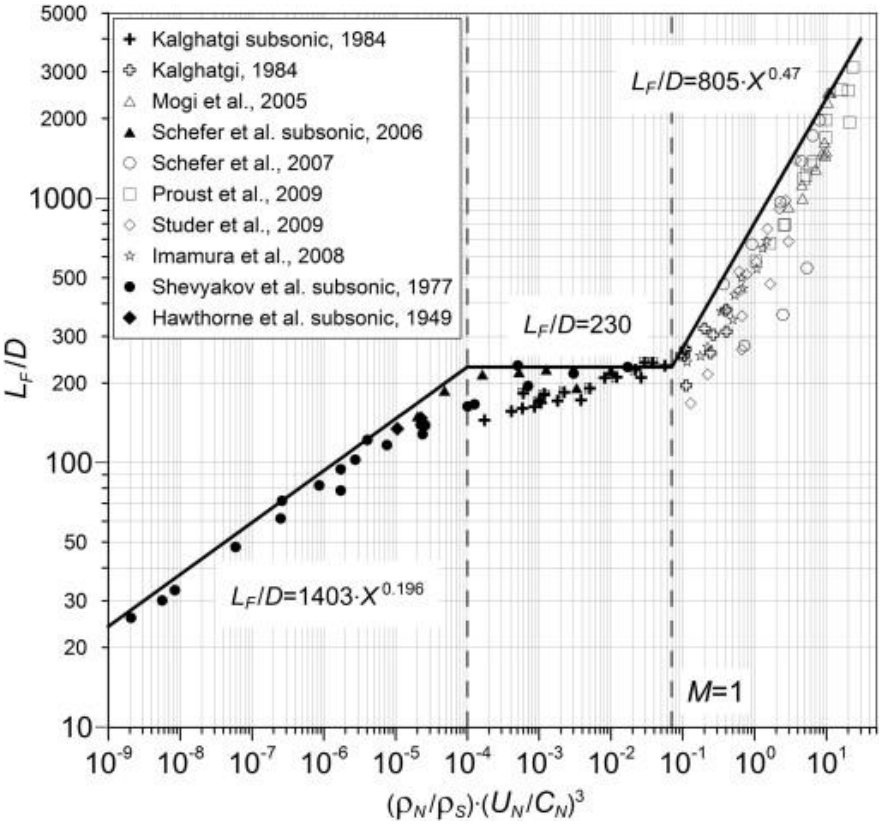

Figure 16. The dimensionless correlation for hydrogen jet flames (in formulas "X" denotes the similarity group $\rho_N/\rho_S)(U_N/C_N)^3$ (Molkov and Saffers, 2013).

The hydrogen flow parameters at the nozzle exit for experiments presented in Figure 16 are taken either directly from experiments or calculated by the under-expanded jet theory (Molkov et al., 2009). The details of experiments used to underpin the dimensionless correlation are given in (Molkov and Saffers, 2011). The correlation covers the whole spectrum of hydrogen reacting leaks, including laminar and turbulent flames, buoyancy and momentum-controlled fires, expanded (subsonic and sonic) and under-expanded (sonic and supersonic) jet fires.

Harm criteria for people can be expressed in terms of injury or death (LaChance, 2010). It is possible to use a "no harm" criterion which limits the level of acceptable consequences to a low enough level that no injury would occur. Temperature 70 °C is taken as "no harm" criterion. Exposures to flames, hot air or radiant heat fluxes can result in first-, second-, or third-degree burns. The resulting level of harm is dependent upon several factors: the amount and location of exposed skin, the person's age, the exposure time, the speed and type of medical treatment, etc.

Figure 17 shows measured axial temperature of hydrogen flame (Barlow and Carter, 1996; Imamura et al., 2008; LaChance, 2010) as a function of distance from the nozzle, x, normalised by the flame length, L_F. Three harm criteria are presented by horizontal lines: 70 °C – "no harm" threshold; 115 °C – pain limit for 5 min exposure; 309 °C – third degree burns for a 20 s ("fatality" limit). Comparison between the axial temperature profile and named criteria provides the separation distances: $x = 3.5L_F$ for "no harm" separation (70 °C), $x = 3L_F$ for pain limit (115 °C, 5 min), $x = 2L_F$ for third degree burns (309 °C, 20 s).

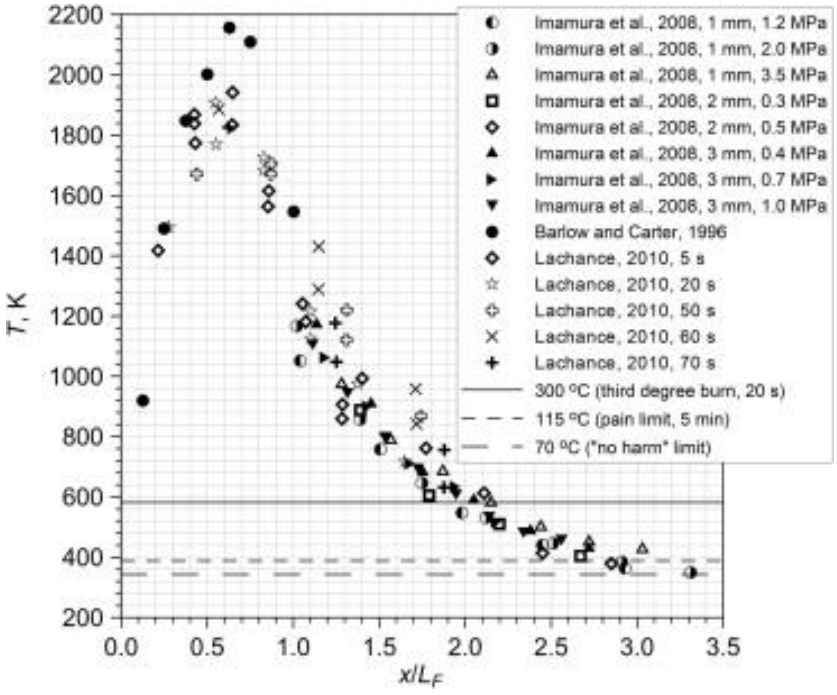

Figure 17. Measured axial temperature as a function of distance expressed in flame calibres, and three criteria for jet fire effects (lines) (Molkov and Saffers, 2013).

3.2.3 Thermal losses effect and thermal loads (URS, UU)

Jet flames originated by pressurised hydrogen ignited releases can cause life threatening conditions in their surroundings, i.e. injury or death of the exposed subject. It could be conservatively assumed that the direct contact with the flame can result in fatality, whereas

exposure to the radiative heat flux of the flame can have as consequent injury harm levels: first-, second- or third-degree burns. The potential damage depends on the vulnerability of the target, which is determined by age, health conditions, etc.

In many numerical simulations heat losses from turbulent hydrogen flames to the confinement structures were usually considered to be negligible or less important (Bray, 1996). The main reason is that the heat loss rate in high-speed flames is usually believed to be too low compared to the energy release rate to impact the dynamics of flame propagation in confined space. However, it has been revealed by many experimental studies that modelling of heat losses from the combustion products is important for accurate prediction of pressure and thermal loads. The neglection of heat transfer in models, i.e. heat conduction, convection, thermal radiation and condensation, may lead to over-prediction of the maximum pressure peak value and under-prediction of pressure decay rate. On the other hand, for the numerical simulations without simulating the heat losses to the structures, it will be difficult to accurately capture many phenomena in the dynamics of flame propagation since the local pressure and temperature could not be precisely predicted.

Xiao et al. (2015) have analysed the importance of various heat transfer mechanisms and their relative contributions to the total energy losses. Numerical investigations on the mechanisms of heat losses caused by propagating turbulent flames were performed using a semi-implicit pressure-based all-speed CFD code GASFLOW-MPI. Heat losses from turbulent sonic flames to the structures of the ENACCEF facility at the Institut de Radioprotection et de Surete Nucleaire (IRSN) were studied. It appears that the effect of heat losses on the flame propagation properties is not significant. However, the impacts of heat losses on the pressure peak and pressure decay after hydrogen combustion should not be neglected. It indicates that the convective heat transfer and thermal radiative heat transfer are the main contributors of the total energy losses to the structures. In all cases, the effect of steam condensation heat transfer is relatively small but not negligible. In general, it is suggested to include the heat transfer mechanisms in order to improve the reliability and accuracy of numerical analyses of hydrogen safety issues.

Few experiments have been carried out to analyse the behaviour of hydrogen jets and the potential hazard connected to it. Grune et al. (2011, 2014) have examined horizontal high-pressure hydrogen jets to investigate the potential hazards associated to accidental release of gas and consequent ignition. Two cases of ignition were considered: forced ignition by a spark and self-ignition. Experimental results showed that the highest values of thermal loads are achieved for the spontaneous ignition of the hydrogen jet. Furthermore, it was noted that highest thermal load was reached close to the nozzle. The heat flux decreases linearly when the distance to the nozzle increases. Typical values of integrated thermal load ranged between 50 and 300 kJ/m^2 when reducing the distance to the jet fire from approximately 170 to 50 cm. The jet fire was originated by a 4 mm release at 200 bar. The results were expressed also in term of critical distance: a critical distance of 2 m for second-degree burns of human skin is reached for a storage pressure of 25 bar, while this value increases to 2.5 m for pressures of for 200 bar. In any case, for the conditions in which these experiments were conducted, the maximum value of critical distance reached was 3 m. Details are given in Figure 27 in section 3.2.4.2 along with a detailed description of the performed experiments.

3.2.3.1 Radiative heat flux (URS, UU)

Consalvi and Nmira (2019) performed a throughout analysis of the literature concerning the mechanisms of radiant heat flux generated by hydrogen flames. Given the absence of soot, the only responsible for emitting radiation are the H_2O^* molecules in the excited state.

To model radiative heat flux, two different semi-empirical models have been applied: the point source model and the surface emitter model (TNO, 2005). The point source model considers heat radiation coming from a single point, located on the centreline of the flame (Figure 18a). The radiative heat flux (kW/m^2) at a distance S (m) from the source to the target is evaluated according to the equation:

$$q_{rad} = \frac{\chi_{rad}\, m_{fuel}\, \Delta H_c\, \tau_a}{4\pi S^2} \tag{3.11}$$

where χ_{rad} is the radiated heat fraction, m_{fuel} and ΔH_c are the mass flow rate (kg/s) and the combustion heat of fuel (kJ/kg) respectively, and τ_a is the atmospheric transmissivity.

The estimation of the radiative heat flux requires the prior evaluation of the radiated heat fraction (χ_{rad}), defined as the fraction of the total emitted radiative power (S_{rad}) and the total heat released by the chemical reaction ($m_{fuel}\, \Delta H_c$) as follows:

$$\chi_{rad} = \frac{S_{rad}}{m_{fuel}\, \Delta H_c} \tag{3.12}$$

Schefer et al. (2006a, 2007) reported that the radiant fraction for hydrogen jet flames exhibits a logarithmic dependence on flame residence time, as observed for hydrocarbon flames. However, the absence of CO_2 and soot in the product stream results in lower overall radiant fractions (<0.1). The authors showed that the point source model results agreed well with experimental measurements from hydrogen jet fires.

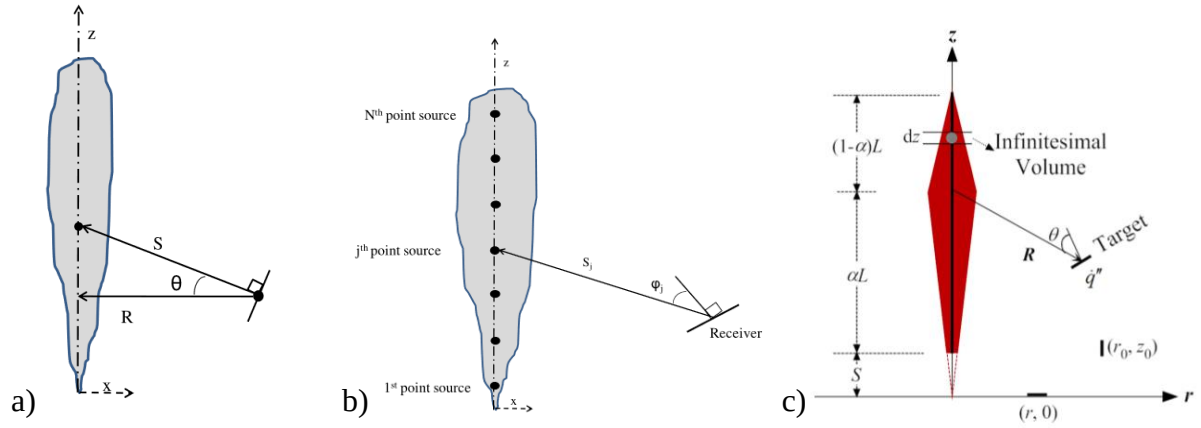

Figure 18. a) Single point source model (Hankinson and Lowesmith, 2012), b) Multi point source model (Hankinson and Lowesmith, 2012), c) Line source model (Zhou and Jiang, 2016).

Molina et al. (2007) developed an expression treating the flame as a blackbody emitter and the radiant fraction as function of flame residence time (ms), adiabatic flame temperature T_{ad} (2390 K for H_2) and Plank's mean absorption coefficient for the product species (H_2O, 0.23 m^{-1}):

$$\chi_{rad} = 0.08916\, log_{10}\left(t_f\, \alpha_p T_{ad}^4\right) - 1.2172 \tag{3.13}$$

and t_f is the flame residence time (ms), obtained as follows:

$$t_f = \frac{\rho_f W_f^2 L_f f_s}{3\rho_f d_j^2 u_j} \quad (3.14)$$

where density (ρ_f), width (W_f,), lenght (L_f,), mass fraction (f_s) and jet diameter (dj) and velocity (u_j) are referred to a stoichiometric flame.

However, the correlation proposed by Molina et al. (2007) was defined for laboratory scale hydrogen momentum-controlled flames, considered optically thin. Large-scale hydrogen flames have a greater thickness and may result in an under-estimated radiant fraction.

A weighted multi-point source model has been proposed by Hankinson and Lowesmith (2012) to improve the predictions of the radiative heat flux (see Figure 18b). Indeed, Ekoto et al. (2012) observed that the conventional single point source models may underpredict the measured radiative heat flux by 40% or more in the near field of a flame. According to the multi-source model, a number *N* of source points is chosen along the flame axis and the total radiation is evaluated as the sum vector of the radiation of each source point. A conceptual scheme is given in Figure 18b and compared to the single point source model in Figure 18a. The details and calculation procedure are available in Hankinson and Lowesmith (2012). The weighted source flame radiation model has demonstrated substantial improvement in the heat flux predictions in the near field. Ekoto et al. (2014) further developed the model to include buoyancy effects on the jet flame trajectory curvature.

Another model proposed in the literature to determine the radiative heat flux is the surface emitter model or solid flame mode that can be found in Hankinson and Lowesmith (2012). It considers the radiative source as the surface of a solid object, generally assumed as a cone or a cylinder. The radiative heat flux is evaluated as follow:

$$q_{rad} = VE\tau_a, \quad (3.15)$$

where V is the view factor and E is the emissive power per flame surface (kW/m^2), defined as the product of the radiative fraction and the total heat released from the chemical reaction per flame surface area ($E = (\chi_{rad}\, m_{fuel} \Delta H_c)/A_f$).

Despite a simple implementation and common use, the cylindrical solid flame model has showed a considerable departure from the measurements. Main reason is the assumption of a constant emissive power over the whole flame, whereas it changes along its length. To fulfil this lack, the line source model was developed by Zhou and Jiang (2016), which integrates the thermal energy radiated from the centreline of the jet flame along its length (see Figure 18c). It is considered that the flame shape as a kite could lead to better estimation of the flame surface area. Furthermore, the effect of the flame lift-off on the radiative heat flux is taken into account. The methodology is detailed in Zhou et al. (2014, 2016). The authors found a better agreement with experimental radiative heat flux from a horizontal propane jet fire compared to the point- and multi-source models. In particular, it was observed that the linear source model can provide good predictions for both small-scale and large-scale jet fires.

Overall, it can be concluded that the point source model is mainly valid in the far field of hydrogen jet flames, whereas the multi-source and solid flame models are more accurate in the near field (Huang et al., 2018), where safety issues are especially important.

Radiative heat flux from hydrogen flame can also be calculated using CFD, especially in complex geometries. The radiation models implemented in CFD codes approximate and solve the following radiation transfer equation (RTE):

$$\frac{dI_v(r,s)}{ds} = -K_{av}I_v(r,s) - K_{sv}I_v(r,s) + K_{av}I_b(v,T) + \frac{K_{sv}}{4\pi}\int_{4\pi} I_v(r,s')\Phi(s\cdot s')d\Omega' + S \qquad (3.16)$$

where ν is the frequency, r and s are the position and the direction vectors, s is the path length, K_a and K_s are the absorption and the scattering coefficients respectively, T is the absolute temperature, I_b is the blackbody emission intensity, Φ is the in-scattering phase function, Ω is the solid angle, S is the relevant radiation intensity source term (ANSYS, 2016).

Several radiation approaches and models are available to be implemented in CFD codes, based on different simplifying assumptions. A summarised description is given below.

1) Fractional heat loss due to radiative heat transfer

The model of the fractional heat loss due to radiative heat transfer does not model radiation but it considers that a certain percentage of total released heat is lost as radiation, depending on the type of fuel and the scenario considered (SFPE, 2008; Ciambelli et al., 2011). It could be assumed that the percentage is around 20-40% for hydrocarbons and of the order of 10% for hydrogen.

2) P-1 Model

The P-1 Model (Differential Approximation model) is a first simplification of the RTE, assuming that the radiation intensity is direction independent at a given location in space (ANSYS, 2016a).

3) Discrete Ordinates model (DO)

The Discrete Ordinates model solves the RTE for a finite number of discrete directions, spanning the round solid angle, in a Cartesian system. (Selcuk and Kayakol, 1996). Namely, this model transforms the RTE in a transport equation for radiation intensity in the spatial Cartesian coordinates (ANSYS, 2016b).

4) Discrete Transfer Radiation Model (DTRM)

The Discrete Transfer model is based on ray tracing between surfaces and solves the RTE along representative multiple rays of radiation travelling through the computational domain in selected directions specified by polar and azimuthal angles (Selcuk and Kayakol, 1996).

5) Monte Carlo model

The statistical Monte Carlo Model allows simulation of the physical interactions between photons and the surrounding environment (ANSYS, 2016a; Ciambelli et al., 2011). Photons are emitted and tracked through the system, along (pseudo-) random directions. This model requires a considerable computational effort and is not generally applied to large scale fires.

A considerable number of numerical studies have been carried out on hydrocarbon flames, whereas only a few are available on hydrogen flames.

Ibas (2005) has carried out numerical simulations of hydrogen and hydrogen-hydrocarbon non-premixed flames, with and without radiation model. The authors compared the P-1 and the

DTRM radiation models on a Fluent platform. Results showed a negligible difference between the two radiative models despite a lower computational cost for P-1 model.

Wang et al. (2014) have performed numerical simulation to characterize the radiation mechanism of hydrogen and hydrogen/methane under-expanded jet fires, with CFD code FireFOAM. The radiation process has been simulated using the finite discrete ordinate (DO) model. Results presented a good agreement with experimental measurements.

A DO model was implemented as well by Cirrone et al. (2019a) to simulate the thermal radiation from cryogenic hydrogen jet fires with release pressure up to 6 bar. The authors found an excellent agreement between simulation results and experiments. The same approach was employed by the authors to analyse a horizontal hydrogen jet fires in under-expanded conditions (900 bar). In this case the comparison with experimental data has showed some discrepancy, especially in the initial phase of the release, where the greatest thermal radiation was emitted in the experiment (Cirrone et al., 2019b).

Location of jet fire close to a surface may affect the radiative heat flux measured in its proximity. Hall et al. (2017) observed that for a jet fire located 5 cm above the ground, the radiative heat flux measured at 2 m from the jet axis was 40% greater than the value measured for a free jet far from the ground. Experimentally measured radiative heat flux is shown in Figure 19. The flame length increased from 2.7 m to 4.4 m respectively. A lower flame length increase was observed for the same release in proximity of the ceiling (3.2 m).

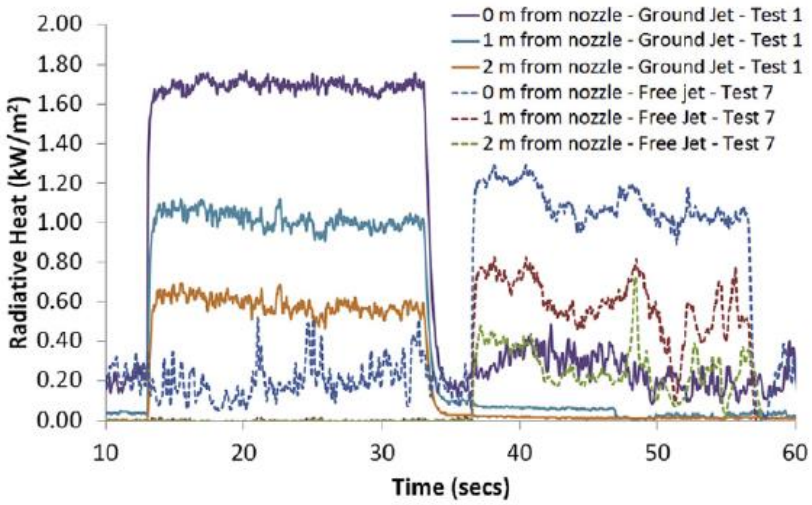

Figure 19. Experimental radiative heat flux at 2 m from release with 150 barg pressure and 1.06 mm orifice (Hall et al., 2017).

3.2.3.2 Thermal dose (UU)

As discussed in the previous sections, exposure to the radiative heat flux of a flame can have the following harm levels: first, second or third degree burns. The resulting level of harm is a function of the exposure duration in addition to the incident thermal flux. Therefore, it is usually expressed in terms of thermal dose (TD):

$$Thermal\ Dose = I^{\frac{4}{3}} \cdot t\ , \tag{3.17}$$

where I is the radiative heat flux (kW/m^2) and t is the exposure time in seconds. The thermal dose unit (TDU) is equal to 1 (kW/m^2)$^{4/3}$s.

Thermal dose can be a comprehensive parameter to estimate hazard distances beside a jet fire, where engineering tools are currently not available. Cirrone et al. (2019c) employed the thermal dose definition to evaluate either the distance or the maximum exposure time for public or first responders. The authors conducted numerical study on jet fires with release temperature in the range 48-78 K and pressure 2-4 bar abs from 1.25 mm orifice. It was found that at 0.5 m distance from the flame axis the public should not be exposed for more than 30 s to not incur in first degree burns. On the other hand, fire fighters may stay as close as 0.27 m from the jet axis up to 3 min, receiving a thermal dose of approximately 1380 (kW/m^2)$^{4/3}$s for the longest jet fire.

Greater distances were found by Hall et al. (2014) for a 60 l/min spillage. In this case, it was found that a distance greater than 8.7 m from the flame extent (~5 m) should be maintained to avoid a harmful thermal dose for an exposure time up to 200 s.

3.2.4 Pressure loads (UU)

In case of ignited release from a high-pressure storage system, overpressure hazards may arise along with thermal hazards. As already discussed in section 3.1.4., unignited high-pressure release in an enclosed space may lead to damage or destruction of the structure due to the pressure peaking phenomena (PPP). The PPP for ignited releases, which will happen with higher probability, can generate higher overpressure compared to unignited release. It will be described in the next section.

A second potential accident scenario is the delayed ignition of high-pressure turbulent hydrogen jet, which can create a significant overpressure. The presence of walls or confinements can affect the overpressure in the surroundings of the jet. This scenario will be described in section 3.2.4.2.

3.2.4.1 PPP for ignited releases (UU, USN)

The pressure peaking phenomena for ignited release is stronger compared to unignited release from the same source. This is because not only the number of gas molecules increases in the compartment, but also the temperature. This will significantly increase the pressure in the compartment compared to an unignited release (Makarov et al., 2018; Hussein et al., 2018; Brennan et al., 2019). Figure 20 shows the pressure history from CFD simulations of pressure peaking phenomena of both ignited and unignited release in a garage. The internal dimensions of the garage are 4.5x2.6x2.6 m and the vent size is 0.35x0.55 m. The release rate of hydrogen into the compartment is 0.2993 kg/s.

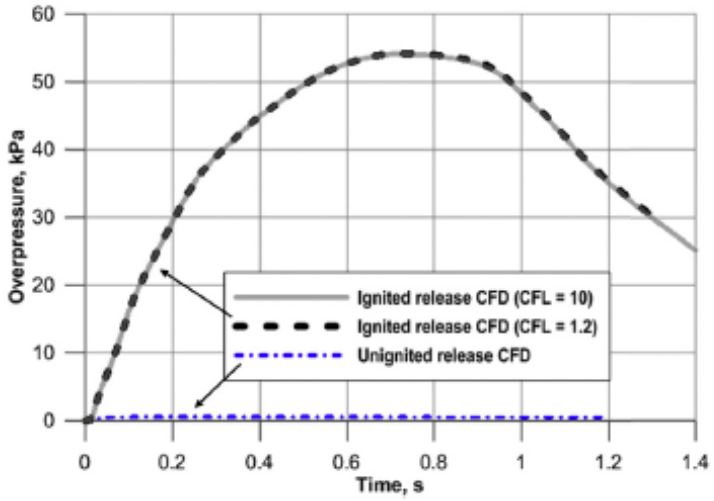

Figure 20. CFD simulations of ignited and unignited hydrogen release in a garage of 30.4 m^3 volume with release rate of 0.2993 kg/s and vent size of 0.35x0.55 m (Brennan et al., 2019).

Makarov et al. (2018) developed a reduced-order model for estimation of the pressure peaking phenomena for ignited releases. The model was validated against experiments in enclosure with dimensions HxWxL=1x0.98x0.96 m. Further development and validation of the reduced engineering tool and contemporary CFD models for simulation of PPP are required. Furthermore, CFD can give insights into further hazardous effects, e.g. calculate thermal effects in addition to pressure loads, both within and without the enclosure.

In section 3.1.5 it was shown that TPRD diameter 2 mm was sufficient to prevent damage to a typical garage by PPP for an unignited release from a 70 MPa storage tank (see as well Figure 21, right). However, pressure increased by factor about 20 when the release from the same source was ignited, creating unacceptable conditions for people and garage structure. Even vents with openings up to 4 bricks were not sufficient to prevent the destruction of the garage, conversely to unignited releases.

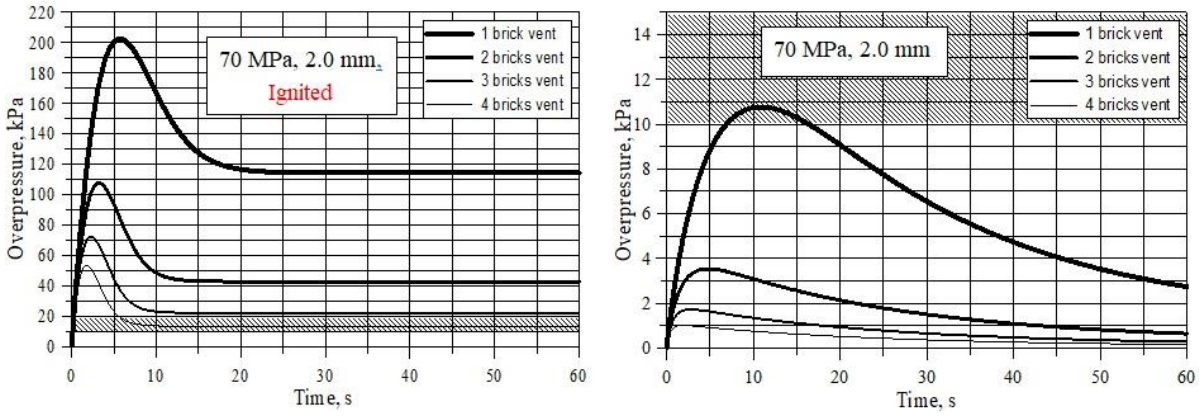

Figure 21. Overpressure dynamics of hydrogen jet fire (left) and unignited release (right) in a garage from a 2 mm TPRD and 70 MPa storage pressure (release rate 107 g/s) (Makarov et al., 2019).

Figure 22 shows that for an ignited release from TPRD with D=0.3 mm and onboard tank storage pressure 700 bar, in a garage of size 2.6x2.6x4.5 m with vent 1 brick (left) or 0.5 brick (right) the garage can withstand overpressure of 10 kPa. The TPRD D=3 mm was taken as an equivalent size of the leak though the wall of leak-no-burst (LNB) tank in a fire. This value is

a round-up from 2.5 mm, as defined by HySAFER through the inverse problem from the experimental blow-down curve. The experiment was also performed with 700 bar explosion-free tank in a fire.

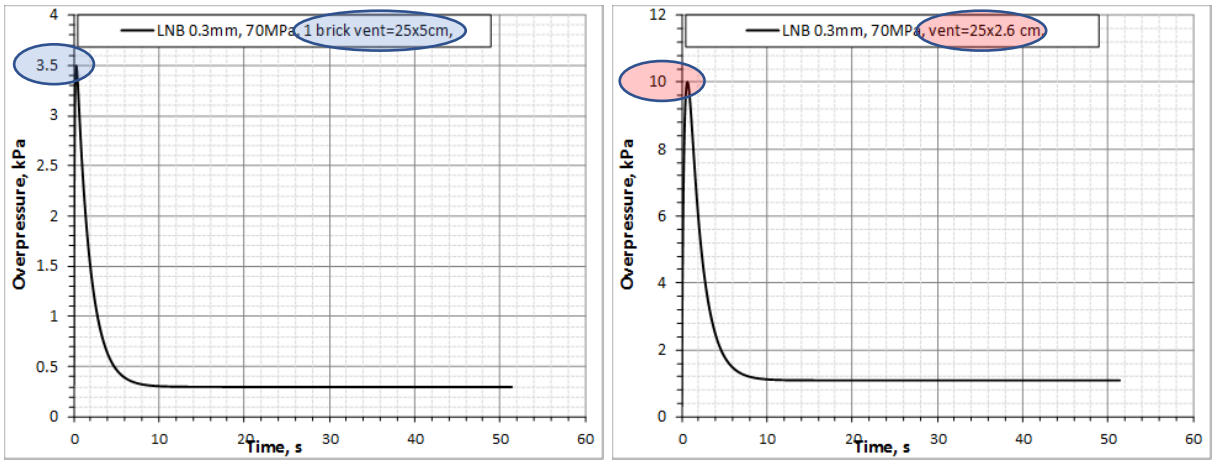

Figure 22. Ignited release from TPRD with D=0.3 mm in a garage 2.6x2.6x4.5 m with vent 1 brick (left) or 0.5 brick (right).

3.2.4.2 Delayed ignition of turbulent hydrogen jets (UU, PS)

If a delay occurs between the opening of the TPRD (beginning of a high-pressure release) and ignition, explosion hazard arises along with the thermal hazard mentioned for jet fires. The produced overpressure depends on several factors such as the leakage diameter, storage pressure and ignition delay time. It can be as high as 0.2 bar at 4 m from the ignition point (Takeno et al., 2007), which is enough to cause eardrum rupture according to the thresholds indicated by LaChance et al. (2011). After the high-pressure peak, a low-pressure wave with longer duration was recorded in experiments. This is because hydrogen continues to burn in non-premixed turbulent regime. The release had pressure 40 MPa and diameter 10 mm. The ignition was triggered after 2 s in a zone with an estimated hydrogen concentration of 40%. The flame front propagation speed had a maximum value of 978 m/s. The reason for such high value is believed to be the strongly turbulent premixed combustion given by the high initial turbulence mixing of the jet, affecting, consequently, the deflagration overpressure.

Daubech et al. (2015) investigated a release with pressure and diameter 40 bar and 12 mm, respectively. Ignition was triggered at 1.8 m from the release point and the highest pressure (0.08 bar) was recorded 2 m downstream the ignition point. The recorded maximum flame speed was 280 m/s. Further experimental investigations on delayed ignition of hydrogen jets were performed by Royle and Willoughby (2011a). The releases were produced by a 205 bar storage through nozzles with diameter equal to 9.5 mm, 6.4 mm, 3.2 mm and 1.5 mm. The authors observed that for a given ignition delay, the maximum overpressure recorded rose with the increase of the release size, achieving a maximum value of 0.054 bar for the 9.4 mm release (400 ms delay). The same proportionality was observed by Takeno et al. (2007) for the range of diameters 0.5-10 mm.

The effect of ignition delay on overpressure could be significant. During the first phase of the release, the hydrogen concentration varies considerably along the jet axis. Thus, if the ignition position is fixed, variations of 100 ms order of magnitude of the ignition delay will determine

if the ignition point is located in the poor or rich mixture portion of the jet. A variation of ignition delay from 400 ms to 2000 ms led to recorded maximum overpressures, respectively, 0.037 bar and 0.095 bar, with a peak value (0.194 bar) achieved for 600 ms (Royle and Willoughby, 2011a).

Zabetakis and Burgess (1961) observed that ignition delay can also affect the total radiant energy and the rate of energy release of different masses of spilled liquid hydrogen.

The presence of surfaces as a barrier to potential jet flame may strongly affect the resulting overpressure in the case of delayed ignition. Royle and Willoughby (2011b) observed that the presence of a surface perpendicular to the direction of the jet can increase up to 2.6 times the overpressure recorded in proximity of the release point, which would correspond to the location of the vehicle and possible occupants in the scenario of a release from a TPRD in a confined space. The maximum recorded value was 0.422 bar for an orifice of 9.4 mm. This is comparatively large diameter of release characteristic for refuelling station rather than for vehicle. However, the effect of the presence of the perpendicular surface was seen to reduce with the decrease of diameter. For a 3.2 mm release pressure increased from 0.035 to 0.041 bar when the wall was included in the configuration. The jet may be not directed perpendicularly to the surface. Royle and Willoughby (2011b) measured an increase of the overpressure by 2.5 times when the surface had a 60˚ tilt for a 3.2 mm release, which is more realistic for automotive applications rather than 9.5 mm.

Friedrich et al. (2007b) investigated the delayed ignition for hydrogen jets impinging on a flat plate with and without sidewalls. The authors observed an increase of overpressure by a factor of 5 when the sidewalls were included in the set up. The presence of the sidewalls prevented the diffusion of hydrogen, retaining a larger amount of hydrogen in higher concentrations.

Further experimental research should be conducted to assess the overpressure hazards from delayed ignition of turbulent hydrogen jets in a tunnel, to be accompanied by the development and validation of engineering correlations and numerical tools to estimate the hazards as function of the release and ignition characteristics.

Ignition of unsteady hydrogen jets (PS)

Accidental hydrogen release from a pressurised hydrogen storage systems leads to unsteady release conditions. Due to the continuously pressure decay in the hydrogen storage systems the hydrogen release rate decays with time. For large hydrogen storage volumes and small hydrogen release rates a quasi-stationary hydrogen release scenario can be assumed, see section 3.2 Hydrogen jet fires. For higher hydrogen release rates from smaller hydrogen storage volumes the hydrogen release time can become short and the result is an unsteady hydrogen jet with strongly unsteady fast transient conditions.

All FC-vehicles operate with two hydrogen systems which are different in their operation pressure range and are separated by a pressure reducer device. The main storage tank is a high pressure system up to 700 bar and has a capacity of several kg hydrogen. The hydrogen feed line from the storage tank to the FC-engine is a low pressure system with values in a range of 5 to 16 bar and hydrogen volumes up to 60 dm^3 (NTP). These parameters were derived from real dimensions of hydrogen supply systems in currently operated cars and buses. Due to the safety concept of the vehicles, the main storage tank valve will be immediately closed if any disturbance, like a crash situation, H_2-leak detection or maintenance and servicing work will

occur. After the tank closing there are still two small but susceptible hydrogen reservoirs in the vehicle. The hazards potential of unsteady hydrogen jet released from the low and high pressure H_2-inventory of FC cars and buses was investigated by Grune et al. (2011 and 2014).

In the study of the low pressure H_2-inventory case, unsteady free hydrogen jets from a 10 mm pipe were simulated experimentally. In the experiments hydrogen amounts up to 60 STP dm^3 at initial pressures of 5 and 16 bar were released. Figure 23 (left) shows the measured and calculated pressure decay in the release reservoirs (vessel B [4 dm^3]), the maximum hydrogen release rates of 24 g/s and 97 g/s were determined for the initial pressures of 5 bar and 16 bar, respectively.

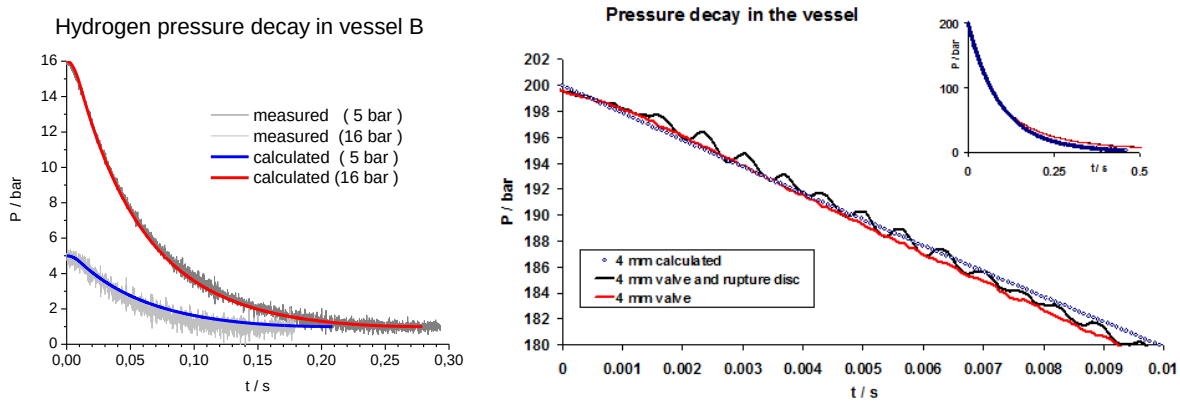

Figure 23. Measured and calculated pressure decay in the release reservoirs. Left: Low pressure, vessel B (4 dm^3), H_2-release through a 10 mm tube nozzle (Grune et al., 2011). Right: High pressure, vessel 0.37 dm^3, 4 mm tube nozzle (Grune et al., 2014).

In the study of the high pressure case, an accidental H_2 release from a small high pressurized reservoir of 0.37 dm^3 was investigated experimentally. Two different starts-up release conditions were simulated. In the first procedure a fast valve opens and different tubular release nozzles with diameters of 3, 4, and 10 mm produce a hydrogen free jet in air. In the second release application, an additional rupture disc was installed in the 4 mm exhaust pipe. The shape of the hydrogen effusion times and the total release time of 250 ms and 380 ms demonstrates the strong transient release condition. The free transient hydrogen jets were ignited on the jet axis by varying ignition position and ignition time delay. Figure 24 shows a sequence from a digital video with a time step 40 ms for an example with early ignition close to the nozzle and highly transient jet fire.

Figure 24. Sequences from digital video, time step 40 ms Vessel [D16; 1.25 dm^3; P = 16 bar] (Grune et al., 2014).

The generated pressure waves and thermal loads were investigated systematically. The time span in which the gas cloud is ignitable is almost identical with the effusion time of the gas

from the vessels. For many ignition times and ignition positions the ignition of the unsteady free jet produced only a local combustion with no detectable pressure wave. In contrast to this, an ignition of the free hydrogen jet shortly after it has reached its maximum effusion rate can lead to a local explosion with detectable pressure waves. For every given amount of hydrogen, a distinct ignition time and ignition position exists for the generation of a maximum pressure wave due to a "local explosion" in the free jet.

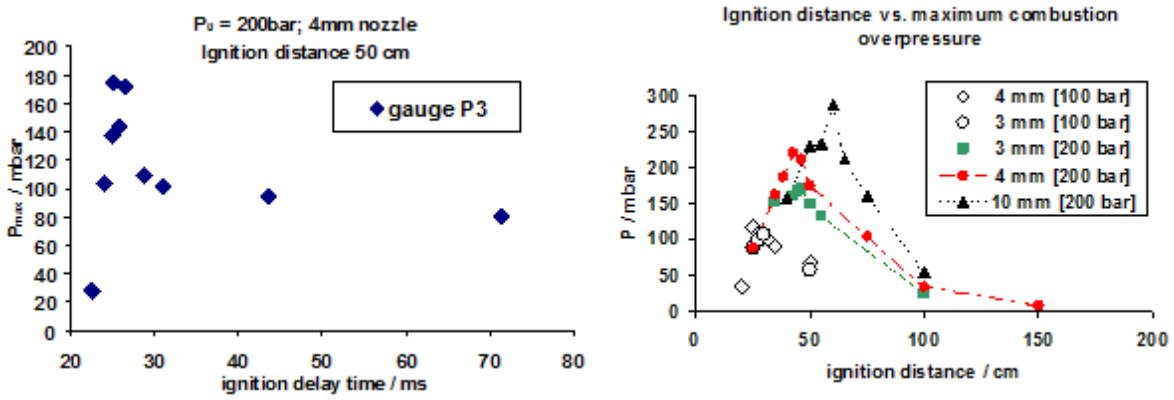

Figure 25. Left: Dependence of the ignition delay time on the generated combustion overpressure. Right: Maximum measured combustion overpressures for different ignition distances (Grune et al., 2014).

The amplitude of the generated combustion overpressure is very sensitive to the ignition delay time. Figure 25 left shows an example (high pressure release) of the dependence of the ignition delay time on the generated combustion overpressure measured reflected in 50 cm distance to the jet axis. There is a narrow ignition time window of 25 ms +/- 1 ms which produces the highest observed overpressure. Also the ignition distance has a strong influence on the amplitude of the pressure load. Figure 25 right summarized the investigated maximum overpressure for different ignition distances, the pressure is measured reflected in 50 cm distance to the jet axis. The mean duration of the positive pressure phase amounts to approximately 1.5 ms in the low and high pressure cases. The maximum measured amplitudes of the pressure waves for the vessels investigated in experiments with initial pressures of 5 bar and 16 bar are plotted against the distance perpendicular to the jet axis in Figure 26. In the low pressure case the maximum measured side-on overpressure amplitudes at a distance of 40 cm to the explosion origin were between 24 and 120 mbar.

A free jet that is ignited early and close to the nozzle generates the maximum thermal load for its ambience. The combustion duration of the released hydrogen lies in the range of the effusion times. Important thermal loads were only detected on the jet axis and due to the strong transient conditions measured as integral heat flux. The maximum integral heat flux measured on the jet axis decreases almost linearly with increasing distance to the nozzle. Close to the nozzle thermal loads of 240 kJ/m^2 (initial pressure 5 bar; released H_2 =48 dm^3 [NTP]) to 22 kJ/m^2 (initial pressure 16 bar; released H_2 =4 dm^3 [NTP]) were measured for the low pressure case. For initial high pressure release a maximum value of 300 kJ/m^2 (initial pressure 200 bar, 4 mm nozzle, released H_2 =72 dm^3 [NTP]) was measured. Figure 27 shows the critical distance to the nozzle for possible second degree burns of human skin for both cases.

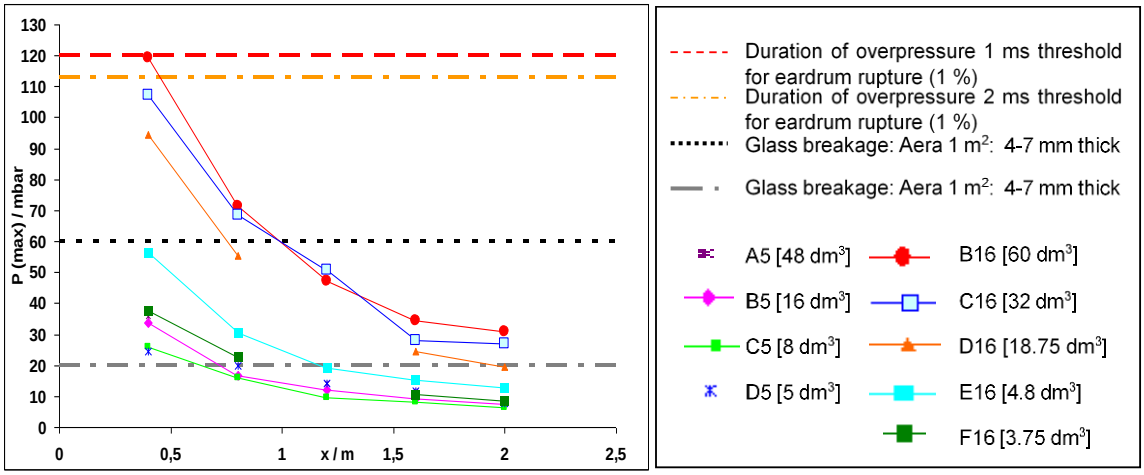

Figure 26. Hazard potential due to peak overpressures from ignited hydrogen releases from the vessels with an initial pressure of 5 and 16 bar (Grune et al., 2011).

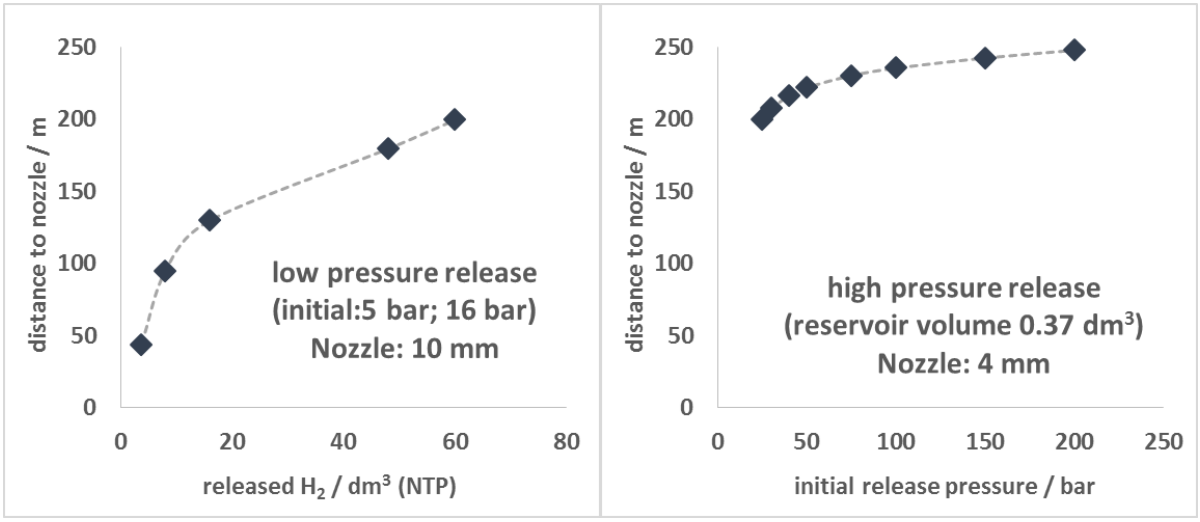

Figure 27. Critical distance to the nozzle for possible second degree burns of human skin (Grune et al., 2011, 2014).

The knowledge of accidental unsteady hydrogen release with subsequent ignition contains a lot of open questions. The main hazard potential, relevant to tunnel safety, is the possibility of triggering a post-crash-fire due to the unsteady hydrogen release.

3.2.5 Hydrogen jet fires in a tunnel (UU)

Tunnels are provided with natural or mechanical ventilation. Several studies have been conducted on the effect of ventilation on hydrogen unignited releases. Fewer studies were performed on the effect on hydrogen jet fires. Wu (2006) analysed the thermal effects and potential back layering of heat and combusted gases. The latter phenomenon describes the scenario in which the smokes produced by a fire may move in direction opposite to the main stream of the flow imposed by the ventilation system. Two releases with mass flow rate equal to 0.1 and 0.5 kg/s were investigated through numerical simulations. A ventilation velocity of 2.5 m/s was imposed 40 m upstream the release point in the tunnel with a 5x5m cross section. It was found that the back-layering effect was eliminated for the 0.1 kg/s release, which was characterised by a heat release rate of 6 MW. However, in the case of the larger release (0.5 kg/s), characterised by a heat release rate of 30 MW, back layering effects were observed up

15 m upstream the release point. Furthermore, the flame impinging on the ceiling, spread underneath it, covering 45 m. The 0.5 kg/s release had a release velocity of 50 m/s. Further research should be conducted for releases in realistic scenarios, characterised by storage pressures up to 700 bar and supersonic velocities at the nozzle. Furthermore, the studies did not include contribution of hydrogen combustion to automobile fire. This scenario will be further developed and discussed in Chapter 3.5.

3.2.6 Structural response to hydrogen jet fires (DTU)

Contrarily to people, structural elements are less affected by smoke and temperatures of local fires, i.e. fires that are in a growing phase and have not heated the surroundings to temperatures higher than 300-400 °C. Therefore, local fires are not generally considered in structural fire safety design, where post-flashover fire models such as standard or hydrocarbon fire curves are generally used as design fires.

However, such assumption is not always conservative. An example is provided by traveling fires (Law et al., 2011). Traveling fires are local fires which moves by consuming a limited part of combustible at a time. They are often visible in large compartments with well-distributed fuel load, such as open-offices, but also car parks and well-ventilated tunnels, where flashover temperatures can hardly be obtained, but a slow spread of the fire from one combustible item to the next one is possible. Since the very long duration of traveling fires makes up for the low fire temperatures, the structural elements get significantly heated and become subjected to degradation of the mechanical properties and possibly to structural failure or collapse.

Another example is provided by the opposite type of thermal solicitation, i.e. a short but very intense flame, as would happen for hydrogen, which is impinging the structural elements. Both steel and concrete elements are negatively affected by such rapid local heating, as explained in paragraph 3.2.6.2 and 3.2.6.3 respectively. Furthermore, the effect of high-pressure hydrogen jet fires on the erosion of tunnel road materials and lining materials is not well understood and further experimental investigations should be conducted.

3.2.6.1 Fire resistance rating (DTU)

The fire resistance of concrete and steel elements is done according to the EURO code requirements. Different scale furnaces are used that simulate post flashover situations to test the fire resistance (R), the integrity (E) and the insulation (I) of a component. The tests provide times and the components are labelled as REI30, REI60, REI90, REI120 according to the time they can last the impact of the standard fire curve ISO 834.

The ISO 834 curve (cellulosic fire curve) defines a minimum standard fire resistance often used for the testing of building components:

$$T(t) = 20 + 345 \log_{10}(8\,t + 1), \tag{3.18}$$

where T is the temperature (°C) and t is the time (min). The Hydrocarbon Curve (HC) is applicable for industrial and off-shore plants reaching 1100 °C. A modified version (HCM) is developed for tunnels reaching a maximum temperature of 1300 °C:

$$T = 20 + 1080(1 - 0.325 * e^{-0.167\,t} - 0.675e^{-2.5t}) \tag{3.19}$$

The Rijks Water Staat (RWS) design fire curve is developed for tunnels reaching 1200 °C in 10 min and 1370 °C in 1 hour. Afterwards, it cools down to a steady level of 1200 °C in 2 hours.

The Eisenbahn Bundesamt (EBA) defines a design curve for railroad tunnels reaching 1200 °C in 5 min.

Parametric design fires are another approach including also cooling phases into the design fire curve:

$$T = 20 + \frac{345 \log_{10}(8\,\Gamma t+1)}{1+0.04\left(\frac{t}{t_d}\right)^{3.5}} \quad \text{with} \quad \Gamma = \frac{\left(O/b\right)^2}{(0.04/1160)^2}, \tag{3.20}$$

where b is the thermal inertial of the compartment and O is the opening factor of the compartment. They can be calculated as:

$$b = (\rho\, c_p\, \lambda)^{0.5} \quad \text{and} \quad O = \frac{A\sqrt{h_{ave}}}{A_{total}}, \tag{3.21}$$

where ρ, c_p, and λ are the density, specific heat capacity and conductivity of the enclosure, respectively, A is the total area of the vertical openings in the compartment, h_{ave} is the average height of the openings weighted by the area of each opening, A_{total} is the total area of the enclosure (i.e. the sum of the wall, ceiling, and floor surfaces).

t_d in eq. (3.20) is the end time of burning and is calculated as:

$$t_d = 7.80 \cdot 10^{-3} \cdot q/O \text{ (in minutes)} \quad \text{with} \quad q = \frac{Q}{A_{tot}}, \tag{3.22}$$

where q is the fuel load density of the compartment.

3.2.6.2 Integrity of steel elements (DTU)

Steel has a high thermal expansion coefficient and is known to expand significantly during fire. The expansion of the structural elements would not be a problem per se, as no limitation on the displacements must be respected during fire, as long as the stability of the structure is ensured. However, due to redundancy of the structural system, structural elements are rarely completely free to expand and “eigen-stresses” arise in the element as a consequence of the hindered expansion.

In case of design with standard or hydrocarbon fire, the Eurocodes do not require the explicit consideration of such indirect stresses (EN 1993-1-2, 2005). Although such simplification has been proven to be non-conservative, it is motivated by the fact that, during a flashover fire, all structural elements are exposed to the same thermal solicitation and heated to similar temperatures. As such, the stiffness of the hindering elements is also reduced (e.g. the flexural stiffness of a column hindering the expansion of the supported beam) and the eigen-stresses that arise in the expanding element are limited.

This is not the case, when an impinging flame heats only one element or a part of an element. In this case, the cold part retains its nominal stiffness and higher eigen-stresses arise in the heated part, while its mechanical properties degrade rapidly. This may lead to early buckling of beam and columns and such failures may propagates to other elements (Gentili et al., 2013).

The proper consideration of hindered thermal expansion is not only important for steel buildings, but is of course paramount in case of highly restrained structures, such as columns of underground parking supporting continuous slabs, arch or truss bridges, vaults, and tunnels.

A different problem related to the exposure of steel structures to jet flames is related to the behaviour of the protective material. Steel elements are normally protected against fire by encasing the profiles with board panels (made of insulating materials such as calcium silicate, mineral fibres, etc.) or painting the surface with intumescent coatings (water-, solvent-, or epoxy-based). In particular, the use of intumescent coatings has been rapidly spreading in the last years, due to less encumbrance, a progressive drop in the prices, and increased performances of such paints in protecting steel profiles under testing conditions.

The testing standards are typically based on (ISO834-1, 1999) for water- and solvent-intumescent coatings used in buildings or hydrocarbon fire for epoxy-based intumescent coatings used in offshore structures or marine environment. However, research has shown that, contrarily to inert insulation, the behaviour of intumescent coatings is not only dependent on the temperature, but also on the heating rate and fire conditions (Lucherini et al., 2018). This means that the fire protection offered to the steel by the intumescent coating in a real fire may be different, and in some cases overestimated, with respect to the value assessed by testing.

Hydrogen fire in particular could expose the coating to very rapid heating regimes and require special consideration in the choice and dimensioning of the fire protection. Although some producers provide special paints to be used against jet fires, the behaviour of such paints under different heating regimes is still under research (Tolstrup et al., 2019) and, at present, it does not seem possible to ensure the same safety of painted elements under different types of fire.

It is particularly important to fill this knowledge gap for structures such as car parks and tunnels, where the fire protection can be exposed to car fires. Due to the nature of the different materials progressively involved in the fire, to the possible traveling nature of the fire, and to the presence of gasoline- and hydrogen –fuelled vehicles, such fires may expose the structure to quite different heating regimes. It is therefore of interest to assess whether or to which extent intumescent coatings aimed at protecting car park and tunnel structures from car fires can also be effective against hydrogen fires. To this purpose, experimental data could be gathered on different type of intumescent paint exposed to radiant heat and jet fires. Furthermore, thermo-gravimetric analysis of the paint could be undertaken, in order to assess the role played by the different chemical components and understand the causes of a possible different response of the coatings to various heating regimes.

3.2.6.3 Integrity and concrete spalling (DTU)

Concrete is a mixture of a cement paste and an agglomerate (see What is concrete?). Cement when mixed with water gives a chemical reaction and provides a paste that sets and hardens to bind the agglomerates in the concrete. The cement is made by heating a mixture of limestone, sand or clay (silicone), bauxite (aluminium) and iron ore constituting the major components. (see What is cement?). Different agglomerates are used providing various types of concrete. Normal concrete is defined having a compression strength < 60 MPa, high strength concrete can take compressive stresses >80 MPa, while ultrahigh-strength concrete is stable to compressive stresses >150 MPa. The difference is mainly that the pores of normal concrete are more and more filled with small particle agglomerates providing the additional strength. This

has implications on the reaction to fire behaviour. For normal concrete, the ratio ξ(T) of e.g. compression stress at a temperature T to the stress at T=20 °C is given as:

$$\xi(T) = k + \frac{1-k}{1 + \frac{T}{T_1} + \left(\frac{T}{T_2}\right)^2 + \left(\frac{T}{T_8}\right)^8 + \left(\frac{T}{T_{64}}\right)^{64}} \tag{3.23}$$

The approach is also valid for calculating the temperature dependence of steel tensile stresses (Hertz, 2019). T is the temperature in °C and T_n are coefficients to describe the temperature dependency of the e.g. compressive stresses to concrete. The coefficient k is the ratio between max and min value of a material and is k=0 for concrete. Figure 28 shows an example of the variation of compression stresses ratio as function of temperature for normal concrete. The curve HOT for normal concrete describes the strength loss during the time of exposure to the fire. The sequent cooling phase provides additional damage to the concrete over a period up to a week. The COLD curve is therefore showing a steeper profile. A rapid heating leads to a faster loss of strengths. Thus, after a tunnel fire special care needs to be taken to observe, secure the structure and avoid further post-fire damages.

The reason is the damage mechanism of concrete. Under heating water vapour in the pores and crystal water in the cement are released resulting in shrinking of this cement phase. The aggregates in contrary expand with heat giving raise to tensile stress in the concrete. After the end of the fire the release of water can be reverted and the concrete may recover. Nevertheless, starting at a temperature of about 300 °C concrete will start forming micro cracks and the strength is lost permanently. After the fire such heated calcium in the concrete will react with water to produce calcium hydroxide crystals. These may work as jacks and widen the cracks in the concrete, making it further lose strength in the cooling phase of a period of up to a week after the fire. At 500 °C large cracks may be observed. At 700 °C the concrete has lost most of its strength and no strength is left at 800 °C. This description is valid for unstressed concrete, as stresses counter act the development of cracks pushing the effects to somewhat higher temperatures. It is also seen that rapid heating give rise to faster loss of strength. This needs to be investigated more in relation to hydrogen jet flames impinging tunnel walls. Russian heat resistant concrete shows a better temperature performance until it melts at about 1300 °C.

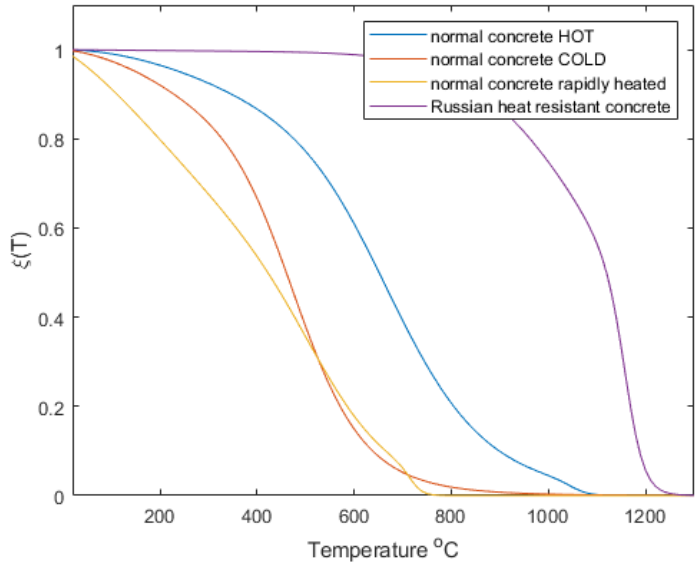

Figure 28. Ratio of compression stress ξ(T) as function of temperature for normal concrete.

Experimental tests to investigate the tunnel lining reaction to fire were performed by Wang et al. (2017). The tests were done with and without additional layer of fire resistant coating. The authors observed concrete spalling in all the tests. The concrete lining without the fire resistant coating showed only minor damage. The measured temperatures of the concrete for the lining without the fire resistant coating were observed to be only a little higher than for linings with a fire resistant coating. However, for the latter a thermal hysteresis was observed, which may be beneficial to mitigate a fast and severe temperature rise, and to possibly prevent potential spalling. Wang et al. (2017) concluded that for typical tunnel fires with smoke temperature below 600 ^{o}C a fire resistant coating is unnecessary. However, further analysis may lead to different conclusions when dealing with fires involving hydrogen.

Explosive spalling is a process where the water in the concrete is heated to vapour inside the material leading to its explosive rupture. It could easily be observed in high or ultra-high strength concrete with a minimum amount of pores. The reinforcement with propylene fibres is found to have a mitigative effect on spalling (Hertz, 2002; Hertz and Sørensen, 2005; Fletcher et al., 2007; Ozawa and Morimoto, 2014; Sýkora et al., 2018).

Explosive spalling of concrete is of concern as it is a violent process and may destroy a structure or cross section. The factors that lead to this phenomenon are reviewed by (Hertz, 2019) as cited in Figure 29. Hertz also found that circular tunnels are more susceptible to explosive spalling than immersed tunnels. The former hinders thermal expansion of the inner surface by the circular shape, while the latter typically provides very thick walls in a non-circular shape to counter act buoyancy while placed under water. This type of construction does not necessitate use of high-strength concrete.

Guidelines to explosive spalling and proper design:

- Explosive spalling of ordinary concrete may occur as spalling of the corners of wet or fresh elements or the sides of wet structures within the first 20 min of a standard fire. As far as possible, bevelled edges should be used [..].
- Concrete appears to be safe from explosive spalling if it has a strength of less than 60 MPa and moisture content less than 3% by weight. The structure should be designed to ensure that the moisture content will not exceed 3%.
- High-strength concrete (>89 MPa) with compressive stresses or hindered thermal expansion usually has a pore structure that makes it susceptible to explosive spalling.
- Ultra-strength concrete (>150 MPa) may spall explosively also if it has no hindrance to thermal expansion.
- If high strength concrete is applied, it should be placed in the cross-section of the structure so that it cannot be heated to more than 350 ^{o}C during a fully developed fire.
- Fibre reinforcement (e.g. polypropylene fibres) may reduce the risk of explosive spalling, especially in tension zones.
- Dry and porous light aggregate concrete with open pores in the matrix surrounding the aggregates does not usually suffer from explosive spalling. Therefore, porous light aggregate concrete can be used to insulate high-strength

Figure 29. Guideline to explosive spalling and proper design (Hertz, 2019, pp. 231–232)

In conclusion, it has been showed that structural integrity of tunnel walls and lining is generally designed and tested for specific time-temperature curves for a fire exposure expected with conventional vehicles. Exposure conditions may be significantly different when dealing with hydrogen jet fires. Further experimental work is needed to assess the integrity of structures exposed to hydrogen fires and determine novel design criteria. A coupled CFD/FEM modelling may greatly support this assessment, providing insights into the structural response to the thermal effects in confined spaces.

3.3 Hydrogen explosions (UU)

The release of hydrogen following an accident in a tunnel or another enclosed space may lead to the formation of a flammable mixture. An ignition of such flammable hydrogen-air cloud may lead to “combustion explosion”, which could be either deflagration or detonation, generating pressure effects presenting a threat to life and property. Deflagration propagates with the velocity below the speed of sound (sub-sonic) in the unburned mixture, while detonation propagates with the velocity above the speed of sound (super-sonic). In the latter case the shock and flame fronts are coupled. The speed of detonation wave depends on a composition of hydrogen-air mixture. In stoichiometric mixture it can be as high as 2000 m/s. The safety of hydrogen automotive applications and the related infrastructure, including garages, maintenance workshops, underground parking, and tunnels, is a main area of concern.

Deflagrations in the open, in the absence of any obstacles, could generate overpressures (pressure above the atmospheric one) of about 10 kPa, which is about the threshold of overpressure to which civil structures could withstand. Deflagrations in the enclosures and/or confined spaces could lead to more significant overpressures up to about 0.7 MPa in strong closed vessel. Deflagration in an enclosure can be mitigated by venting, the most cost-effective and widespread explosion mitigation technique. Detonation cannot be mitigated by venting technique and is characterised by higher overpressures, ranging up to approximately 1.5 MPa.

Vehicles in a tunnel or other structure in an enclosed space may significantly affect the combustion and pressure dynamics. Numerous experimental and numerical studies on an obstructed even small-scale tube showed that reflection of a developing shock on obstacles and associated flame instabilities, including Rayleigh-Taylor and Richtmayer-Meshkov instabilities, may lead to deflagration-to-detonation transition, see for example insights into the process in numerical study (Gamezo et al., 2007).

A deep understanding of combustion and pressure dynamics is required to assess accident consequences for public, emergency personnel of underground transportation infrastructure and property, including vehicles and structure itself. These encompass understanding of thermal and pressure effects. Thermal effects include contact with the burning matter, exposure to high temperature combustion products and radiative heat flux. Pressure effects include overpressure and impulse from the blast wave. Later may direct impact people and property, or indirectly by projectiles. Furthermore, drivers in tunnels will be likely located in vehicles. In case of small blast overpressures this circumstance may attenuate the direct pressure effects of the blast, yet may lead to secondary injuries due to windows glass breakage or the activation of airbags. The latter eventuality was observed in the accident happened in Sandvika, Norway, in June 2019 (the accident at hydrogen refuelling station is under investigation). No fatalities or major injuries were reported. However, two drivers suffered injuries caused by the inflation of the airbags because of the blast impact (NewsinEnglish, 2019).

3.3.1 Deflagration (UU)

A release of hydrogen in a tunnel or any other confined space will lead to formation of a flammable cloud of different size depending on release parameters. The cloud may be close to uniform but most probably it will have non-uniform distribution of hydrogen in air. The consequences of deflagrations in uniform hydrogen-air mixtures are discussed in section 3.3.1.1. The flammable cloud is expected to be in the jet area (flammable envelope) and at some circumstances it can accumulate beneath the ceiling. This hydrogen-air layer under the ceiling is most likely to have a stratified concentration. The consequences of non-uniform mixture deflagration for this scenario are presented in section 3.3.1.2.

3.3.1.1 Uniform hydrogen-air mixture deflagration (UU)

Groethe et al. (2007) conducted experiments in a 78.5 m long tunnel with section equal to 3.74 m^2. The tunnel represents approximately $1/5^{th}$ scaled real tunnel for vehicles. Facility and dimensions are showed in Figure 30 (left). The uniform hydrogen-air mixture occupied 35 m^3 volume at the centre of the tunnel and it was contained within plastic barriers that were cut prior to ignition. The content of hydrogen varied in different experiments in the range 9.5-30%. The 9.5% mixture was unable to produce a pressure high enough to be sensed at the pressure probes. On the other hand, the 20% hydrogen mixture resulted in an overpressure of 35 kPa throughout the length of the tunnel without pressure decay with distance. The maximum pressure measured at the end of the tunnel increased to 150 kPa for the mixture containing 30% of hydrogen by vol. This value is 15 times the maximum overpressure recorded for an equivalent unconfined test. It is more than 100 times higher than “no harm” threshold for humans of 1.35 kPa. One of key conclusions from this experimental programme that blast wave propagating in a tunnel is practically not decaying with distance. Thus, all should be done that a system vehicle-structure does not create such size of flammable cloud that can deflagrate.

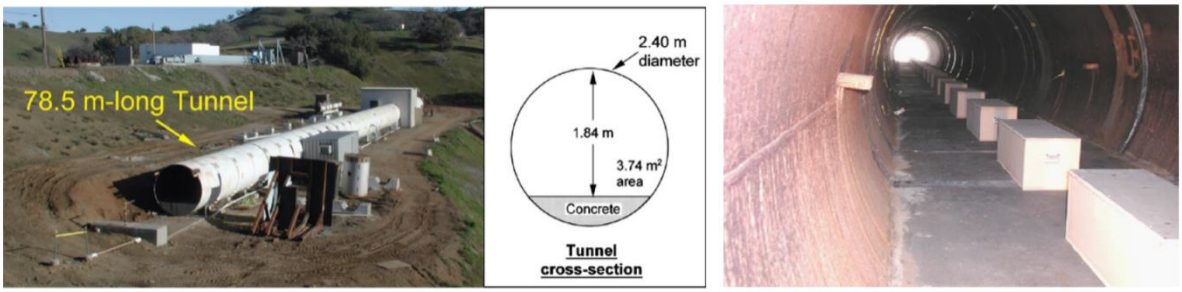

Figure 30. Tunnel facility (left) and placement of mock vehicles for test with obstacles (right) (Groethe et al., 2007).

Tests in conditions of partial confinement were performed by Groethe et al. (2007) to assess the possibility of deflagration enhancement. Such conditions were recreated by igniting the mixture within two aluminium plates separated by a 10 mm gap. The authors did not observe any increase in the flame speed. The measured overpressure was approximately the same or slightly lower than the case without the two aluminium barriers.

Groethe et al. (2007) conducted additional tests with the presence of mock vehicles inside the tunnels, placed as shown in Figure 30 (right). The overall areal blockage ratio was 0.03. Experimental dynamics of overpressure and impulse is given in Figure 31. Results are compared to the test without obstacles and they showed that the vehicle presence did not produce any significant effect on the pressure dynamics. The authors suggested that this may

be due to the low blockage ratio. The resulting overpressure may change for higher blockage ratios, which could be given by the presence of trucks or buses in a tunnel. Therefore, further investigations should be conducted to asses overpressure in such conditions.

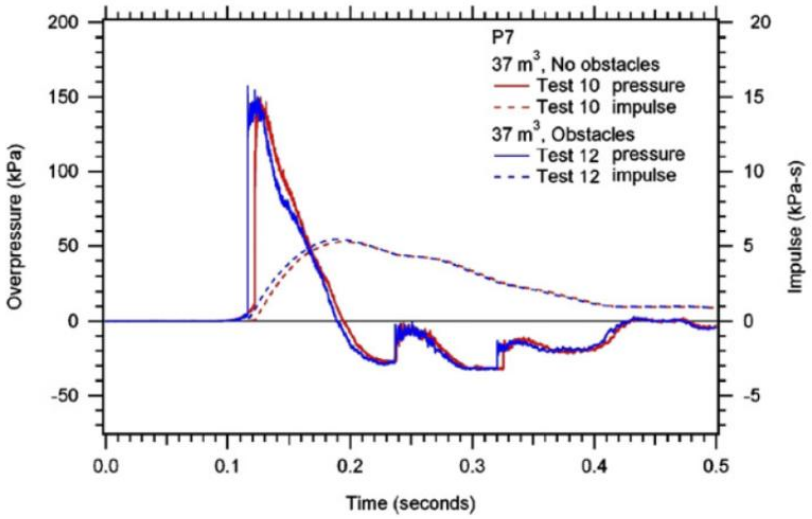

Figure 31. Pressure and impulse measurement towards the end of the tunnel for tests with and without mock vehicles (Groethe et al., 2007).

Groethe et al. (2007)'s deflagration tests in the tunnel were simulated numerically by Molkov et al. (2008). A LES model was employed, and it reproduced well the experimental data. Simulations also provided insights into the dynamics of flame propagation and pressure build-up inside and outside the tunnel. It was observed that for the case including obstacles, the explosion overpressure on the side surface of the obstacle was significantly higher than the overpressure at the ceiling. The difference increases with the distance from the ignition point, due to more steeper leading front of the blast wave transforming with distance to the shock and thus larger reflected on the obstacle pressure. The maximum overpressure was practically the same along the tunnel (~140kPa). Fatality and serious injury to people and damage to structure is expected at such pressures. Outside the tunnel, the maximum overpressure decreased to 5 kPa in less than 1 m. The flame front reached the tunnel exit in 270 ms. The flame was observed to accelerate in an initial stage and decelerate afterwards at 85 ms. The shock wave reached the tunnel exit in 131 ms and a rarefaction wave propagated inside the tunnel immediately after. This wave caused the flame front to accelerate again until it reached the tunnel exit.

Similar conclusions on the blockage ratio for deflagration tests in tunnels by Grothe et al. (2007) were achieved by the same authors for uniform hydrogen-air mixtures contained in a 300 m^3 tent placed in the open atmosphere. Hydrogen content was in the range 15-30% by volume. Cylindrical obstacles with diameter and height 0.46 m and 3 m, respectively, were placed in the centre of the cloud. This scenario may be representative of a semi-confined space such as a refuelling station. The authors compared the resulting deflagration overpressure against a case without obstacles. They concluded that there was no enhancement of deflagration. This is contrary to a smaller scale experiment with the same volume blockage ratio (Groethe et al., 2002). The authors indicated that a possible reason may be due to the dimension of the obstacles, which may be large enough to not induce a significant level of turbulence into the mass flow (0.46 m), opposite to the 2.1 cm pipes used in the small-scale experiments.

3.3.1.2 Localised uniform and non-uniform hydrogen-air mixture deflagration (UU)

A release of hydrogen in a tunnel or any other confined space may lead to the formation of a flammable cloud beneath the ceiling. This layer is likely to be stratified, i.e. it will have a concentration gradient along the vertical direction. The thickness of the stratified layer is function of the released mass of hydrogen and the geometry of the enclosed space. Another example of inhomogeneous mixture is given by the formation of gas "pockets", leading to the creation of a so-called localised mixture. Deflagration in a mixture with a hydrogen gradient may be more dangerous in sense of generated overpressure than a uniform mixture deflagration containing the same amount of hydrogen (Whitehouse et al., 1996).

Uniform localised mixture deflagration in closed space

Makarov et al. (2018a) developed a thermodynamic model to calculate the maximum overpressure from localised uniform mixture deflagration in a closed space. The model assumes two stages of combustion, which are shown in Figure 32. The first stage is an isochoric combustion. Afterwards, the combustion products expand adiabatically. Threating the gas as ideal, the authors derived eq. (3.22) for the final deflagration overpressure:

$$p_2 = \Phi\, p_{b1} \left(\frac{p_2}{p_{b1}}\right)^{\frac{\gamma_b - 1}{\gamma_b}} (1-\Phi)\, p_0 \left(\frac{p_2}{p_0}\right)^{\frac{\gamma_{air}-1}{\gamma_{air}}} \tag{3.24}$$

where Φ is the flammable volume fraction, p is the pressure at the stages described in Figure 32 and γ is the specific heat ratio.

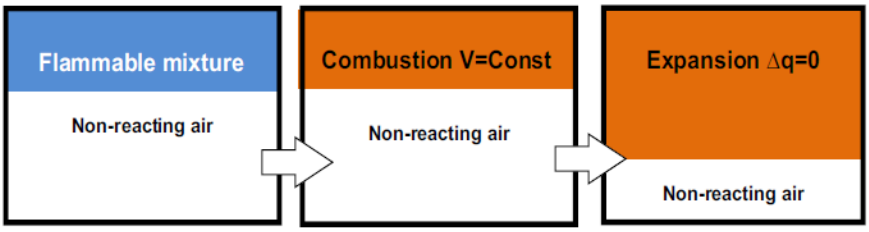

State "0": Initial state	State "1": Combustion V=Const	State "2": Expansion Δq=0
Initial state: T_0, p_0 Fuel-air mixture: m_m, M_m, V_{m0} Air: m_{air}, M_{air}, V_{air0}	Burnt mixture: m_b, T_{b1}, p_{b1} Air: m_{air}, M_{air}, T_0, ps_0	Final state of burnt mixture: T_{b2}, p_2, m_b, M_b, V_{b2} Final state of air: m_{air}, M_{air}, T_{air2}, p_2

Figure 32. Schematic problem formulation for localised deflagration in a closed space (Makarov et al., 2018a).

The burnt mixture pressure after combustion in a constant volume(p_{b1}) is not known in advance and any suitable technique to find it may be applied. The authors (Makarov et al., 2018) demonstrated two methodologies to retrieve p_{b1} value. The first procedure derives the equation to calculate temperature T_{b1} and pressure p_{b1} at the state 1 based on the internal energy conservation equation in the isochoric combustion process and a single step reaction assumption:

$$T_{b1} = \frac{T_0\left(c_{pb} - R/M_m\right) - \Delta h_c}{c_{pb} - R/M_b}, \tag{3.25}$$

$$p_{b1} = p_0 \frac{M_m\, T_{b1}}{M_b\, T_0}, \tag{3.26}$$

where Δh_c is the hydrogen heat of combustion. The second methodology used thermodynamic equilibrium model implemented using GASEQ software to find the burnt mixture temperature and pressure for a constant volume process. Both techniques provided very close solutions with temperature difference within 1% and pressure difference within 3.3% maximum (in the range from LFL to stoichiometric mixtures).

The thermodynamic model was compared against experiments by Stamps et al. (2009) for the hydrogen-air ratio of 0.997 and the flammable volume fraction (Φ) in the range 0.469-0.878. In the first stage the experimental measurements for p_{b1} were used to calculate the maximum deflagration pressure p_2. The Ulster's model calculations agreed well with experimental measurements with a deviation of 13% for one test, whereas it was within 6% for the remaining 5 tests. Ulster's model results showed a reduced scattering from experimental measurements compared to the model suggested in Boyack et al. (1993). In the second stage, equation (3.26) was used to calculate the burnt mixture pressure p_{b1} independently from experiments. The analytical solutions for p_{b1} and p_2 resulted in pressures higher than experiments, due to the assumption of an adiabatic combustion whereas in reality heat losses were present in the experiment. However, predictions were conservative, and it was concluded that the thermodynamic model can be used as engineering tool for hydrogen safety.

The developed model was used to calculate the maximum possible hydrogen inventory which deflagration in a closed space, such as a warehouse, will be non-destructive. The study considered a maximum overpressure of 10 kPa, as a typical threshold value for structural damage to civil buildings. The authors found that the non-destructive limit for deflagration overpressure (i.e. 10 kPa) will be generated from combustion of localised 4% hydrogen-air mixture occupying only 7.9% volume fraction of the sealed (no vents) enclosure. This corresponds to the averaged through the whole volume concentration below 0.31% of hydrogen by volume - much below 4% of LFL.

The above solution was presented as an engineering correlation for the maximum amount of hydrogen (kg) allowable to be released in an enclosure of volume V (m³) without vents and not to exceed 10 kPa overpressure in case of its deflagration:

$$m_{H2} < 2.61 \cdot 10^{-4}\, V. \qquad (3.27)$$

One should keep in mind that this 10 kPa threshold is a generic value and smaller overpressure values may be found in literature for lower damage levels, e.g. of 4.8 kPa is suggested in Baker et al. (1983) and Mannan (2005) to avoid minor damages to structures. As realistic enclosures are likely to leak, which is not considered in the model, the developed model is expected to provide conservative predictions.

Vented deflagration of non-uniform localised mixture

In the case of vented deflagration, the pressure increase due to combustion will be counterposed by the pressure decrease due to the outflow of gases through the vent. Makarov et al. (2018a) elaborated a model for localised vented deflagration following theory by Molkov (1996). The model is based on the volume conservation in the enclosure and the equation of mass flow rate for the sub-sonic release through the vent, additionally to the mass conservation for burnt and unburnt mixture and the equation for conservation of internal energy. The correlation for the non-dimensional pressure $\Delta\pi = p/p_i$ is given as:

$$\Delta\pi = \left(Br_t^{-B}\sqrt{\frac{E_i}{2}}\right)\cdot MIN\left\{1.0;\ \left[E_i^{2/3}\left(\frac{1+\left(\frac{1}{\varphi}-1\right)\frac{M_{air}}{M_f}}{1+\left(\frac{1}{\Phi\varphi}-1\right)\frac{M_{air}}{M_f}}\right)^{2/3}\right]^2\right\}, \quad (3.28)$$

where Br_t is the turbulent Bradley number, B is a coefficient, E_i is the combustion products expansion coefficient, Φ is the volumetric fraction of localised flammable fuel-air mixture in enclosure and φ is the volumetric fraction of fuel in localised fuel-air mixture. The term in parenthesis is additional to traditional correlation for vented deflagration of uniform mixture fully occupying an enclosure and it represents the contribution due to the localised mixture instead. A detailed description of the model and its derivation is given in Makarov et al. (2018a).

The authors concluded from their theoretical analysis that the maximum overpressure of a localised vented deflagration is defined by a small fraction of the non-uniform mixture with the highest burning velocity and the largest expansion coefficient, whereas contributions of slower burning parts of flammable mixture to the vented deflagration overpressure are expected to be negligible. In order to be applied to non-uniform mixtures, correlation (3.28) needs to consider the volume fraction of the fastest burning flammable mixture responsible for the pressure build-up, Φ*. The correlation was applied to experiments performed at KIT (Germany) and HSL (UK) on vented deflagration of uniform and non-uniform hydrogen-air flammable layer in an enclosure from medium to large scale (Kuznetsov et al., 2015; Hooker et al., 2017). The best fit was found for a burning velocity taken as 95-100% of the maximum burning velocity of the mixture in the enclosure, which in most cases will be under the ceiling. The derived correlation reproduced the experiments with a reasonable engineering accuracy for such complex phenomenon.

Deflagration of non-uniform localised mixture in a tunnel

Groethe et al. (2007) investigated the combustion of accidental hydrogen releases in a 78.5 m long tunnel. Two tests were performed on the release of 0.1 kg of hydrogen in 20 s at the centre of the tunnel. Concentration measurements showed that the mixture was lean prior to the successful ignition. However, pressure was lower than the instruments capability, preventing its measurements. A second set of tests was performed on releases of 0.1 kg and 2.2 kg of hydrogen in 20 s and 420 s respectively. The release point was located toward one end of the tunnel, which had a forced ventilation rate of 1.6 m^3/s. for both releases, the mixture failed to ignite, in spite of a recorded concentration higher than LFL.

Bie & Hao (2017) investigated the explosion overpressure produced by the ignition of a hydrogen release from a 6 mm TPRD of a 70 MPa onboard storage in a subsea tunnel with dimensions WxHxL=13.5x5x500 m. Hydrogen distributions prior to ignition (3.1 s) are presented in Figure 14 and Figure 15. A maximum overpressure of 11 kPa was recorded at 5 m from the vehicle. When a ventilation rate of 6 m/s was applied in the tunnel, the overpressure recorded in the flow direction was slightly affected by the ventilation rate, whereas the overpressure upstream the vehicle reduced by 30% at both 5 and 10 m. If the mixture was ignited after 6.1 s the maximum recorded overpressure at 5 and 10 m increased to 13 kPa for the case without ventilation. When ventilation was included in simulations (6 m/s), pressure in downstream direction recorded a slight decrease to 12 kPa at 10 m, whereas it remained

unvaried at 5 m. Similarly to the case with ignition after 3.1 s pressure upstream the vehicle decreased by approximately 30%.

Further experimental and numerical studies should be conducted on the deflagration of non-uniform hydrogen-air clouds in tunnels, e.g. assessing the effect of the tunnel geometry (horse-hoe or rectangular), the effect of vehicles presence, etc.

3.3.2 Deflagration-to-Detonation Transition (KIT)

The criteria for Deflagration-to-Detonation Transition (DDT) are based on a shock tube experiments. The DDT criteria were mainly developed for enclosed geometry with a uniform concentration of hydrogen in oxidiser (air or oxygen). Since the detonation is the shock driven exothermic reacting front, propagating steady-state with a velocity higher than speed of sound, it needs to provide transient conditions for flame acceleration from laminar to sonic velocity with formation of a complex "shock wave – reaction zone" propagating in a stationary manner with so-called Chapman-Jouguet velocity.

Being ignited, the deflagration flame front propagates as a piston producing a flow ahead the flame surface. The flow, in turn, produces a turbulence leading to further flame acceleration. Depending on flame acceleration law, a precursor shock wave can be formed at some distance from flame surface (Landau and Lifshitz, 1989). Typically, the strength of precursor shock wave can be in the range Mach number M=1.2–1.7. Such weak shock cannot initiate the detonation. Then, if efficient flame velocity reaches or exceeds the speed of sound, a sequence of secondary advanced shock waves may collapse into a local explosion leading to detonation, preferentially at the sidewall or exactly at the flame surface. Rough walls and obstructions may promote the detonation onset and shorten the run-up-distance (RUD) to DDT. However, not each combustion process leads to detonation.

The critical conditions for DDT can be formulated as follows.

Detonability limits. For hydrogen-air mixtures, detonability limits should be at least within the flammability limits 4-75% vol of hydrogen.

Fast flame condition. The criteria are based on expansion ratio σ, Zeldovich number β and Lewis number Le, that can be used to estimate a priori a potential for effective flame acceleration for a given fuel-air composition (Dorofeev et al., 2001). For hydrogen-air mixtures at ambient conditions the critical expansion ratio is given as:

$$\sigma^* = 3.75. \tag{3.29}$$

This corresponds to the mixture of 10.5% vol of hydrogen. For instance, the mixtures with hydrogen concentration below 10% will not be able to accelerate to the speed of sound due to flame instability and local flame extinction. No speed of sound means no detonation.

Spatial conditions. The space or characteristic dimensions for the system with potentially detonable composition have to be sufficiently large. Usually, the scale of detonable system is characterized in terms of dimensionless ratio L/λ of characteristic size L of the problem over the detonation cell size λ as a measure of detonability of the mixture:

$$\frac{L}{\lambda} > N^*, \tag{3.30}$$

where N^* is the critical value for detonation onset (DDT) or detonation propagation dependent on geometry of the system: linear tube or channel with rough or smooth walls; 2D-structure similar to a thin layer in between two solid plates; multi-chamber structure similar to a chain of rooms or a tube with obstacles; unconfined geometry (see Table 4). Most of practical cases are covered by so called 7λ criterion (Dorofeev et al., 2000), i.e. a ratio $L/\lambda>7$, based on large-scale experiments and theoretical analysis.

Table 4. Dimensionless scale for different processes.

Dimensionless scale, L/λ	Critical value N*, (-)	Detonation relevant phenomenon	References
d/λ	1	Detonation propagation in obstructed tubes with orifice size d (BR*<0.43)	Teodorczyk et al., 1988
L/λ	7	Detonation onset in obstructed tubes	Dorofeev et al., 2000
L/λ	7	Detonation onset in multi-chamber structure	Dorofeev et al., 2000
d/λ	24-65	Jet-initiation of detonation in unconfined cloud with jet orifice size d	Bezmelnitsyn, 1998
L/λ	>1000	Detonation onset in unconfined cloud with a size L	Khokhlov et al., 1997

*Note: Blockage ratio is $BR=1-d^2/D^2$, where D is the inner tube diameter; d is the obstacle orifice size.

Detonation cell size λ is the characteristic size of cellular pattern produced on a sooted plate by triple points of collided transverse waves occurred during the detonation process. Detonation cell size is the measure of mixture sensitivity. The less the detonation cell size is, the more easily the mixture can detonate. Detonation cell size can be measured experimentally or calculated using a chemical kinetics mechanism and an assumption about gas dynamic nature of detonation cells (Gavrikov et al., 2000). Table 5 shows the calculated detonation cell sizes for hydrogen-air mixtures at normal conditions (T=293 K, P=1 bar).

Table 5. Calculated detonation cell sizes for hydrogen-air mixtures at ambient conditions.

Hydrogen concentration, % vol	Detonation cell size λ, mm	Hydrogen concentration, % vol	Detonation cell size λ, mm
9	18040	29.586	9.8
10	5095	30	9.7
11	2319	35	9.7
12	1289	40	11.9
13	798	45	16.8
14	531	50	27.3
15	361	55	57.4
16	252	60	148
18	114	65	362
20	44.6	70	930
22	24.6	75	2957
25	14.5	80	21230

Integral scale. Run-up-distance (RUD) to DDT. The importance of conditions associated with a required level of turbulence due to high enough flow velocity and strength of precursor shock wave is well-known. It was experimentally found time ago that the ratio of length over the channel diameter L/D=20–40 is required for detonation onset. Based on study by Kuznetsov et al. (2005), for smooth unobstructed channel the RUD required for DDT can be expressed as:

$L_D = 500\lambda$ (broad channels, $D/\lambda > 20$), (3.31)

$L_D = 25D$ (narrow channels, $10 < D/\lambda < 20$). (3.32)

If the channel size is very narrow ($D/\lambda < 10$) then the detonation may occur at shorter distance in a relatively short tube due to the shock–flame interaction of reflected precursor shock wave with a flame brush leading to Richtmayer-Meshkov instability and strong flame acceleration (Kuznetsov et al., 2017).

Of course, in presence of single or multiple obstacles blocking the channel, the RUD to fast sonic flame and DDT can be reduced due to the blockage of the channel and flow velocity increase (Veser et al., 2002). Figure 33 shows an effect of blockage on flame acceleration in dimensionless co-ordinates independent of mixture reactivity (Kuznetsov et al., 2002).

Depending on the blockage ratio (BR=1–d^2/D^2, where d is the orifice diameter; D is the channel cross-section), it needs only few obstacles spaced by a channel diameter to accelerate the flame to speed of sound or to detonation. The more is the blockage, the less will be RUD to fast flame or detonations, L_D:

L_D = (10-12)D (BR = 0.3) (3.33)

L_D = (3-4)D (BR = 0.6) (3.34)

L_D = (2-3)D (BR = 0.9) (3.35)

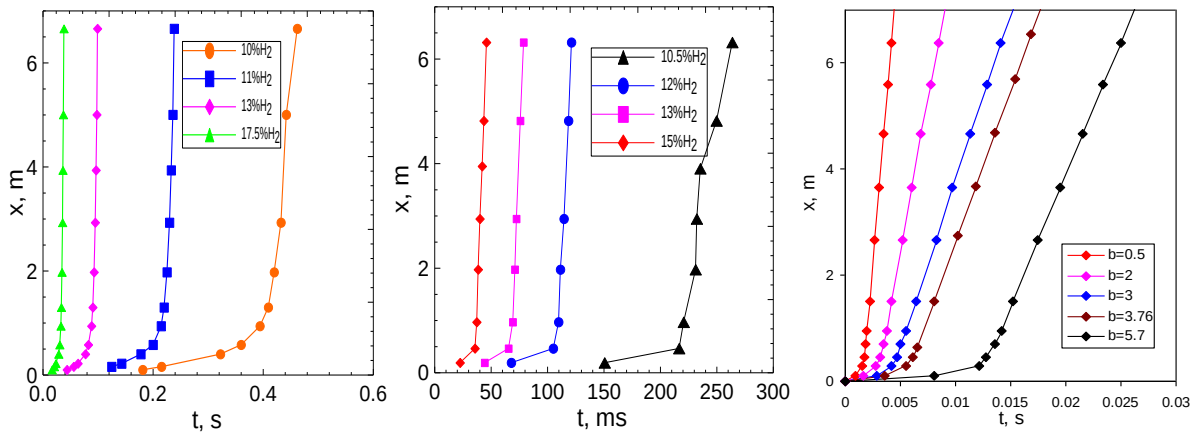

(a) (b) (c)

Figure 33. Distance-time (x-t) diagrams for hydrogen-air flame propagation in obstructed channel with different blockage ratios: (a) BR = 0.3; (b) BR =0.6; (c) BR = 0.9, b=[N_2]/[O_2](Kuznetsov et al., 2002).

3.3.2.1 Criteria for flame acceleration and DDT in a tunnel geometry (KIT)

All these afore mentioned conditions are still valid for specific tunnel geometry and can be considered as a worst-case accident scenario. However, due to hydrogen leak or an accidental hydrogen release from high-pressure tank in a tunnel, a non-uniform, e.g. stratified, hydrogen–air mixture can be formed preferentially at the ceiling part of a tunnel structure.

Several experiments and numerical simulations have been recently done with respect to combustion and detonation in a semiconfined stratified layer of hydrogen-air mixture typical for accident scenario in a tunnel geometry. Experiments on hydrogen combustion in a thin

semiconfined layer have been performed inside the safety vessel with a volume of 100 m^3 (Kuznetsov et al., 2011). The cylinder volume has 3.5 m internal diameter and 12 m length. A wall thickness of 80 mm allows to perform detonation experiments directly inside of the volume. A rectangular box with dimensions of 9x3x0.6 m was installed inside the safety vessel, as shown in Figure 34. With respect to geometry and dimensions, such experimental layout is very suitable to experimentally simulate hydrogen accident in tunnel environment.

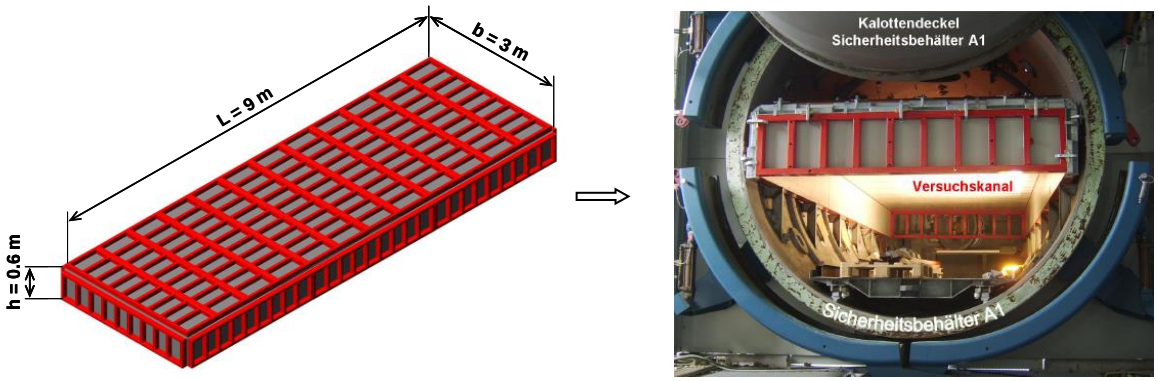

Figure 34. Main dimensions of the flat layer box (left) and a photo of the thin layer box installed inside the safety vessel (right) (Kuznetsov et al., 2011).

All experimental data on characteristic pressures and flame velocities for uniform compositions are summarized in Figure 35. The figure shows that in semi-open channel experiments the threshold between the slow and fast flame regimes is the sonic speed in reactants c_r, while in closed channels it is the sonic speed of the products (Alekseev et al., 2001). Figure 35 demonstrates that the thinner is the layer (thickness h), the higher hydrogen concentration or more reactive mixture has to be to reach the speed of sound.

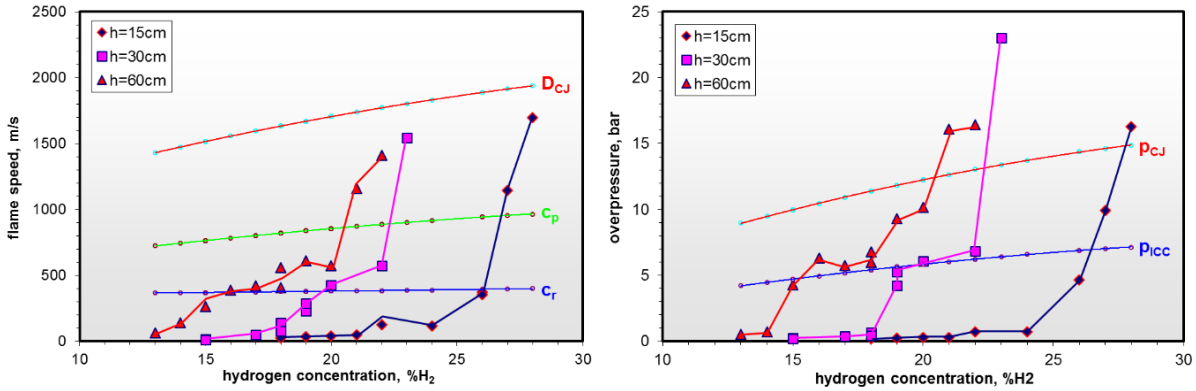

Figure 35. Characteristic flame velocity and overpressure for different layer thicknesses as function of hydrogen concentration: c_r, c_p, D_{CJ} are sonic speed in reactants, products and CJ-detonation velocity respectively; p_{ICC} and p_{CJ} are adiabatic isochoric complete combustion pressure and CJ-detonation pressure respectively (Kuznetsov et al., 2011).

In terms of hydrogen concentration, the critical conditions for fast sonic flames for different layer thickness are as follows (see Figure 35):

h = 0.15 m for 26% H_2 ($\sigma^* > 4.63$), (3.36)

h = 0.3 m for 19% H_2 ($\sigma^* > 5.42$), (3.37)

h = 0.6 m for 15% H_2 ($\sigma^* > 6.6$). (3.38)

Since expansion ratio is a critical indicator of the potential for flame acceleration (Dorofeev et al., 2001; Alekseev et al., 2001), Figure 36 summarizes all experiments as a dependence of expansion ratio versus layer thickness *h* and spacing between obstacles for semi-confined layer *s*.

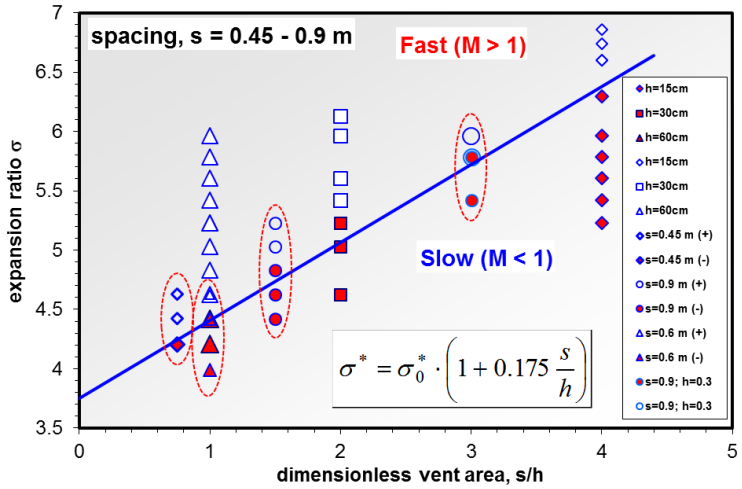

Figure 36. Critical conditions for an effective flame acceleration as function of expansion ratio vs. dimensionless vent area: sonic flame and detonations (open points); subsonic flame (solid points). Different spacing is labelled (Kuznetsov et al., 2011).

A linear correlation between the critical expansion ratio σ* for fast flame propagation in a flat layer and the reciprocal layer thickness 1/*h* or spacing between the obstacles, *s*, was derived from the experiments (Figure 36) and theoretical considerations:

$$\sigma^* = \sigma_0^*(1+K \cdot s/h), \quad (3.39)$$

where K=0.175 is a constant depending on the blockage ratio (BR).

As follows from Figure 35, for uniform mixtures the detonation occurs at different hydrogen concentration depending on layer thickness:

h = 0.15 m for 27% H_2, (3.40)

h = 0.3 m for 23% H_2, (3.41)

h = 0.6 m for 21% H_2. (3.42)

Thinner layer needs more reactive mixture to be detonated than a thicker one. Since the energy losses and the mixture reactivity are reciprocally correlated with layer thickness and detonation cell width λ, the dimensionless ratio of the layer thickness over the detonation cell width *h*/λ can expected to be a constant value for the critical detonation conditions. Figure 37 confirms that dimensionless layer thickness for critical conditions for detonation onset are almost the same for three investigated layer thicknesses (Kuznetsov et al., 2011):

h/λ=13-14. (3.43)

This value agrees very well with previous experiments performed on a smaller scale facility, *h*/λ=7-15 (Friedrich et al., 2007a).

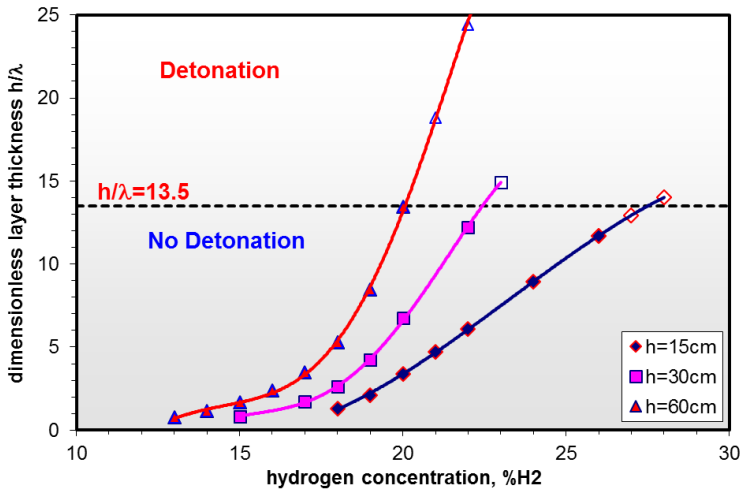

Figure 37. Critical conditions for DDT in the relationship between the dimensionless layer thickness and hydrogen concentration: detonation (open points); no detonation (solid points) (Kuznetsov et al., 2011).

To experimentally reproduce a natural hydrogen stratification in a tunnel geometry, different hydrogen concentration gradients of 0.2, 0.3 and 0.6% H_2/cm have been created inside a thin layer box by using an effect of turbulent diffusion during the gas filling procedure (Kuznetsov et al., 2015b). Figure 38 shows an example of the tests on formation of linear concentration gradient by varying of the mixture composition at constant pressure (Figure 38a) or changing of initial pressure in a mixing tank at the same hydrogen concentration (Figure 38b).

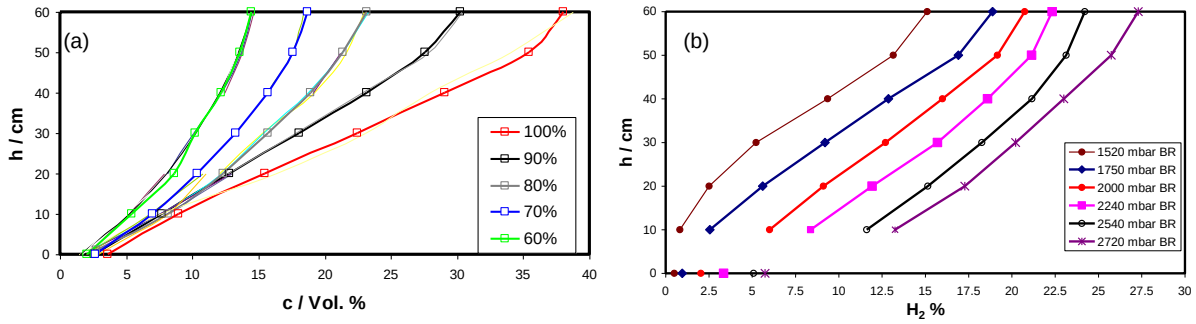

Figure 38. Hydrogen distribution in an obstructed layer: (a) by varying of the hydrogen concentration in a mixing tank; (b) by pressure changing in a mixing tank (Kuznetsov et al., 2015b).

Because experiments demonstrated almost no influence of hydrogen stratification on critical conditions for flame acceleration, formula (Eq. 3.39) to evaluate the critical expansion ratio remains the same as for uniform compositions:

$$\sigma^* = \sigma_0^*(1 + 0.175 \cdot s/h), \quad (3.44)$$

where σ^* is the critical expansion ratio for maximum hydrogen concentration at the ceiling of the channel. Except the highest gradient of 0.6% H_2/cm, there is almost no influence of the gradient on flame propagation velocity for stratified compositions. The process of combustion in a stratified atmosphere is governed by the maximum hydrogen concentration at the ceiling of the channel. Then, the critical conditions for DDT in a stratified atmosphere remain the same as in Eq. 3.43 with the difference that for stratified atmosphere efficient layer thickness h^*

should be evaluated up to the lower detonable hydrogen concentration of 13-14% H_2 (Grune et al., 2017):

$$h^*/\lambda=13\text{-}14, \tag{3.45}$$

where h^* is the efficient height of detonable layer of hydrogen-air mixture; λ is the detonation cell size of hydrogen-air mixture at the ceiling.

3.3.3 Detonations (KIT)

Detonation is the stationary explosive process of supersonic combustion propagating with so-called Chapman-Jouguet velocity D_{CJ} and characteristic Chapman-Jouguet pressure P_{CJ} which are thermodynamic functions of energy of reaction Q and do not depend on chemical kinetics:

$$D_{CJ} = \sqrt{2(\gamma^2 - 1)Q}, \tag{3.46}$$

$$P_{CJ} = \frac{1+\gamma(D_{CJ}/c_s)}{\gamma+1}, \tag{3.47}$$

where γ is the adiabatic coefficient; c_s is the speed of sound. The parameters of stationary detonation can be calculated using thermodynamic data base similar to STANJAN. According to Eq. (3. 46), loss of energy Q due to a narrow channel or congested area or surface friction may lead to detonation velocity deficit up to 25-30% compared to theoretical D_{CJ} velocity (Dorofeev et al., 2000; Kuznetsov et al., 2002) and then detonation fails with velocity drop up to speed of sound in reactants or in combustion products c_r or c_p (Figure 39).

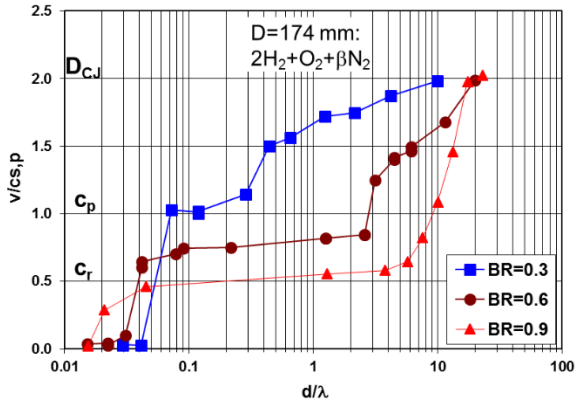

Figure 39. Effect of blockage ratio on characteristic flame velocity for stoichiometric H_2-O_2 mixtures diluted with nitrogen, β=[N2]/[O2] (Kuznetsov et al., 2015b).

Critical dimensionless ratio d/λ for detonation propagation and detonation transition in different geometries and channels of different blockage degree BR are collected in Table 6. Higher blockage degree leads to larger energy losses and needs more reactive or detonable mixture (with smaller detonation cell size λ) to be able to detonate. Another near L/λ limit regime for detonation propagation is the galloping detonation when the velocity deficit may reach $0.5D_{CJ}$ due to failure of detonation behind the obstacle and then re-initiation before the next one.

Approaching to a tunnel geometry a series of experiments was performed in a cylinder chamber with a layer of uniform or stratified hydrogen-air mixture (Figure 34). Detonation was initiated with a buster of stoichiometric hydrogen-air mixture then a layer of uniform test mixture

without obstacles has detonated. A critical condition for uniform layer of hydrogen-air mixture was found (Rudy et al., 2013):

h/λ=3-4, (3.48)

where h is the thickness of hydrogen-air mixture and λ is the detonation cell size of hydrogen-air mixture. For a layer of stratified hydrogen-air composition the critical condition for detonation propagation looks almost the same (Grune et al., 2017):

h^*/λ^*=3-4, (3.49)

where h^* is the efficient height of detonable layer of hydrogen-air mixture which is associated with h_{Det} (see Figure 40); λ^* is the efficient detonation cell size corresponding to the average hydrogen concentration within a detonable layer. According to paper (Boeck et al., 2016) the dimensionless detonable layer thickness changes from 1 to 3 for a stratified hydrogen-air mixture within a channel 6x30 cm. Such experiments cannot be reliable to a tunnel geometry because of fully enclosed geometry and an influence of shock reflections from bottom wall on detonation propagation. Thus, larger scale experiments are needed.

Table 6. Critical dimensionless scale $L/\lambda=N^*$ for detonation propagation.

Dimensionless scale L/λ	Critical value N*	Detonation relevant phenomenon	References
d/λ	$1/\pi$	Detonation propagation in a smooth tube with inner diameter d	Moen et al. (1981)
d/λ	1	Detonation propagation in obstructed tubes with orifice size d (BR*<0.43)	Teodorczyk et al. (1988)
d/λ	2.5-3	Detonation propagation in obstructed tubes with orifice size d (BR=0.6)	Kuznetsov et al. (2000)
d/λ	10	Detonation propagation in obstructed tubes with orifice size d (BR=0.9)	Kuznetsov et al. (2002)
h/λ	0.4	Detonation propagation in a thin gap between 2 solid plates with a gap size h	Ishii et al. (2002), Wu & Kuo (2013), Kuznetsov & Grune (2019)
$\Delta x/\lambda$	10	Detonation transition trough a gradient of reactivity with nonuniformity size Δx	Kuznetsov et al. (1997)
d_c/λ	13	Critical tube diameter d_c of detonation exit in unconfined mixture	Mitrofanov & Soloukhin (1965), Moen et al. (1986)

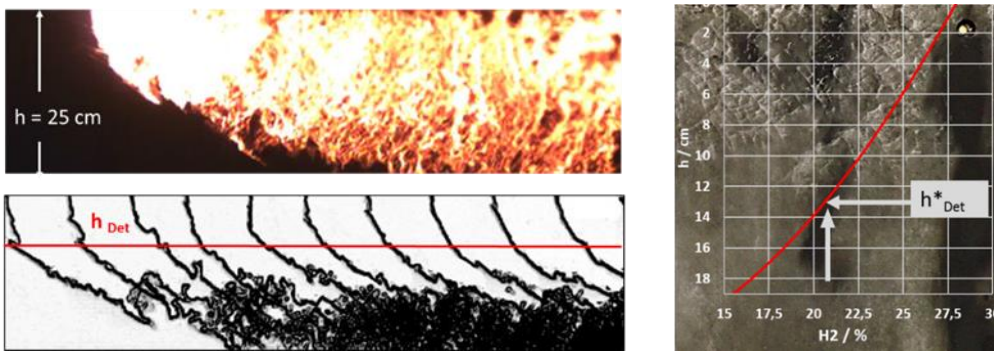

Figure 40. Snapshot of the detonation front and detonation front propagation history (left) and a soot plate record with corresponding H_2-concentration profile (right) (Grune et al., 2017).

3.4 Behaviour of high-pressure hydrogen storage tank in a fire (UU)

The FCVs with zero emission are already on roads with compressed gaseous hydrogen (CGH2) storage onboard at a typical nominal working pressure 70 MPa. There are about 5500 FCVs in California and about 2800 FCVs in Japan (Wenger, 2019). Hydrogen refuelling stations for FCV operate at even higher pressures, i.e. up to 100 MPa; number of stations worldwide is growing, e.g. there are 62 in Germany, 40 in California, 100 in Japan (Wenger, 2019). FCV may be involved in a fire, exposing the high-pressure tank to high temperature and heat flux. The following sections analyse such scenarios, discussing first the fire resistance rating of tank, and then hazards in case of failure of the storage system in a fire.

To prevent tank rupture in a fire it is equipped by TPRD. However, there is a non-zero failure probability of TPRD that makes risk unacceptable if fire resistance rating of a tank is below about 50 minutes (Dadashzadeh et al., 2018). The problem of tank rupture is especially important for tunnels, where generated by rupture blast wave could propagate through the whole length of the tunnels with little decay in pressure (thus threatening life and property along the whole tunnel). The development of explosion-free in a fire tank is the most effective way to solve most of safety problems not only for a system vehicle-confined structure but for all possible applications of composite Type IV cylinders for hydrogen storage. The breakthrough solution for inherently safer onboard storage is presented in Molkov et al., 2017).

3.4.1 Fire resistance rating (UU, FHA)

For FCV there are two major failure modes associated with hydrogen system, i.e. storage tank rupture and hydrogen line break. Composite cylinders for CGH2 with plastic liner (Type IV) for the gas tightness are selected by major original equipment manufacturers (OEMs) due to lightweight and high strength to provide competitive driving range. Rupture of a container can occur either due to the internal pressure exceeding the tank strength (low probability event for cylinders with regulated safety factor 2.25) or due to any external/internal factor reducing the tank strength, e.g. fire (higher probability event). For instance, when exposed to a fire, the tank wall starts to degrade, and tank gradually loses its load bearing strength over the time. The fire resistance rating (FRR), i.e. time from a fire start to tank rupture in the case of a faulty TPRD or its blockage during an accident, of current tanks is about 6-12 min (Kashkarov et al., 2018; Makarov et al., 2016; Weyandt, 2005, 2006).

Reported recently accidents with cylinder rupture in CNG vehicles have demonstrated quite devastating consequences (“CNG explosion,” 2016), (Schmitt, 2016). The QRA study (Dadashzadeh et al., 2018) demonstrated that composite hydrogen storage tanks with FRR=6-12 min have a risk of human life loss in a road accident escalating to a fire and consequently the tank rupture of $3.14 \cdot 10^{-3}$ fatality/vehicle/year on London roads. This is two and half orders of magnitude above the acceptable level of risk of 10^{-5} fatality/vehicle/year as indicated in (LaChance et al., 2009 & 2011; Haugam et al., 2013; Dadashzadeh et al., 2018). The cost associated with loss of life in the accident in this case is 4.03M £/accident (Dadashzadeh et al., 2018). To make risk acceptable FRR should be about 50 minutes or explosion-free in a fire tanks should be used by OEMs.

Ulster University suggested a tank failure mechanism in a fire capable of predicting the time to tank rupture (FRR), which is based on the regulated initial burst pressure (IBP) for a carbon fibre reinforced polymer (CFRP) overwrapped Type IV tank of 225% of nominal working

pressure (NWP) (United Nations Economic Commission for Europe, 2013). Therefore, considering the tank's safety factor is 2.25, the load bearing fraction of the composite wall thickness becomes $P_{current}/(2.25 \cdot NWP)$, where $P_{current}$ (MPa) is the current pressure inside the tank. When the tank is filled at 70 MPa, i.e. NWP, this value is 70 MPa / (70 MPa ·2.25) = 0.44, i.e. not the whole wall thickness, but only 0.44 fraction of the wall thickness holds the pressure of 70 MPa. The remaining fraction, i.e. 1-0.44=0.56, becomes a safety margin, which decreases with the increase of pressure inside the tank due to heat transfer from the fire to hydrogen. When exposed to the fire, the temperature grows in the tank and the pressure, $P_{current}$, increases too; hence the initial fraction of the wall thickness 0.44 increases too to bear the load. It is expected that the rupture occurs at the time when the safety margin fraction of the tank wall is consumed, that is when it is equal to $1 - [P_{current}/(2.25 \cdot NWP)]$. Another assumption of the failure mechanism developed at Ulster is that the composite degradation is associated with thermal decomposition of the resin. The temperature of resin decomposition is typically ranging within 573-673 K, which is below the decomposition temperature of the carbon fibres, i.e. typically 873 K. Depending on the curing temperature of the composite tank manufacturing process, the temperature of resin decomposition could be even lower. Once the resin degrades, the fibre reinforcement loses its optimal position and cannot support the mechanical load, causing the composite failure.

The tank FRR depends on the fire heat release rate (HRR). This in turn correlates with heat flux to the tank. The study (Kashkarov et al., 2018) introduces the suggestion to the UN GTR#13 to improve the fire test reproducibility. This is achieved through the FRR saturation at the HRR≥350 kW. The study revealed that not only control of temperatures under the cylinder as required by GTR#13 regulation, but also the burner heat release rate (HRR) strongly affects the FRR. However, the effect of burner size and tank size was not yet addressed in the study. To improve the fire test reproducibility and account for variety of tank sizes, it is proposed to relax the fixed burner dimensions in GTR#13 and fix not simply HRR but the specific heat release rate HRR/A, where A is the burner area. This changes the previously proposed FRR saturation correlation (Kashkarov et al., 2018) to the new one on the figure below (Figure 41).

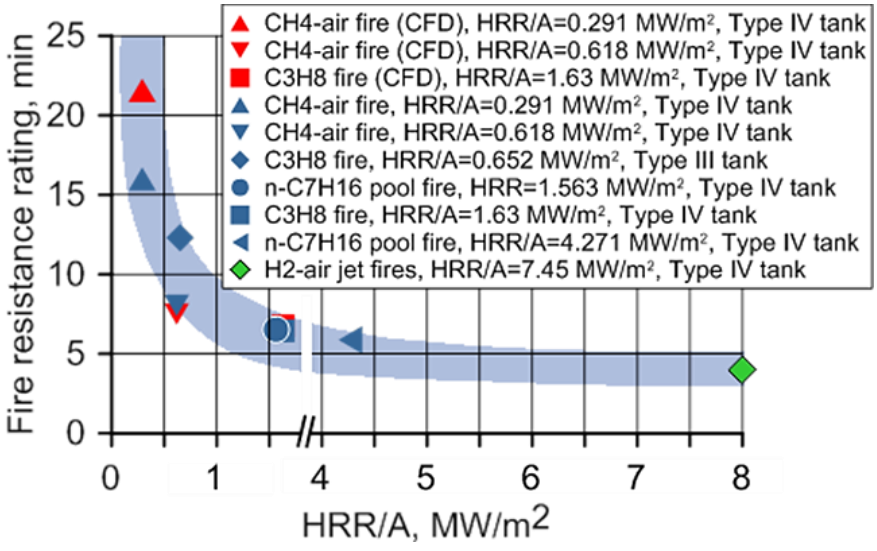

Figure 41. FRR dependence on the burner's HRR/A: experimental data and CFD simulations (Makarov et al., 2016); (Weyandt, 2006, 2005), (Blanc-Vannet et al., 2019); (Bustamante-Valencia et al., 2016); (Ruban et al., 2012).

The above graph shows the range of most common fire scenarios, i.e. diffusion non-premixed fire (gas and pool fire), premixed fire and high-momentum jet fire to the tank. The saturation of FRR with increase of HRR/A above 1 MW/m^2 is in a full agreement with typical values of HRR/A=1-2 MW/m^2 for gasoline combustion in automobile fires. This is clear that fire testing of tanks at lower values of HRR/A doesn't reflect real conditions and could "facilitate" passing the regulated test but would not provide acceptable level of risk.

One of scenarios where the composite tank can be degraded till rupture is the smouldering fire. The effect of such fire on composite tanks is not yet investigated. A recent accident with an explosion of a CNG tank on board of a garbage truck was caused by a smouldering fire: "…natural-gas powered garbage truck began smouldering… neighbour was recording just as the truck exploded", "…garbage truck exploded after catching fire … and blasted a hole in the front of a nearby house". "A total of four houses were damaged in the explosion" (Shea, 2016; Today, 2016). It has to be underpinned that these CNG tanks were equipped by TPRD but they were not initiated by smouldering fire. Figure below shows the smoke from the CNG truck being in smouldering fire and explosion of the onboard CNG tank.

Figure 42. CNG garbage truck explosion in the US (Today, 2016).

There are different means to increase the FRR, e.g. insulation blankets, protection shell, etc. The FRR increase up to 2 hours, which is comparable with longest car fire duration (Mangs and Keski-Rahkonen, 1994), has been demonstrated recently by the use of intumescent paint in the UK funded by EPSRC project (Makarov et al., 2016). Pötzsch et al. (2018) also mentions the intumescent laminate and other coatings and fire-resistant gelcoat.

The recently discovered phenomenon of the rupture prevention in a fire by the gas leak was demonstrated in the study (Bustamante-Valencia et al., 2016). The authors showed 4 tests with 70 MPa tanks filled by different percentage of the NWP, i.e. 100%, 75%, 50% and 25%, see Figure 43. It is shown that the 70 MPa tank filled at pressure 100% and 75% of NWP (70 and 52.5 MPa) ruptured, whereas the tanks filled at 50% and 25% (35 MPa and 17.5 MPa) leaked instead without explosion. This can be explained by the fact that the load-bearing fraction of wall thickness for lower pressure is smaller than that for 70 MPa and it takes longer for degradation front to travel through the wall and reach it. At the same time, plenty of heat to melt liner was transferred inside causing liner melting and initiation of gas release through the load bearing wall. Unfortunately, this "safety effect" does not work for fully filled tanks and the solution is still required to improve life safety and property protection of onboard storage.

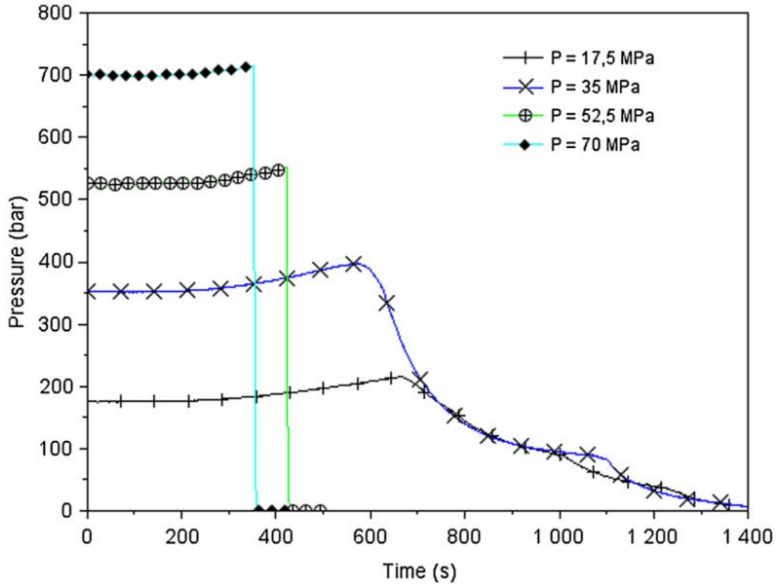

Figure 43. Tank pressure histories in fires at 4 different initial pressures (Bustamante-Valencia et al., 2016).

The breakthrough leak-no-burst (LNB) safety technology (Molkov et al., 2017), which is being developed at Ulster, excludes tank rupture in a fire at any storage pressure by allowing an insignificant leakage of hydrogen though the tank composite wall after melting a liner. The insignificant leak flow rate is equivalent to flow rate through an orifice of only 0.2-0.3 mm diameter. This is essential for safety provisions to address other safety concerns as well. In particular, such engineering solution excludes long flames and the pressure peaking phenomenon (PPP), i.e. the unique only for hydrogen phenomenon when leak is inside the enclosure like garage or maintenance shop (Brennan and Molkov, 2013; Hussein et al., 2018; Makarov et al., 2018). Figure 44 shows the schematic operation of the composite tank wall in a fire: ordinary tank (left) and an LNB tank (right).

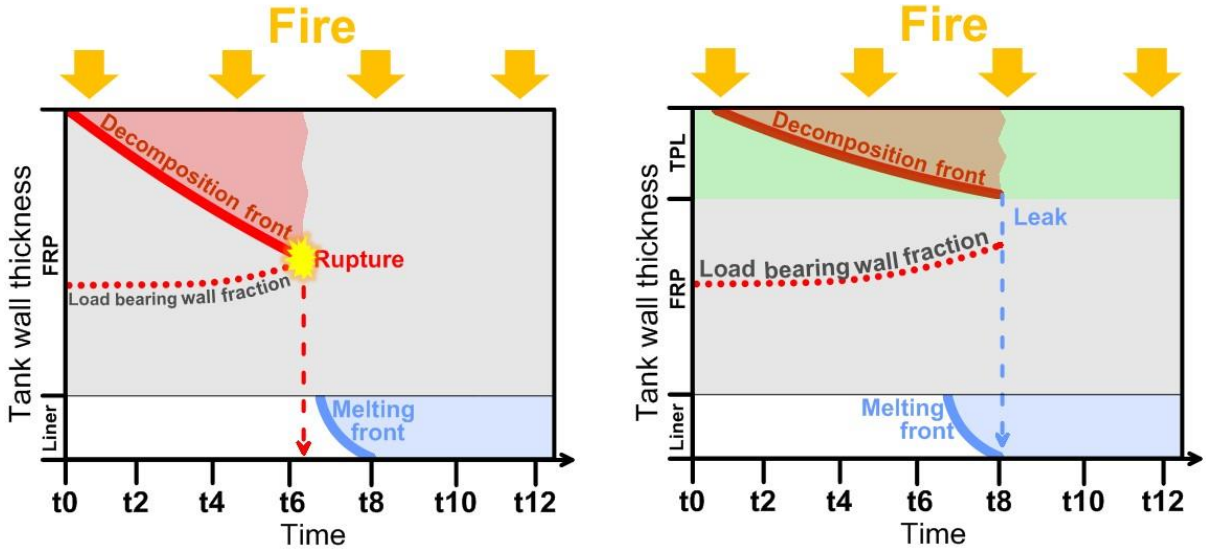

Figure 44. Burst criterion for the tank in a fire.

The decomposition front is represented by a temperature range of the CFRP is 613-633 K (Chiang et al., 2007; Kashkarov et al., 2017b; Liu et al., 2007; Niranjana et al., 2007; Régnier

and Fontaine, 2001). The decomposition front of the wall propagates inside the wall thickness and, therefore, reduces the safety margin thickness of the wall. The load bearing wall fraction (increasing due to growing temperature and pressure inside the tank) tends to come in contact with the decomposition front in some point. The rupture occurs once the load bearing wall fraction is decomposed (two fronts intersect) before the liner melting front travels through the liner thickness meaning the liner has melted (Figure 44, left). Figure 44 (right) shows the performance of the explosion-free in a fire tank. Due to the added thermal protection layer (TPL), the decomposition front curve is less steep and decomposition of resin propagates inside the tank slower, although allowing for the heat transfer inside sufficient to melt the liner before the decomposition front comes in contact with load bearing wall fraction.

3.4.2 Rupture of hydrogen storage tank in a fire (UU)

There is a non-zero failure probability of the high-pressure storage tank rupture in a fire, e.g. due to TPRD activation failure or its blockage in a car accident. The high-pressure hydrogen tank rupture in a fire is followed by devastating blast wave and fireball, which diameter may reach tens of meters for cars. These pressure and thermal effects may cause fatalities and serious injuries of people as well as damaging buildings, even severely enough to fully demolish them, leaving no possibility for evacuation or rescue in the least case.

3.4.2.1 Blast wave (UU)

The stand-alone cylinder for hydrogen storage, e.g. a cylinder at refuelling station, and the under-vehicle onboard hydrogen storage cylinders are two typical applications. There is an essential difference in blast waves' strength after ruptures of such two storage applications. This is due to the fact that under-vehicle tank rupture is accompanied by a significant loss of released mechanical energy of compressed gas directed to destroy a vehicle and to displace its body frame from its original location by tens of meters, as observed in the experiment and then discussed in the relevant report (Weyandt, 2006). It should be noted that from the blast strength calculation point of view, an under-vehicle cylinder rupture may be considered as a "stand-alone" application in some scenarios. For instance, this can be applicable to the cases when the vehicle is overturned in an accident or in the case of tank(s) storage on a vehicle roof, e.g. like in current buses, or on a vehicle side. Yet, this is a conservative approach as the loss of energy to damage a car body would be neglected.

The rupture of an onboard hydrogen tank located under a vehicle produces lower overpressures in a blast wave in near field compared to the case of rupture of stand-alone tank of the same volume and with the same pressure. This difference is due to losses of a significant part of the compressed hydrogen mechanical energy in the onboard tank on the vehicle destruction and its translation by 22 meters in the test (Weyandt, 2006). The estimated difference in fractions of hydrogen mechanical energy contributed to the blast wave strength for stand-alone and onboard (under-vehicle) tanks is 1.8/0.12=15 times (if comparing 350 bar tanks) (Molkov and Kashkarov, 2015). At the same time, such a reduction of the mechanical energy is practically "compensated" in a far field by nearly doubling of the fraction of chemical energy released during combustion (for 350 bar tanks). The fire test with under-vehicle 35 MPa tank performed in USA (Weyandt, 2006) demonstrated the FRR=12 min and that the car frame was a projectile itself as it travelled by 22 ms from its initial location (Figure 45).

Figure 45. Rupture of an under-vehicle tank in a fire, i.e. equivalent to scenario with failed to initiate or blocked TPRD (Weyandt, 2006).

The CFD study on the blast wave in tunnel from high-pressure tank rupture (Shentsov et al., 2018) aims to understand a blast wave dynamics after a hydrogen tank rupture in a tunnel based on a conservative scenario, i.e. tunnel with one of smallest cross-section area and one of the highest amount of onboard hydrogen storage in a vehicle. It has been shown that the tank rupture in the tunnel generates multiple interacting shocks due to reflections from walls, ceiling and floor. For the smallest double lane cross-section area and one of the latest tanks with volume 140 L and storage pressure 70 MPa, it was shown that the quasi one-dimensional geometry of the tunnel practically prevents the blast wave decay as compared to the tank rupture in the open atmosphere, when the blast wave decays quickly due to continuous increase of the blast wave area. In the near field and contrary to the tank rupture in the open, people and vehicles will undergo a harm and damage from a series of shocks. Then, the more uniform by height blast wave propagates throughout the whole length of the tunnel practically without or small decrease of its peak at distances further than 40 m for the case without combustion and 30 m for the case with combustion. Total impulse of the blast was calculated for every 5 m from the tank location until 50 m at the height of 1.5 m and 0.25 m. Knowledge of overpressure and impulse allows to use the Baker's harm diagram (Figure 46) taken from (Molkov and Kashkarov, 2015) to estimate harm to people in the tunnel following the considered here scenario. The harm effects of blast wave on people present in the tunnel do not account for any "protecting" effects, e.g. people inside a vehicle which stays intact, etc.

The hazard thresholds at height of 1.5 m were studied and shown in Figure 46 (crosses) as it is the closest to the lungs and ears damage for a standing person. The "fatality" overpressure threshold (horizontal dashed line at 100 kPa) is associated with 1% chance of lung haemorrhage by the blast, and the "injury" threshold with 1% of eardrum rupture (horizontal dashed grey line at 16.5 kPa). However, these two "simplified" thresholds do not consider the impulse. The "lung damage threshold" curve is more appropriate to estimate the possibility of fatalities. People standing at 5 m from the hydrogen tank are about to reach the fatality threshold. Closer to the tank distances the chance of lung haemorrhage increases drastically.

From 10 m to the end of the tunnel, people will have serious injuries, in particular, their eardrums will rupture. There is no "no harm" zone in the tunnel for this conservative scenario.

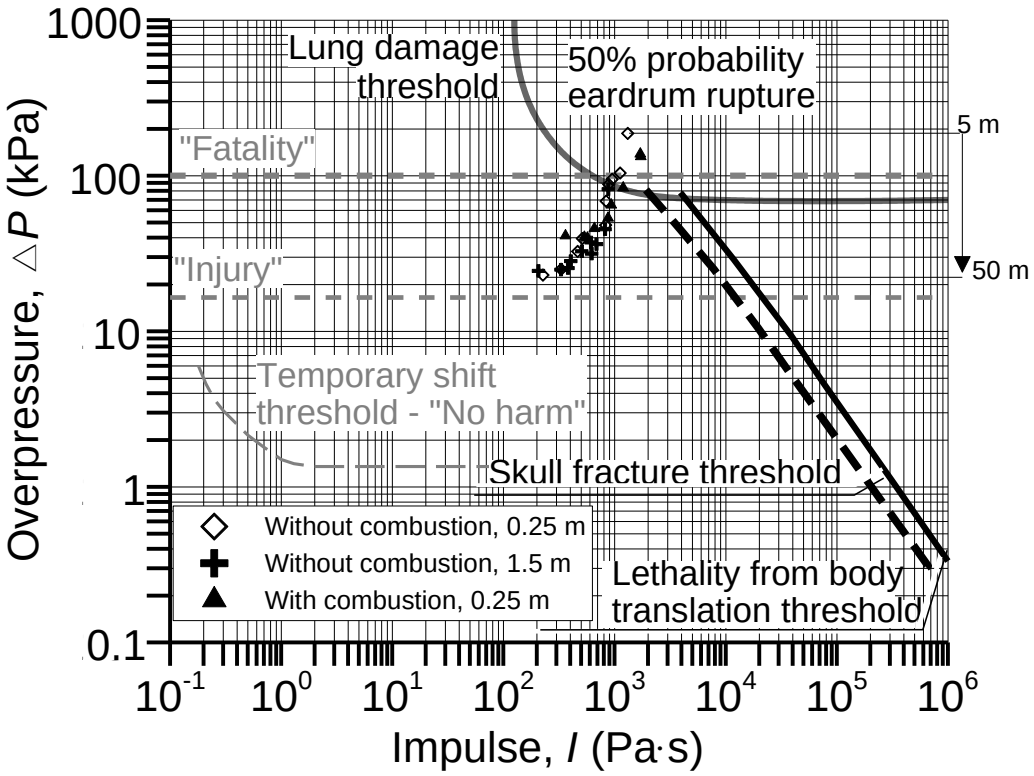

Figure 46. The blast pressure and impulse at 0.25 m (diamonds and triangles) and 1.5m (crosses) heights, (Molkov and Kashkarov, 2015).

For different reasons people may lay or sit on the ground after an accident occurs, whether in the case where victims are injured or unconscious, people who fall when trying to leave the tunnel or wait for emergency services to come. In such scenarios, the pressure and impulse they are exposed to are higher. As can be seen in Figure 46 (diamonds and triangles) at 5 m from the tank, survival chances are very low. If the impulse is not taken into account, an overpressure of 200 kPa at distance 5 m leads to 99% chance of lung haemorrhage (Mannan, 2005), causing the death of almost all the persons hit by the blast wave. At distances between 10 m and 20 m from the ruptured tank, the fatality threshold is still met but the probability drops to a smaller percentage. However, the chance of serious injury with eardrum rupture remains high at about 50%. Similar to the 1.5 m height case, the further from the tank (until 40 m for the case without combustion), the smaller the probability of eardrum rupture. Humans do not have time to react on the blast wave. It takes less than 0.2 s after tank rupture for all blast waves to exit the tunnel passing distance of 50 m in the considered problem. Besides the pressure effects from the blast wave, other hazards and associated risks exist. People can be hurt by projectiles or pushed down by the blast causing secondary injuries. Furthermore, injuries may be provoked to people in vehicles by the airbag inflation because of the blast impact and by pieces of shattered windows. Surely, the thermal effects of a fireball and projectiles are other sources of hazards and risks to be investigated.

The paper by Shen et al. (2018) deals with theoretical assessment of consequences of accidental catastrophic explosion in the case of high-pressure tank (165 L, 35 MPa) rupture during fire test. The pressure effect was one of the damage patterns that was analysed. It was found that for the overpressure of blast wave, the slight injury for human and minor damage for equipment are expected in the radius range of within 14 m and 65.4 m respectively.

Recent numerical study on the blast wave in tunnel has shown the effect of hydrogen inventory of a tank with pressure before burst equal to 94.5 MPa on blast wave strength in far field (Shentsov et al., 2019). Figure 47 shows dependence of the maximum blast overpressure recorded at 140 m i.e. 10 m before the exit for all three tunnels and various tank inventories. Symbols represent the exact tank inventory for each simulation. Connecting lines give approximate estimation of the overpressure for certain tunnel cross-sections with different amounts of hydrogen inventory. For the singe-lane tunnel hydrogen inventory above 0.75 kg would create overpressure above "injury" threshold. For the two-lane tunnel, this minimum inventory mass value is doubled to around 1.6 kg. For the five-lane tunnel, all cases are below the "injury" limit up until 7 kg of hydrogen inventory, the enlarged confinement of the tunnel facilitating a more pronounced pressure decay and lower level of pressure peak in "established" blast. The "no harm" limit is however exceeded at 140 m in any considered tunnel for hydrogen mass inventories down to 0.58 kg. All cases are well below the "fatality" threshold of 100 kPa. It should be underlined that this is a very preliminary study of mainly academic interest rather than a source of safety guidelines for storage tank and hydrogen-powered vehicle developers. To make realistic recommendations the HyTunnel-CS project plans to apply coupled CFD+FEM simulations to account for losses of mechanical energy on vehicle demolition and translation in space as well as effect of under-vehicle tank location on efficiency of hydrogen combustion that contributes to the blast wave strength.

More research should be done in order to exclude injuries and/or fatalities and develop innovative safety technologies to exclude tank rupture in a fire at all. One of such technologies, i.e. the leak-no-burst technology, is currently under development and primary testing at Ulster University.

The research in the HyTunnel-CS project includes real scale experiments of tank rupture in tunnels. This will give invaluable data and will be applied to validate the reduced-order and CFD models.

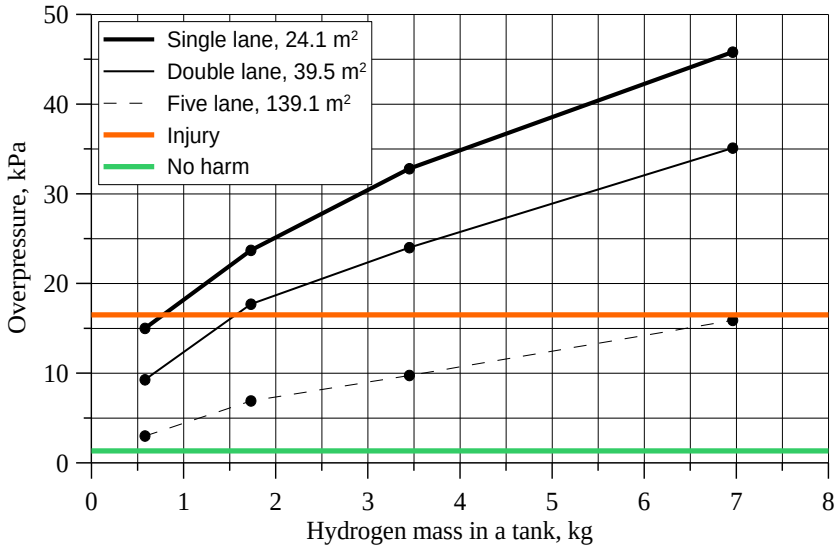

Figure 47. Maximum blast wave pressure recorded at 140 m from the 94.5 MPa tank as a function of tank mass for three tunnel cross-sections (Shentsov et al., 2019).

3.4.2.2 Fireball (UU)

There are definitions of fireball in literature. For example, Martinsen and Marx (1991) defined a fireball is a dynamic phenomenon, whereby a ball of fire grows spherically in size and upwardly due to buoyant forces soon reaching its maximum diameter and the limited fuel supply is consumed. The life cycle of a fireball is relatively short, and during its existence the fireball passes through various distinctive stages chronologically: growth, steady burning and burnout (Mannan, 2005) as it is shown in Figure 48. During the growth stage, rapid mixing and combustion occurs. It lacks a distinct shape whereas in the steady burning stage the fireball is roughly spherical and conforms into a mushroom shape later.

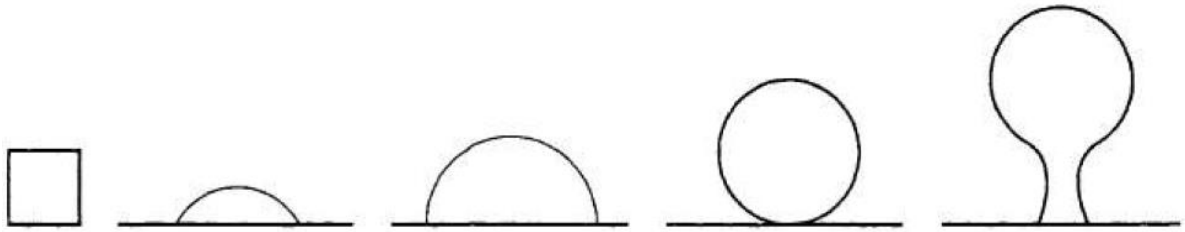

Figure 48. Development of a typical fireball from a source at ground level (Mannan, 2005).

Barry (2002) characterised a fireball as an atmospheric combustion of an air-fuel mixture cloud during which the released energy is mainly due to radiative heat. In fact, fireball propagates as the released fuel mixes with air. The outer fireball boundary, where combustion takes place, forms the flammable mixture. Further on, as the heated gases start to lead, the flame elevates above the ground and tends to become of a cloud shape (sometimes spherical).

A rapid fuel release from a high-pressure container may result in a fireball of a short duration. Such an accident may begin with a vessel rupture. Due to a high internal pressure or degradation of composite wall the vessel containment may be rapidly released outside. A fireball may produce a significant amount of radiation within its short lifetime (typical onboard storage amount hydrogen will be consumed in a fireball combustion in a couple of seconds). Thus, it could result in fatality or injury of humans and serious damage to civil structures. The area affected is several times greater than the actual size of fireball (Martinsen and Marx, 1991).

During the first fractions of a second, the released flammable gas mixes with air. More often, the ignition happens due to fire, which may decompose the vessel and it eventually fails to hold the gas under high pressure.

The harm from a fireball may be recognized as direct thermal effect on human or as damage from burnt material. The hazardous area around a fireball is influenced by vessel size, its design (type) and internal pressure value. Tests with Type III and IV vessels exposed to fire (Weyandt, 2006, 2005; Zalosh, 2007) are the only experiments documented in a way useful to current research. These tests were conducted to define FRR, i.e. time to vessel rupture in a fire, and obtain the characteristics of the blast wave, fireball and scattering of projectiles. Tanks were filled with hydrogen at NWP 35 MPa. Figure 49 shows the fireballs formed after Type III (under-vehicle) and Type IV (stand-alone) vessels rupture.

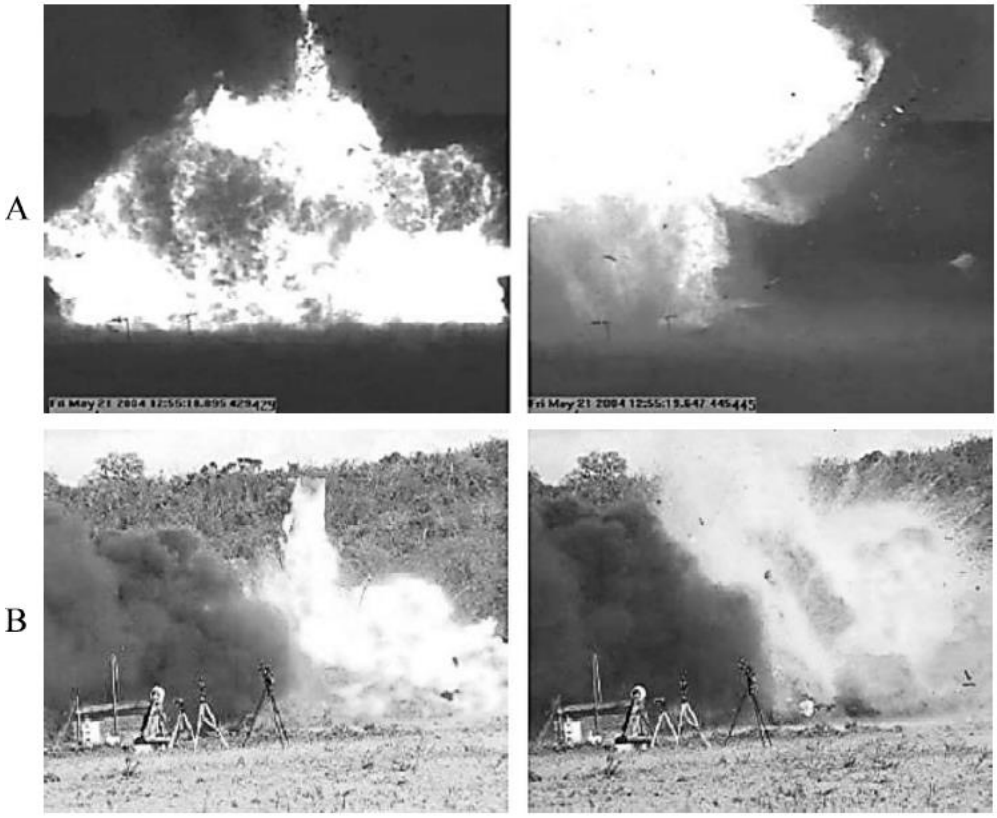

Figure 49. A: fireball from stand-alone vessel rupture 45 ms (left) and 997 ms (right) (Zalosh, 2007); B: fireball from the under-vehicle vessel rupture 70 ms (left) and 170 ms (right) (Weyandt, 2006; Zalosh, 2007).

More experimental observations from these tests are as follows. Burning of the tank composite layers started in 45 s (Type IV) and 20 s (Type III) as observed by the black soot appearance. For the test with Type III tank under the vehicle the earlier appearance of soot could be as well due to polymeric material in the SUV. Maximum fireball diameter of 7.6 m was observed for Type IV tank at 45 ms after the tank rupture. Fireball lifted in 1 s. For Type III tank under the vehicle the fireball diameter was significantly larger, i.e. 24 m. A correlation applied by (Zalosh and Weyandt, 2005) for the fireball diameter gave 9.4 m (for hydrogen mass of 1.64 kg). In both tests the duration of fireball was about 4.5 s (by IR video), and twice shorter by high-speed visible range cameras. A correlation applied by (Zalosh and Weyandt, 2005) gave a shorter duration of only 0.6 s. This means that existing correlations, which were built on data for hydrocarbon fireballs, cannot be directly applied to hydrogen fireballs. The deeper understanding of underpinning physical phenomena is needed to build new correlations for hydrogen safety engineering with higher predictive accuracy. The heat flux measured in test with Type III tank, at the distance 15.2 m, was assessed in short spikes. The values were in the range 210-300 kW/m^2, as being quite high and dangerous to people (to compare with, for example, the effect from the heat flux of about 35 kW/m^2 is characterised by 1% fatality in 10 seconds).

3.4.2.3 Projectiles (UU)

The paper by Shen et al. (2018) deals with theoretical assessment of consequences associated with the accidental rupture of high-pressure tank (165 L, 35 MPa) in a fire. The flying fragments is one of the hazards that was analysed. As can be expected it was found that the

flying distance of the destructed tank increases with the increment of projection angle. After tank rupture the fragment projectiles flied along various directions. The main part of the tank shown in Figure 50 (a) flew forward and then stopped at the distance of 32.5 m when hitting a truck as shown in Figure 50 (b). The truck was moved forward by 0.5 m. The weights of the truck and the main part of the tank were 1.5 tons and 79 kg respectively. The wind shields and high-pressure pipes were also severely destroyed and broken down into debris. A fragment was found at least 40 m from the initial position of the fire test, and the other was 16.8 m away as shown in Figure 50 (c) and (d).

During another fire test by Shen et al. (2018) shown in Figure 51, the inner pressure of the tank reached 43.73 MPa when the tank ruptured. The tank flew out, first hit an object between the side of a small truck and the cockpit, then bounced up, scraped a high-voltage wire and finally hit a wall and stopped. The stop position of the tank is about 200 m from the tank site. Figure 52 shows the flying trajectory of the tank.

More detailed information of the two accidents is recorded as follows. The schematic diagram of position relationship of the first fire test is shown in Figure 53.

It was found by Shen et al. (2018) that the theoretical flying distances are 148 m and 365.3 m when the projection angles are 0° and 10°, respectively.

Figure 50. The consequences of the first explosion test: (a) the damaged hydrogen storage tank; (b) the damaged truck; (c) (d) the debris of accident site (Shen et al., 2018)

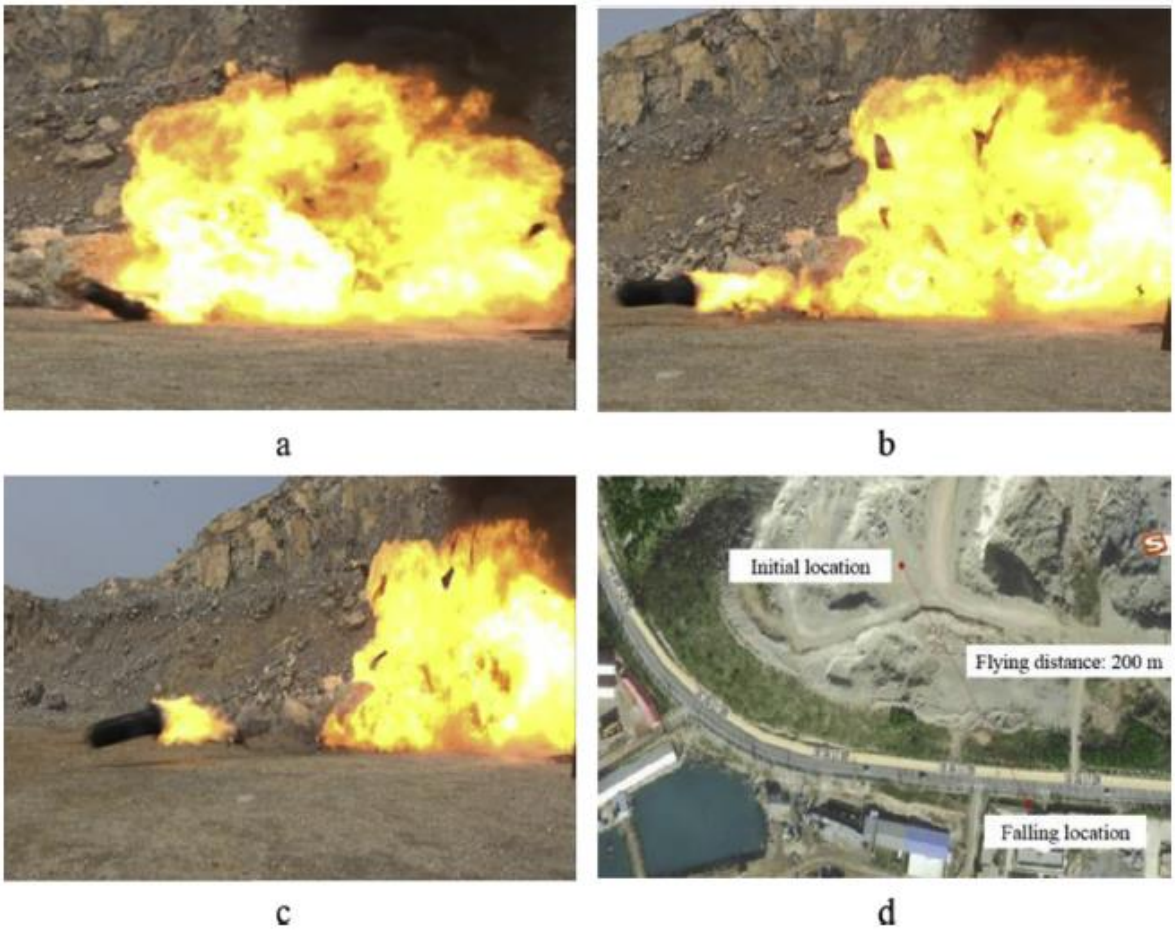

Figure 51. The second explosion test: (a), (b), (c) - the flying tank and fireball; (d) - satellite map of the explosion test site (Shen et al., 2018).

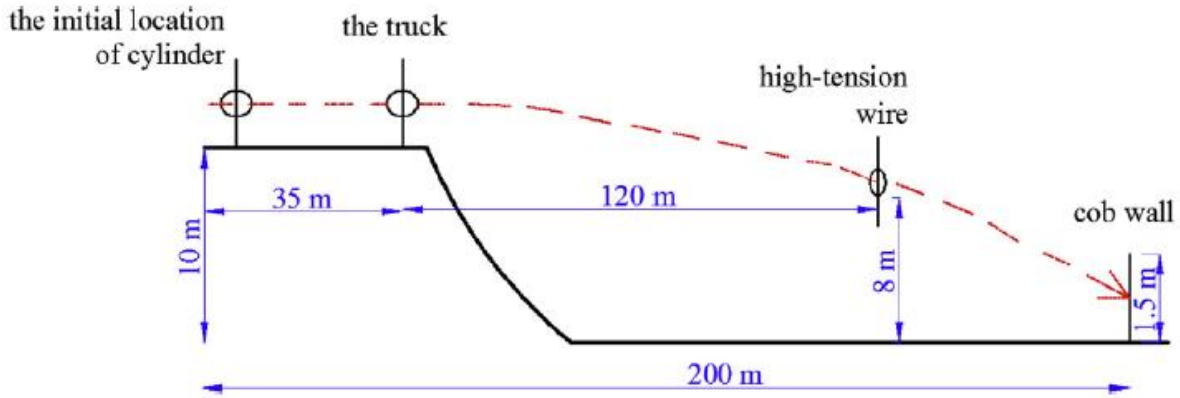

Figure 52. The flying trajectory of the tank of the second test (Shen et al., 2018).

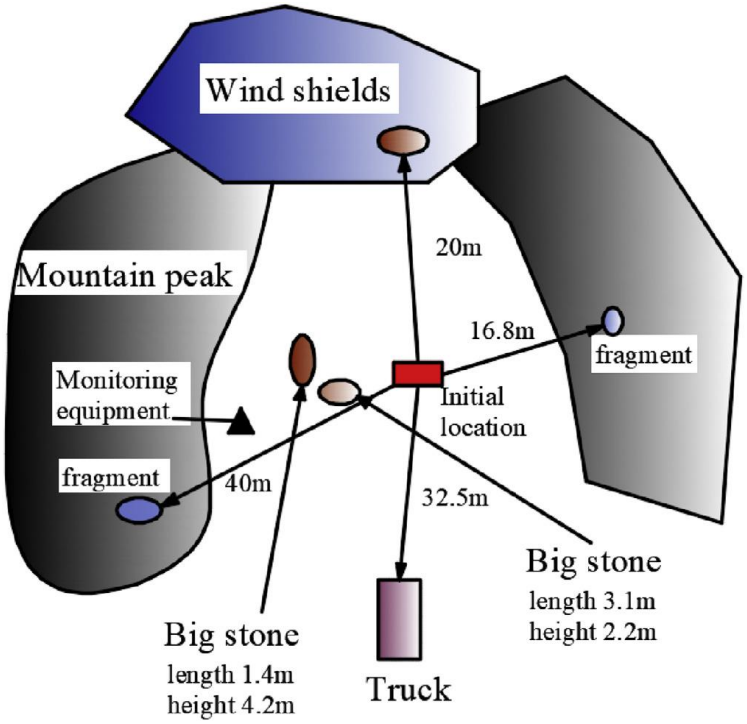

Figure 53. Schematic diagram of the first fire testing spot (Shen et al., 2018).

The test by Weyandt (2006) was performed for the hydrogen cylinder of 88 L at 34.5 MPa located under SUV vehicle. The hydrogen cylinder failed after 12 min 18 sec of exposure, destroying the burnt remains of the automobile. The rear of the vehicle projected upwards and twisted counter clockwise and over the front half of the vehicle. As the rear of the vehicle twisted the cylinder projected horizontally out of the top of the vehicle. The vehicle rotated clockwise about 90 degrees. A trail of aluminium liner fragments of various sizes was left in the path of the cylinder to its final resting place, 40 m of the explosion. Various parts of the cylinder, vehicle, and bonfire system were strewn about the test site in all directions, up to 107 m away. Figure 54 shows the location of the major components found around the test site. The main portion of the cylinder, thrown approximately 40 m northward, weighed approximately 48 kg. The portion of steel thrown approximately 107 m southward of the test location weighed approximately 2.3 kg.

Pittman (1976) carried out investigation with seven vessels pressurized with argon until they burst. The area was instrumented to measure the blast and fragment parameters generated by vessel rupture. All vessels were T-l steel spheres with an internal volume of 1 ft^3. Design burst pressures were 15000, 30000, and 50000 psi. All vessels burst into two pieces. Of these 14 pieces, 10 were recovered. Weights of the recovered sections ranged from 51.1 pounds to 271 pounds. The recovered sections were those that hit the arena walls and were stopped or those that hit the ground or firing pad and travelled only a short distance. The recovered fragments were found at distances between 168 m and 423 m for different pressures.

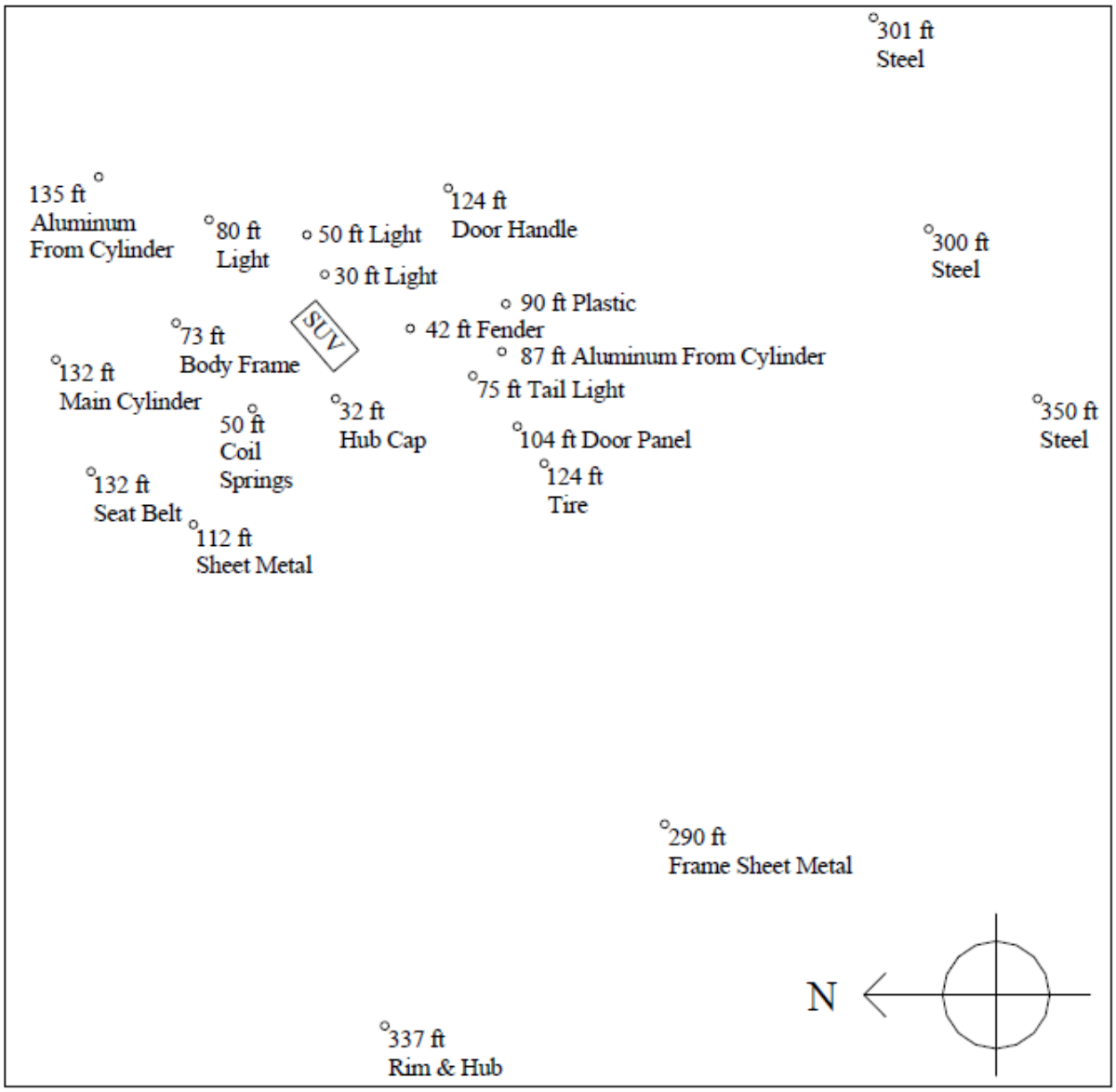

Figure 54. Location of various parts following the explosion (Weyandt, 2006).

3.4.2.4 Structure response (DTU, UU)

The above described phenomena also have impact on structures. The effect of temperature and the response of structures made of steel and concrete are already described in chapter 3.2.6. During explosions the generated overpressure loads are to be absorbed by the structures. In tunnels the pressure in blast wave after deflagration or tank rupture can be predicted with advanced CFD codes due to various reflections and influence of obstacles providing congestion. The tunnel structure allows blast wave to travel along the tunnel and may lead to the damage of the tunnel and destruction of its equipment such as ventilation fans, lightning, sensors etc. Projectiles from ruptured pressure vessels may contribute to this. The travelling of the fireball after tank rupture in a fire in a tunnel gives rise as well to both thermal (temperature and heat radiation) and pressure (pressure and impulse) loads. It is important to know both the blast wave and fireball dynamics in a tunnel to fully assess their harmful effect on people and damaging effect on structure. Further studies of both experimental and numerical nature should be conducted for a better understanding of the phenomena.

3.5 Interaction between hydrogen fire and conventional vehicle fire (DTU)

The section will focus on vehicle fires as conventional fires and their interaction with hydrogen fire from TPRD. Furthermore, third vehicles nearby a hydrogen vehicle may likely be the cause of fire and fire spread in tunnels and confined spaces. Also, it is assumed that the amount of combustible construction materials is reduced to a minimum in such infrastructures.

3.5.1 Heat release rate (UU, DTU)

The statistics on fires occurred in hydrogen-powered vehicles (HPV) is absent up to date. Nevertheless, as the hydrogen infrastructure develops in different countries, the HPV fleet will also grow. This implies that these vehicles are subject to risk of fires as much as gasoline vehicles. In such a fashion, the assessment of the nature of a vehicle fire gets more importance.

In Great Britain, for the period since 1994 to 2005 it was registered 3096 car park fires (in buildings); nearly half of these, i.e. 1592, were initiated in vehicles (Department for Communities and Local Government, 2010). From 2004 to 2008 the number of fires and explosions at public service stations in USA comprised 5020 (Evarts, 2011). At these service stations from 2004-2008 the outside and other fires comprised 770, structure fires were 600, outside trash/rubbish fires were 600 and vehicle fires comprised 3050 (2500 of passenger vehicle fires, 270 of mobile property (unclassified), 220 of road freight or transport vehicles, 30 of camper or recreational vehicles, 20 of off-road or heavy equipment and 10 of others) (Evarts, 2011). The average annual number of car fires in Great Britain comprised about 64,100 during the period from 2000 to 2012 (Department for Communities and Local Government, 2010). The average annual number of vehicle fires in the USA during the period from 2003 to 2007 comprised 287,000 (93% from these were highway vehicles, 85% – passenger road vehicles, 8% – trucks or fright road vehicles) (NFPA, 2010).

Besides the numbers of the vehicle fires, it is important to pay attention to the durations and HRRs reached in the fires for different vehicles. The highest values of HRRs are produced by heavy goods vehicles (HGV). The recent research indicated the HRRs in HGV fires reached 100-200 MW (Jönsson and Herrera, 2010; SOLIT, 2007; UPTUN 251, 2006) as well as the latter higher value was also mentioned in (Tarada, 2011) and (McCory et al., 2008). Tarada (2011) provides the data on HRR of the fires with HGVs and vehicles with dangerous goods as high as 120 MW; the petrol tanker fuel spills fires can reach 200-300 MW. (Tarada, 2011) also gave the typical HRRs for different vehicle fires: passenger car (5-10 MW); light duty vehicle (LDV, 15 MW); coach, bus (20 MW); lorry, HGV up to 25 tonnes (30-50 MW); HGV, 25-50 tonnes (70-150 MW); petrol tanker (200-300 MW).

The heat release rate (HRR) is not only a property of the burning material but is strongly influenced by the characteristics of the encloser around the fire. The HRR from a car in open air is usually lower than the similar car burning in an enclosure due to radiative feedback from the heated surfaces of the structure. Therefore, HRR time histories cannot just be transferred from one geometry to another and needs careful considerations. As experiments are expensive it is necessary to develop suitable models to predict HRR in different types of enclosures. This is important to predict fire spread and the thermal and mechanical stresses in the structures caused by a fire.

The tunnel ventilation conditions have additional essential influence on the HRR time histories. In general, the higher the air velocity is, the higher the HRR would be (Cheong et al., 2008).

The data on fires in tunnels, especially spills, shows that the HRR can be quite large. For instance, the USA accident with gasoline tanker in Caldecott tunnel had 33.3 m^3 of gasoline burnt in 40 min, giving a 430 MW fire (Larson et al., 1983; Ingason and Li, 2017). The Skatestraum tunnel incident involved a 16.5 m^3 tanker trailer that collided with the tunnel wall and ruptured. The initial spilled gasoline burned at estimated HHR up to 440 MW for a duration of 7 min, while the gasoline left in the tank was burning for about 41 min at an estimated HRR of 220 MW. Some of the gasoline reached the sewer and is assumed to be burned there (Statens havarikommisjon for transport (SHT), 2016).

In case of a single passenger car fire the HRR is not as large as in case of spill of a tanker. The on-road vehicles vary from motorcycles to HGVs or even petrol tankers. Okamoto et al. (2013) described car fires lasting as long as 2 hrs with peak HRR as high as 4 MW. Tohir and Spearpoint (2013) described the vehicle fires from mini to heavy passenger cars, SUVs, MPVs, etc., as long as 1 hr 40 min, and achieved range of HRRs up to nearly 8.85 MW. In experiments by Mangs and Keski-Rahkonen (1994) the peak HRR in a car fire reached about 1.9 MW. The car fire experiments (Department for Communities and Local Government, 2010) demonstrated the peak HRR of 3.8-16 MW (latest denotes several vehicles).

The total HRR of a car fire may be increased by an additional TPRD activation and combustion of released hydrogen. It is important to understand how this number changes with different TPRD sizes and what safety technology will allow to release gas safely without rupture and not increase the HRR significantly. Let us assume the HPV passenger car is caught on fire and the TPRD is activated, supposedly at the peak HRR of a fire. Let us take the realistic hydrogen tank of 62.4 L volume and 700 bar storage pressure (Yamashita et al., 2015) and 3 different TPRD diameters, i.e. 3 mm (Mattelaer, 2018), 1 mm and 0.25 mm. The latest value is the TPRD orifice diameter equivalent to the overall opening size of the explosion-free in a fire tank (Molkov et al., 2017) releasing the gas estimated by the authors from the experimental data in the blowdown part of the test. Using the blowdown engineering tool of “e-Laboratory” (2019) based on the background theory (Molkov, 2012), we shall estimate the dynamic mass flow rate from the TPRD during the tank blowdown. Using the hydrogen gas heat of combustion 119.93 MJ/kg, we estimate the dynamically changing HRR of hydrogen jet fire from TPRD, assuming the release is ignited in a fire, where the maximum HRR will be at the start of release. The two passenger car fires HRR curves were taken for comparison against the TPRD HRR curves: (Mangs and Keski-Rahkonen, 1994) and (Okamoto et al., 2013) – designated as experiment A and B respectively. Figure 55 shows the plot of HRR of hydrogen jet fire from 3 mm TPRD against the HRR curves of the above two car fires.

It is seen from Figure 55 (left and right) that the 3 mm jet fire HRR reaches its maximum of up to 29 MW in the beginning and very quickly decreases. Although the hydrogen jet fire duration is less than 2 min, its peak is higher by almost 9 times the peak HRR of conventional car fire experiment B and almost by 14 times car fire experiment A. There is a disruption in the Y-axis at HRR value above 4 MW to demonstrate the peak HRR from 3 mm TPRD activation jet fire comparable with car fires’ HRR. Figure 55 (right) shows the scaled-up blow-down history over X-axis to make the blow-down history distinguishable, even through such a “big” TPRD orifice diameter.

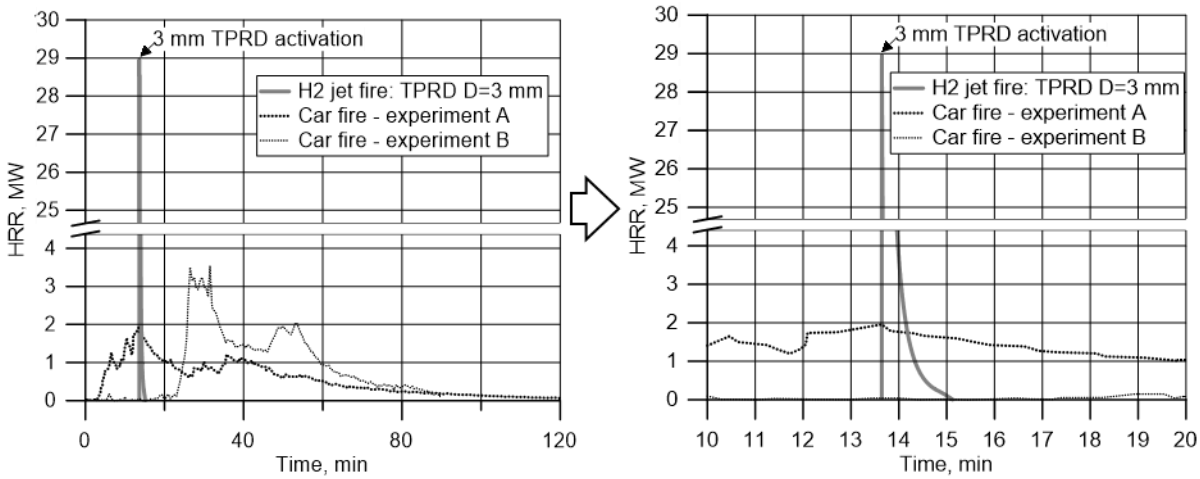

Figure 55. Hydrogen jet fire HRR from 3 mm TPRD (grey solid curve) and car fire HRRs histories (black dash curves): A - Mangs and Keski-Rahkonen (1994), B - Okamoto et al. (2013): left – overall HRR histories, right – scaled up TPRD jet fire history.

Let us now compare the car fires' HRR curves against the jet fire HRRs through 1 mm and 0.25 mm TPRDs, see Figure below.

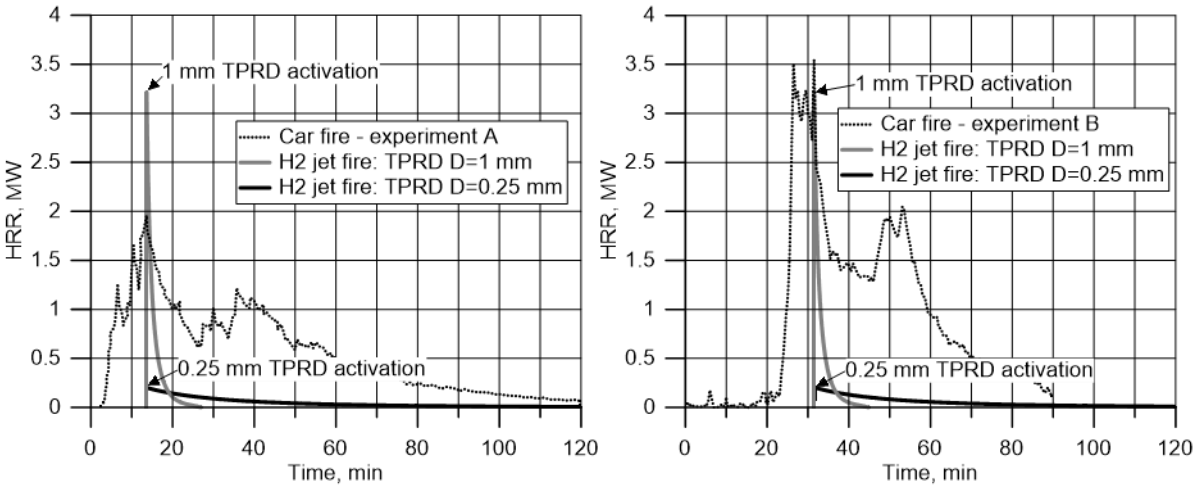

Figure 56. Hydrogen jet fire HRR from 1 mm TPRD and 0.25 mm TPRD (black and grey solid curves respectively) and car fire HRRs histories (black dash curves): experiment A (left) and experiment B (right).

Figure 56 (left) shows that the blowdown through 1 mm diameter TPRD gives the short duration jet fire with the maximum HRR value of 3.21 MW. This is by about 62% higher than the peak HRR in car fire experiment A and by about 9% lower than the peak HRR value of car fire experiment B (right). The TPRD activation time was "set" to the car fire peak HRR for the comparison purposes only. The blowdown from the 0.25 mm diameter TPRD or tank manufactured following explosion-free in a fire technology (providing an equivalent leak size), gives significantly less HRR than car fire HRRs. For test A its maximum HRR is less than car fire HRR peak by 10 times and by about 17.5 times for test B. This means that there is practically no total HRR increase for hydrogen vehicle in the case of use of TPRD diameters of factions of millimetre or using explosion-free in a fire tanks.

From results in Figure 55 and Figure 56, it can be concluded that the explosion-free in a fire safety technology is the promising way forward as it not only excludes tank rupture but doesn't

increase the total HRR in vehicle fire. This engineering solution also excludes long jet flames from TPRD, and eliminates such catastrophic consequences of tank rupture as blast wave, fireball and projectiles. The last but not least, the use of this safety technology eliminates one of the most hazardous phenomenon for hydrogen cars in garages, i.e. the pressure peaking phenomenon.

The HyTunnel-CS project aims to study the effect of TPRD diameter and the use of explosion-free in a fire tanks on fire dynamics of vehicle fires.

3.5.2 Toxicity (DTU)

Hydrogen is a non-toxic compound and the only direct toxic impact to humans is by asphyxiation. Hydrogen has also no ecotoxic effects and is readily degraded in nature.

However, the vehicle fires in tunnels or confined space will involve various combustible materials that may give certain yields of toxic emissions depending on the fire conditions. A single car fire in a tunnel may normally be regarded as a well-ventilated fire. This provides the most effective combustion. Depending on the specific material such a fire may release about 60 to 90% of the possible total combustion heat. The main products are carbon dioxide, water vapour and various amounts of soot. The latter depends on the chemical nature of the burning material. Incomplete combustion of organic materials produces carbon monoxide with yields depending on the ventilation conditions. A minimum is produced under well-ventilated conditions, while under-ventilated fires will produce much higher yields. Similar, materials containing nitrogen atoms in their chemical structure yield hydrogen cyanide in under-ventilated conditions, while mainly nitrogen oxides are yielded under well-ventilated conditions. From burning PVC the toxic emission will be hydrogen chloride and hydrogen fluoride is expected from fluorinated compounds. Hereunder, it is found that Li-ion batteries may emit additional amounts of hydrogen fluoride in a battery fire (Truchot et al., 2018). These gases are providing the acute toxic load of a burning vehicle.

Soot that contains various amounts of poly-aromatic hydrocarbons (PAH) will provide a chronic toxicological effect that endangers the work of firefighters as they are repeatedly exposed over many years. Other partly degraded organic compounds are typically found in fire emissions, such as aldehydes or dioxins.

Several authors investigated the fire emissions from vehicles (Wichmann et al., 1995; Lönnermark and Blomqvist, 2006; Truchot et al., 2018). Truchot et al. (2018) found the yields listed in Table 7. Lönnermark and Blomqvist (2006) found in their vehicle fire tests a total PAH yield of 1.1 g/kg, while the total dioxine content (PCDD) yielded 0.0021 mg/kg. The total amount of particles is given to yielding 64 g/kg. The volatile organic compounds are yielding 8.5 g/kg. The total amounts per burned car are listed in Table 8. Additional to organic emissions, a number of metallic compounds were measured by the authors, such as arsenic, cadmium, chromium, lead, zinc, and others. The yields of lead (820 mg/kg) and Zinc (3200 mg/kg) are by far the dominating emissions in the test.

The threshold values for the toxicity for some of the emitted gases is in the lower ppm range (see Table 9 and therefore such emissions need to be regarded in fire scenarios in closed spaces as they may be of importance with evacuation scenarios).

Table 7. Fire emissions testing selected specific vehicle components (Truchot et al., 2018).

Product category	Plastics	Tyres	Cables
Amount burned [kg]	48	49	36
Yields [g/kg]:			
Carbon dioxide	2034	1469	728
Carbon monoxide	20	42	9.1
Hydrogen chloride	2.2	0.2	2.1
Hydrogen fluoride	0.014	0.003	0.11
Nitrogen oxides	5.0	2.8	2.5
Sulphur dioxide	–	10	–

Table 8. VOC fire emissions for a burned car (Lönnermark and Blomqvist, 2006).

Compound	**Total mass per car (g)**
Benzene	322
Toluene	71.9
Styrene	54.1
Ethylbenzene	19.2
Phenol (partly benzaldehyde)	39.1
Benzonitrile	25.0
Indene	15.3
Total amount of VOC	**928**

Table 9. Data for the toxicity thresholds of inorganic gases (10 min non-reversible threshold limit) (Truchot et al., 2018).

Compound	**Non-reversible threshold (10 min) ppm**
Carbon monoxide	2600
Hydrogen fluoride	600
Hydrogen chloride	240
Hydrogen cyanide	62
Nitrogen monoxide	150
Nitrogen dioxide	60
Sulphur dioxide	128

3.5.3 Visibility (DTU)

An important parameter in any fire safety engineering (FSE) scenario is the visibility and its development during a fire. This is modelled as the density of particles (soot) and its distribution over time in the enclosures. Threshold limits depending on the size of the enclosure are defined and the time to reach this threshold limits is calculated, which may be used for calculating the available safe egress time (ASET). This is one of the tenability criteria used in FSE.

Hydrogen is not generating any soot while burning, but other materials does. Materials generate various amount of soot. This is assessed using the smoke potential parameter. In modelling, the Lambert Beers law is used to implement the calculation of the distance for visibility.

There are a number of other tenability criteria defined, such as a humidity level and upper layer gas temperatures, toxicity, heat radiation criteria, etc. For hydrogen jet flames, water vapour is produced and the humidity in enclosures is influenced. The heat radiation from hydrogen fires is less than from fossil fuel fires. However, the soot produced by conventional fires, as well as dust particles or erosion processes, may increase the radiation to a higher level when entraining and mixing into the hydrogen flames.

In order to define an overall ASET, the tenability criteria (ISO/TR 13571-2, 2016) with the fastest time to reach ASET is compared to the required safe egress time (RSET) value.

3.5.4 Escape time (DTU)

The escape or required safe egress time (RSET) is an essential parameter to predict a safe fire design. The RSET is compared to the ASET. If the RSET is lower than the ASET, a safe evacuation may be possible. The RSET may be determined through various models. In cases where only a few people are present, hydraulic type of models maybe applicable, while more sophisticated models are needed for complex infrastructures with many people present. There is a vast literature on this item, e.g. Hurley et al. (2016). An overview on evacuation modelling is provided by Ronchi (2013). The author performed a number of tunnel evacuation experiments in a Swedish tunnel and modelled these scenarios with different degree of modelling sophistications:

A) The analytical calculations described in the Society of Fire Protection Engineers (SFPE) handbook (Hurley et al., 2016);
B) An individual use of evacuation models;
C) A multi-model approach. Six evacuation models were employed, namely FDS+Evac, BuildingEXODUS, STEPS, Pathfinder, Gridflow and Simulex.

The results showed that:

1) The use of model default settings produced significant differences in the results;
2) The calibration of models input required different degrees of effort in relation to the model sophistication level, i.e. whether it used deterministic assumptions or not;
3) Analytical calculations were not a sufficient method to simulate complex tunnel evacuation processes, i.e., exit choice in smoke;
4) The use of a single model was not sufficient if the modellers had not information to calibrate the input;
5) The multi-model approach was a useful tool to test the sensitivity of the results to the model employed and the model sub-algorithms.

3.5.5 Fire spread scenarios (DTU)

Chapter 3.5.1 described tunnel accidents involving HGV that may start major fires and which are known to be a threat to the tunnel structures. The event of a fire initiating in a smaller vehicle may as well escalate to a scenario where the fire spread to several vehicles in a tunnel or similar confined spaces as e.g. car parks. The specific scenario depends on the location and time, as they determine the number of cars and traffic. As an example, during the night only a minor traffic is expected, whereas a major traffic is expected at rush hours and big events as concerts, football matches, festivities, etc.

Assuming that in a first instance a single car is burning, the fire may spread to a neighbour vehicle depending on the parking distance between cars (see Figure 57) or queuing distance in a tunnel (Tohir and Spearpoint, 2013; Tohir et al., 2018). The latter is defined by traffic regulations for the specific tunnel, which had been implemented after major accidents as the Mont Blanc tunnel fire (see Figure 58). It may be intuitive that the shorter the parking distance, the higher is the probability of ignition of a second car and fire spread to other cars. Car parks are designed assuming that fire may only spread to a few cars before the fire brigade gets control over the situation. Literature studies assume a 12 minutes period for the fire spread from one gasoline fuelled car to another. Statistical research and tests from the European commission of steel structures stated that in an open car park at most 3-4 vehicles are expected to be on fire at the same time. Nevertheless, there may be more disastrous scenarios. As an example, the recent Liverpool multi-storey car park fire on December 31, 2017, destroyed 1400 cars, and led to the collapse of parts of the building structure. Such events question the validity of current design praxis of car parks.

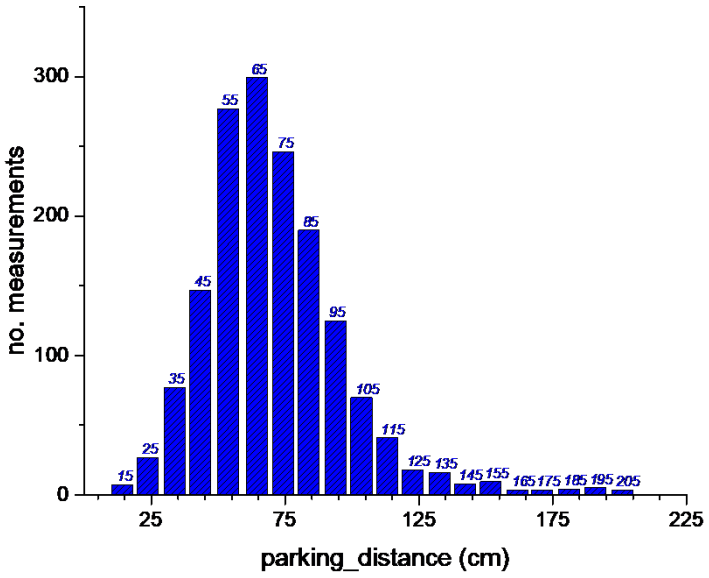

Figure 57. Distribution of parking distances (Franssen et al., 1997).

Road rules & regulations

Safety is the utmost priority for the operators of the Mont Blanc Tunnel and **speed limits** must therefore be strictly adhered to. Anyone caught flouting the speed regulations are liable to a hefty fine or confiscation of their licence.

1. Minimum Speed limit: 50 km/h
2. Maximum Speed limit: 70 km/h
3. Minimum distance between vehicles: 150 m

All moving vehicles must use dipped headlights whilst in the tunnel and stopping and/or parking on the carriageway is strictly forbidden, as is overtaking, U-turning and reversing. Each driver is issued with a Mont Blanc Tunnel safety leaflet on payment of the toll which explains the road and safety regulations in three languages (English, French & Italian). Motorists are also asked to listen to the radio whilst driving through the tunnel.

There are 120 cameras located within the tunnel which are able to detect the slightest incident. From the control room, 18 traffic safety operators monitor the tunnel 24 hours a day, using an automated assistance system which implements an appropriate operating procedure depending on the type of incident detected – e.g. activation of message boards, ventilation, initiating emergency responses and sending warning messages to emergency response personnel. Fire engines are positioned at both entrances and in the middle of the tunnel so that the anticipated response time for any incident is estimated at no longer than 6 minutes.

Figure 58. Road rules & regulations for the Mont Blanc Tunnel (Chamonet, 2019).

A number of investigations have been made concerning vehicles performance in car park fires, but only a few are concerned with hydrogen-powered vehicles (HPV) (Wu, 2008; Schneider et al., 1999; Middha and Hansen, 2009; Tamura et al., 2014; Søgaard et al., 2018). It is therefore important to investigate in more detail tunnel and confined space scenarios to involve fire spread and structural damage as well as evacuation scenarios. Furthermore, new types of car park should be evaluated as e.g. automatic parking facilities where cars are closely placed using a robotic system.

3.5.6 Firefighters' intervention and hazards (IFA)

Firefighters responding to the scene of an accident in a tunnel or other confined spaces may be exposed to both hazards associated to conventional vehicles fires and specific hazards associated to hydrogen powered vehicles. This section describes the major hazards for firefighters.

3.5.6.1 Smoke (IFA)

A major hazard for firefighters is smoke. Firefighters protect themselves by using self-contained breathing apparatus (SCBA), sometimes referred to as a compressed air breathing apparatus (CABA) or simply breathing apparatus (BA).

One of the most important objectives of the preventive fire protection is to delay or control the direction of smoke and heat expansion dividing the facility into sections. Naturally this is difficult in tunnels. The tunnel tube between the two portals cannot be segmented without great effort and in consequence they present one continuous fire compartment per tube. Nevertheless, the venting regimes aim to keep partitions of the tunnel free from smoke.

Chances of survival in the smoke are low. As a rule, distances in a road tunnel are too long to hold one's breath and escape through the smoke. Furthermore, smoke can spread faster than people can run. Victims who do not manage to flee from an area filled with dense smoke to a

safe area, have little chance of survival. Thus, operations utilising breathing apparatus in a tunnel are even less failure tolerant than fire operations in residential structures, which is why safety rules have to be taken extraordinarily seriously. Even so, at search and rescue operations it cannot be presumed that no one can survive in a tunnel filled with smoke. In the year 2000 during a lorry fire in the Norwegian Seljestad road tunnel, one person survived exposure to smoke for over an hour. At the fire in the Tauern road tunnel (A) in 1999, firefighters saved three lorry drivers trapped in the smoke.

3.5.6.2 Heat (IFA)

Although very high temperatures can occur at vehicle fires in confined spaces this can be overcome utilising the appropriate tactics. While still problematic, the heat radiation and convection of the fire are not the greatest stresses placed on the firefighter. Thermal stress caused by great physical strain in combination with the now common turnout gear is more of an issue. Working with breathing apparatus under the considerable weight of personal protective equipment is difficult enough. However, when this is combined with the enormous effort required to complete the necessary tasks such as carrying a victim over long distances it can lead to critical heat accumulation, resulting in a loss of performance and potentially to a serious risk to health. Therefore, the physical strains on firefighters should be limited as much as possible, like using transport aids such as a basket stretcher with wheels. If such equipment is not available, more personnel must be deployed, for example four instead of just two persons for rescuing a heavy victim (Brauner et al., 2016).

Vehicle fires can produce temperatures locally exceeding 1000 °C (Schneider & Horvath, 2006). However, it cannot be concluded that fire services cannot achieve anything at the scene. Such temperatures can also occur in structure fires (Drysdale, 1999). Regardless, an interior fire attack is a common procedure in Central Europe.

For fire operations it is not that important whether unbearable high temperatures arise, but rather where they arise. On the downstream side of a fire unbearably high temperatures can arise, despite the use of good protective equipment (Guigas et al., 2006). The highest temperatures are expected at the ceiling, but they can also occur at ground level (Schneider & Horvath, 2006). On the upstream side, bearable working conditions can exist at least up to the height of the head. Firstly, because there is a vertical temperature gradient: highest temperature at the ceiling, lower temperatures at the floor. The high ceiling of road tunnels supports this effect even more. Secondly, most of the heat generated by the fire is discharged on the downstream side with the conveying smoke. Thirdly, cool fresh air flows constantly towards the fire on the upstream side. All of these effects enable a firefighter to approach the seat of fire close enough to fight it effectively (Blennemann, 2005). However, for these effects to aid the firefighter the flow of air must remain sufficient.

The enormous heat radiation from a vehicle fire can keep the firefighters at the distance outside of the casting distance of their water streams. If so, firefighters can only advance slowly while constantly cooling the construction and other vehicles and by staying behind cover.

In practice firefighters will protect themselves simply by keeping distance to the heat sources. If necessary special extinguishing equipment will be used to bring in the water over large distances. Never ever will firefighters try to measure heat radiation and act on results from that.

They rely on their senses and experience. This is the reason why burn injuries to firefighters are very seldom.

In the majority of tunnel fires, an approach from the upstream side should allow to reach casting distance, whilst using a shielding water spray and constantly cooling down the structure, ceiling and walls. After calculations of the Fire Research Institute of Saxony-Anhalt (Institut der Feuerwehr Sachsen-Anhalt) an approach of up to 24 m, even at a fully developed lorry fire, should be possible (Pleß and Seliger, 2009; Koinig, 1999).

Vehicle fires in tunnels spread mainly through means of heat convection in the direction of air flow. Therefore, the thermal load on the downstream side develops to the maximum, with the top vertical air layers being the hottest. Lorries pose the biggest hazard; due to their height they reach up into the highly heated air layers close to the ceiling. Because of this, the fire can spread over longer distances with no vehicles and spanning distances up to 50 m are to be expected (Pleß & Seliger, 2009, p. 19). To prevent such fire spreads, many tunnel carriers try to control the traffic in order to increase the distance between lorries. The Gotthard road tunnel for example regulates the inflow of lorries. Road markings and signs aiding the drivers in maintaining a safe distance between them and the next vehicle can also be used.

3.5.6.3 Electricity (IFA)

Firefighters can be harmed by electrical systems in vehicles. They try to protect themselves by using main shut-off switches if available and by using the appropriate extinguishing techniques. Hazards of electricity are not a hydrogen specific issue but are rather associated with the fuel cell system in the vehicle.

3.5.6.4 Hazards of explosion (IFA, UU)

Fire fighters cannot protect themselves against direct impact from shockwaves from explosions. The only way to protect themselves is to recognize that an explosion may occur and then to keep appropriate distance. However, it is known that in tunnels blast wave propagate along the whole duration of the tunnel with little decay. Thus, all possible should be done to eliminate the blast wave hazards in tunnels and similar confined spaces. One important issue to be addressed is given by the capability to recognise an explosion potential and assess its consequences.

3.5.6.5 Firefighter's reconnaissance in clean air (SPFI)

Assessments during firefighter's intervention and reconnaissance are typically done in the timeframe of minutes or even seconds. Easy recognizable elements should therefore be triggers to support a fast decision-making process. Typically, the available time frame is within fractions of the one available for academic environments. However, the fire service relies heavily on the work delivered by scientists to aid their preparation for interventions, extracting from these studies easy and practical elements for a fast decision-making process. The following hydrogen combustion characteristics may influence the reconnaissance and intervention strategy of the fire services.

3.5.6.6 Invisible flame (SPFI)

As mentioned in section 2.2, the flames provided by hydrogen's combustion in clean air are nearly invisible to the human eye due to the absence of soot. Thermal imaging cameras are therefore an indispensable tool at a fire scene. In the open space and simple configurations, the

hydrogen jet flame may likely stand out among the non-burning elements. However, in confined areas such as tunnels and underground parking lots, fires from other burning cars may surround the hydrogen jet fires from a TPRD, hiding them within their flames.

3.5.6.7 Low radiative fraction (SPFI)

Due to the lack of soot, a hydrogen flame emits a limited radiant heat. If no thermal imaging cameras are used to observe the hydrogen flame, firefighters may be posed to danger as they approach the seemingly unburned object. Firefighters may expose themselves to the flame without feeling a warning while approaching it, given the absence of a heated transition area close to the flame as consequence of the low radiant heat and invisible flame.

3.5.6.8 Heat Release Rate (SPFI)

Hydrogen has a heat of combustion per unit of mass significantly higher than conventional fuels: it is 10 times higher than the value of cellular materials (e.g. wood), and up to 4 times higher than an average petrol fire. The main method used by the fire service to put out fires is by relying on the heat absorption of water. Theoretically, 3 MJ is required to heat up 1 litre of water, vaporize it and further heat it up to 300 °C. Although it is difficult to assess the portion of water applied to a fire actually reaching the fire and absorbing the heat, or to what temperature the steam actually rises, it can be said that there is a correlation between the HRR of a fire and the water flow required to extinguish it. Since hydrogen has such a higher heat of combustion, it is of interest to assess the water flow required for a certain ignited hydrogen release and thus its HRR. Furthermore, correlations for other parameters such as flame height or temperature reached at a certain distance from the fire could be as well useful indicators during a reconnaissance.

3.5.6.9 Structures protection (SPFI)

Firefighting in large confined spaces requires different tactics from fires in open space or small compartments. Tunnels typically require longer intervention times which may result in higher heat impact on the structure. To deal with this, the fire service dedicates part of its intervention on cooling the structure (Vogt, 2017). In Belgium 2/3 of the water flow is aimed at this, whereas 1/3 is provided on the fire source itself. Although these general practices vary according to a large set of parameters including HRR, tunnel cross section, ventilation, etc., it is unknown whether they may or may not be sufficient for incidents with hydrogen.

4. Harm and damage criteria (UU)

The main aim of predicting the consequences of a possible accident scenario is to analyse the potential harm to people and damage to infrastructures to avoid the occurrence of injury/fatality or property destruction, respectively. The definition of acceptance and harm criteria is of utmost importance to assess the effect of the hazards associated to hydrogen powered vehicles or hydrogen transport presented in Chapter 3. As a consequence, the hazard distances to certain harm levels can be calculated. In the following sections, a review of the available in literature harm and damage criteria is presented. However, stakeholders should be aware that different standards and thresholds may be in act according to the country of application.

4.1 Harm criteria for unprotected and protected people (UU)

Harm criteria for people can be expressed in terms of injury or fatality. It may be possible to define an acceptable level defined as “no harm” criterion. Below this limit, accident consequences are low enough to not incur in any injury. The definition of globally applicable harm criteria is challenging. Indeed, the potential damage depends on the vulnerability of the target, which is determined for people by age, health conditions, etc…

As discussed in section 3.1.1., hydrogen is not a poisonous gas. However, its release in a fully/partially confined space can form an oxygen-deficient atmosphere, leading to asphyxiation. The effects of oxygen depletion on humans were already presented in Table 2 and are not repeated here. Therefore, the present section will focus on the thermal and overpressure effects associated to hydrogen combustion and explosions.

4.1.1 Thermal harmful effects (UU, IFA)

The exposure to hydrogen fires or direct contact with flames may result in first, second or third degree burns. It may conservatively be assumed that the direct contact with flames would result in fatality (LaChance et al., 2011).

During a hydrogen fire, the surrounding air may be heated up significantly, causing harm to people in the fire vicinity. Direct contact with the hydrogen flame and hot combustion products can cause severe thermal burns. Exposure to high temperature air may also lead to difficult breathing and respiratory tract burns (HyResponse, 2015b). Table 10 presents the effects of the air high temperature on people.

Table 10. Effect of air temperature on people (HyResponse, 2015b).

Temperature of air, °C	Physiological response
70	No fatal issues in a closed space except uncomfortable situation
115	Threshold for pain (exposure longer than 5 minutes)
127	Difficulty breathing
149	Breathing via mouth is difficult, temperature limit for escape
150	Skin burns occur in less than 5 minutes
160	Rapid, unbearable pain with dry skin
182	Irreversible injuries in 30 seconds
203	Respiratory system tolerance time is less than 4 minutes with wet skin
309	Third degree burns for 20 seconds exposure, causes burns to larynx after a few minutes, escape is not possible

A second source of hazard is given by the radiative heat flux emitted by the fire. The associated effects on unprotected people were reported by LaChance et al. (2011) and HyResponse (2015b). Values are showed in Table 11. A radiative heat flux level of 1.6 kW/m^2 is identified as a no harm criterion. Below this limit no effects are expected on people for long exposures.

Table 11. Effects of radiative heat flux on people (LaChance et al., 2011; HyResponse 2015b).

Thermal radiation intensity, kW/m^2	Effects on people
1.6	No harm for long exposures; safe for the general public and the stationary personnel
2.5	Intensity tolerable for 5 min; severe pain above this exposure time
3	Intensity tolerable for non-frequent emergency situations above 30 min
4-5	Pain for 20 s exposure; first degree burn
9.5	Second degree burn after 20 s
25	Significant injury in 10 s; 100 % lethality in 1 min
35-37.5	1% lethality in 10 s

Operators not wearing protective clothing should not be exposed to radiative heat flux above 1.5 kW/m^2 (Heus and Denhartog, 2017). This value agrees with the acceptable radiative heat flux indicated by Pleß and Seliger (2009) for firefighters for a long exposure and shown in Table 12. However, both sources report a limit slightly lower than the "no harm" level of 1.6 kW/m^2 reported by LaChance et al. (2011). Firefighters responding to an accident scene will be equipped with thermal protective clothing and equipment. Therefore, they can withstand higher levels of thermal radiation. Heus and Denhartog (2017) reported that firefighters wearing protective clothing (EN469) can perform emergency operations for a duration of approximately 3 minutes when exposed to heat fluxes up to 4.6 kW/m^2, which agrees with the intensity indicated as tolerable for emergency personnel in (HyResponse, 2015b). Citing Koinig (1999), Pleß and Seliger (2009) provided values in Table 12 on acceptable heat radiation for firefighters. However, it should be noted that these are indicative thresholds, following the considerations presented in section 3.5.6.2 on firefighters' strategies and distances to heat sources.

Table 12. Acceptable heat radiation for fire fighters.

Heat radiation kW/m^2	**Effect on firefighters**
1.5	Bearable for a long time.
4.5	Bearable with normal protective turn-out coats.
8.0	Need of cooled protective coats.

The harm level is function of both thermal radiation intensity and exposure duration, thus it is usually expressed in terms of thermal dose (TD), as discussed in section 3.2.3.2. LaChance et al. (2011) reported the thermal dose ranges available in literature leading to first, second or third degree burns. The thermal dose levels are different depending on whether emitted radiation is included in the ultraviolet or infrared range of the spectrum. Threshold doses for both the spectrum ranges are given in Table 13. Exposure to infrared radiation results to be more dangerous, as shown by the lower and more conservative TD limits.

Table 13. Effects of thermal dose on people (LaChance et al., 2011).

Burn Severity	Threshold Dose $(kW/m^2)^{4/3}s$	
	Infrared	Ultraviolet
First Degree	80-130	260-440
Second Degree	240-730	670-1100
Third Degree	870-2640	1220-3100

4.1.2 Overpressure harmful effects (UU)

Humans can be strongly affected by a blast wave directly through injuring human organs sensitive to pressure, e.g. eardrum rupture and lung haemorrhage. Indirect effects to a human involve body displacement with possible fatal injuries, e.g. a human may hit the head or receive lethal fractures, e.g. if the body is projected against obstacles. The people are more vulnerable to harm when being indoors. This is due to fragment effect, e.g. skin lacerations by flying glass, injuries from falling building parts, e.g. shattered walls and brickworks. Harm criteria which are given in this study were gathered from different national and international sources, including codes, guidelines and best practices. The harm effects to people due to blast wave overpressure, ΔP, and impulse, I, are shown in Table 14.

Table 14. Effects on people from blast waves.

Effects on people	**ΔP, kPa**	**I, Pa·s**
People indoors		
10% occupant vulnerability (probability of serious injury/death) - wood-frame and non-reinforced masonry bldg.) (API, 1995)	6.9	-
Injuries likely from broken glass and structure debris, personnel are highly protected from fatality and serious injury (API, 1995)	8.27	-
20% occupant vulnerability (non-reinforced masonry) (API, 1995)	8.62	-
40% occupant vulnerability (steel-frame bldg.) (API, 1995)	10.34-17.24	-
Injuries from secondary blast effect (e.g. debris) (API, 1995)	11.72	-
Temporal loss of hearing / injury from secondary blast effect (structure debris / body translation); no fatality or serious injury; injuries from fragments to personnel in open (API, 1995)	15.86	-
100% vulnerability (non-reinforced masonry) (API, 1995)	20.68	-
20% fatality probability (Health and Safety Executive, 2010)	21	-
Personnel serious injury (fragments/firebrands) (API, 1995)	24.13	-
100% vulnerability (wood- & steel-frame bldg.) (API, 1995)	34.47	-
Serious injury is likely to be brought by blast, missiles, debris and translation of a body (API, 1995)	55.16	-
100% fatality probability (unprotected structures) (Health and Safety Executive, 2010)	70	-
People (unprotected) outdoors		
50% blowdown (NFPA, 2011)	-	60
Lung haemorrhage threshold (NFPA, 2011)	-	180
Severe lung haemorrhage (NFPA, 2011)	-	360
1% serious injury from displacement (NFPA, 2011)	-	370

1% fatality probability (NFPA, 2011)	-	590
50% fatality probability (NFPA, 2011)	-	900
Irreversible effects from “grave” danger threshold (Ministère de l’Interieur, 2013)	5	-
People are knocked down (Jeffries et al., 1997)	10.3-20	-
Fatality effects threshold from “grave danger” (Ministère de l’Interieur, 2013)	14	-
Eardrum rupture threshold (Jeffries et al., 1997)	13.8	-
Possible fatality by projection against obstacles (Jeffries et al., 1997)	13.8	-
1% eardrum rupture probability (Fugelso et al., 1972; Mannan, 2005)	16.5	-
Maximum survivable blast overpressure (Health and Safety Executive, 2010)	17-21	-
Fatal effects from “very grave” danger threshold (Ministère de l’Interieur, 2013)	20	-
1% eardrum rupture (NFPA, 2011)	23	-
1% fatality probability (Health and Safety Executive, 2010)	25-35	-
Eardrum rupture (AIChE Center for Chemical Process Safety, 1999; CCPS, 1994; Federal Emergency Management Agency, 1987)	34.47	-
50% eardrum rupture probability (Jeffries et al., 1997)	34.5-48.3	-
15% fatality probability (Health and Safety Executive, 2010)	35	-
50% eardrum rupture probability (Fugelso et al., 1972; Mannan, 2005)	43.5	-
Internal injuries threshold (Jeffries et al., 1997)	48.3	-
50% fatality probability (Health and Safety Executive, 2010)	50-100	-
Lethal head injury (AIChE Center for Chemical Process Safety, 1999; CCPS, 1994; Federal Emergency Management Agency, 1987)	55.16	-
Standing people are thrown by distance (Jeffries et al., 1997)	55.2-110.3	-
90% eardrum rupture probability (Jeffries et al., 1997)	68.9-103.4	-
Severe lung damage (AIChE Center for Chemical Process Safety, 1999; CCPS, 1994; Federal Emergency Management Agency, 1987)	68.95	-
Lethal injury to body (AIChE Center for Chemical Process Safety, 1999; CCPS, 1994; Federal Emergency Management Agency, 1987)	75.84	-
Lung haemorrhage threshold (Jeffries et al., 1997)	82.7-103.4	-
90% eardrum rupture probability (Fugelso et al., 1972; Mannan, 2005)	84	-
1% fatality probability (lung haemorrhage) (Fugelso et al., 1972; Mannan, 2005)	100	-
50% eardrum rupture probability (NFPA, 2011)	110	-
50% fatality probability (lung haemorrhage) (Jeffries et al., 1997)	137.9-172.4	-
50% fatality probability (lung haemorrhage) (Fugelso et al., 1972; Mannan, 2005)	140	-

99% fatality probability (lung haemorrhage) (Fugelso et al., 1972; Mannan, 2005)	200	-
90% fatality probability (lung haemorrhage) (Jeffries et al., 1997)	206.8-241.3	-
Instant fatalities (Jeffries et al., 1997)	482.6-1379	-

4.2 Damage criteria for structures and equipment (UU)

Structures, equipment and environment will be affected by exposure to radiant heat flux emitted by hydrogen combustion. Table 15 shows the damage criteria according to the radiant heat flux level reported in HyResponse (2015b). An exposure of 30 minutes to a radiant heat flux of 4 kW/m^2 would be sufficient to cause the breakage of glass. Domino effects may be present for levels of 8 kW/m^2.

Table 15. Effect of radiant heat flux on structures, equipment and environment (HyResponse, 2015b).

Radiant heat flux, kW/m^2	Effects on structures, materials, equipment and environment
4	Glass breakage (30 min exposure)
5	Significant windows breakage
8-12	Radiation intensity threshold capable to cause domino effects
10	Heating structures; increase of temperatures and pressures in LH2/GH2 storages
10-12	Ignition of vegetation
10 or 20	Ignition of fuel, oil (120 or 40 s, respectively)
12.5-15	Piloted ignition of wood; melting of plastics (>30 min exposure)
16	Failure of structures (except concrete) in prolonged exposures
18-20	Cable insulation degradation (>30 min exposure)
20	Intensity, which concrete structures can withstand for several hours
25-32	Unpiloted ignition of wood; steel deformation (>30 min exposure)
35-37.5	Process equipment and structural damage, including storage tanks (>30 min exposure)
100	Steel structure collapse (>30 min exposure)
200	Concrete structures failure (in several dozen of min)

The overpressure hazards associated to hydrogen explosions may severely damage the structure or equipment of a tunnel or confined space. Overpressure above 1 kPa may lead to the breakage of glass and windows. This may carry harmful effects, e.g. for people inside vehicles in a tunnel. Overpressure above 15 kPa may already cause collapse of unreinforced concrete walls. A list of the overpressure thresholds and associated damage is reported in Table 16.

Table 16. Effects of overpressure on structures and equipment (LaChance et al., 2011).

Overpressure, kPa	Description of damage
1	Threshold for glass breakage
15-20	Collapse of unreinforced concrete or cinderblock walls
20-30	Collapse of industrial steel frame structure
35-40	Displacement of pipe bridge, breakage of piping
70	Total destruction of buildings, heavy machinery damaged
50-100	Displacement of cylindrical storage tank, failure of pipes

The effect of overpressure on structures and equipment depends on the combined effect with the impulse of a pressure wave. Table 17 describes the damage associated to the levels of overpressure and impulse, as reported in HyResponse (2015b).

Table 17. Combined effect of overpressure and impulse on the level of damage (HyResponse, 2015b).

Overpressure peak, kPa	Impulse, kPa·s	Description of damage
3.6	0.10	Border of minor structural damages
14.6	0.30	Threshold for moderate structural damages: failure of some load-bearing elements
34.5	0.52	Threshold for partial destruction: 50-75% of walls destroyed
70.1	0.77	Total destruction of buildings

4.3 Tenability criteria in relation to safe egress (DTU)

People in a tunnel may be exposed to different hazards during a fire. The most likely exposures are to heat radiation, toxic smoke gases and hot gases as well as dense smoke reducing the visibility. In order to enable a safe egress, a certain tenability level or acceptance criteria need to be evaluated (ISO/TR 13571-2, 2016). The standard is to ensure safe egress in the early stages of any fire, supporting persons individual egress and not the rescue by the fire brigades. The support of the people tenability when a fire is starting is regarded as an essential safety objective of regulations. The ISO standard recognizes the following tenability conditions:

1. Loss of visibility;
2. Thermal effects: hyperthermia of human body, skin burns, burns in the lungs;
3. Toxic effects.

ISO 13571 is a tool developed to quantify the performance level related to the above conditions in a fire event.

Ad 1) the visibilities are calculated using the optical density of smoke based on Lambert Beers law. The standard uses the equations of safe egress that links visibility to walking speed. Such speeds have been experimentally measured and may be calculated using the equations by Nelson and Mowrer that also allow to predict the speeds of crowds. In situations of good visibility (>= 10 m), the movement speed may be 0.5 m/s, while less visibility reduces the movement speed by 50%. Here an acceptance criterion may be formulated that relates the time to evacuate, such as required time to safe egress (RSET), with the available time (ASET) until the visibility is reaching the defined threshold value. Comparison of the ratio ASET/ RSET being less or greater than 1 provides the acceptance of any scenario.

Ad 2) the ISO standard identifies a number of necessary models to predict the thermal effects, such as exposure models predicting temperature impacts on persons being dressed normally or being almost naked. The relative humidity in such scenarios should be less than 10%. The impact on persons can be calculated by dose models using the thermal model FED equation stated in ISO 13571.

Ad 3) the toxic impact is calculated based on a categorization of the gases into asphyxiating gases (as CO, HCN) and irritating gases (as HCl, HBr). Some threshold values are shown in Table 18. Conditions like low oxygen concentration causing hypoxia or high carbon monoxide causing hyperventilation are also recognized. There may be other effects as well as clogging

of the respiratory tracts due to soot. The toxicity of a gas composition is calculated using the fractional effective Dose FED. The FED is defined in ISO 13344:2015 as a "ratio of the exposure dose for an asphyxiant toxicant to that exposure dose of the asphyxiant expected to produce a specified effect on an exposed subject of average susceptibility". This subject is in other words a healthy male adult.

Table 18. Threshold values examples for incapacitation and lethal effects of toxic impacts during a fire taken from (Ingason et al., 2015, p. 394).

Species	**Exposure 5 min**		**Exposure 30 min**	
	Incapacitation	*Lethal*	*Incapacitation*	*Lethal*
CO [ppm]	6000-8000	12000-16000	1400-170	2500-4000
HCN [ppm]	150-200	250-400	90-120	170-230
O_2 [%]	10-13	<5	<12	6-7
CO_2 [%]	1-8	>10	6-7	>9

Another exposure could lead to incapacitation that impacts the evacuation and may lead to lethality. The fractional effective dose can be calculated with the type of equations shown below. The additive effects of several gases present are summed to provide the total dose. Such doses are used as acceptance criteria as shown in Table 19 for the following technical recommendations:

- EU-UPTUN: EU project established acceptance criteria;
- SE-FKR-BV: performance-based requirements and recommendations for fire safety in road tunnels (FKR-BV12) SP Technical Research Institute of Sweden;
- TRVR tunnel 11 from the technical council transport authorities in Sweden publ. nr. 2011:088;
- BBRAD: performance-based design of buildings in Sweden for comparison with building requirements.

It may be seen that the recommended Swedish acceptance criteria for tunnels are close or identical to those of the building requirements.

$$F_{IN,n} = \left(F_{I_{CO},n} + F_{I_{CN}}\right) V_{CO_2,n} + F_{I_{O2},n} \tag{4.1}$$

where $F_{IN,n}$ is the fraction of incapacitating dose calculated on the respective doses for carbon monoxide ($F_{I_{CO},n}$) and hydrogencyanide ($F_{I_{CN}}$) as well as low oxygen concentration ($F_{I_{O2},n}$). V_{CO2} is the carbon dioxide volume in the room that lead to more frequent respiration

The partial incapacitation fractions $F_{I,n}$ are calculated e.g by the following type of expressions given by Purser (2008) exemplified for the carbon monoxide fractional incapacitation dose:

$$F_{I_{CO},n} = \frac{3.317*10^{-5}[CO]^{1.036}\, RMV(t_n - t_{n-1})}{I} \tag{4.2}$$

where $F_{I_{CO},n}$ is the CO fractional incapacitation dose, [CO] is the CO concentration in ppm at time step t_n in min, RMV is the breathing rate (typically 25 L/min for light activity), I is the indicator for incapacitation; the blood COHb (carboxy haemoglobin) value for incapacitation is equal to 30% for light activity. The individual fractions are summed to obtain the fractional effective dose for incapacitation FI($t=t_N$) after a certain exposure time t_N:

$$FI(t = t_N) = \sum_{n=2}^{N} F_{IN,n} \quad (4.3)$$

Table 19. Acceptance criteria for tunnel fires in Sweden (Ingason et al., 2015).

Parameter	EU UPTUN	SE-FKR-BV	SE-TRVR	SE-BBRAD
Visibility [m]	>= 10	-	10 (unknown place) 5 (known place)	10 (space >100 m^2) 5 (space < 100 m^2)
Smoke layer height [m]	-	-	1.6 + H*0.1	1.6 +H_{room}*0.1
Gas temperature [^oC]	<= 60	< 80	<80	<80
Radiation [kW/m^2]	<= 2	<2.5	<2.5 < 10 (short time)	<= 2.5
Toxic gas	FI_{tot} < 1	5% CO_2 <2000 ppm CO 15 % O_2 (max 1 min) or FI_{tot} 0.3 (min. CO, CO_2, O_2 HCN)	-	5% CO_2 <2000 ppm CO < 15% O_2

5. Quantitative Risk Assessment (DTU)

The European Directive 2004/54/EC "Minimum safety requirements for tunnels in the Trans-European Road Network" requires a specific quantitative risk assessment (QRA) for the transportation of dangerous goods in tunnels. This category currently includes hydrogen-powered vehicles and hydrogen transport in tunnels, for which there is not a specifically designed QRA methodology, yet. The reasons are mainly due to a limited knowledge of the consequences of accidents involving hydrogen in confined spaces and the specifics of the associated scenarios, such as first responder's intervention procedures. The present chapter aims at providing an overview of the current QRA methodologies and their potentialities to be applied to accident scenarios involving hydrogen.

5.1 Hazards identification (DTU)

Hazard identification is one of the first steps in the risk assessment procedure. The start is to get to know the infrastructure and the technical installations provided in a tunnel or similar confined space as a car park. Hazard identification is a qualitative measure and some simple schemes have been developed over time to help collecting the identified hazards in a systematic manner. Methods may be "What –if" questions. More advanced methods is the FMEA failure mode and effect analysis that is very suitable to identify component failures and to estimate the importance of these. In case of flow systems as the piping in hydrogen vehicles, hydrogen refuelling stations or industrial process equipment, HAZOP (hazard and operability study) is very useful and is applied in process industries for decades. Other methods that may be applied for hazard identification are fault trees and event trees. These may be used qualitatively but may also be used quantitatively to predict the likelihood of an accident scenario.

As typically hazard identification provides a huge number of potential hazards, some ranking is performed to enable prioritisation between the various hazards identified. The outcome maybe semi qualitative by applying few categories for the likelihood of a hazard to happen (e.g. high, medium, low, extremely low) and also for the consequences of such hazard (e.g. catastrophic, major, minor, negligible). The results may be presented in a risk matrix where the impacts are coloured red, yellow, green for instances (traffic light matrix).

5.2 QRA methodology by PIARC (URS)

The QRAM software (Quantitative Risk Assessment Model) provides a methodology to assess the risks associated with transport of dangerous goods (DG) through road tunnels (INERIS, 2005a,b; PIARC 2008, 2012). It was committed by OECD (Organisation for Economic Co-operation and Development) and PIARC (the World Road Association), and was developed by INERIS (France), with contribution of WS-Atkins (UK) and the Institute for Risk Research (CA). The QRAM is used in many European countries where a specific quantitative risk assessment (QRA) methodology for the transportation of dangerous goods in tunnel is not provided, in order to comply with the European Directive 2004/54/EC of the European Parliament and Council (2004). The model is based on spreadsheet tools running in Microsoft Excel/VBA installed on Windows OS (INERIS, 2005b), and permits the calculation of societal and individual risks. The consequences can be evaluated in terms of fatalities or fatalities and injuries for tunnel users and local population. The general description of the QRAM provided in this section is based on INERIS (2005a, b) and PIARC (2008, 2012), unless otherwise specified. A detailed description can be found in the mentioned references.

5.2.1 Overview (URS)

The QRAM requires the definition of the system by inputs in terms of:

- tunnel geometrical characteristics: length, cross section, vertical and horizontal alignment, number of lanes, lay-bys, escape routes, emergency exits, uni- or bi-directional traffic, etc.;
- meteorological data and statistics;
- tunnel equipment: lighting, ventilation, drainage, water supply, warning, monitoring, control and communication systems, road signs, access for emergency services, fire resistance of structure and equipment;
- traffic data and characteristics for each route section and traffic direction: average annual and seasonal daily traffic through the tunnel per lane, overall traffic composition (vehicle mix) and percentage of heavy goods vehicles, speed limits, congestion statistics;
- specific data on dangerous goods transportation (composition, type, traffic volume, amount, type);
- historical statistics and frequencies of potential accident types on tunnel/open air routes;
- statistics and frequencies of fires and dangerous events;
- data on alternative routes (both tunnel and open air routes);
- data on surrounding population (urban/rural area).

The QRAM is based upon a limited number of scenarios involving a selection of dangerous goods, still representative of the main effects that can be generated in the event of accidents involving hazardous goods (large fires, explosions with or without thermal effects, toxic effects from accidental releases). The resulting 13 scenarios are reported in Figure 59:

Scenario Nr:	Description	Capacity of tank	Size of breach (mm)	Mass flow rate (kg/s)
1	HGV fire 20 MW	-	-	-
2	HGV fire 100 MW	-	-	-
3	BLEVE of LPG in cylinder	50 kg	-	-
4	Motor spirit pool fire	28 tonnes	100	20.6
5	VCE of motor spirit	28 tonnes	100	20.6
6	Chlorine release	20 tonnes	50	45
7	BLEVE of LPG in bulk	18 tonnes	-	-
8	VCE of LPG in bulk	18 tonnes	50	36
9	Torch fire of LPG in bulk	18 tonnes	50	36
10	Ammonia release	20 tonnes	50	36
11	Acrolein in bulk release	25 tonnes	100	24.8
12	Acrolein in cylinder release	100 litres	4	0.02
13	BLEVE of liquefied CO2	20 tonnes	-	-

Figure 59. QRAM scenarios (INERIS, 2005a).

Scenarios 1 and 2 (HGV fires), which do not specifically concern dangerous goods, are used for comparison. Scenario 13 (BLEVE of liquefied refrigerated CO_2) is representative of class 2 DG substances, i.e. inflammable, non-toxic gases but potentially able to lead to a BLEVE with significant pressure effects.

Based on the input data, which can be default nationwide average values (when local data are not available), the QRAM performs:

- quantitative frequency analysis of the sequence of events from any potential initial event (breakdown, accident) to all possible consequence scenarios, in terms of conditional probabilities for different boundary conditions (tunnel/open air routes, urban/rural areas);
- quantitative consequence analysis, by means of 1D tools implemented in the software, with specific models/equations calculating physical and physiological consequences of each scenario within tunnels or along open air routes for tunnel users and local population. The tools (INERIS, 2005a) take into account effects of hazards (such as heat, smoke, toxics, pressure, etc. for each scenario) on people including escape and sheltering impact. First the physical consequences are evaluated for each scenario. Then, their physiological effects on people are derived by means of Probit functions for lethality and/or injuries. Besides physiological consequences, structural damage can be evaluated by means of specific tools. An estimate of refurbishing cost can be provided in terms of the relative percentage of building cost for a similar new tunnel. Moreover, the main environmental effects in terms of atmospheric dispersion, water and ground contamination can be evaluated too.

The combination of quantitative frequency and consequence analyses allows the evaluation of the societal risk (i.e. the whole range of possible outcomes of all possible DG scenarios for tunnel/route users and local population) in terms of frequency-consequence log-log graphs (F/N curves), showing the cumulative frequencies (F, $year^{-1}$) of incidents involving N or more fatalities and/or injuries. Societal risk can also be evaluated in terms of the Expected Value (EV), which is a single value representing the average number of fatalities per year.

Although less common, the QRAM also allows the evaluation of the individual risk (i.e. the risk related to an individual person who lives near the tunnel/route, expressed as a probability to be injured or killed) by means of two-dimensional spatial iso-risk contours.

As a methodological approach, the QRAM can be used in two steps, outlined in Figure 60 (PIARC, 2008). In the first step, the QRAM allows the evaluation of an expected risk value (called “intrinsic risk”, IR) for the tunnel/route under investigation, which represents the yearly expected number of victims due to dangerous goods transportation, on the assumption that all dangerous goods are authorized.

According to PIARC (2008), an intrinsic risk of 0.001 can be considered as the threshold limit, above which a second QRA step is required to support the decision of the administrative authority on the authorisation (totally or partially) or total ban of DG transport in the tunnel under investigation.

Specifically, the QRAM can be used to calculate and compare the risk levels of:

- the investigated tunnel and possible alternative tunnel configurations and/or measures, as well as alternative routes, in terms of societal risk (F/N curves, expected values), with reference to acceptance criteria;
- various options for DG transport limitations (for the whole traffic, for some groups of dangerous goods, or for predetermined periods of time), assessing for example the societal risks for each ADR category (A to E) for the tunnel under investigation.

The QRAM can also be used also to perform a sensitivity analysis on the main parameters (like DG and global traffic, population data, accident rates).

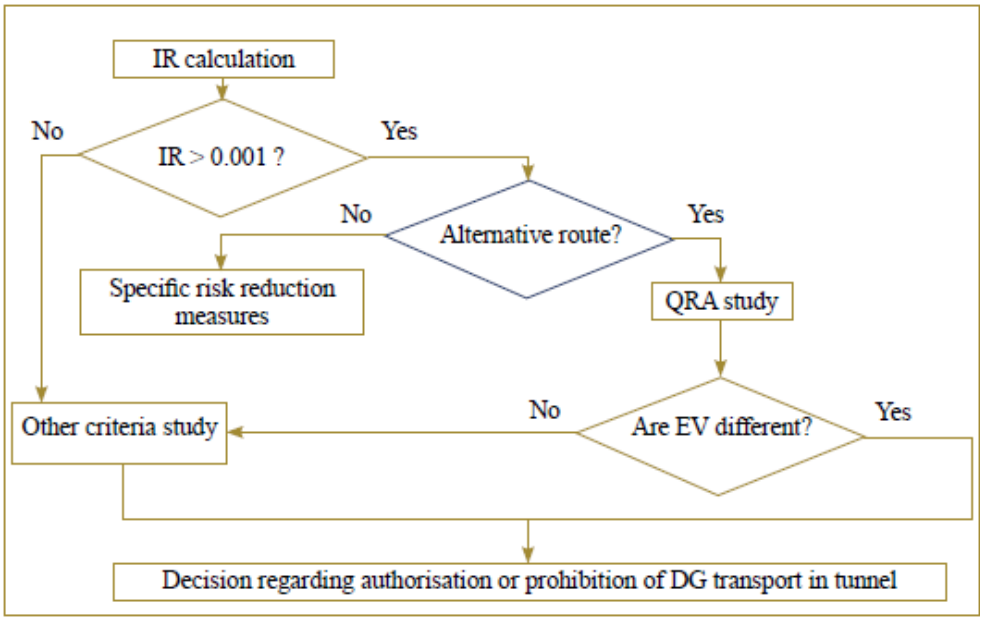

Figure 60. QRAM methodological approach (PIARC, 2008).

According to PIARC (2008), if the QRA study does not allow a clear choice between tunnels/routes, further criteria can be accounted for: i) accidents without hazardous material (specifically, HGV scenarios 1 and 2); ii) risk aversion, i.e. the fact that some accidents are perceived to be much worse than their direct consequences would indicate, as defined by PIARC (2012); iii) route vulnerability from economic and environmental perspectives.

With regards to the range and limits of application, PIARC (2008, 2012) indicates that the QRAM is well suited to take decisions on DG traffic authorisation or not in a tunnel. On the contrary, it is not suitable for a general risk analysis for road tunnels. Indeed, QRAM algorithms, procedures and tools were specifically developed for risk assessment of transportation of dangerous goods through road tunnels and routes, and should not be used beyond this purpose. However, the availability of a limited number of DG scenarios on which the QRAM is based, makes it necessary to consider such substances as representative of other materials able to produce the same type of danger, according to the DG class. A correspondence per class of different dangerous goods is proposed as reported in Figure 61 (INERIS, 2005b).

Moreover, according to INERIS (2005a, b), the simplifications required at the different stages of QRAM procedure may globally produce a considerable level of uncertainty to the final evaluation (about 300%), depending on the case study (range 250-400% with a 95% confidence interval, including both frequency and consequence aspects). Moreover, whenever reliable local data (best estimates) are available, they should be used rather than software default values, derived from nationwide averages.

In order to perform an overall assessment of the tunnel system to achieve a required global tunnel safety level, the QRAM should be applied in conjunction with other tools, such as CFD models for the evaluation of smoke spread, toxic cloud distribution and ventilation, and evacuation models for the evaluation of people egress (PIARC website).

DG directly associated with a scenario	Types of DG correspondence to base traffic rate upon	Scenarios
DG potentially leading to a large (100MW) fire (except liquids)	rough amount of DGs that are combustible (roughly class 4)	2
Propane 50kg	class 2F , part in cylinders	3
Flammable liquids in bulk (Motor spirit, diesel oil, ...)	class 3	4
Fraction of flammable liqs potentially leading to VCE (excl diesel oil)	Motor Spirit (3F1 does not seem to be a good correspondence, it is wiser to use danger code 33)	5
Chlorine in Bulk	Chlorine (and other very toxic gases with IDLH <= 50ppmv) in Bulk	6
Propane in Bulk	class 2F , part in bulk	7, 8, 9
Ammonia in Bulk	class 2T (TF, TC,TO, TFC, TOC) transported in bulk except Chlorine and very toxic gases	10
Acrolein in Bulk	class 6 , part in bulk	11
Acrolein in Cylinder	class 6 , part in cylinders	12
liquefied CO2 in Bulk	class 2 gases which have not been taken into account already because flammable or toxic	13

Figure 61. Types of DG correspondence to base traffic rates upon (INERIS, 2005b).

5.2.2 Frequency analysis (URS)

The probabilities of occurrence associated to each of scenario are evaluated through a fault tree as reported by INERIS (2005a). The scenarios to be included in the analysis depend on the vehicle involved in the accident. Below a list of examples of relevant scenarios for each vehicle type is given:

- HGV without dangerous goods: fire is the most relevant scenario, influenced by fire load (in the case of non-flammable goods, QRAM scenario 1, or for flammable goods, QRAM scenario 2) and ignition conditions (in case of an accident, ignition can start either on another damaged vehicle, or on the truck itself);
- Motor spirit: relevant scenarios are pool fire and vapour cloud explosion (VCE), QRAM scenarios 4 and 5 respectively;
- LPG: relevant scenarios are BLEVE (QRAM scenarios 3 and 7), VCE (QRAM scenario 8) and torch fire (QRAM scenario 9).

In the event of a continuous release through a breach in the tank, due to an accident or rupture, the sequences of events can lead to pool fires (hydrocarbons), and torch (jet) fires or VCE depending on ignition, i.e. early ignition for fires and delayed for VCE. A detailed description of all the possible scenarios, associated fault trees and probabilities is given in (INERIS, 2005a). Here are reported only examples of the event fault trees for a VCE and BLEVE, Figure 62 and Figure 63 respectively, given that a similar scenario may be present in accidents involving hydrogen.

The probability associated to a VCE can be calculated according to the corresponding event tree, see Figure 62, as:

$$P_{VCE} = P'' \times P4 = P' \times P3 \times P4 = P1 \times P2 \times P3 \times P4 = P1 \times (Px + Py) \times P3 \times P4 \quad (5.1)$$

The probability associated to a torch (jet) fire can be evaluated by an event tree similar to VCE (Figure 62), but considering P4 being relative to an early ignition instead of delayed one:

$$P_{torch\ fire} = P1 \times (Px + Py) \times P3 \times P4 \quad (5.2)$$

According to the pertaining event tree (reported in Figure 63), the probability associated to BLEVE is:

$$P_{BLEVE} = P11 \times P12 = (P8 + P9 + P10) \times P12 =$$
$$= [(P1 \times P2) + (P3 + P4 \times P5) + (P6 \times P7)] \times P12 \quad (5.3)$$

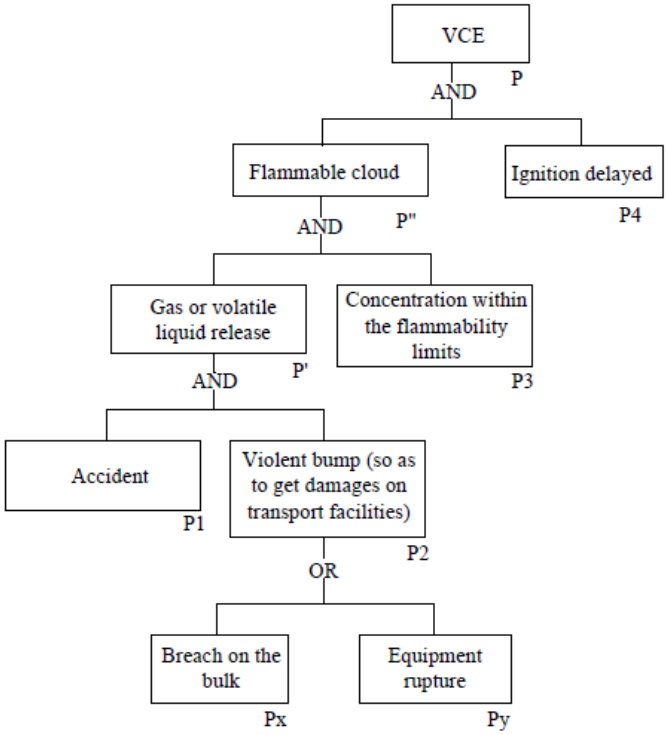

Figure 62. VCE fault tree (INERIS, 2005a).

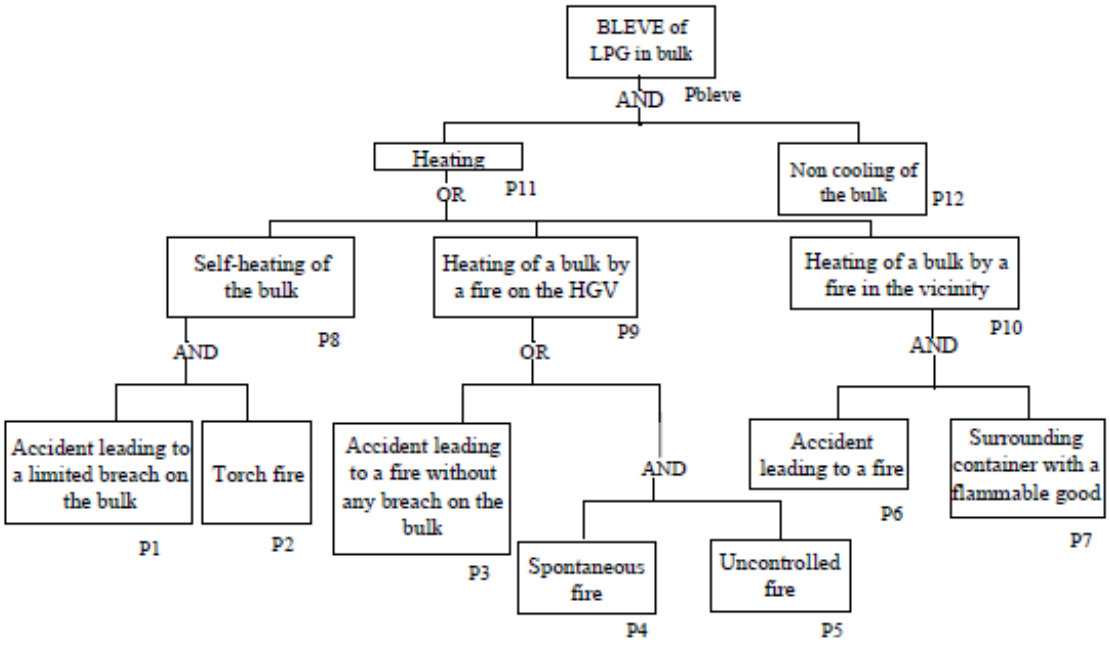

Figure 63. BLEVE fault tree (INERIS, 2005a).

The final results of the analysis are expressed in terms of scenarios rates per kilometre of given sections. These values consider both data on HGV and DG-HGV traffic on different sections of the route, and data on accident involvement rates per MVKm (million vehicle kilometre), either entered by the user or by default values from French, Canadian or Norwegian databases (INERIS, 2005a, b).

If AH_i is defined as the number of HGV involved in an accident per MVKm, the number NHA_{ij} of scenarios j per year on a section R_i is calculated as:

$$NHA_{ij} = SHA_{ij} \times AH_i \times TH_i \times L_i \times 365 \times 10^{-6}, \quad (5.4)$$

where SHA_{ij} is the scenario j rate once an accident involving an HGV has taken place in section R_i, TH_i *is* the HGV traffic in section R_i, L_i is the length of section R_i, R is the route considered and R_i the i section of this route.

Similarly, AD_i is defined as the number of DG-HGV involved in an accident per MVKm. It can be obtained as $AD_i = kD \times AH_i$, where kD is a corrective factor between HGV accident rates and DG-HGV accident rates.

Then, the number NDA_{ijk} of scenarios jk per year on section R_i is calculated by:

$$NDA_{ijk} = SDA_{ijk} \times AD_i \times TD_{ij} \times L_i \times 365 \times 10^{-6} \quad (5.5)$$

where SDA_{ijk} is the scenario j_k rate once an accident with a DG-HGV of type j has taken place on section R_i, TD_{ij} is the traffic of DG-HGV of type j on section R_i. The latter is calculated as $TD_{ij} = \alpha_j \times \beta_i \times TH_i$, where α_j is the fraction of DG-HGV of type i in the whole DG-HGV traffic and β_i is the fraction of DG-HGV in the HGV traffic on section R_i.

5.2.3 Consequence Analysis (URS)

5.2.3.1 Evaluation of physical consequences (URS)

The QRAM employs different spreadsheet tools to model and evaluate the physical consequences (in terms of heat, smoke, pressure, toxics) according to the scenario and its main hazards (Figure 64). The tools are based on literature correlations as reported by INERIS (2005a) in Section 8.

Few approximations of tunnel parameters are used to simplify the consequence modelling, e.g.: i) the tunnel cross-section is considered rectangular in shape, with dimensions being uniform along the tunnel length; ii) the tunnel is considered as formed by a number of longitudinal segments, and a different setting may be used in each segment in terms of gradient, drainage and different ventilation systems (natural, longitudinal, semi-transverse, transverse).

Regarding the properties used for calculations, LPG is assumed as propane, and motor spirit as gasoline. The detailed description of all the scenarios reported below is available in (INERIS, 2005a) and it includes all the tools used to calculate the physical consequences of the accidents. Below only scenarios for BLEVE and VCE are treated in more detail to provide an example of the proposed methodology to the reader.

	Accident Scenario	Main hazard(s)
1	HGV fire, 20 MW (unladen or laden with little combustible material)	Fire and smoke
2	HGV fire, 100 MW (loaded with combustible material)	Fire and smoke
3	LPG BLEVE, 50kg cylinder	Fireball and pressure effects
4	Motor spirit pool fire, 28 tonne capacity tanker	Fire and smoke
5	Motor spirit vapour cloud explosion (VCE), 28 tonne tanker	Thermal and pressure effects
6	Chlorine release, 20 tonne capacity tanker	Toxic gas
7	LPG BLEVE, 18 tonne capacity tanker	Fireball and pressure effects
8	LPG VCE, 18 tonne capacity tanker	Thermal and pressure effects
9	LPG torch fire, 18 tonne capacity tanker	Fireball and pressure effects
10	Ammonia release, 20 tonne capacity tanker	Toxic gas
11	Acrolein release, 25 tonne capacity tanker	Toxic liquid
12	Acrolein release, 100 l capacity cylinder	Toxic liquid
13	Liquefied refrigerated CO2, 20 tonne capacity tanker	Pressure effects

Figure 64. QRAM accident scenarios and their hazards (INERIS, 2005a).

5.2.3.1.1 HGV and motor spirit fires

The fire size for HGV scenarios is considered equal to 2.5×10 m, with fire lasting 1 hour. For the motor spirit scenario, the fire size and duration depend on the pool that is formed following the release from a tanker. Their calculation account as well the gradient and camber of the road, and the drainage system.

The flow rate of combustion products is calculated as function of the fire and tunnel characteristics. For the prediction of smoke movement, a simple approach has been adopted in QRAM: the variation of the velocity and the depth of the smoke layer are calculated on the basis of a level, naturally ventilated tunnel. For longitudinal and semi-transverse systems, the smoke regime, i.e. stratified flow in one or both directions, will depend on the basis of the tunnel geometry and ventilation flow rate.

The methodology allows the calculation of the CO concentration to determine the toxicity of the produced smoke and visibility. Smoke concentration effects are assumed to be significant only in the case of fully mixed regime. In this case the concentration of combustion products is assumed to be uniform over the tunnel length. Finally, the thermal effects of the high temperature smoke can be calculated in terms of incident radiation flux and thermal dose.

5.2.3.1.2 Toxic vapour clouds

The mass flow rate for a liquid release is assessed, including effect of eventual flash off and vaporisation of the remaining liquid fraction. The model considers the conditions in the tunnel, such as ventilation and slope, to calculate the characteristics of the layer of toxic gas within the enclosed space. Finally, the toxicity effects are estimated in terms of toxic dose from the substance concentration and exposure time.

5.2.3.1.3 LPG – BLEVE

BLEVEs can occur when the cylinder or tank is engulfed in a fire; thermal stresses would cause the metal vessel to rupture, and the high flammability of the exposed liquid would lead to the generation of a fireball. Because the current understanding of the development of fireballs in tunnels is limited, it is assumed here that the total volume of the fireball in the tunnel accident scenario is the same as for a fireball in the open. The fireball is assumed to be spherical, and the diameter *D* (m) and duration *t* (s) are calculated as a function of the mass of fuel *M* (kg):

$$D = 5.8M^{1/3} \tag{5.6}$$

$$t = 0.45M^{\frac{1}{3}} \text{ if } M < 37\ ton \quad \text{or} \quad t = 8.6M^{1/6} \text{ if } M > 37\ ton \tag{5.7}$$

The corresponding length of affected tunnel is calculated by equating the volume of a tunnel section with that of the fireball.

Thermal radiation effects

The thermal radiation effects from an LPG fireball are calculated assuming a surface emissive power I_r =270 kW/m² in the estimation of the incident radiation flux *I* (kW/m²) as:

$$I = v_f T_r I_r, \tag{5.8}$$

where v_f is the view factor and T_r the atmospheric transmissivity.

The thermal radiation dose L_t ([W/m²]$^{4/3}$s) over an exposure time of *t* (s) is calculated by:

$$L_t = I^{4/3} t. \tag{5.9}$$

A probit function can then be used to determine the percentage of fatalities.

Pressure effects

The overpressure effects are evaluated in terms of peak pressure *c* and impulse *I* as a function of distance *z*, tunnel cross-sectional area *A* and source size *m*:

$$z = Im^{-1/3}, \tag{5.10}$$

$$c = m^{1/3} A^{-1/2}, \tag{5.11}$$

while the equivalent-charge mass of TNT M_{TNT} (kg) is calculated by:

$$M_{TNT} = \alpha_e \frac{M_f H_f}{H_{TNT}}, \tag{5.12}$$

where M_f is the mass of fuel in the cloud (kg), H_f is the heat of combustion of fuel (MJ/kg), H_{TNT}=4.68 MJ/kg is the heat of combustion of TNT, α_e =TNT-equivalency=0.03.

5.2.3.1.4 LPG and motor spirit - Vapour Cloud Explosions

For LPG, the liquid mass flow rate is calculated as for the toxic vapour clouds (i.e. chlorine and ammonia) scenarios:

$$\dot{m} = C_D A_h \rho u, \tag{5.13}$$

where C_D=0.6 is the discharge coefficient, A_h the hole area (m^2), ρ the liquid density (kg/m^3), u (m/s) is the release velocity according to $\frac{u^2}{2} = gh + \frac{\Delta P}{\rho}$, with h=2 m the depth of liquid in tank and ΔP= 7 × 10^5 (N/m^2).

For motor spirit, the evaporation rate is obtained as:

$$\dot{m}_E = 1.2 \times 10^{-10} \left(\frac{Mp^\circ}{T}\right) u^{0.78} x^{0.89} y, \quad (5.14)$$

where $\dot{m}_E$ is the evaporation rate (g/s), M is the molecular weight, p° is the vapour pressure of liquid (dyn/cm²), T is the absolute temperature of liquid (K), u is the mean wind speed (cm/s), x and y the downwind and crosswind dimensions of pool (cm), respectively.

The spread of the flammable gas cloud is assumed to be uniform over the tunnel cross-section, moving at the airflow speed. The ignition is assumed to trigger at the earliest among the time the cloud front reaches the portal, the time the tank becomes empty or a time of 10 minutes. The explosion duration has been taken arbitrarily as 15 seconds.

The QRAM tool has not been validated for hydrogen accidental scenarios up to date.

Tunnel overpressures

When the explosion is confined, as in a tunnel, the increase of volume causes rapid rises in pressure. The portals will provide venting routes in the event of an explosion (with exclusion of detonation which venting technique is not applicable to). Even if the tunnel is only partially filled with a flammable gas cloud, the expanding combustion products will push the unburned gas ahead of themselves, filling the tunnel as they progress. Overpressures produced in such situations may be as high as those produced if the tunnel was completely full.

A distinction is made between cases where the expanded gas would fill a significant portion of the tunnel and those where the gas volume is relatively small. The threshold has been arbitrarily chosen as expanded volume equal to 25% of the tunnel volume. Below this threshold volume, the overpressures are estimated using the TNT-equivalent approach described previously. Above this threshold, the method used to calculate overpressures is as follows:

$$\Delta p = 58 k_1 k_2 k_3 \beta S_0 \frac{\left(\frac{n_x}{100} V\right)^{2/3}}{A_x}, \quad (5.15)$$

where k_1 is the gas composition constant (k_1=1.2 for propane and 1.0 for motor spirit), k_2 is the flame path length constant (k_2=1, assuming worst case overpressures), k_3 is the blockage ratio constant, β is the turbulence factor = 12.0, S_o is the laminar burning velocity (S_o=0.52 m/s for propane or 0.4 for benzene), n_x is the percentage of gas venting through opening x, A_x is the area of vent, e.g. tunnel cross-sectional area (m²), V is the free volume in tunnel (m³).

Regarding these parameters the following comments are made below:

- k_3: this parameter depends on the area blockage ratio, which is defined as the free area available for flame acceleration divided by the total cross-sectional area of the tunnel. It is assumed that most of the blockage in the tunnel is due to stationary vehicles in the tunnel. The values of k_3 is 0.5 for 5% blockage ratio, 1.0 for 20% and 2.0 for 30% blockage ratio.

- n_x: it is assumed that only 2 openings exist. If the ignited cloud volume is less than the tunnel volume, the openings are taken to be at the location of the two cloud fronts, otherwise the tunnel portals are assumed. The gas is vented equally through both ends: n_x = 50%.
- V: the free volume is taken as the volume occupied by the gas cloud minus the volume occupied by the vehicles.
- the calculated overpressure is considered to be constant in the tunnel because the overpressure decay in the tunnel is assumed to be negligible. Hence, the overpressure is assumed to be unchanged at the portals.

5.2.3.1.5 BLEVE of a tanker filled with refrigerated liquefied CO_2

Overpressures are estimated using the TNT-equivalent approach.

Analogous specific tools can be used for the evaluation of physical consequences outside of a tunnel and on open air route, as reported in INERIS (2005a).

5.2.4 Evacuation in tunnels (URS)

Depending on the accident scenario, tunnel occupants may be subjected to either one or a combination of thermal, smoke, explosion or toxic effects. In addition, the behaviour of people in tunnel emergencies has not been sufficiently addressed and may be significantly different from those observed in building fire emergencies. Therefore, reasonable assumptions need to be made where insufficient information is available.

The total time (t_{evac}) required to evacuate the tunnel or reach a safe place (or relatively safe) is very complex. It comprises: a) the recognition time (t_{rec}) after a cue; b) the response time (t_{res}) to prepare to evacuate; c) the movement time (t_{mov}). The recognition time and the response time constitute the pre-movement time t_{pre}. It depends principally upon the type of warning system provided, and on occupants' characteristics.

As regards the warning system, four categories are available in QRAM: W0) No warning system; W1) warning system using alarm bell, siren or similar; W2) public address system (PA), with pre-recorded voice systems and/or informative warning visual display; W3) PA + CCTV, with live voice directives e.g. from a control room.

With regards to occupants' characteristics, a series of parameters can be tuned (in a range 1-5) in the QRAM to account for their influence, from the worst situation for escape (for which a value of 1 is assigned) to the best situation (for which a value of 5 is assigned). A 'neutral' value of 3 (i.e. neither high or low influence) is suggested for parameters which are difficult to evaluate. Such parameters concern both recognition and response times.

Recognition is the period after an alarm or cue is evident but prior occupants begin to respond. In this case the parameters comprise: a) occupant characteristics: people alertness, mobility, social affiliation, commitment in activities; b) wayfinding: familiarity to the tunnel emergency exit routes; c) hazard identification: distance from incident, traffic density, tunnel gradient, tunnel curvature, perceived severity of situation.

Response time is the period after occupants recognise the alarm or cue and begin to respond to it, e.g. stop vehicle and gather belongings, but before they begin to move directly to an exit. With reference to the response time, the parameters to set in QRAM comprise: vehicle travel speed and vehicle type.

On the basis of warning system and the aforementioned parameters, the occupant pre-movement time (t_{pre}) is evaluated as follows:

$$t_{pre}adjusted = t_{pre}(bps, W) * w_{eff}, \quad (5.16)$$

where t_{pre} *(bps,W)* is the best possible scenario (BPS) reference value for warning system, evaluated according to a matrix of baseline estimates related to different warning systems and scenarios, see Figure 65. $w_{eff} = 5/average\ t_{pre}parameters$ is the occupancy response efficiency weighting, derived from aggregate ratings of the t_{pre} parameters (Figure 66).

warning system	Pre-movement time (t_{pre})		
	best scenario (bps) (seconds)	average scenario (seconds)	worst scenario (seconds)
W0	< 300	420	> 720
W1	< 180	360	> 540
W2	< 120	240	> 360
W3	< 60	120	> 180

Figure 65. QRAM matrix of baseline estimates of t_{pre} (INERIS, 2005a).

	Recognition time (trec)									
	Occupant characteristics				Wayfinding	Hazard identification				
	B	C	D	E	F	G	H	I	J	K
Proportion of distance from incident to safety	Alertness	Mobility	Social affiliation	Commitment	Familiarity	Distance from incident	Traffic density	Tunnel gradient	Tunnel curvature	Perceived severity of situation
1.0	4	4	3	3	2	1	1	5	5	4
0.8	4	4	3	3	2	2	2	5	5	4
0.6	4	4	3	3	2	3	3	5	5	4
0.4	4	4	3	3	2	4	4	5	5	4
0.2	4	4	3	3	2	5	5	5	5	4

Coding scheme for asterisk ratings

Rating	asleep	low	group	high	unfamiliar	distant	high	high	curved	toxic gas
1	*	*	*	*	*	*	*	*	*	*
2	**	**	**	**	**	**	**	**	**	**
3	***	***	***	***	***	***	***	***	***	***
4	****	****	****	****	****	****	****	****	****	****
5	*****	*****	*****	*****	*****	*****	*****	*****	*****	*****
	awake	high	alone	low	familiar	close	low	low	straight	VCE

Figure 66. Occupant response model (INERIS, 2005a).

The pre-movement time used in the evacuation analysis is the lowest between the time calculated in eq. (5.16) or the time for the smoke or toxics to reach the occupants.

The movement time is the time spent in direct movement towards an exit or place of relative safety. The movement time is calculated dividing the distance required to travel to a safe place by people travel speed, set as a QRAM input (a default travel speed is 0.5 m/s).

In the event of a fire, people will probably not use an emergency exit if tunnel conditions in the vicinity of the exit are hazardous due to heat or smoke. The distance where people may perceive conditions to be too hazardous can be specified in QRAM (default value is 100 m).

5.2.5 Evaluation of physiological, structural and environmental consequences (URS)

The combined evaluation of physical consequences in terms of hazardous loads for each scenario and the total time required to evacuate or take shelter, allows the estimation of the physiological consequences (in terms of fatalities and/or injuries).

The total dose (thermal radiation, toxicity, etc.) absorbed by evacuees is calculated by integrating the doses received in each tunnel segment according to the time spent travelling each segment, according to the correlations reported above. Then Probit functions of total doses are used to estimate the probability of fatalities and injuries from the different hazardous effects.

The typical form of a Probit function is:

$$Pr = a + bln(L), \quad (5.17)$$

where a and b are constants and L is the load (dose) related to the studied effect.

The specific functions used by the QRAM to evaluate lethality and injuries are based on relevant literature data, all reported by INERIS (2005a).

5.2.5.1 Probit equations for lethality in tunnel (URS)

- *Thermal effect from fires and BLEVEs:*
  $Pr = -14.9 + 2.56\ln(q^{4/3} * t)$ (5.18)
  where t is a time of exposure (s), q is the thermal radiation flux (kW/m²).
- *Toxic effect from fires:*
  $Pr = -37.98 + 3.7\ln(C * t)$ (5.19)
  where C is the CO concentration (ppmv) and t is the time of exposure (min).
- *Overpressure direct effects from VCEs:*
  $Pr = -77.1 + 6.91\ln(p°)$ (5.20)
  where $p°$ is the peak overpressure (Pa).
- *Toxic effects from toxic releases:*
  $Pr = -5 + 0.5\ln(C^{2.75} * t)$ for chlorine (5.21)
  $Pr = -35.95 + 1.85\ln(C^{2} * t)$ for ammonia (5.22)
  $Pr = -3.18 + \ln(C * t)$ for acrolein (5.23)
  where t is a time of exposure (min) to a concentration C (ppmv).

5.2.5.2 Probit equations for injuries/time to incapacitation in tunnel (URS)

- *Thermal effect from fires and BLEVEs:*
  $Pr = -39.83 + 3.0186\ln(q^{4/3} * t)$ for first degrees burns (5.24)
  $Pr = -43.14 + 3.0186\ln(q^{4/3} * t)$ for second degrees burns (5.25)

where t is a time of exposure (s), q is the thermal radiation flux (kW/m²).

- *Toxic effect from fires:*
  The time to incapacitation t (min) for exposure to CO is evaluated for a 70 kg human engaged in light activity by:
  $t = D/K(C_{CO}{}^{1.036})$ (5.26)
  where D is the percentage Carboxyhemoglobin concentration at incapacitation (30% for light activity), K=8.2925×10^{-4} for light activity (25 L/m volume of air breathed), C_{CO} the CO concentration (ppmv).

- *Overpressure effects from VCEs:*
  $Pr = -15.6 + 1.93\ln(p°)$ for eardrum rupture (5.27)
  $Pr = -27.1 + 4.26\ln(J)$ for injury from missiles (glass) (5.28)
  $Pr = -39.1 + 4.45\ln(J)$ for injury from whole body translation (5.29)
  where $p°$ is the peak overpressure (Pa) and J the impulse (Pa s).

- *Toxic effects from toxic releases:*
  $Pr = -10.085 + \ln(C^{2.75} * t)$ for chlorine (5.30)
  $Pr = -21.43 + \ln(C^{3.33} * t)$ for ammonia (5.31)
  $Pr = -2.34 + \ln(C * t)$ for acrolein (5.32)
  where t is a time of exposure (min) to a concentration C (ppmv).

Besides physiological consequences, structural and environmental consequences can also be evaluated by means of specific tools reported by INERIS (2005a).

Damage to tunnel structures and ancillary equipment due to explosions and fires are evaluated in terms of overpressure and temperatures in comparison with critical values for tunnel collapse, concrete cracking, spalling and thermally induced reduction in strength for concrete and steel structures, as well as for failure of mechanical and electrical equipment. Moreover, an estimation of restoration costs can also be calculated, in terms of the relative percentage of the building cost for a new tunnel of similar design.

As regards environmental effects, a qualitative evaluation can be obtained, as a function of the scenario and in terms of atmospheric dispersion, water and ground contamination, as shown in Figure 67. Results are given as qualitative indicators for negligible, low, medium or high severity.

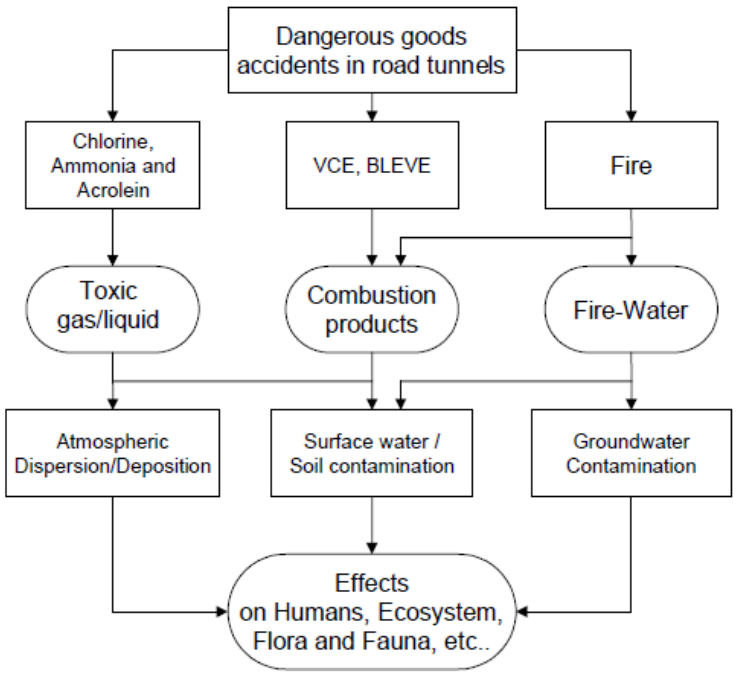

Figure 67. Environmental impacts of DG accidents in road tunnel (INERIS, 2005a).

5.2.6 Evaluation of societal and individual risk (URS)

The combination of quantitative frequency and consequence analyses allows the evaluation of the societal risk in terms of F/N curves, which are built in the QRAM once every set of frequencies/consequences couples have been calculated for all possible DG scenarios, tunnel/road users and local populations. Societal risk can also be evaluated in terms of the Expected Value (EV), i.e. a single value representing the average number of fatalities per year.

Considering each single scenario, the QRAM evaluates that any set of circumstances (differing e.g. in terms of weather conditions, traffic, period of the year, epicentre location, etc.) produces N fatalities (or injuries) with a probability of P_1, P_2, …, P_k, … , P_{kmax}.

The resulting probability to get N victims or more over all the circumstances is given by:

$$P_{global}(N) = P_{global}(N+1) + \sum_{k=1}^{k_{max}} P_k. \quad (5.33)$$

This estimate is then iterated for N from 1 to N_{max} (the calculated maximum number of victims for the considered scenario), in order to build the global F/N curve.

In order to simplify the very complex calculation of all the frequencies/consequences couples due to all possible combinations of scenarios, circumstances and tunnel settings, the QRAM assumes classes of number of victims, with a representative value for each one. Each class in the F/N curve is associated to the corresponding yearly frequency, given by the sum of all the contributions to this class of number of victims.

As an example, the F/N curves reported by PIARC (2008) for a QRAM case study aimed to compare risk levels of an investigated tunnel and a possible alternative route are shown in Figure 68.

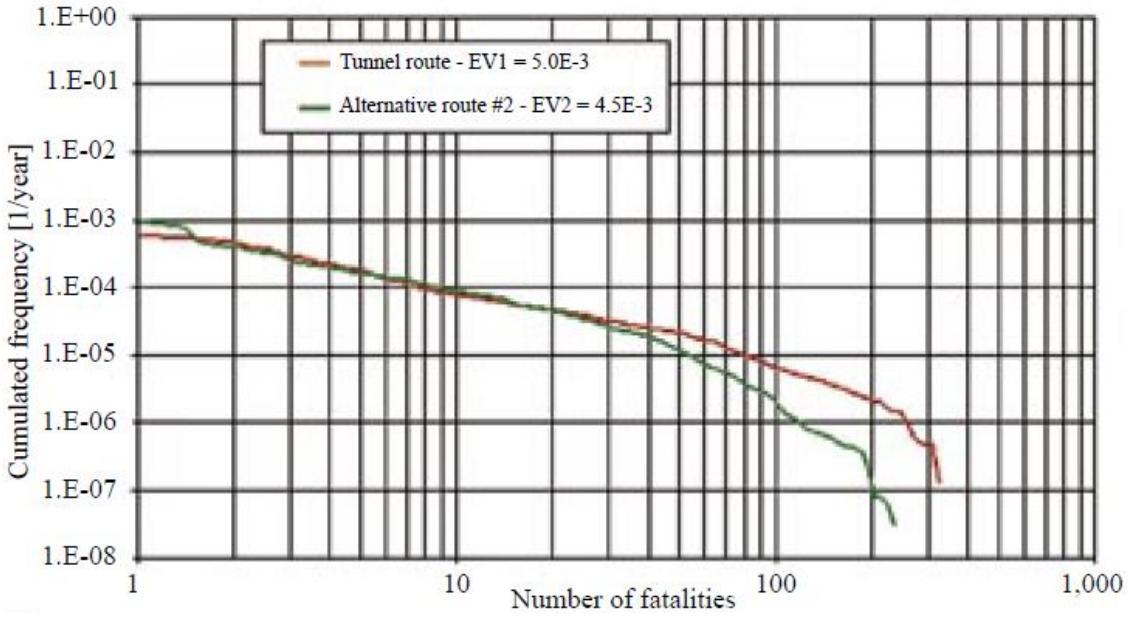

Figure 68. QRAM F/N curves (PIARC, 2008).

The QRAM also allows the evaluation of the individual risk for local population, expressed as a probability to be injured or killed, depending on the people position assumed as fixed. This individual risk is expressed as a frequency per year, or otherwise as the reverse value representing a response time, i.e. an average number of safe years between two accidents for a person remaining at a fixed location. It is shown by means of two-dimensional spatial iso-risk contours and is calculated as follows.

At each location (X,Y) near the tunnel/route, for all the accidents Acc_i which can occur due to DG transportation, and in all the possible circumstances, the probability $P(Acc_i)$ of occurring in one year is evaluated. The occurrence of a consequence (e.g. death) for a person at (X,Y) location is given by $Probit(X,Y,Acc_i)$. The individual risk $I(X,Y)$ is then calculated by:

$$I(X,Y) = \sum P(Acc_i) * Probit(X,Y,Acc_i). \quad (5.34)$$

5.3 Probabilistic risk assessment (DTU)

The QRA described in section 5.2 uses a combination of deterministic and probabilistic inputs to evaluate tunnel accidents. There are, however, other probabilistic risk assessment methodologies (Meel and Seider, 2008; Musharraf et al., 2013; Khakzad et al., 2014; Liu and Zio, 2016). One of these is the application of Bayesian Belief Networks (BBN) that have been increasingly used to predict structural reliability of civil structures, e.g. (Janda et al., 2018), and in process industry safety, e.g. (Al-shanini et al., 2014).

The BBN theory is based on Bayes theorem to calculate the conditional probabilities P of events A and B:

$$P(A|B) = P(B|A)\,P(A)/P(B) \quad (5.35)$$

Nelisse and Vrouwenvelder (2017) developed and predicted the "Probability of a Large Fire in a Road Tunnel Bayesian Inference" based on BBN theory and historical data. The objective was to calculate the probability for large tunnel fires (>25 MW).

Few works have been conducted on hydrogen systems, as e.g. “Challenges to improve confidence level of risk assessment of hydrogen technologies” by Pasman (2011). The author states that a large-scale distribution and a successful use of hydrogen require an adequate risk control by employing risk assessments. One problem is the uncertainty as it may influence decision support. This is a weakness of the QRA. The way forward is seen in better scenario generation, taking advantage of historical incident data and newer methods such as Bayesian belief nets applied to the entire hydrogen distribution system and not only to single installations. The results shall present confidence intervals.

Another development is given by dynamic models. They are seen as a supplement to fault and event trees as these latter common tools are difficult to apply for dynamic situations (Duijm et al., 2013; Markert et al., 2016). Such models are assumed to better predict a large number of scenarios and to use the outcome of these scenarios to e.g. predict the worst-case situation, which is currently most often predicted using expert judgement. The dynamic risk models can deal with time dependent events that are difficult to assess using normal event trees. The methodology enables modelling of the reliability of the safety functions in a tunnel in terms of technological failures and in terms of human and organisational factors. On the other hand, the method can be linked to scenarios predicting the safe egress of people in different tunnel accident scenarios in relation to hydrogen risks.

5.4 QRA for an onboard storage system (UU)

There are several important differences between the expected damage and injuries of an explosion in open and confined space, i.e. considerably greater pressure build-up in a confined space in a tunnel which results into higher effect on the tunnel structure and humans; higher probability of explosion as a result of an accident. Hence, even if the probability is very low, the severity of damage or injury could be so high which is not tolerable. This high potential catastrophe could occur if all three conditions below are met:

- transportation of dangerous goods in the tunnel;
- poor design of construction for the prevention of structural damages or fatalities in the buildings above the decking if the explosion event is above the permissible load of 16 tons;
- high degree of exploitation above the deck which leads to the larger number of individuals affected by the accident (Lundin, 2018).

The evacuation from a tunnel during the emergency condition is also a complicated situation which is influenced by various factors, e.g. tunnel physical characteristics; human behaviour; etc. (Derudi et al., 2018). The evacuation time of people reacting to the fire and the time lapse between the occurrence of fire and reaction to it are also important parameters. The effects of an accidental event are influential parameters as well which affects the occupants’ actions, e.g. the release of toxic gasses and the smoke dispersion can lead to the evacuation speed reduction. The safety measures are however the factors with positive influence, e.g.:

- the presence of firefighters/firefighting systems to reduce or eliminate the consequences of the accident;
- devices to close the tunnel to stop more individuals to be exposed;
- loud speakers and signs to effectively direct exposed individuals to the safe place;
- etc.

In a review study by Kazaras and Kirytopoulos (2014), several QRA models in the road tunnel were introduced which include but are not limited to:

- Austrian tunnel risk model TuRisMo;
- Dutch TUNPRIM RWS-QRA model;
- OECD/PIARC DG-QRAM model (see section 5.2);
- QRAFT model;
- Italian risk analysis model;
- German BASt model.

These models are based on event/fault tree analysis conjugated with consequences estimation models and evacuation methods. Fires, explosions and toxic dispersion are the focus of these models and the risk is defined in the form of societal risk, i.e. FN curves. The results are either compared to a reference tunnel, i.e. a tunnel with the same characteristics complying with EU directives, or to an absolute risk criteria (Kazaras and Kirytopoulos, 2014).

Considering accident frequencies (extracted from historical datasets), incident consequences inside tunnels and the open routes, escape routes and sheltering effects, and effects of hazards (i.e. heat and smoke) on people, the risk is calculated in term of societal risk, i.e. F/N curves. F/N curves, where F is the frequency of N or more fatalities/injuries, are employed to illustrate the results with respect to a low chance of injuring most people in an area or high chance of injuring only a few of people. In section 5.2.1 it was discussed that a variety of parameters must be defined as input to QRAM, i.e. routes; tunnel geometry; ventilation condition; emergency escape measures; traffics' details, directions, accident rates; population density along the path; etc. (Hall et al., 2001). Caliendo and De Guglielmo (2017) employed the QRAM software to analyse the level of risk in the bi-directional Varano road tunnel, located in the South of Italy. The impact of the hourly traffic volume (VHP), percentage of HGVs and failure of emergency ventilation system was investigated, and it was concluded that the increase of these factors would lead to higher levels of risk (Caliendo and De Guglielmo, 2017).

The use of a commercial risk assessment model QRAM, however has some deficiencies: e.g. the models used behind the software are still black-box with not enough transparent details on how the consequences are calculated, how the effects are modelled, etc.; the scenarios considered in the model only focus on the fire accident and release, hence "low frequency high consequence events" are ignored in this software. An example of "low frequency high consequence events" is the rupture of a compressed hydrogen storage tank in a fire with the consequent blast wave and fireball (Molkov and Kashkarov, 2015). This latter scenario was employed in the recent risk assessment study of Dadashzadeh et al. (2018) for an onboard hydrogen storage volume of 62.4 L (Type IV; NWP 70 MPa) of (Toyota Motor Corporation, 2016; Yamashita et al., 2015) applied to roads in London. It was concluded (Dadashzadeh et al., 2018) that the risk of human life loss in an accident when hydrogen tank ruptures in a fire $3.14 \cdot 10^{-3}$. This is two and half orders of magnitude larger than the acceptable level of risk of $1.00 \cdot 10^{-5}$. The cost associated with loss of life in the accident in this case is 4.03 M £/accident.

While all proposed models for the QRA in tunnels focused on the societal risk, i.e. FN curves, with respect to the safety issues and safety measures of the tunnel, a QRA methodology in a tunnel considering the safety issues and safety measures of the vehicle itself is a clear lack. Indeed, when it comes to the first responders' intervention strategies and tactics for hydrogen accidents in a tunnel, the individual risk, i.e. annual fatality probability, associated with a

hydrogen powered vehicle is of importance at the same level of societal risk associated with the tunnel if not more. In such emergency conditions, the individual risk which provides the fatality probability at a specific distance from the onboard hydrogen storage in a fire is a more influential risk indicator. The effectiveness of vehicle safety measures, e.g. increasing fire resistance rating (FRR) of onboard storage, to eliminate or to decrease the risk to an acceptable level is a practical way forward.

To this end, Ulster original QRA methodology (Dadashzadeh et al., 2018) will be expanded to tunnels. The focus will be on low frequency high consequence events, i.e. the rupture of a tank in a fire with the consequent blast wave and fireball, which hazards to be quantified during the HyTunnel-CS project. The aim is to investigate the impact of FRR of onboard storage on a level of risk and its acceptance for hydrogen-powered vehicles in tunnels using QRA and its application to an example tunnel. The QRA will employ publicly available data on FRR of onboard hydrogen storage, TPRD failure frequency, tunnels' statistical accident data to evaluate the impact of safety engineering on emerging hydrogen-powered transport in tunnel. Flowchart of the proposed QRA methodology is shown in Figure 69. The QRA output is a value of risk in terms of human fatality probability per year (Figure 69). The risk in terms of fatality probability per year (Figure 69) is assessed using the frequency of fire accidents per 10^6 vehicle-mile per year (Bassan 2016; National Highway Traffic Safety Administration (NHTSA) 2015; Lafleur et al. 2017). The consequence analysis aims to identify dominant hazards in an accident fire and their consequences, which are considered here only as fatality probability per rupture.

The first step in the consequence analysis is the identification of the key hazards relevant to the accident scenario with a high-pressure composite tank in a fire. They are identified, based on other studies at Ulster University, as a blast wave and fireball following a catastrophic tank rupture in a fire. The detailed comparative analysis of other hazards, including jet fires from TPRD and projectiles emanating from a tank explosion, is out of the scope of the study.

The next step is the estimation of hazard distances at which pressure cause fatality, serious injury, slight injury, and where there is no harm from the fireball and blast wave. The engineering tool for the calculation of the hazard distances for the blast wave in tunnels is under development in the HyTunnel-CS project. This is a methodology report and the authors would carry out QRA when tools are available for assessment of hazards, i.e. pressure hazards of blast wave and thermal hazards of fireball are available.

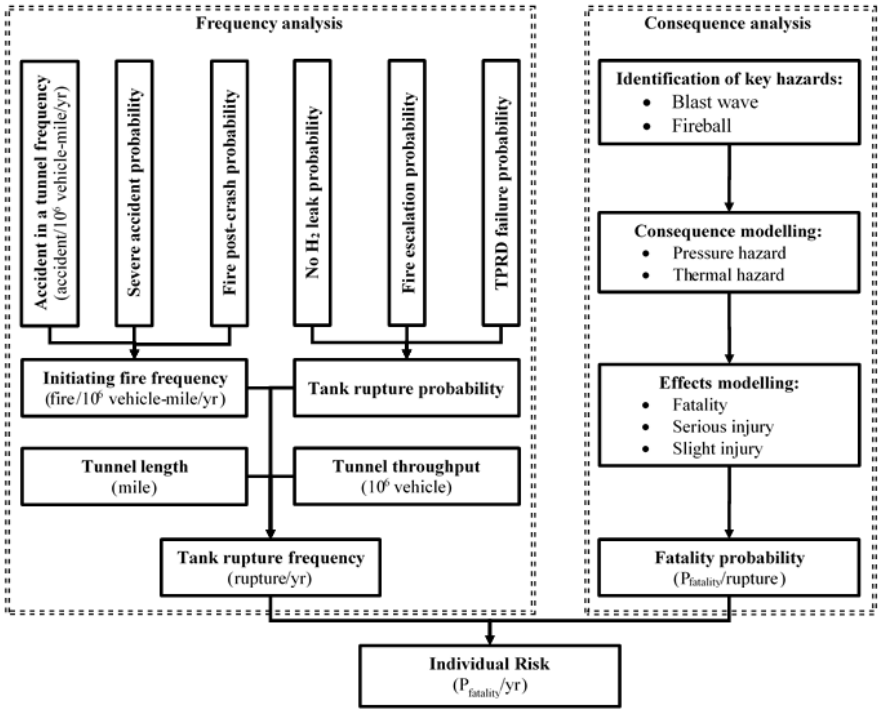

Figure 69. The QRA methodology flowchart: risk in terms of fatality probability per year.

The effects' probability of the blast wave overpressure on an individual were considered as (Kashkarov et al., 2017a) in Figure 70a:

- fatality probability ($P_{fatality}$) of 1 for the distances with the overpressure above 100 kPa,
- serious injury probability ($P_{serious\ injury}$) of 1 for the distances with the overpressure above 16.5 kPa and below 100 kPa,
- slight injury probability ($P_{slight\ injury}$) of 1 for the distances with the overpressure above 1.35 kPa and 16.5 kPa,
- probability of 0 for all above mentioned effects for the distances with the blast overpressure below 1.35 kPa.

The acceptance criteria for the IR value is defined as $1 \cdot 10^{-4}$ fatality probability/yr which is proposed by (Norsk Hydro, 2003) as an acceptable level of risk for the first responders in a hydrogen fuel station. There is no acceptance criteria for injury risk. Hence, injury risks are usually combined with fatality risk to be evaluated (European Maritime Safety Agency, 2015). In this method, injuries are weighted and treated as equivalent fraction of fatality by multiplying to a relative ratio. There are various relative ratios for serious injury and slight injury in different countries and industries. This study employs the relative values of 0.1 and 0.01 (Figure 70b) for serious injury and slight injury which is suggested by road transport sector in UK (European Maritime Safety Agency, 2015).

The techniques and tools mentioned above are used to calculate the fatality probability of individuals who are affected as per flowchart in Figure 69.

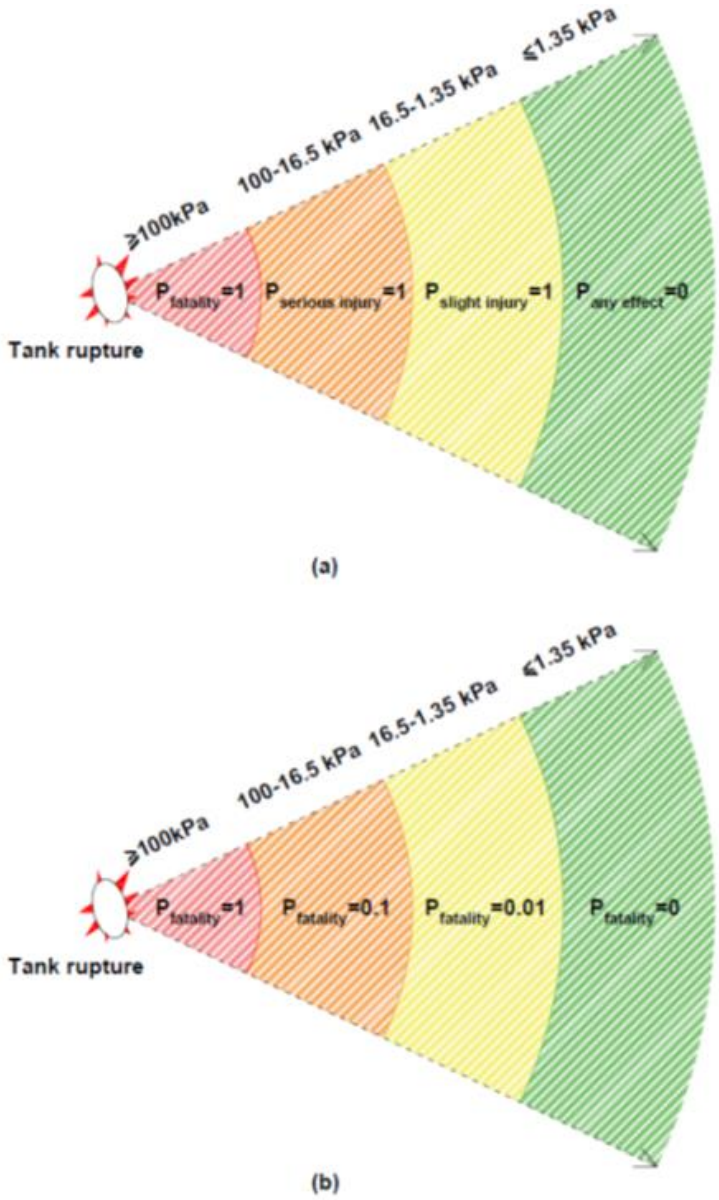

Figure 70. Graphic representation of probabilities associated with (a) fatality, serious injury and slight injury (Kashkarov et al., 2017a), (b) equivalent fraction of fatality.

The frequency analysis includes estimation of the initiating event (fire) frequency (fire/10^6 vehicle-mile/yr), TPRD failure, and calculation of the escalating probability of emergency operations failing to extinguish fire (EP) leading to a tank rupture in a fire. In this study, the initiating fire frequency is calculated by multiplying accident in a tunnel frequency (accident/10^6 vehicle-mile/yr) (Bassan, 2016), severe accident probability (Bassan, 2016; National Highway Traffic Safety Administration (NHTSA) 2015; Lafleur et al., 2017) and fire post-crash probability (Bassan, 2016).

Given that a tank rupture in a fire is considered as the accident scenario in the present study, no leak is considered before the rupture, which introduces the probability of no H_2 leak in the formulation (Lafleur et al., 2017). The tank rupture frequency is calculated here by multiplying four parameters: initiating fire frequency (fire/10^6 vehicle-mile/yr), tank rupture probability, tunnel length (mile) and tunnel throughput (10^6 vehicle) (Road Tunnel Association, 2019).

Finally, the risk in terms of fatality probability ($P_{fatality}$/year) is calculated as a product of fatality per rupture and frequency of a rupture (Figure 69).

Overall, it was showed that current QRA methodologies do not take account for the specific scenarios involving accidents of hydrogen powered vehicles in tunnels or other confined spaces. The causes are to be looked for in the lack of data, such as failure frequencies, and limited knowledge of accident consequences in such scenarios. The engineering tools and model to be produced in this project will assist the development of an overarching QRA methodology merging together hydrogen specifics, first response and rescue procedures used to tackle accidents in tunnels, etc. Alternative risk reduction measures for hydrogen vehicles should be used or reinforced to ensure a level of safety equal or higher than for fossil fuel vehicles.

6. Safety knowledge gaps and technological bottlenecks (DTU, UU)

The main aim of the present critical review of the state of the art is to define the areas where knowledge gaps and technological bottlenecks for characterisation of hazards and associated risks in tunnels are present, and where current knowledge is insufficient to calculate hazards and risks of hydrogen-powered vehicles and other transport in tunnels and other confined spaces. This deliverable is used to shape extensive experimental campaigns, analytical and numerical studies. A list of identified knowledge gaps and technological bottlenecks, which are grouped in a number of research areas, is as follows (it covers safety concerns beyond those directly related to hazards and associated risks):

Hydrogen releases

- Effectiveness of regulated ventilation systems in case of hydrogen release accident.
- Hazard distances of unignited release, i.e. location of flammable hydrogen-air mixture for releases and dispersion in realistic scenarios at storage pressures up to 700 bar.
- The upper limit of hydrogen release rate that will not require change in ventilation system.
- Engineering tool for the assessment of ventilation system parameters to prevent and mitigate flammable mixture formation in tunnels and especially its ventilation systems.
- Tank blowdown model with frictional effects during release of hydrogen.
- Non-adiabatic blowdown of hydrogen storage tank, including scenario of a storage tank behaviour in a fire.
- Engineering tool for mechanical ventilation in an underground parking.
- Experimental data and tools for hydrogen release in enclosure with more than two vents.
- Mechanical ventilation in underground parking with hydrogen-powered vehicle.
- Dynamics of release and dispersion of hydrogen in a tunnel, including hydrogen release and dispersion in a tunnel with forced ventilation.
- Difference between hydrogen dispersion in tunnels with regulated slope (below 5%) and without slope in sense of hazard distance.
- The effect of using fans in confined spaces.
- The pressure peaking phenomenon validation for garage-like enclosures for unignited releases.
- The effect of ventilation and its interaction with other mitigation systems, e.g. water spray and mist, bulkheads, etc.
- Predictive tool for the design of tunnel ventilation systems and corresponding ventilation protocols.
- Impinging hydrogen unignited jets.

Fires

- Effect of decreased ventilation rate in a fire, and innovative ventilation systems.
- The pressure peaking phenomenon validation for garage-like enclosures for jet fires from TPRD.
- Fire dynamics of hydrogen vehicles with understanding that standard curves cannot be applied.
- Relation between concrete spalling and a way structural elements and linings are fixed.
- Impact of impinging hydrogen jet fires on high strength concrete types, which may lead to concrete degradation and (explosive) spalling effects.

- Effect of water vapour generated by hydrogen combustion from TPRD on the visibility and the choice of "cross passage" distance.
- Coupling fire dynamics and evacuation simulations for accidents involving hydrogen.
- Effect of hydrogen combustion on smoke back-layering.
- Efficiency of hydrogen fire suppression systems by water sprays and oxygen depletion.
- Need for reassessment of current design criteria of underground car parks or threshold for TPRD diameter to keep current RCS requirements for hydrogen vehicles.
- Reduced-order and CFD tools for the pressure peaking phenomenon prediction.
- Hydrogen non-premixed turbulent combustion in scaled underground parking.
- Coupled CFD+FEM modelling of the structure's reaction to fire.
- Effect of hydrogen releases to fire spread scenarios in underground transportation systems.
- Thermal effects of hydrogen non-premixed turbulent combustion on a vehicle fire behaviour, structure and evacuation conditions in underground parking.
- Effect of hydrogen jet fire on structure integrity and concrete spalling.
- Effect of hydrogen jet fires on the erosion of tunnel road materials and lining materials.
- Effect of hydrogen combustion from TPRD on vehicle fire dynamics in tunnel.
- Effect of water sprays on mitigation of hydrogen jet fires.
- Impinging hydrogen jet fires.
- Dynamics of total and radiative heat flux on under-vehicle hydrogen storage and surroundings from the "conventional" car fire before and after TPRD initiation.
- Effect of water generation during hydrogen combustion from TPRD on soot density from car fire.

Deflagrations and deflagration-to-detonation transition (DDT)

- Conditions for DDT in ventilation system of tunnels, including horizontal and vertical ventilation systems with non-uniform hydrogen-air mixtures in the presence of obstacles.
- Maximum pressure of turbulent LFL mixture deflagration in closed space.
- Deflagration of non-uniform hydrogen-air cloud in a tunnel, including effect of cross-section geometry (round or rectangular).
- Foam and water spray/mist system effect on premixed combustion and DDT.
- Prediction of blast wave from deflagrations of hydrogen-air mixtures in tunnels.
- Thermal and pressure effects of turbulent hydrogen jet delayed ignition in confined space.
- Engineering model for assessment of overpressure during spurious hydrogen release, e.g. during operation of TPRD.
- Engineering tool for prevention and mitigation of composite hydrogen storage tank explosion in a fire.
- Validated CFD model for deflagration of non-uniform hydrogen-air cloud created by release in a tunnel.
- CFD model accounting for effect of water spray/mist system effect on deflagration.
- Flame acceleration and transition to detonation in tunnel structures, including bulkheads smoke mitigation systems and ventilation channels.
- Influence of heat transfer to structure on pressure and temperature decays for deflagration strength.

Blast wave and fireball

- Behaviour of high-pressure storage tanks in a tunnel fire.
- Coupling blast wave pressure load CFD simulations and structural FEM simulations.

- Physical modelling and CFD+FEM simulations of tank rupture under-vehicle accounting for losses on vehicle demolition and translation in space.
- Hydrogen combustion and pressure dynamics in presence of vehicles and other obstacles in a tunnel.
- Prediction of blast wave and fireball dynamics after hydrogen tank rupture in a tunnel fire.
- Engineering models for assessment of blast wave and fireball of tank rupture in a tunnel, using parameters of a storage vessel and of a tunnel.
- Dependence of inherently safer hydrogen inventory on tunnel parameters (cross-section area, length, etc.).
- Coupled CFD/FEM modelling and simulation of a tunnel structure reaction to the blast produced by hydrogen storage tank rupture in a fire.
- Experimental data and engineering tools for the assessment of a fireball and blast wave dynamics in a tunnel.

Prevention and mitigation techniques

- Prevention and mitigation techniques eliminating hydrogen tank rupture in a tunnel and its devastating consequences: blast wave, fireball, projectiles, e.g. leak-no-burst safety technology for prevention of tank rupture in a fire.
- Safety of high-pressure storage tanks: alternative TPRD designs and development of advanced materials for pressure vessels to prevent and mitigate hydrogen storage tank explosion in a fire.
- Shock wave attenuation by water and mist systems, absorbing materials, soft bulkheads, sacrificial pre-evacuated volumes.
- Comparison of efficiency of cheaper water spray systems with more expensive water mist systems.
- Establishing best practice for TPRD activation, e.g. would a piloted ignition on activation be a safer option?
- Guidelines for sprinkling and fire ventilation.
- Protection of humans and critical equipment against pressure effects.
- Difference in prevention and mitigation techniques to accidents with hydrogen cars, buses, heavy goods vehicles and rail vehicles.

First response

- Operator’s actions as the first responder in case of accident involving hydrogen vehicle.
- Consequences of TPRD cooling by firefighters.
- Difference in response to accidents with hydrogen cars, buses, heavy goods vehicles and rail vehicles.
- Best practise for safe egress in tunnels in the context of hydrogen energy accidents.

Safety management and risk assessment

- Risk assessment methodology and frequencies and consequences effects data on the use of hydrogen-powered vehicles in road and railway tunnels and similar confined spaces.
- Permitting procedure for dangerous goods transportation through tunnels.
- Eurocodes inapplicability for explosions produced by hydrogen tank rupture in a tunnel.
- Preservation of self-evacuation principle for accidents involving hydrogen.
- Effect of blast wave demolition in a tunnel on cost of a tunnel closure.

It should be mentioned that the knowledge gaps and technological bottlenecks identified and listed in this report are complementary and shared with those identified in the co-report of deliverable D1.1 “Report on assessment of effectiveness of conventional safety measures in underground transportation systems and similar confined spaces”.

7. Conclusions (UU)

A critical review of the hazards and risks of hydrogen powered vehicles and transport in tunnels or other confined spaces is presented. Relevant experimental, analytical and numerical studies are presented and discussed. Available reduced-order and CFD models and tools to quantify consequences of possible accidents are critically analysed. The shortcomings of available models and tools are underlined. The areas where understanding of hazard is insufficient are highlighted. The harm to humans and damage to civil structures criteria are of utmost importance to assess the effect of accident consequences on humans and infrastructure. Harm and damage criteria are used to define the hazard distances. The QRA methodologies, which are considered potentially applicable to tunnels applications are discussed. The critical review led to the identification of knowledge gaps and technological bottlenecks, which are in the HyTunnel-CS project domain.

The report is the state-of-the-art and beyond the state-of-the-art analysis of research that assists in understanding of relevant physics to underpin the advancement of hydrogen safety engineering for tunnels, etc. It includes incentives to develop innovative explosion and fire prevention and mitigation strategies and engineering solutions. The report will support shaping the research within HyTunnel-CS. The goal is to underpin inherently safer entering underground traffic systems by hydrogen vehicles at risk below or the same as for fossil fuel transport. The report informs intervention strategies and tactics for first responders to be developed and paves a way to recommendations for inherently safer use of hydrogen vehicles in underground transportation systems. The complementarities and synergies of partners in theoretical, numerical and experimental research will be used to close identified knowledge gaps and resolve technological bottlenecks.

References

AIChE Center for Chemical Process Safety (1999) Guidance for Consequence Analysis of Chemical Releases, Center for Chemical Process Safety, American Institute of Chemical Engineers, New York: American institute of Chemical Engineers.

Al-shanini, A., Ahmad, A. and Khan, F. (2014) Accident modelling and analysis in process industries. Journal of Loss Prevention in the Process Industries, 32, 319–334.

Alcock, J.L., Shirvill, L.C. and Cracknell, R.F. (2001) Comparison of existing safety data on hydrogen and comparative fuels. Deliverable report of European FP5 project EIHP2, May 2001. Available from: www.eihp.org/public/documents/CompilationExistingSafetyData_on_H2_and_ComparativeFuels_S..pdf [Accessed on 13.05.19].

Alekseev, V.I., Kuznetsov, M.S., Yankin, Yu., G., Dorofeev, S.B. (2001) Experimental study of flame acceleration and DDT under conditions of transverse venting. J. Loss Prev. Proc. Ind., 14/6: 591-596.

ANSYS (2016a), CFX help, Release 17.2.

ANSYS (2016b) FLUENT help, Release 18.0.

API (1995) Management of hazards associated with location of process plant buildings (API Recommended Practice 752). American Petroleum Institute, Washington D.C.

Baker, W.E., Cox, P.A., Westine, P.S., Kulesz, J.J., Strehlow, R.A. (1983) Explosion hazards and evaluation. Elsevier Scientific Publishing Company.

Baratov, A.N., Korolchenko, A.Y. and Kravchuk, G.N. (Eds.) (1990) Fire and explosion hazards of substances and materials. Moscow: Khimia. 496 p., ISBN 5-7245-0603-3 part 1, ISBN 5-7245-0408-1 part 2 (in Russian).

Barbato, L., Cascetta, F., Musto, M., Rotondo, G. (2014) Fire safety investigation for road tunnel ventilation systems – An overview, Tunn. Undergr. Sp. Technol. 43, 253–265.

Barlow, R.S., Carter, C.D. (1996) Relationships among nitric oxide, temperature, and mixture fraction in hydrogen jet flames. Combust. Flame 104, 288–299.

Barry, T.F. (2002) Risk-informed, performance-based industrial fire protection. 1st ed, An Alternative to Prescriptive Codes. Tennessee Valley Publishing, USA.

Bassan, S. (2016) Overview of Traffic Safety Aspects and Design in Road Tunnels. IATSS Research 40 (1), 35–46.

Bezmelnitsyn, A.V. (1998) Experimental study of conditions for detonation initiation by a jet of combustion products. PhD thesis, RRC Kurchatov Institute, Moscow (in Russian).

Bie, H.Y. and Hao, Z.R. (2017) Simulation analysis on the risk of hydrogen releases and combustion in subsea tunnels. International Journal of Hydrogen Energy, Volume 42, Issue 11, 7617-7624.

Birch, A.D., Brown, D.R., Dodson, M.G., Swaffield, F. (1984) The structure and concentration decay of high pressure jets of natural gas. Combustion Science Technology 36, 249–261.

Birch, A.D., Hughes, D.J., Swaffield, F. (1987) Velocity decay of high pressure jets. Combustion Science and Technology 52 (1-3), 161-171

Blanc-Vannet, P., Jallais, S., Fuster, B., Fouillen, F., Halm, D., van Eekelen, T., Welch, S., Breuer, P., Hawksworth, S. (2019) Fire tests carried out in FCH JU Firecomp project, recommendations and application to safety of gas storage systems. International Journal of Hydrogen Energy, Special issue on The 7th International Conference on Hydrogen Safety (ICHS 2017), 11-13 September 2017, Hamburg, Germany 44, 9100–9109.

Blennemann, F. et al. (2005) Brandschutz in Fahrzeugen und Tunneln des ÖPNV. Fire protection in vehicles and tunnels for public transport. Alba-Fachverlag, Düsseldorf, pp. 55, 57.

Boeck, L.R., Berger, F.M., Hasslberger, J., Sattelmayer, T. (2016) Detonation Propagation in Hydrogen-Air Mixtures with Transverse Concentration Gradients. Shock Waves, 26: 181-192

Bourgeois, T. et al. (2015) Evaluating the temperature inside a tank during a filling with highly-pressurized gas. International Journal of Hydrogen Energy. Pergamon, 40(35), 11748–11755.

Boyack, K.W., Tieszen, S.R., Stamps, D.W. (1993). Internal pressure loads due to gaseous detonations. Proc R Soc Lond A, 443:343-66.

Brauer, R. L. (2006) Pressure, safety and health for engineers, 2nd edition, John Wiley & Sons, Hoboken, New Jersey, pp. 359–370.

Brauner, C. et al. (2016) Firefighting operations in road tunnel. Tactics – Techniques – Background. Kehsler Verlag, Saulheim. p. 60.

Bray, K. N. C. (1996) The challenge of turbulent combustion. Proc Combust Inst, vol. 26, pp.1-26.

Brennan, S., Makarov, D., Molkov, V. (2010) Dynamics of flammable hydrogen-air mixture formation in an enclosure with a single vent, in: Proceedings of the 6th International Seminar on Fire and Explosion Hazards. Leeds.

Brennan, S., Molkov, V. (2013) Safety assessment of unignited hydrogen discharge from onboard storage in garages with low levels of natural ventilation. International Journal of Hydrogen Energy, 38(19), 8159–8166.

Brennan, S., Molkov, V. (2018) Pressure peaking phenomenon for indoor hydrogen releases. International Journal of Hydrogen Energy 43, 18530–18541.

Brennan, S., Hussein, H.G., Makarov, D., Shentsov, V., Molkov, V. (2019) Pressure effects of an ignited release from onboard storage in a garage with a single vent. International Journal of Hydrogen Energy 44, 8927–8934.

BRHS (2009) Biennal Report on Hydrogen Safety. The European Network of Excellence "Safety of Hydrogen as an Energy Carrier" (NoE HySafe). Available from: www.hysafe.org [Accessed 28.12.11].

British Standards Institution (2001) British standard 7974:2001, Application of fire safety engineering to the design of buildings – Code of Practice. 7974:2001 (2001).

BS 7345-7:2013, The British Standards Institution, Components for smoke and heat control systems Part 7: Code of practice on functional recommendations and calculation methods for smoke and heat control systems for covered car parks, 2013.

Buncefield Investigation (2010) The Buncefield Major Incident Investigation Board. Available from: http://www.buncefieldinvestigation.gov.uk/index.htm [Accessed 26.12.11].

Bustamante-Valencia, L., Blanc-Vannet, P., Heudier, L., Jamois, D. (2016) Thermal history resulting in the failure of lightweight fully-wrapped composite pressure vessel for hydrogen in a fire experimental facility. Fire Technology 421–442.

Cadwallader, L.C. and Zhao H. (2016) Personnel Safety with Pressurized Gas Systems, INL/JOU-14-32059.

Caliendo, Ciro, and Maria Luisa De Guglielmo (2017) Quantitative Risk Analysis on the Transport of Dangerous Goods Through a Bi-Directional Road Tunnel. Risk Analysis 37 (1): 116–29.

Cariteau, B., & Tkatschenko, I. (2012) Experimental study of the concentration build-up regimes in an enclosure without ventilation. International Journal of Hydrogen Energy, 37(22), 17400–17408.

CCPS (1994) Guidelines for Evaluating the Characteristics of Vapour Cloud Explosions, Flash Fires and BLEVEs. New York: American institute of Chemical Engineering.

Cerchiara, G.M., Mattei, N., Schiavetti, M., Carcassi, M.N. (2011) Natural and forced ventilation study in an enclosure hosting a fuel cell. International Journal of Hydrogen Energy 36, 2478–2488.

Chamonet (2019) The Mont Blanc Tunnel. Road rules & regulations. Available from https://www.chamonet.com/travel/driving/the-mont-blanc-tunnel [accessed 30.07.2019]

Chen, C.J., Rodi, W. (1980) Vertical turbulent buoyant jets: a review of experimental data. NASA STIRecon Tech. Rep. A 80, 23073.

Cheong, M.K., Spearpoint, M.J., Fleischmann, C.M. (2008) Design fires for vehicles in road tunnels. Presented at the 7th International Conference on Performance-Based Codes and Fire Safety Design Methods, Auckland, New Zealand, pp. 229–240.

Chiang, C.-L., Chang, R.-C., Chiu, Y.-C. (2007) Thermal stability and degradation kinetics of novel organic/inorganic epoxy hybrid containing nitrogen/silicon/phosphorus by sol–gel method, Thermochim. Acta 453, 97–104.

Choi, J., Hur, N., Kang, S., Lee, E.D., Lee, K.-B. (2013) A CFD simulation of hydrogen dispersion for the hydrogen leakage from a fuel cell vehicle in an underground parking garage. International Journal of Hydrogen Energy 38, 8084–8091.

Ciambelli, P., Meo, M., Russo, P., Vaccaro, S. (2011) Thermal radiation modelling in tunnel fires. Advanced in Applied Mathematics and Mechanics, vol.3, 327-353.

Cirrone D., Makarov D. and Molkov V. (2019a) Thermal radiation from cryogenic hydrogen jet fires. International Journal of Hydrogen Energy, vol.44, 8874-8885.

Cirrone, D. M. C., Makarov, D., Molkov, V. (2019b) Simulation of thermal hazards from hydrogen under-expanded jet fire. International Journal of Hydrogen Energy, vol.44, 8886-8892.

Cirrone D., Makarov D. and Molkov V. (2019c) Near Field Thermal Dose of Cryogenic Hydrogen Jet Fires, International Seminar on Fire an Explosion Hazards, 21-26 April 2019, St. Petersburg, Russia.

Cirrone, D., Makarov, D., Molkov, V. (2019d) Cryogenic hydrogen jets: flammable envelope size and hazard distances for jet fire, in: International Conference on Hydrogen Safety. Presented at the International Conference on Hydrogen Safety, Accepted, Adelaide, Australia.

Cleaver, R. P., Marshall, M. R., & Linden, P. F. (1994) The build-up of concentration within a single enclosed volume following a release of natural gas. Journal of Hazardous Materials, 36, 209–226.

CNG explosion (2016) [WWW Document] Wwwerdgasfahrer-Forumde. URL http://www.erdgasfahrer-forum.de/viewtopic.php?t=14568 (accessed 3.15.18).

College of the Desert (2001) Hydrogen Fuel Cell Engines and Related Technologies Course. Module 1. Available from: https://www.energy.gov/eere/fuelcells/downloads/hydrogen-fuel-cell-engines-and-related-technologies-course-manual [accessed 24.08.2019]

Commission Regulation (EU) No 406/2010 — European Environment Agency [WWW Document], n.d. URL https://www.eea.europa.eu/policy-documents/commission-regulation-eu-no-406-2010 (accessed 4.22.19).

Consalvi, J. L., Nmira, F. (2019) Modeling of large-scale under expanded hydrogen jet fires. Proceedings of the combustion Institute, vol. 37, 3943-3950.

Coward, H.F. and Jones, G.W. (1952) Limits of flammability of gases and vapors. Bulletin 503, Bureau of Mines, p. 155.

Dadashzadeh, M., Makarov, D. and Molkov, V. (2017) Non-adiabatic blowdown model: a complimentary tool for the safety design of tank-TPRD system, in International Conference on Hydrogen Safety, September 11-13, 2018, Hamburg, Germany.

Dadashzadeh, M., Kashkarov, S., Makarov, D., Molkov, V. (2018) Risk assessment methodology for onboard hydrogen storage. International Journal of Hydrogen Energy 43, 6462–6475.

Daubech, J., Hebrard, J., Jallais, S., Vyazmina, E., Jamois, D., Verbecke, F. (2015) Un-ignited and ignited high pressure hydrogen releases: Concentration – turbulence mapping and overpressure effects. Journal of Loss Prevention in the Process Industries, Volume 36, 439-446.

Department for Communities and Local Government (2010) Fire spread in car parks, BD2552.

Department for Communities and Local Government, n.d. Fire Statistics Great Britain 2011/12 [WWW Document]. URL https://data.gov.uk/dataset/vehicle_fires.

Derudi, M., Borghetti, F., Favrin, S., Frassoldati, A. (2018) TRAM: A New Quantitative Methodology for Tunnel Risk Analysis. Chemical Engineering Transactions 67: 811–16.

Dorofeev, S.B., Sidorov, V. P., Kuznetsov, M. S., Matsukov, I. D., Alekseev, V. I. (2000) Effect of scale on the onset of detonations. Shock Waves, v. 10, pp. 137-149.

Dorofeev, S.B., Kuznetsov, M.S., Alekseev, V.I., Efimenko, A.A., Breitung, W. (2001) Evaluation of limits for effective flame acceleration in hydrogen mixtures. J. Loss Prev. Proc. Ind., 14 (6): 583-589.

Drysdale, D. (1999) An introduction to fire dynamics. Wiely, 2nd. Edition, Chichester, p. 351.

Duijm, N. J., Kozine, I. O. and Markert, F. (2013) Assessing risks on offshore platforms by dynamic simulation of accident scenarios', in Society for Risk Analysis - Europe (SRA-E). Trondheim, Norway: Society for Risk Analysis - Europe (SRA-E).

Ekoto, I. W., Houf, W. G., Ruggles, A. J., Creitz, W. L., Li, J. X. (2012) Large-scale hydrogen jet flame radiant fraction measurements and modelling. Proceedings of the International Pipeline Conference, Calgary, Canada, September 24-28.

Ekoto, I. W., Ruggles, A. J., Creitz, W. L., Li, J. X. (2014). Updated jet flame radiation modeling with buoyancy corrections. International Journal of Hydrogen Energy, vol. 39, 20570-20577.

E-Laboratory [WWW Document], n.d. URL https://elab-dev.iket.kit.edu/#/ (accessed 6.27.19).

EN 1993-1-2 (2005) Eurocode 3: Design of steel structures - Part 1-2: General rules - Structural fire design (English) [Authority: The European Union Per Regulation 305/2011, Directive 98/34/EC, Directive 2004/18/EC].

European Maritime Safety Agency (2015) Risk acceptance criteria and risk based damage stability. Final Report, Part 1: Risk Acceptance Criteria.

European Parliament and Council (2004) Directive 2004/54/EC of The European Parliament and of The Council on minimum safety requirements for tunnels in the Trans-European Road Network, 29 April 2004.

Evarts, B. (2011) Fires at U.S. Service Stations. NFPA.

Federal Emergency Management Agency (1987) Handbook of Chemical Hazard Analysis Procedures, Washington, D.C.

Fletcher, I. A., Welch, S., Torero, J. L., Carvel, R. O, Usmani, A. (2007) Behaviour of concrete structures in fire. Thermal Science, 11(2), 37–52.

Fluent Incorporated, Fluent 6.1.22 (2003), User's Guide.

Franssen et al. (1997) Development of design rules for steel structures subjected to natural fires in closed car parks.

Friedrich, A., Grune, J., Jordan, T., Kotchourko, A., Kotchourko, N., Kuznetsov, M., Sempert, K., Stern, G. (2007a) Experimental study of hydrogen-air deflagrations in flat layer. In: Proc. 2nd ICHS International Conference on Hydrogen Safety. September 11 - 13, 2007 San Sebastian – SPAIN, paper 1.3.106, 1-12.

Friedrich, A., Grune, J., Kotchourko, N., Kotchourko, A., Sempert, K., Stern, G., Kuznetsov, M. (2007b) Experimental study of jet-formed hydrogen-air mixtures and pressure loads from their deflagrations in low confined surroundings. International Conference on Hydrogen Safety, San Sebastian, Spain.

Fugelso, L.E., Weiner, L.M., Schiffman, T.H. (1972) Explosion effects computation aids (No. GARD Prog. 1540), Gen. Am. Div., Gen. Am. Transportation Co., Niles, Illinois, US.

Gamezo, V.N., Ogawa, T., and Oran, E.S. (2007). Numerical simulations of flame propagation and DDT in obstructed channels filled with hydrogen-air mixture. Proc. Combust. Instit., 31, 2463–2471.

Gavrikov, A.I., Efimenko, A.A., Dorofeev, S.B (2000) A model for detonation cell size prediction from chemical kinetics. Combustion and Flame, 120 (1-2): 19-33.

Gentili, F., Giuliani, L., Bontempi, F. (2013) Structural Response of Steel High Rise Buildings to Fire: System Characteristics and Failure Mechanisms. Journal of Structural Fire Engineering. 4. 9-26.

Groethe, M., Colton, J., Chiba, S. (2002) Hydrogen deflagration safety studies in semi-open space, in the 14th World Hydrogen Energy Conference, Montreal, Canada, 9-13 June 2002.

Groethe, M., Merilo, E., Colton, J., Chiba, S., Sato, Y., and Iwabuchi, H. (2005) Large-scale hydrogen deflagrations and detonations, Paper No. 120105, in Proceedings of the First International Conference on Hydrogen Safety, Pisa, Italy, 8–10 September 2005.

Groethe, M., Merilo, E., Colton, J., Chiba, S., Sato, Y., and Iwabuchi, H. (2007) Large-scale hydrogen deflagrations and detonations. International Journal of Hydrogen Energy, 32, 2125-2133.

Grune, J., Sempert, K., Kuznetsov, M., Breitung, W. (2011) Experimental study of ignited unsteady hydrogen jets into air. International Journal of Hydrogen Energy, vol. 36, pp. 2497-2504.

Grune, J., Sempert, K., Kuznetsov, M., Jordan, T. (2014) Experimental study of ignited unsteady hydrogen releases from a high pressure reservoir. International Journal of Hydrogen Energy 39, 6176-6183.

Grune, J., Sempert, K., Friedrich, A., Kuznetsov, M., Jordan, T. (2017) Detonation wave propagation in semi-confined layers of hydrogen–air and hydrogen–oxygen mixtures. International Journal of Hydrogen Energy, Volume 42, Issue 11, 7589-7599.

Guigas, X. et al. (2006) Water mist tests for the A86 East tunnel. In: INTEVIA Technical Institute of Traffic and Transportation (pub.): 2nd International Symposium on Tunnel Safety & Security. pp. 233–241, Madrid.

Haddad, R.K., Maluk, C., Reda, E., Harun, Z. (2019) Critical Velocity and Backlayering Conditions in Rail Tunnel Fires: State-of-the-Art Review. J. Combust. 2019, 1–20.

Hall, R., Knoflacher, H., Pons., P. (2001) Quantitative Risk Assessment Model for Dangerous Goods Transport through Road Tunnels. PIARC Ref. RR329-086. https://www.piarc.org/ressources/publications/3/5089,RR329-UK.pdf.

Hall, J. E., Hooker, P. and Willoughby, D. (2014) Ignited Releases of Liquid Hydrogen: Safety Considerations of Thermal and Overpressure Effects. International Journal of Hydrogen Energy, vol. 39, no. 35, 20547–20553.

Hall, J. E., Hooker, P., O' Sullivan, L., Angers, B., Hourri, A., Bernard, P. (2017) Flammability profiles associated with high-pressure hydrogen jets released in close proximity to surfaces. International Journal of Hydrogen Energy, vol. 42, 7413-7421.

Hankinson, G., Lowesmith, B. J. (2012) A consideration of methods of determining the radiative characterstics of jet fires. Combustion and Flame, vol. 159, 1165-1177.

Haugom, G., Rikheim, H. and Nilsen, S. (2003) Hydrogen Applications. Risk Acceptance Criteria and Risk Assessment Methodology, in European Hydrogen Energy Conference, Grenoble (France), 2003.

Hawthorne, W.R., Weddell, D.S., Hottel, H.C. (1949) Mixing and combustion in turbulent gas jets. Proc. Combust. Inst. 3, 266–288.

Health and Safety Executive (1975) The Flixborough Disaster: Report of the Court of Inquiry, HMSO, ISBN 011360750.

Health and Safety Executive (2010) Methods of approximation and determination of human vulnerability for offshore major accident hazard assessment.

Hertz, K. D. (2002) Limits of spalling of fire-exposed concrete, Elsevier, 1, 113–116.

Hertz, K. D. (2019) Design of fire-resistant concrete structures. 1st edn. Edited by Bhattacharyya and Hobbs. London (UK): ICE Publishing; Thomas Telford limited. Available at: www.icebook.com.

Hertz, K. D. and Sørensen, L. S. (2005) Test method for spalling of fire exposed concrete, Fire Safety Journal, 40(5), 466–476.

Heus, R., Denhartog, E. A. (2017) Maximum allowable exposure to different heat radiation levels in three types of heat protective clothing. Ind Health. 2017;55(6): 529–536.

Hooker, P., Hoyes, J., Hall, J., Willoughby, D. (2017) Experimental studies on vented deflagrations in a low strength enclosure, International Journal of Hydrogen Energy, 42(11):7 565-76.

Houf, W.G., Evans, G.H., Merilo, E., Groethe, M., James, S.C. (2012) Releases from hydrogen fuel-cell vehicles in tunnels, International Journal of Hydrogen Energy 37, 715–719.

Hourri, A., Angers, B. and Bénard, P. (2009) Surface effects on flammable extent of hydrogen and methane jets, International Journal of Hydrogen Energy 34(3), 1569-1577

Hourri, A., Angers, B., Bernard, P., Tchouvelev, A., Agranat, V. (2011) Numerical investigation of the flammable extent of semi-confined hydrogen and methane jets. International Journal of Hydrogen Energy, vol. 36, pp. 2567-2572.

Hu, L.H., Huo, R., Chow, W.K. (2008a), Studies on buoyancy-driven back-layering flow in tunnel fires, Exp. Therm. Fluid Sci. 32, 1468–1483.

Hu, L.H., Peng, W., Huo, R. (2008b), Critical wind velocity for arresting upwind gas and smoke dispersion induced by near-wall fire in a road tunnel, J. Hazard. Mater. 150, 68–75.

Huang, Y., Li, Y., Dong, B. (2018) Radiant heat flux profile of horizontally oriented rectangular source fuel jet fires. Industrial & Engineering Chemistry Research, 57, 1078-1088.

Hurley, M.J., Gottuk, D.T., Hall Jr., J.R., Harada, K., Kuligowski, E.D., Puchovsky, M., Torero, J.L., Watts Jr., J.M., Wieczorek, C.J. (2016) SFPE handbook of fire protection engineering, fifth edition. 4th edition, SFPE Handbook of Fire Protection Engineering, Fifth Edition. 4th edition. Edited by M. J. Hurley et al., Springer.

Hussein, H.G., Brennan, S., Shentsov, V., Makarov, D., Molkov, V. (2018) Numerical validation of pressure peaking from an ignited hydrogen release in a laboratory-scale enclosure and application to a garage scenario. International Journal of Hydrogen Energy 43, 17954–17968.

Hussein, H.G., Brennan, S., Makarov, D., Shentsov, V., Molkov, V. (2019), Safety considerations of an unignited hydrogen release from onboard storage in a naturally ventilated covered car park, 9th International Seminar on Fire and Explosion Hazards, St. Petersburg, Russia, April 21-26.

HyResponse (2015a) Lecture – Hydrogen properties relevant to safety, Accessible from: www.hyresponse.eu/training-mat-1.php [Accessed on 13.05.19].

HyResponse (2015b) Lecture – Harm criteria for people and environment, damage criteria for structures and equipment. Accessible from: www.hyresponse.eu/training-mat-1.php [Accessed on 13.05.19].

HyTunnel-D111 (2009) Internal project on investigating the use of hydrogen vehicles in road tunnels, Deliverable D111, 15 April 2009. Accessible from:

http://www.hysafe.net/download/1763/Hyunnel_Final%20ReportDraft_20Feb09_final.pdf [Accessed on 30.06.2019]

HyTunnel-CS (2019). Deliverable D1.1. Report on assessment of effectiveness of conventional safety measures in underground transportation systems and similar confined spaces. Fuel Cells and Hydrogen Joint Undertaking (FCH JU), Grant Agreement Number 826193.

Ibas, M. (2005) The effect of thermal radiation and radiation models on hydrogen- hydrocarbon combustion modelling, International Journal of Hydrogen Energy, vol.30, 1113-1126.

IEC 60079-10-1 (2015) International Electrochnical commission IEC 60079-10-1. Explosive atmospheres - Part 10-1: Classification of areas - Explosive gas atmospheres. (No. IEC 60079-10-1).

Imamura, T., Hamada, S., Mogi, T., Wada, Y., Horiguchi, S., Miyake, A., Ogawa, T. (2008) Experimental investigation on the thermal properties of hydrogen jet flame and hot currents in the downstream region. International Journal of Hydrogen Energy 33, 3426–3435.

INERIS (2005a) Transport of Dangerous Goods Through Road Tunnels: Quantitative Risk Assessment Model (v. 3.60 and v. 3.61) - Reference Manual. Research Report N° 20504, 1 August 2005.

INERIS (2005b) Transport of Dangerous Goods Through Road Tunnels: Quantitative Risk Assessment Model (v. 3.60 and v. 3.61) - User's Guide. Research Report N° 20504, 1 December 2005.

Ingason, H., Li, Y. Z. and Lönnermark, A. (2015) Tunnel Fire Dynamics. New York, NY: Springer New York.

Ingason, H., Li, Y.Z. (2017) Spilled liquid fires in tunnels. Fire Safety Science: Proceedings of the 12th International Symposium 91, 399–406.

Ishii, K., Itoh, K., Tsuboi, T. (2002) A study on velocity deficits of detonation waves in narrow gaps. Proceedings of the Combustion Institute, 29 (2), pp. 2789-2794.

ISO 834-1:1999 (1999) Fire-resistance tests - Elements of building construction - Part 1: General requirements.

ISO 13344:2015 (2015) Estimation of the lethal toxic potency of fire effluents.

ISO 19882 (2018) Gaseous hydrogen – Thermally activated pressure relief devices for compressed hydrogen vehicle fuel containers.

ISO/DIS 19880-1 (2018) 19880-1 TI organization for standardization I. Gaseous hydrogen – fuelling stations. Part 1: General requirements. 2018.

ISO/TR 15916:2004 (2004) Basic considerations for the safety of hydrogen systems. ISO/TR 15916:2004

ISO/TR 13571-2 (2016) Life-threatening components of fire - Part 2: Methodology and examples of tenability assessment.

Janda, T., Šejnoha, M. and Šejnoha, J. (2018) Applying Bayesian approach to predict deformations during tunnel construction. International Journal for Numerical and Analytical Methods in Geomechanics. Edited by D. Felix, 42(15), 1765–1784.

Jeffries, R.M., Hunt, S.J., Gould, L. (1997) Derivation of fatality probability function for occupants buildings subject to blast loads (Contract research report for HSE No. 147/1997). Contract research report. WS Atkins Science & Technology.

Jönsson, J., Herrera, F. (2010) HGV traffic – Consequences in case of a tunnel fire, Presented at the Fourth International Symposium on Tunnel Safety and Security, Frankfurt am Main, Germany, pp. 125–134.

Karpov, V.P. and Severin, E.S. (1980) Fiz. Goreniya Vzryva 16, No. 1, 45.

Kashkarov, S., Li, Z.Y., Molkov. V. (2017a) Hazard distance nomograms for a blast wave from a compressed hydrogen tank rupture in a fire, 7th International Conference on Hydrogen Safety (ICHS7).

Kashkarov, S., Makarov, D., Molkov, V. (2017b) Model of 3D conjugate heat transfer and mechanism of compressed gas storage failure in a fire, in: 7th International Conference on Hydrogen Safety (ICHS), Hamburg, Germany.

Kashkarov, S., Makarov, D., Molkov, V. (2018) Effect of a heat release rate on reproducibility of fire test for hydrogen storage cylinders. International Journal of Hydrogen Energy 43, 10185–10192.

Kazaras, K. and Kirytopoulos, K. (2014) Challenges for current Quantitative Risk Assessment (QRA) models to describe explicitly the road tunnel safety level. Journal of Risk Research 17 (8): 953–68.

Khakzad, N., Khan, F. and Paltrinieri, N. (2014) On the application of near accident data to risk analysis of major accidents. Reliability Engineering & System Safety, 126(0), 116–125.

Khokhlov, A.M., Oran, E.S., Wheeler, J.C. (1997) A theory of deflagration-to-detonation transition in unconfined flames. Combust. Flame 108, 503–517.

Kim, H. J., Hong, S. W., Kim, H.D., Yang, S. Y., Chung, S. H. (2001) Quenching distance measurement for the control of hydrogen explosion. Proceedings of the 18th International Colloquium on the Dynamics of Explosions and Reactive Systems, Seattle, Washington.

Koinig H. (1999) Referenzszenarien zur Richtlinie 96/82/EG, erstellt im Auftrag des Bundesministeriums für Umwelt, Jugend und Familie, Wien 1999, Allg. beeid. und gerichtl. zert. Sachverständiger, Technisches Büro für Technische Physik, Donaustr. 101/1, 2344 Maria Enzersdorf.

Kuznetsov, M.S., Dorofeev, S. B., Efimenko, A. A., Alekseev, V. I., Breitung, W. (1997) Experimental and numerical studies on transmission of gaseous detonation to a less sensitive mixture. Shock Waves, vol. 7, 297-304.

Kuznetsov, M.S., Alekseev, V. I., Dorofeev, S. B. (2000) Comparison of critical conditions for DDT in regular and irregular cellular detonation systems. Shock Waves, v. 10, pp. 217-224.

Kuznetsov, M., Alekseev, V., Matsukov, I. (2002) Deflagration-to-Detonation Transition in H_2 -Air and H_2 -O_2 -N_2 mixtures in channels with obstructions. Advances in Confined Detonations (eds. G. Roy, S. Frolov, R. Santoro, S. Tsyganov), Torus Press Ltd., Moscow, pp 26-30.

Kuznetsov, M., Alekseev, V., Matsukov, I., Dorofeev, S. (2005) DDT in a smooth tube filled with a hydrogen–oxygen mixture. Shock Waves (2005) 14: 205-215.

Kuznetsov, M., Grune, J., Friedrich, A., Sempert, K., Breitung, W., Jordan, T. (2011) Hydrogen-air deflagrations and detonations in a semi-confined flat layer. In: Fire and

Explosion Hazards, Proceedings of the Sixth International Seminar (Edited by D. Bradley, G. Makhviladze and V. Molkov), 125-136.

Kuznetsov, M., Friedrich, A., Stern, G., Kotchourko, N., Jallais, S., L'Hostis, B. (2015a) Medium-scale experiments on vented hydrogen deflagration. J Loss Prev Process Ind, 36:416-28.

Kuznetsov, M., Yanez, J., Grune, J., Friedrich, A., Jordan, T. (2015b) Hydrogen combustion in a flat semi-confined layer with respect to the Fukushima Daiichi Accident. Nuclear Engineering and Design, 286: 36-48.

Kuznetsov, M., Lelyakin, A., Alekseev, V., Matsukov, I. (2017) Detonation transition in relatively short tubes. In: Ben-Dor G., Sadot O., Igra O. (eds) 30th International Symposium on Shock Waves 1. Springer Publ., 481-485.

Kuznetsov, M. and Grune, J. (2019) Experiments on combustion regimes for hydrogen/air mixtures in a thin layer geometry. International Journal of Hydrogen Energy, 44 (7): 8727-8742.

LaChance, J., Houf, W., Middletoon, B. and LaFluer, C. (2009) Analyses to support development of risk-informed separation distances for hydrogen codes and standards. Sandia National Laboratories (2009) SAND2009–0874, unlimited release, March, 2009.

LaChance, J. (2010) Analyses to support development of risk-informed separation distances for hydrogen codes and standards, in: 6th ISCARW. Belfast.

LaChance, L., Tchouvelev, A., Engebo, A. (2011) Development of uniform harm criteria for use in quantitative risk analysis of the hydrogen infrastructures. International Journal of Hydrogen Energy 36, 2381-2388.

LaFleur, C., Bran-Anleu, G., Muna, A.B., Ehrhart, B.D., Blaylock, M. and Houf, W.G. (2017) Hydrogen fuel cell electric vehicle tunnel safety study.

Lamoureux., N., Djebaili-Chaumeix, N., Paillard, C.E. (2003) Laminar flame velocity determination for H2-air-stream mixtures using the spherical bomb method, J. Phys. IV France, 12, 445-458.

Landau, L. D. and Lifshitz, E. M. (1989) Fluid Mechanics. Pergamon Press. Oxford.

Larson, D., Reese, R., Wilmot, W. (1983) Caldecott Tunnel fire thermal environments: regulatory considerations and probabilities (Report No. SAND--82-1949C).

Law, A., Stern-Gottfried, J., Gillie, M., Rein, G. (2011) The influence of travelling fires on a concrete frame. Engineering Structures, Volume 33, Issue 5, 1635-1642.

Li, Z. Y., Makarov, D., Keenan, J., Molkov, V. (2015) CFD study of the unignited and ignited hydrogen releases from TPRD under a fuel cell car, International Conference on Hydrogen Safety, Yokohama, Japan.

Lind, C.D. (1975) What Causes Unconfined Vapour Cloud Explosions? Loss Prevention, vol.9, 101-105.

Liu, W., Varley, R.J., Simon, G.P. (2007) Understanding the decomposition and fire performance processes in phosphorus and nanomodified high performance epoxy resins and composites. Polymer 48, 2345–2354.

Liu, J. and Zio, E. (2016) System dynamic reliability assessment and failure prognostics, Reliability Engineering & System Safety.

Lönnermark, A. and Blomqvist, P. (2006) Emissions from an automobile fire. Chemosphere. Pergamon, 62(7), 1043–1056.

Lucherini, A., Giuliani, L., Jomaas, G. (2018) Experimental study of the performance of intumescent coatings exposed to standard and non-standard fire conditions. Fire Safety Journal, vol. 95, 42-50.

Lundin, J. (2018) Risk evaluation and risk control in road overbuilding of transport routes for dangerous goods, In Proceedings of Eighth International Symposium on Tunnel Safety and Security, Borås, Sweden, March 14-16, 2018.

Makarov, D., Kim, Y., Kashkarov, S., Molkov, V. (2016) Thermal protection and fire resistance of high-pressure hydrogen storage, Presented at the Eighth International Seminar on Fire & Explosion Hazards (ISFEH8), Hefei, China.

Makarov, D., Hooker, R., Kuznetsov, M., Molkov, V. (2018a) Deflagrations of localised homogeneous and inhomogeneous hydrogen-air mixtures in enclosures. International Journal of Hydrogen Energy, Volume 43, Issue 20, 9848-9869.

Makarov, D., Shentsov, V., Kuznetsov, M., Molkov, V. (2018b) Pressure peaking phenomenon: Model validation against unignited release and jet fire experiments. International Journal of Hydrogen Energy. Pergamon, 43 (19), 9454–9469.

Mangs, J., Keski-Rahkonen, O. (1994) Characterization of the fire behaviour of a burning passenger car, part I: car fire experiments. Fire Safety Journal 23, 17–35.

Mannan, S. (2005) Lees' Loss Prevention in the Process Industries. 3rd ed, Hazard Identification, Assessment and Control, Elsevier Butterworth-Heinemann.

Markert, F., Kozine, I. and Duijm, J. N. (2016) Process risk assessment using dynamic simulation of scenarios. Chemical Engineering Transactions, 48(2015), 181–186.

Martinsen, W., Marx, J. (1991) An improved model for the prediction of radiant heat from fireballs, in: International Conference and Workshop on Modeling Consequences of Accidental Releases of Hazardous Materials. San Francisco.

Matsuura, K., Nakano, M., Ishimoto, J. (2010) Forced ventilation for sensing-based risk mitigation of leaking hydrogen in a partially open space. International Journal of Hydrogen Energy 35, 4776–4786.

Mattelaer, V. (2018) Private communication, in: Toyota Europe.

McCory, T., Sprakel, D., Christensen, E. (2008) Workpackage 2 Fire development and mitigation measures, D251. Engineering Guidance for Water Based Fire Fighting Systems for the Protection of Tunnels and Sub Surface Facilities (Official deliverable).

Meel, A. and Seider, W. D. (2008) Real-time risk analysis of safety systems. Computers & Chemical Engineering, 32(4–5), 827–840.

Middha, P., Hansen, O.R. (2009) CFD simulation study to investigate the risk from hydrogen vehicles in tunnels. International Journal of Hydrogen Energy 34, 5875–5886.

Middha, P., Hansen, O. R., Grune, J., Kotchourko, A. (2010) CFD calculations of gas leak dispersion and subsequent gas explosions: validation against ignited impinging hydrogen jet experiments. Journal of Hazardous Materials, vol. 179, 84-94.

Ministère de l'Interieur (2013) NIO Risque hydrogène [WWW Document]. interieur.gouv.fr. URL http://www.interieur.gouv.fr/Le-ministere/Securite-civile/Documentation-

technique/Les-sapeurs-pompiers/Doctrines-et-techniques-professionnelles/Notes-operationnelles (accessed 12.10.15).

Mitrofanov, V. V., Soloukhin, R. I. (1965) The diffraction of multi-front detonation waves. Sov. Phys.-Dokl. 9: 1055.

Moen, I. O., Donato, M., Knystautas, R., Lee, J. H. S. (1981) The influence of confinement on the propagation of detonations near the detonability limit. Symp. (Int.) Combust., 18th, pp. 1615--23. Pittsburgh, Pa : Combust. Inst.

Moen, I.O., Sulmitras, A., Thomas, C.O., Bjerketvedt, D., Thibault, P.A. (1986) Influence of cellular regularity on the behaviour of gaseous detonations. In: Bowen JR, et al., editors. Dynamics of Explosions, vol. 106. Washington DC: AIAA Progress in Astronautics and Aeronautics; p. 220–43.

Molina, A., Schefer, R. W., Houf, W. G. (2007) Radiative fraction and optical thickness in large-scale hydrogen-jet fires. Proceedings of the Combustion Institute, vol. 31, pp. 2565-2572.

Molkov, V. (1996) Venting gaseous deflagrations. DSc Thesis, Moscow: VNIIPO; [in Russian].

Molkov, V., Verbecke, F., Makarov, D. (2008) LES of hydrogen-air deflagrations in a 78.5-m tunnel. Combustion Science and Technology, 180:5, 796-808.

Molkov, V. (2009) Hydrogen non-reacting and reacting jets in stagnant air: overview and state-of-the-art, in Proceedings of the 10th International Conference on Fluid Control, Measurements, and Visualization (FLUCOM 2009), 17-21 August 2009, Moscow, Russia.

Molkov, V., Makarov, D. and Bragin, M. V. (2009) Physics and modelling of underexpanded jets and hydrogen dispersion in atmosphere. Physics of Extreme States of Matter, 146–149.

Molkov, V., Bragin, M., Brennan, S., Makarov, D., Saffers, J.-B. (2010) Hydrogen safety engineering: Overview of recent progress and unresolved issues. International Congress Combustion and Fire Dynamics, Santander, Spain, 63-81.

Molkov, V., Saffers, J. (2011) The Correlation for Non-premixed Hydrogen Jet flame Length in Still Air. Fire Saf. Sci. 10, 933–943.

Molkov, V (2012) Fundamentals of Hydrogen Safety Engineering I, download free book at bookboon.com.

Molkov, V., Saffers, J.B. (2013) Hydrogen jet flames. International Journal of Hydrogen Energy 38, 8141–8158.

Molkov, V., Makarov, D., Keenan, J., Volodymyr, S., Venetsanos, A. G., Tolias, I. C., Duclos, A. (2014a) D 2.1 Review: The state-of-the-art in physical and mathematical modelling of safety phenomena relevant to FCH technologies 31. Report of the SUSANA Project, 1–341.

Molkov, V., Shentsov, V., Quintiere, J. (2014b) Passive ventilation of a sustained gaseous release in an enclosure with one vent. International Journal of Hydrogen Energy 39, 8158–8168.

Molkov, V., and Kashkarov, S. (2015) Blast wave from a high-pressure gas tank rupture in a fire: stand-alone and under-vehicle hydrogen tanks. International Journal of Hydrogen Energy, International Journal of Hydrogen Energy 40, 12581–12603.

Molkov, V., Makarov, D., Kashkarov, S. (2017) Composite Pressure Vessel for Hydrogen Storage, PCT International Application P119851PC00.

Mukai, S., Suzuki, J., Mitsuisho, H., Oyakawa, K., Watanabe, S. (2005) CFD simulation on diffusion of leaked hydrogen caused by vehicle accident in tunnels, in: 1st International Conference on Hydrogen Safety (ICHS 2005), Pisa, Italy, September.

Musharraf, M., Hassan, J., Khan, F., Veitch, B., MacKinnon, S. & Imtiaz, S. (2013) Human reliability assessment during offshore emergency conditions. Safety Science 59: 19-27.

NASA (1997) Safety standard for hydrogen and hydrogen systems. Guidelines for hydrogen system design, materials selection, operations, storage, and transportation. Technical Report NSS 1740.16, Office of Safety and Mission Assurance, Washington.

National Highway Traffic Safety Administration (NHTSA) (2015) Traffic Safety Facts 2015: a compilation of motor vehicle crash data from the fatality analysis reporting system and the general estimates system.

Nelisse, R. M. L. and Vrouwenvelder A. (2017) Probability of a large fire in a road tunnel Bayesian Inference, 4th International Probabilistic Workshop. Springer International Publishing, 123-134.

NewsinEnglish (2019) Hydrogen explosion under probe. Available at: https://www.newsinenglish.no/2019/06/11/hydrogen-explosion-under-probe/ [Last access: 11.08.2019]

NFPA (2010) U.S. vehicle fire trends and patterns.

NFPA 2 (2011) NFPA® 2 Hydrogen Technologies Code. Batterymarch Park, Quincy, MA 02169-7471.

Niranjana Prabhu, T., Hemalatha, Y. J., Harish, V., Prashantha, K., Iyengar, P. (2007). Thermal degradation of epoxy resin reinforced with polypropylene fibers. J. Appl. Polym. Sci. 104, 500–503.

NIST website (2019) Thermophysical Properties of Hydrogen. Available from: https://webbook.nist.gov/cgi/fluid.cgi?ID=C1333740&Action=Page [Last access: 24.08.19]

Norsk Hydro (2003) Risk acceptance criteria for hydrogen refuelling stations, no. February.

Okamoto, K., Otake, T., Miyamoto, H., Honma, M., Watanabe, N. (2013) Burning behavior of minivan passenger cars. Fire Safety Journal, Fire Safety Journal 62, 272–280.

Ono, R., Nifuku, M., Fujiwara, S., Horiguchi, S., Oda, T. (2007) Minimum ignition energy of hydrogen-air mixture: Effect of humidity and spark duration. Journal of Electrostatics, 65, 87-93.

Ozawa, M. and Morimoto, H. (2014) Effects of various fibres on high-temperature spalling in high-performance concrete. Construction and Building Materials. Elsevier, 71, 83–92.

Pasman, H. J. (2011) Challenges to improve confidence level of risk assessment of hydrogen technologies. International Journal of Hydrogen Energy, 36(3), 2407–2413.

Patankar, S. V. (1980) Numerical heat transfer and fluid flow (Series in computational methods in mechanics and thermal sciences). New York: McGRAW-HILL BOOK COMPANY.

PIARC Technical Committee C 3.3 on Road Tunnel Operation (2008) Risk analysis for road tunnels. Report n° 2008R02.

PIARC Technical Committee C.4 on Road Tunnel Operation (2012) Current practice for risk evaluation for road tunnels. Report n° 2012R23.

PIARC website, Tunnels - QRA model webpage. Available at https://www.piarc.org/en/knowledge-base/road-tunnels/qram_software/ [Accessed 15.06.19].

Pittman, J.F. (1976) Blast and fragments from superpressure vessel rupture. Defense Technical Information Center.

Pleß, G. and Seliger, U. (2009) Forschungsbericht Nr. 158. Untersuchung der Bedingungen für die Feuerwehren bei der Bekämpfung von Bränden in Verkehrstunneln unter Berücksichtigung der in den Risikoanalysen der OECD-PIARC zugrundeliegenden Brandszenarien für verschiedene Unfälle. Fire Research Institute of Saxony-Anhalt, Heyrothsberge, p. 19, 20.

Pötzsch, S., Krüger, S., Sklorz, C., Borch, J., Hilse, T., Otremba, F. (2018) The fire resistance of lightweight composite tanks depending on fire protection systems. Fire Saf. J. 100, 118–127.

Purser, D. A. (2008) Chapter 2: SFPE Handbook of Fire Protection Engineering (Ed. P.J. DiNenno) Fourth Edition. Quincy MA, USA: National Fire Protection Association.

Régnier, N., Fontaine, S. (2001) Determination of the thermal degradation kinetic parameters of carbon fibre reinforced epoxy using TG. J. Therm. Anal. Calorim. 64, 789–799.

Road Tunnel Association (RTA) (2019) UK & Eire Road Tunnel Directory. UK & Eire Road Tunnel Directory.

Ronchi, E. (2013) Testing the predictive capabilities of evacuation models for tunnel fire safety analysis. Safety Science. Elsevier, 59, 141–153.

Royle, M. and Willoughby, D.B. (2011a) Consequences of catastrophic releases of ignited and unignited hydrogen jet releases. International Journal of Hydrogen Energy 36, 2688-2692.

Royle, M. and Willoughby, D.B. (2011b) The interaction of hydrogen jet releases with walls and barriers. International Journal of Hydrogen Energy 36, 2455-2461.

Ruban, S., Heudier, L., Jamois, D., Proust, C., Bustamante-Valencia, L., Jallais, S., Kremer-Knobloch, K., Maugy, C., Villalonga, S. (2012) Fire risk on high-pressure full composite cylinders for automotive applications. International Journal of Hydrogen Energy, International Journal of Hydrogen Energy 37, 17630–17638.

Rudy, W., Kuznetsov, M., Porowski, R., Teodorczyk, A., Grune, J., Sempert, K. (2013) Critical conditions of hydrogen–air detonation in partially confined geometry. Proceedings of the Combustion Institute, 34 (2): 1965-1972.

SAE J2579 (2009) Technical information report for fuel systems in fuel cell and other hydrogen vehicles, in: SAE International, Detroit MI, U.S.

Saffers, J.B (2010) Principles of hydrogen safety engineering. PhD Thesis. University of Ulster.

Schefer, R. W., Houf, W. G., Bourne, B., Colton, J. (2006) Spatial and radiative properties of an open-flame hydrogen plume. International Journal of Hydrogen Energy, vol. 31, 1332-1340.

Schefer, R.W., Houf, W.G., San Marchi, C., Chernicoff, W.P., Englom, L. (2006) Characterization of leaks from compressed hydrogen dispensing systems and related components. International Journal of Hydrogen Energy 31, 14.

Schefer, R. W., Houf, W. G., Williams, T. C., Bourne, B., Colton, J. (2007) Characterization of high-pressure, underexpanded hydrogen-jet flames. International Journal of Hydrogen Energy, vol. 32, 2081–2093.

Schefer, R. W. and Houf, W. G. (2008) Analytical and experimental investigation of small-scale unintended releases of hydrogen. International Journal of Hydrogen Energy, vol.33, 1435-1444.

Schefer, R. W., Houf, W. G., & Williams, T. C. (2008), Investigation of small-scale unintended releases of hydrogen: buoyancy effects. International Journal of Hydrogen Energy, 33(17), 4702–4712.

Schmitt, B. (2016) Reports of volkswagen cars exploding in european gas stations [WWW Document]. URL https://www.forbes.com/sites/bertelschmitt/2016/09/16/europe-volkswagen-cars-explode-in-gas-stations/#205848a211fa (accessed 3.15.19).

Schneider, A., Kairies, S. and Rose, K. (1999) Synthesis of Akoxysilyl Substituted Cyclophosphazenes and their properties in the Sol-Gel process, Monatshefte für Chemie. Fraunhofer Institute for Silicate Research, D-97082 Würzburg, Germany: Springer, 130, pp. 89–98.

Schneider, U. and Horvath, J. (2006) Brandschutz-Praxis in Tunnelbauten. Brandverhalten, Brandschutzmaßnahmen, Sanierung mit Projektbeispielen. Bauwerk-Verlag, 1. Aufl., Berlin, pp.45, 54.

Scott, A. R. (1983) Occupational high-pressure injection injuries: Pathogenesis and prevention. J Soc Occup Med, 33 (1983), 56–59.

Selcuk, N., Kayakol, N. (1996) Evaluation of discrete ordinates and discrete transfer methods for radiative transfer, Conference Paper.

SFPE (2008) The SFPE Handbook of Fire Protection Engineering. 4th Edition. Di Nenno P.J. et al. Eds., National Fire Protection Association, Quincy (USA).

Shea, K. (2016) WATCH: Garbage truck explodes in fireball, rips hole in nearby house [WWW Document]. NJ.com. URL https://www.nj.com/mercer/2016/01/garbage_truck_explosion_damages_hamilton_house.html [accessed 5.20.19].

Shen, C., Ma, L., Huang, G., Wu, Y., Zheng, J., Liu, Y., Hu, J. (2018) Consequence assessment of high-pressure hydrogen storage tank rupture during fire test. J. Loss Prev. Process Ind. 55, 223–231.

Shentsov, V., Makarov, D., Molkov, V. (2018) Blast wave after hydrogen storage tank rupture in a tunnel fire, in: International Symposium on Tunnel Safety and Security 2018, Presented at the International Symposium on Tunnel Safety and Security 2018, Borås, Sweden.

Shentsov, V., Makarov, D., Dery, W. (2019) Stand-alone hemisphere-tank rupture in tunnel fire: effect of hydrogen inventory on blast wave strength in far field, in: International Seminar on Fire & Explosion Hazards (ISFEH) 9.

Shevyakov, G.G., Komov, V.F. (1977) Effect of noncombustible admixtures on length of an axisymmetric on-port turbulent diffusion flame. Combust. Explos. Shock Waves 13, 563–566.

Shevyakov, G.G., Tomilin, V.P., Kondrashkov, Y.A. (1980) Influence of buoyancy on the mixing length in a free turbulent jet. Eng. Phys. J. deposit with VINITI, 18.

Shevyakov, G.G., Savelyeva, N.I. (2004) Dispersion and combustion of hydrogen jet in the open atmosphere. Int. Sci. J. Altern. Energy Ecol. 1, 23–27.

SOLIT (2007) Safety of life in tunnels – Water mist fire suppression systems for road tunnels (Final Report).

Søgaard, D., Giuliani, L. and Markert, F. (2018) Fire spread by hydrogen fueled vehicles in semi-open car parks, in Nordic Fire Safety Days. Trondheim, Norway, p. 1.

Stamps, D., Cooper III, E., Egbert, R., Heerdink, S., Stringer V. (2009) Pressure rise generated by the expansion of a local gas volume in a closed vessel. Proc R Soc A, 465, pp. 3627-3646.

Statens havarikommisjon for transport (SHT) (2016) Rapport om brann i tanktilhenger i Skatestraumtunnelen i Sogn og Fjordane 15, juli 2015.

Stephenson, R.R. (2005) Fire safety of hydrogen-fueled vehicles: System-level bonfire test.

Sýkora, J., Jarušková, D., Šejnoha, M., Šejnoha, J. (2018) Fire risk analysis focused on damage of the tunnel lining. Fire Safety Journal. Elsevier, 95, 51–65.

Takeno, K., Okabayashi, K., Kouchi, A. Nonaka, T., Hashiguchi, K., Chitose, K. (2007) Dispersion and explosion field tests for 40MPa pressurized hydrogen. International Journal of Hydrogen Energy, Volume 32, Issue 13, 2144-2153.

Tamura, Y., Takabayashi, M. and Takeuchi, M. (2014) The spread of fire from adjoining vehicles to a hydrogen fuel cell vehicle. International Journal of Hydrogen Energy, 39(11), 6169–6175.

Tarada, F. (2011) Fires in tunnels – can the risks be designed out? Eurotransport Magazine, Eurotransport Magazine, 9, 46–49.

Teodorczyk, A., Lee, J.H., Knystautas, R. (1988) Propagation mechanism of quasi-detonations. 22nd Symposium (Int.) on Combustion. The Combustion Institute, Pittsburgh, 1723–1731.

TNO (2005) Methods for the calculation of physical effects due to releases of hazardous materials (liquid and gases), Yellow book, van den Bosh, C.J. H., Weterings, R.A.P.M. (Eds), TNO, The Hague.

Today (2016) Caught on Camera: Natural-gas powered garbage truck explodes [WWW Document]. Today. URL https://www.today.com/video/caught-on-camera-natural-gas-powered-garbage-truck-explodes-609780803613 [accessed 6.1.19].

Tohir, M., Spearpoint, M. (2013) Distribution analysis of the fire severity characteristics of single passenger road vehicles using heat release rate data. Fire Science Reviews 2:5.

Tohir, M. Z. M., Spearpoint, M. and Fleischmann, C. (2018) Prediction of time to ignition in multiple vehicle fire spread experiments. Fire and Materials. John Wiley and Sons Ltd, 42(1), 69–80.

Tolias, I.C., Venetsanos, A.G. (2015) Comparison of convective schemes in hydrogen impinging jet CFD simulation. International Conference on Hydrogen Safety, Yokohama, Japan.

Tolstrup, J., Giuliani, L., Narasimhan, H., Laigaard Jensen, J., Jomaas, G (2019) Experimental study of epoxy coatings for fire protection of bridge cables. The 14th Nordic Steel Construction Conference (NordicSteel2019), 18-20 September 2019, Copenhagen, Denmark.

Toyota Motor Corporation (2016), 2016 Mirai Product Information, 1–3. http://pressroom.toyota.com/releases/2016+toyota+mirai+fuel+cell+product.htm.

Truchot, B., Fouillen, F. and Collet, S. (2018) An experimental evaluation of toxic gas emissions from vehicle fires. Fire Safety Journal, 97, 111–118.

Tse, S.D., Zhu, D. L., Law, C. K. (2000) Morphology and burning rates of expanding spherical flames in H2/O2/inert mixtures up to 60 atmospheres, Proceedings of the 28th Symposium (International) on Combustion, The Combustion Institute, Pittsburgh, PA, 1793-1800.

United Nations Economic Commission for Europe (2013) Global technical regulation on hydrogen and fuel cell vehicles, Addendum 13: Global technical regulation No. 13. Global Registry. (Global Registry). UNECE.

UPTUN 251 (2006) UPTUN 251: Engineering guidance for water based fire fighting for the protection of tunnels and subsurface facilities (EU Research Project).

Veser, A., Breitung, W. Dorofeev, S.B. (2002) Run-up distances to supersonic flames in obstacle-laden tubes, J. Phys. IVFrance 12.

Vogt, M. (2017) Consulting, Tunnel training under realistic conditions, 1–66.

Wang, F., Wang, M. and Huo, J. (2017) The effects of the passive fire protection layer on the behavior of concrete tunnel linings: A field fire testing study. Tunnelling and Underground Space Technology. Elsevier, 69(March), 162–170.

Wang, C., J., Wen, J., X., Chen, Z., B., Dembele S. (2014) Predicting radiative characteristics of hydrogen and hydrogen/methane jet fires using FireFOAM. International Journal of Hydrogen Energy, vol. 39, 20560-20569.

Wenger, D. (2019) State of H2-technology in Germany, Japan & California, E-mail distribution, Wenger Engineering GmbH.

Weyandt, N. (2005) Analysis of induced catastrophic failure of a 5000 psig yype IV hydrogen cylinder (No. 01.06939.01.001). Southwest Research Institute report for the Motor Vehicle Fire Research Institute.

Weyandt, N. (2006) Vehicle bonfire to induce catastrophic failure of a 5000-psig hydrogen cylinder installed on a typical SUV. Southwest Research Institute report for the Motor Vehicle Fire Research Institute.

Whitehouse, D.R., Greig, D.R., Koroll, G.W. (1996) Combustion of stratified hydrogen-air mixtures in the 10.7 m3 combustion test facility cylinder. Nucl Eng Des, 166:453-62.

Wichmann, H., Lorenz, W. and Bahadir, M. (1995) Release of PCDD/F and PAH during vehicle fires in traffic tunnels. Chemosphere, 31(2), 2755–2766.

Woodfield, P. L., Monde, M. and Takano, T. (2008) Heat transfer characteristics for practical hydrogen vessels being filled at high pressure. Journal of Thermal Science and Technology, 3, 241–253.

Wu, Y. (2006) Initial assessment of the implication on ventilation system of transporting hydrogen cars through existing road tunnels. In Proc. International 12th Symp. Aerodynamics & Ventilation of Vehicle Tunnels, Portoroz, Slovenia, 11-13 July 2006, 873-881.

Wu, Y. (2008) Assessment of the impact of jet flame hazard from hydrogen cars in road tunnels. Transportation Research Part C: Emerging Technologies, 16(2), pp. 246–254.

Wu, M.H., Kuo, W.C. (2013) Accelerative expansion and DDT of stoichiometric ethylene/oxygen flame rings in micro-gaps. Proceedings of the Combustion Institute, 34 (2), 2017-2024.

Yamashita, A., Kondo, M., Goto, S., Ogami, N. (2015) Development of high-pressure hydrogen storage system for the Toyota “Mirai.” SAE Tech. Pap. SAE International.

Yang, J.C., Pitts, W.M., Fernandez, M. and Kuldeep, P. (2013) Measurements of effective diffusion coefficients of helium and hydrogen through gypsum. International Journal of Hydrogen Energy, Volume 38, Issue 19, 8125-8131.

Xiao, J., Travis, J. R., Kuznetsov, J. (2015), Numerical investigations of heat losses to confinement structures from hydrogen-air turbulent flames in ENACCEF facility, International Journal of Hydrogen Energy, vol.40, 13106-13120.

Zabetakis, M. G. and Burgess, D.S. (1961) Research on the hazards associated with the production and handling of liquid hydrogen, United States Department of the Interior Bureau of Mines, Report of Investigations 5707.

Zalosh, R. and Weyandt, N. (2005) Hydrogen fuel tank fire exposure burst test. SAE Pap. 2005-01–1886.

Zalosh, R. (2007) Blast waves and fireballs generated by hydrogen fuel tank rupture during fire exposure, in: 5th International Seminar on Fire and Explosion Hazards, Edinburgh, UK.

Zhang, S., Shi, L., Wang, J., Li, X., Han, Y., He, K., Cheng, X. (2019) Critical ventilation velocity of two fire sources with different separating distances in road tunnel. J. Fire Sci. 073490411985754.

Zhou, K, Jiang, J (2016) Thermal radiation from vertical turbulent jet flame: line source Model. Journal of Heat Transfer, vol.138, 042701-042708.

Zhou, K., Liu, N., Zhang, L., and Satoh, K. (2014) Thermal radiation from fire whirls: revised solid flame model. Fire Technol., vol. 50 (6), 1573–1587.

Zimont, V. L. and Liptnikov, A. N. (1995) A numerical model of premixed turbulent combustion of gases. Chem. Phys. Reports, vol. 14, no. 7, 993-1025.